A helper NLR, NRC4, accumulates at the plant-pathogen interface to provide disease resistance against the Irish potato famine pathogen *Phytophthora infestans*

Cian Joseph Duggan

Thesis submitted to the Department of Life Sciences at Imperial College London for the degree of Doctor of Philosophy (PhD)

31 August 2020

All the work here is my own, except where cited, referenced or acknowledged.

'The copyright of this thesis rests with the author. Unless otherwise indicated, its contents are licensed under a Creative Commons Attribution-Non Commercial 4.0 International Licence (CC BY-NC). Under this licence, you may copy and redistribute the material in any medium or format. You may also create and distribute modified versions of the work. This is on the condition that: you credit the author and do not use it, or any derivative works, for a commercial purpose. When reusing or sharing this work, ensure you make the licence terms clear to others by naming the licence and linking to the licence text. Where a work has been adapted, you should indicate that the work has been changed and describe those changes. Please seek permission from the copyright holder for uses of this work that are not included in this licence or permitted under UK Copyright Law.'

Abstract

Plants and animals both rely on nucleotide-binding, leucine-rich repeat proteins (NLRs) to provide disease resistance. Plant NLRs often co-operate as pairs or networks. A sensor NLR detects the pathogen and a helper NLR executes cell death and/or downstream signalling. NLRs are believed to localise to the cytoplasm, plasma membrane or nucleus. However, these localisation patterns were observed in the absence of infection, not during infection with relevant pathogens due to the HR triggered by the NLR making it impossible to perform microscopy. Many plant proteins re-locate within the cell upon infection by microbes. Therefore the localisation of NLRs during infection may be different to those without infection. Additionally, determining the localisation of NLRs can help us understand what function the NLR provides and how it detects effectors and elicits an immune response. Here I study the localisation of a solanaceous helper NLR, NRC4 during live cell imaging of *Nicotiana benthamiana* leaves with and without infection by the Irish potato famine pathogen, *Phytophthora infestans*. I use transient gene expression and confocal microscopy to show that during NRC4, accumulates from the cytoplasm to a membrane surrounding the pathogen finger-like appendages called haustoria. The extra-haustorial membrane is a newly formed plant membrane interface surrounding the pathogen haustoria. This reveals that NLRs can be motile and alter localisation during infection to accumulate at pathogen contact sites. I overcome the problem of NLRs triggering cell death when their cognate effector is present by either studying the helper NLR NRC4 in the absence of a sensor, or by disarming NRC4 by mutating the first alpha helix of the NLR's cell death eliciting coiled-coil domain. When activated, we found that NRC4 forms puncta which associate with the EHM or in the absence of infection, the plasma membrane. These puncta may represent inflammasome-like 'resistosomes' or groups of resistosomes. A phylogenetically and functionally related NLR, ZAR1, was recently shown to form a resistosome and is proposed to execute cell death by possibly forming pores in the host membrane. Further evidence is required in the future to determine if NRC4 is forming resistosomes and whether these are eliciting cell death directly. Intriguingly, efforts to prevent NRC4 accumulation at the EHM, by mutation, truncation or chimeric NLR generation, led to loss of NRC4's cell death function. As a whole, this thesis provides evidence that NRC4 accumulates to the host-pathogen interface to

provide disease resistance against *P. infestans.* This thesis reveals that NLRs can alter their localisations upon infection and that they can even focally accumulate at the host-pathogen interface. Further understanding into how NRC4 focally accumulates during infection and exactly what it achieves by doing so may help us understand how resistance to fungi and oomycetes occurs. Ultimately, this may allow us to engineer disease resistant crops by, for instance, altering NRC4's specificity to recognise other EHM localised effectors, without altering NRC4's localisation.

Table of Contents

Abstract ***2***

List of Figures ***7***

List of Tables: ***12***

Abbreviations ***13***

Contributions ***15***

Acknowledgements ***20***

1. Introduction ***23***

1. *Phytophthora infestans* **23**

1.1. Surface immunity **26**

1.2. Effector triggered immunity **29**

1.3. Types of NLRs **30**

1.4. Models for NLR mode of action **30**

1.5. Aims & summary of chapters **35**

2. Materials & Methods ***36***

2.1. Summary **36**

2.2. Cloning **37**

2.2.1. Molecular cloning techniques 37

2.2.2. Fluorescent-tagging 40

2.3. Growth, maintenance and experimental conditions with plants and *Phytophthora infestans* **40**

2.3.1. Growth of plants 40

2.3.2. Transient gene expression in *Nicotiana benthamiana* 40

2.3.3. Cell Death Assays 41

2.3.4. *Phytophthora infestans* maintenance and infection of plant leaves 42

2.3.5. Virus Induced Gene Silencing (VIGS) 43

2.3.6. Gene silencing by RNAi 45

2.3.7. Suppression of Rpi-blb2 resistance 45

2.3.8. Complementation of Rpi-blb2/NRC4-mediated resistance or HR 45

2.3.9. Generation of transgenic 35S::NRC4-GFP plants 45

2.4. Protein-based and biochemical experiments 47
2.4.1. Crude protein extraction and western blotting 47
2.4.2. Co-immunoprecipitation 51
2.4.3. Membrane enrichment 53
2.4.4. Callose stain 53
2.4.5. RT-PCR 54
2.5. Microscopy, Imaging and Image analysis 54
2.5.1. Confocal microscopy 54
2.5.2. UV imaging of infection assays 55
2.5.3. Quantification of focal accumulation 55
2.5.4. Fluorescence recovery after photobleaching (FRAP) assay 55
2.6. Details of constructs 56
3. Results Chapter I: Where and when does NRC4-mediated resistance against P. infestans occur? 79
3.1. Chapter Summary 79
3.2. Introduction 79
3.3. Aims 80
3.4. Results & Discussion 81
3.4.1. NRC4, but not Rpi-blb2, accumulates at an EHM microdomain, co-localising with AVRblb2 81
3.4.2. Rpi-blb2/NRC4 does not prevent the initial penetration 109
3.5. Chapter Conclusions 113
4. Results Chapter II: What intramolecular properties of NRC4 determine immunity? 117
4.1. Chapter Summary 117
4.2. Introduction 117
4.3. Aims 118
4.4. Results & Discussion 119
4.4.1. The extended C-terminal domain of NRC4 is required for EHM localisation, stability and immunity 119
4.4.2. 4Tail suppresses NRC4 immunity by an unknown mechanism 129
4.4.3. The CC domain of NRC4 mediates EHM accumulation and programmed cell death 155

4.5. Chapter Conclusions 180

5. Results Chapter III: Does an intermolecular system enable NRC4-mediated immunity? 186

5.1. Chapter Summary 186

5.2. Introduction 186

5.3. Results & Discussion 189

5.3.1. NRC4 accumulation towards haustoria is unlikely to occur due to passive diffusion but instead by a dynamic process 189

5.3.2. Summary of gene silencing screen to determine the cellular components of NRC4 EHM transport 193

5.3.3. VIGS screen of candidate NRC4 interactors reveals secretory components that may positively contribute to Rpi-blb2 mediated resistance 198

5.3.4. The exocyst complex is deployed to the EHM but does not seem to regulate NRC4-Rpi-blb2 mediated immunity 200

5.3.5. HOPS/CORVET complexes involvement in NRC4-mediated resistance 207

5.3.6. RabE1 involvement in NRC4-mediated resistance 219

5.3.7. RabD2a involvement in NRC4-mediated resistance 225

5.4. Conclusions 230

6. General Discussion & Conclusions 233

1. Where does NRC4 localise in the cell? 233

6.1.1. Inactive state – pre-infection 233

6.1.2. Inactive state – during infection (intermediate) 234

6.1.3. Activated state - pathogen activated vs autoactivated 235

6.2. How does NRC4 accumulate at the EHM? 236

6.2.1. Transport pathway for NRC4 deployment to the EHM 236

6.2.2. Diffusion and EHM association/insertion of NRC4 237

6.3. Why does NRC4 accumulate at the EHM? 237

6.3.1. NRC4 accumulation at the EHM increase chances of effector detection 238

6.3.2. NRC4 guards a defence-related secretory pathway that targets the haustorial interface 241

6.3.3. The EHM is required for pathogenesis and targeting NRC4 there allows for efficient destruction of it upon pathogen recognition 243

6.4. Concluding remarks and future challenges 244

7. Bibliography..... 247

List of Figures

Figure 1.1: Infection of epidermal leaf cells by *Phytophthora infestans*. 24
Figure 1.2: Cellular compartments surrounding the haustorium..... 26
Figure 1.3: Pathogens are detected on the plant cell surface by PRRs and in the cell by NLRs..... 28
Figure 1.4: [Fig. S15 An NRC-dependent NLR immune signalling network confers resistance to diverse pathogens..... 33
Figure 1.5: α1 helix of NRC4 is predicted to protrude out upon activation and form a pentameric resistosome. 34
Figure 2.1: Summary of methods. GOI = gene of interest..... 36
Figure 2.2: *ccdB* Gibson Assembly vector generation for fluorescent tagging. 39
Figure 2.3: HR index used for some experiments. 41
Figure 2.4: Generation of pTRV2gg vector for compatibility with PCR fragments produced for pRNAiGG vector..... 44
Figure 2.5: Alignment of RabE family proteins tested for silencing by hpRabE1a. .. 77
Figure 3.1: NRC4, but not NRC2 or ZAR1, accumulates at the EHM. 83
Figure 3.2: Western blot analysis shows studied NLRs stably produced. 84
Figure 3.3: NRC4 associates with the plasma membrane as well as being cytoplasmic. 86
Figure 3.4: Membrane enrichment of transgenically expressed NRC4-GFP, in the absence of *Agrobacterium* or pathogen challenge, shows NRC4 is more cytoplasmic than membrane localised. 87
Figure 3.5: NRC4 accumulates at the EHM during infection with *P. infestans*. 89
Figure 3.6: NRC4 localises to an EHM microdomain, partially but not fully co-localising with EHM markers. 92
Figure 3.7: NRC4 cage-like haustorial structure is not due to localisation to ER surrounding the EHM..... 94
Figure 3.8: NRC4 perihaustorial cage-like localisation pattern does not co-localise with cytoskeletal markers..... 95

Figure 3.9: Fluorescent signal from NRC4 peaks on the host side of an EHMx marker. 96
Figure 3.10: NRC4-GFP fluorescence does not originate from to callose deposits. 98
Figure 3.11: AVRblb2 localises to an EHM microdomain in the absence of NRC4 and in the presence of NRC4 partially co-localises with it. 99
Figure 3.12: Rpi-blb2 is cytoplasmically distributed in the presence of haustoria. . 101
Figure 3.13: NRC4 co-immunoprecipitates with Rpi-blb2 but AVRblb2 pulls down non-specifically. 103
Figure 3.14: NRC4 co-immunoprecipitates with Rpi-blb2 but it is unclear if AVRblb2 CoIPs or not. 104
Figure 3.15: Hairpin RNAi of NRC4 compromises Rpi-blb2 resistance locally. 106
Figure 3.16: Hairpin RNAi of NRC4 compromises Rpi-blb2 resistance in the agro-infiltrated zone only. 108
Figure 3.17: Infection vesicles form in both WT and Rpi-blb2 transgenic lines. 110
Figure 3.18: NRC4 accumulates at the tips of the membrane surrounding hyphal leaders that emerge from infection vesicles. 112
S1 Figure 3.19: RFP-Rpi-blb2 is functional but GFP-NRC4 is not and causes a dominant negative effect. 115
Figure 4.1: InterProScan reveals c-terminal extension of NRC4 with no annotated domain or motif. 119
Figure 4.2: NRC4Δtail truncate does not accumulate at the EHM, but instead remains cytoplasmic 120
Figure 4.3: NRC4Δtail is non-functional and suppresses immunity. 123
Figure 4.4: 4Tail suppresses Rpi-blb2 resistance (in a lysine dependent manner), but 2tail does not. 126
Figure 4.5: Multiple sequence alignment of NRC C-terminal extensions reveals conservation in charged amino acids. 127
Figure 4.6: Western blot showing mKOk-FLAG proteins are correctly cloned and stably expressed. 128
Figure 4.7: 4Tail weakly suppresses NRC4-mediated HR. 130
Figure 4.8: 4Tail expression does not lead to NRC4 degradation. 132
Figure 4.9: Full-length NRC4 does not coimmunoprecipitate with 4Tail. 134
Figure 4.10: Rpi-blb2 or NRC4 does not coimmunoprecipitate with 4Tail. 136

Figure 4.11: 4Tail co-immunoprecipitates with NRC4 but also the negative control EV:GFP. 137
Figure 4.12: 4Tail co-immunoprecipitates with GFP-Rpi-blb2 but also the negative control GFP-RFP tandem. 138
Figure 4.13: 4Tail expression does not seem to effect NRC4-NRC4 interaction. .. 140
Figure 4.14: 4Tail expression does not seem to effect NRC4-Rpi-blb2 interaction. 141
Figure 4.15: 4Tail expression reduces NRC4-GFP perihaustorial fluorescence. ... 143
Figure 4.16: NRC4 focal accumulation is suppressed by 4Tail expression..... 144
Figure 4.17: NRC4 membrane association is not altered by overexpression of 4Tail. 146
Figure 4.18: Model of Rpi-blb2 and Rx1 mediated resistances. 147
Figure 4.19: Rpi-blb2 and Rx1 resistance is broken by 4Tail. 149
Figure 4.20: NRC4^{2Tail} chimera is functional for immunity. 151
Figure 4.21: Internal tagging of NRC4^{2Tail} reveals it accumulates at haustoria. 154
Figure 4.22: Western blotting shows NRC4-NRC2 chimeras are correctly cloned. 155
Figure 4.23: The CC domain of NRC4 is required for EHM accumulation. 156
Figure 4.24: The CC domain of NRC4 can inefficiently focally accumulate to the EHM unlike NRC2. 158
Figure 4.25: NRC4 does not lose perihaustorial focal accumulation when its CC domain is swapped with that of NRC2. 160
Figure 4.26: NRC2 gains perihaustorial focal accumulation when its CC domain is swapped with that of NRC4. 161
Figure 4.27: ZAR1 does not gain full perihaustorial focal accumulation when its CC is swapped with that of NRC4, but did show EHM labelling. 162
Figure 4.28: The first half of the CC domain of NRC4 does not appear to contain the signal for haustorial targeting. 164
Figure 4.29: NRC4 with the second half of the CC domain from NRC2 or ZAR1 still accumulates at the EHM. 166
Figure 4.30: The second half of the CC domain of NRC4 permits haustorial targeting to NRC2 but not ZAR1. 168
Figure 4.31: HR complementation assay in Rpi-blb2 nrc4a/b plants shows that NRC4 varients which remove, swap or add a domain on NRC4 lead to loss of HR function, except for C-terminal fusions. 170

Figure 4.32: Western blot analysis confirms chimeras are cloned correctly and of expected molecular weight. 171
Figure 4.33: The first alpha helix of ZAR1 is functional in NRC4 and does not alter its localisation. 173
Figure 4.34: Mutations in the MADA motif of NRC4 lead to loss of immune function but do not alter localisation. 175
Figure 4.35: Activated NRC4 forms puncta which associate with the PM and/or EHM but is unable to focally accumulate. 178
Figure 4.36: NRC4^{D478V} does not prevent necrotic lesion spread associated with *P. infestans* infection. 179
Supplementary 1 = Figure 4.37: 4Tail-mKOk and RFP-4Tail suppress Rpi-blb2 immunity despite the latter having two amino-acid polymorphisms. 183
Supplementary 2 = Figure 4.38: 4Tail expression does not seem to effect NRC4-NRC4 interaction. 184
Supplementary 3 = Figure 4.39: 4Tail expression does not seem to effect NRC4-Rpi-blb2 interaction. 185
Figure 5.1: Fluorescence Recovery After Photobleaching of NRC4-GFP recovers faster than RFP-Rem1.3. 191
Figure 5.2: NRC4-mKOk fluorescence recovers much slower than cytoplasmic EV-GFP. 192
Figure 5.3: Reverse genetics screen to identify proteins involved in NRC4-mediated resistance. 196
Figure 5.4: VIGS based RNAi screen of candidate NRC4 interactors reveals some possible regulators of Rpi-blb2/NRC4 mediated immunity to *P. infestans.* 199
Figure 5.5: hpExo70A1 seems to have no effect on NRC4 or I2 mediated HR. 201
Figure 5.6: Western blotting shows no effect on NRC4 protein levels upon *Exo70A1* silencing. 203
Figure 5.7: Exocyst complex is deployed to the haustorial interface. 205
Figure 5.8: Western blotting of GFP fusion proteins confirms stable expression of most constructs. 207
Figure 5.9: Diagram summarising what is known about HOPS and CORVET complexes. 208
Figure 5.10: Hairpin RNAi of HOPS/CORVET components amplifies NRC4-mediated HR. 209

Figure 5.11: Hairpin RNAi of HOPS/CORVET components does not seem to alter R3a-mediated HR. 210
Figure 5.12: Hairpin RNAi of HOPS/CORVET core component VPS18 seems to amplify NRC3-mediated HR, but there is insufficient statistical power present to be conclusive. 211
Figure 5.13: NRC4 co-immunoprecipitates with StVPS18-GFP. 212
Figure 5.14: NRC4 co-immunoprecipitates with VPS41-GFP. 213
Figure 5.15: HOPS/CORVET core component StVPS18 is deployed to the haustorial interface. 215
Figure 5.16: HOPS specific component VPS41 is deployed to the haustorial interface. 216
Figure 5.17: Western blotting shows no effect on NRC4 protein levels upon HOPS/CORVET component silencing. 218
Figure 5.18: Western blotting inconclusive in determining whether hpVPS18 alters NRC4 stability. 218
Figure 5.19: Hairpin RNAi of RabE1 amplifes NRC4-mediated HR but not R3a HR. 220
Figure 5.20: hpRabE1 increases the intensity of NRC4 or I2 mediated HRs. 221
Figure 5.21: Semiquantitative RT-PCR confims silencing by hpRabE1 of RabE1 specifically. 222
Figure 5.22: Western blotting shows no effect on NRC4 protein levels upon RabE1 silencing, but probable increase in *Agrobacterium* virulence. 224
Figure 5.23: Expression of Dominant Negative RabD2a mutant suppresses NRC4-mediated HR. 226
Figure 5.24: Expression of Dominant Negative RabD2a mutant suppresses NRC4 or NRC3 mediated HR. 227
Figure 5.25: Western blotting shows RabD2a suppresses *Agrobacterium* mediated gene expression. 229

List of Tables:

Table 1: Composition of shooting and rooting media 46
Table 2: Recipe for SDS-PAGE Separating Gels 49
Table 3: Antibodies used for western blotting 50
Table 4: Common Buffers 52
Table 5: Laser excitations on Leica SP5 and SP8 microscopes 54
Table 6: Details of constructs cloned in this study 56
Table 7: Pre-existing constructs 67
Table 8: PK7 vectors and their derivatives 71
Table 9: Constructs created by gene synthesis (GeneWiz) 73
Table 10: RT-PCR primers 77
Table 11: Summary of Mass Spec candidate interactors investigated for involvement in NRC4-mediated immunity 197
Table 12: List of perihaustorial effectors (data from (Wang et al., 2018a)) 240

Abbreviations

Agroexpression	*Agrobacterium*-mediated transient gene expression
Agroinfiltration	infiltration of *Agrobacterium*
AVR	Avirulence protein
BFP	blue fluorescent protein (TagBFP)
CC	Coiled-coil
ccdB	toxin killing bacteria without ccdA antitoxin
CNL	CC-NLR
DAMP	Danger Associated Molecular Pattern
dpai	days post *agro*infiltration
dpi	days post infection
DTT	Dithiothreitol
FLAG	FLAG tag (non-fluorescent epitope tag with sequence 'DYKDDDDK')
FP	fluorescent fusion protein
GFP	green fluorescent protein (eGFP)
HA	Haemagglutinin tag (non-fluorescent epitope tag with sequence 'YPYDVPDYA')
HR	Hypersensitive Response
LRR	Leucine Rich Repeat
MHD	Methionine-histidine-aspartate
mKOk	monomeric Kusabira Orange 'k' protein
NBD	Nucleotide Binding Domain
NLR	nucleotide-binding, leucine-rich repeat protein
NRC	NLR required for cell death
OD_{600}	optical density at 600 nm
PRRs	Pattern Recognition Receptors
PVX	Potato Virus X

R	Resistance
RFP	red fluorescent protein (mRFP1)
Rpi	Resistance to *Phytophthora infestans*
RPW8	Resistance to Powdery Mildew 8
TIR	Toll/interleukin 1 receptor
TNL	TIR-NLR
VIGS	Virus Induced Gene Silencing

Contributions

Throughout the entirety of this project many individuals contributed. They were mostly Undergraduate and Masters students at Imperial College supervised by me, but some were interns or collaborators. In this thesis I have written the results section using the first-person singular “I” where I alone was involved, or the first-person plural “we” where others were involved with me. The degree to which they contributed varied from experiment to experiment. I could not have got to this stage without them and a single author Thesis is not sufficient to recognise that. Therefore, in an effort to properly recognise their hard work and dedication, here I present a list of contributions based on figures.

Results Chapter I:

Figure 3.1
A-E Experiments by Eleonora Moratto, supervision and experimental design by Cian Duggan
E-M Experiments by Cian Duggan
I & M Transgenic plants produced by Alexandre Y Leary
N-U Experiments by Cian Duggan
3xHA-AVRblb2 cloned by Seda Nohut

Figure 3.2
Experiments by Cian Duggan and Eranthika Hamilton, supervision and experimental design by Cian Duggan

Figure 3.3
Experiments by Cian Duggan

Figure 3.4
Experiments by Cian Duggan and Eranthika Hamilton, supervision and experimental design by Cian Duggan

Figure 3.5-10
Experiments by Cian Duggan

Figure 3.11
Experiments by Cian Duggan
BFP-AVRblb2 cloned by Seda Nohut

Figure 3.12-15
Experiments by Cian Duggan

Figure 3.16
Experiments by Zachary Savage, supervision and experimental conception by Cian Duggan

Figure 3.17-18
Experiments by Cian Duggan

Figure 3.S1
Experiments by Cian Duggan

Results Chapter II:

Figure 4.1-4.5
Experiments by Cian Duggan

Figure 4.6
Experiments by Eranthika Hamilton & Cian Duggan, Supervision and Experimental Design by Cian Duggan

Figure 4.7-17
Experiments by Cian Duggan

Figure 4.18
Figure by Cian Duggan, adapted from Jess Upson

Figure 4.19
Experiments by Fengqi Tian and Cian Duggan, Experimental design and Supervision by Cian Duggan, Analysis by Fengqi Tian

Figure 4.20
Experiments by Cian Duggan

Figure 4.21
Experiments and experimental design by Zachary Savage and Cian Duggan, Supervision by Cian Duggan.

Figure 4.22
Experiments by Zachary Savage

Figure 4.23
Experiments by Cian Duggan

Figure 4.24
Experiments by Eranthika Hamilton and Cian Duggan, Experimental design and Supervision by Cian Duggan, constructs made by Hiroaki Adachi

Figure 4.25
Experiments by Zachary Savage, Eleonora Moratto and Cian Duggan, Experimental design and Supervision by Cian Duggan, constructs made by Zachary Savage

Figure 4.26

Experiments by Eleonora Moratto and Cian Duggan, Experimental design and Supervision by Cian Duggan, constructs made by Eleonora Moratto

Figure 4.27
Experiments by Eranthika Hamilton and Cian Duggan, Experimental design and Supervision by Cian Duggan, constructs made by Eranthika Hamilton

Figure 4.28
Experiments by Eleonora Moratto and Cian Duggan, Experimental design and Supervision by Cian Duggan, constructs made by Eleonora Moratto

Figure 4.29
A
Experiments by Eleonora Moratto and Cian Duggan, Experimental design and Supervision by Cian Duggan, constructs made by Eleonora Moratto
B
Experiments by Eranthika Hamilton and Cian Duggan, Experimental design and Supervision by Cian Duggan, constructs made by Eranthika Hamilton

Figure 4.30
A
Experiments by Eleonora Moratto and Cian Duggan, Experimental design and Supervision by Cian Duggan, constructs made by Eleonora Moratto
B
Experiments by Eranthika Hamilton and Cian Duggan, Experimental design and Supervision by Cian Duggan, constructs made by Eranthika Hamilton

Figure 4.31
Experiments by Eranthika Hamilton and Cian Duggan, Experimental design and Supervision by Cian Duggan

Figure 4.32
Experiments by Eleonora Moratto and Cian Duggan, Experimental design and Supervision by Cian Duggan

Figure 4.33
Experiments by Eranthika Hamilton and Cian Duggan, Experimental design and Supervision by Cian Duggan. Hiroaki Adachi made NRC4-ZAR1alpha1-GFP, and controls, Eranthika Hamilton made ZAR1-NRC4alpha1-GFP

Figure 4.34
Experiments by Eranthika Hamilton and Cian Duggan, Experimental design and Supervision by Cian Duggan. Hiroaki Adachi made NRC4-L9E-GFP, NRC4-3A-GFP and controls

Figure 4.33
Experiments by Cian Duggan. Hiroaki Adachi made the GFP tagged constructs, RFP ones are published.

Figure 4.34
Experiments by Cian Duggan. Hiroaki Adachi made the GFP tagged constructs, RFP ones are published.

Results Chapter III:

Figure 5.1-2
Experiments by Cian Duggan

Figure 5.3
Figure by Cian Duggan

Table 11
Pull down by Tolga Bozkurt, MS by Dr Jan Sklenar, Analysis and selection by Cian Duggan
Initial VIGS screen with NL07434 was performed by Seda Nohut. Seda Nohut also cloned TRV2gg:TM, hpTM, TRV2gg:TPR, hpTPR, hpVSR3,TRV2gg:VSR3. Cindy Peillex cloned TRV/hp:Sec5, Sec3, Exo70A1, VPS18 and VPS41 with Cian Duggan.

Figure 5.4-6
Experiments by Jiaming Liang and Cian Duggan, Supervision and Analysis by Cian Duggan

Figure 5.7
Experiments by Cian Duggan, Sec3 made by Cian Duggan, Exo70B1-GFP made by Cindy Peillex, Exo70A1-GFP made by Jiaming Liang, Exo84b-GFP made by Yasin Dagdas

Figure 5.8
Experiments by Jiaming Liang and Cian Duggan, Supervision and Analysis by Cian Duggan

Figure 5.9
Figure made by Cian Duggan

Figure 5.10-17
Experiments by Cian Duggan

Figure 5.18
Experiments by Jiaming Liang and Cian Duggan, Supervision and Analysis by Cian Duggan

Figure 5.19
Experiments by Cian Duggan

Figure 5.20

Experiments by Jiaming Liang and Cian Duggan, Supervision and Analysis by Cian Duggan

Figure 5.21
Experiments by Cian Duggan

Figure 5.22
Experiments by Jiaming Liang and Cian Duggan, Supervision and Analysis by Cian Duggan

Figure 5.24-26
Experiments by Cian Duggan

Acknowledgements

First and foremost, I want to thank my supervisor, mentor and friend Dr Tolga Bozkurt. He has taught me so much during our five years working together and continues to inspire me. I am really privileged to have met him during my Master's degree at Imperial as he introduced me to the field of plant-microbe interactions. Working with him is what made me excited to pursue a PhD. He has motivated me through the ups and downs of this project and has always kept me well-fed with Bosphorus Kebabs and Oddono's Gelato; and hyped-up on Fernandez & Wells Coffee. I look forward to pursuing more science with him and more importantly, finding the best pistachio ice cream.

Next I'd like to thank all the members of the Bozkurt lab. The culture in our lab through the years has been incredible and I want to pay special thanks to my PhD lab mates. As well as being fantastic friends, Yasin has always brightened my day, Alex has been great for the 'DMCs', and Zac has always been there to discuss ideas – no matter how ridiculous ('The Wizard of OD_{600}' and 'The Mel Gibson Assembler' excel calculators did not make it into this thesis but deserve an acknowledgement here). Thank you to Pooja for her help and competition with plant transfer. I might go over the 100,000 word-limit for this thesis if I acknowledge all the temporary or recent additions to our lab, but I must pay respect and thanks to all of those who have worked on this project with me from this lab: Eleonora, Eranthika, Francesca, Cindy, Mike, Juyeon, Lucie, Han, Fengqi, Jiaming, Kavan, Seda and Zac (again). Eleonora in particular deserves a huge amount of recognition for her work which you can see in the contributions section.

I'd like to thank the FILM facility at Imperial College for teaching me so much about image analysis and microscopy and for all their help with the project more recently. Allison Hunter, Lukas Bukowski and the rest of the tech team at the Department of Life Sciences at Imperial College have done such a fantastic job over the years and particularly during COVID-19. Their work is largely behind the scenes and is often taken for granted. Thank you for making our work possible, we are so lucky to work with you.

I would also like to thank members from the Kamoun lab in TSL, Norwich – where Tolga made the initial discoveries for this project. First, Prof Sophien Kamoun himself for his mentorship. In addition to this, his tweets about progressive publishing and margaritas have inspired me to be more vocal about my views. Next, Dr Chih-hang Wu, Dr Lida Derevnina, Dr Joe Win, and more recently Dr Hiroaki Adachi, all of whom gave me so much of their time and patience – not to mention constructs (see contributions and construct tables). Past Kamounity members Dr Sebastian Schornack for his comments, suggestions and discussions; Dr Khaoula Belhaj for an unpublished construct; and Dr Angela Chaparro-Garcia for her advice. I'd also like to acknowledge the PhD students (at the time) Ola, Erin, Mau and Juan who were great peers and friends.

Thank you to everyone who contributed constructs to this project. Those not already named are Prof Shunyuan Xiao, Dr Henrik Buschmann, and big thanks to Dr Shumei Wang and Prof Paul Birch for the transgenic *Phytophthora*! Details of the constructs are in my constructs table in Materials & Methods chapter and also the contributions section.

There are many people who have taught me and given me opportunities which were integral for me to get to where I am today. I'd like to thank them all. A few, deserve to be mentioned specifically, because I never had a chance to truly thank them in person: Dr Owen Ross for giving me the chance to work in his lab in Mayo Clinic Florida when I was an undergraduate, and his Post-doc at the time Dr Alexandra Ortolaza who taught me how to not contaminate pipettes and PCRs. Next, my high school home economics teacher Mr Dooley, who fostered my love for science (and food), taught me the structure of an amino acid, and always chatted to me like an adult.

Last but not least, I want to thank those in my personal life (who I won't name here). My friends for the good times and for keeping me grounded. My girlfriend for her love, support and knowledge of food. My brothers for their friendship and help through the years. My extended family for their support. My grandfather for teaching me to value an education and to always work hard. Finally, my parents who have loved me, provided for me and taught me from day one. Their wonderful combination of creativity and work ethic has shaped me into who I am.

I couldn’t have finished this without you all, and many more not named here. On top of this, I want to recognise that I’ve benefitted for an enormous amount of privilege to get to where I am. I’m extremely grateful for my opportunities in life and will continue to work hard to contribute what I can to society.

1. Introduction

1. *Phytophthora infestans*

The oomycete *Phytophthora infestans*, the causative agent of late blight disease, was responsible for triggering the Irish potato famine of the mid-19th century. Today it remains the most destructive pathogen of potatoes, also infecting several other solanaceous plants including tomato and the model plant *Nicotiana benthamiana* (Grünwald and Flier, 2005; Yoshida et al., 2013). *P. infestans* has a hemibiotrophic lifestyle (Figure 1.1), beginning when a spore lands and germinates on the epidermal tissue of a host plant. A successful penetration of host tissue results in formation of an intracellular hyphal structure, known as the infection vesicle (IV). Precluding pathogen penetration of the first cell is critical for preventing infection (Whisson et al., 2016). Successful infection then leads to generation of intracellular hyphal-like structures, known as hyphal leaders, which direct the pathogen growth towards the extracellular space. Here intercellular hyphae are formed, which expand throughout the apoplast, forming lateral digit-like penetrations into plant cells. These appendages are known as haustoria and serve as specialised feeding structures for the pathogen and sites for secreting virulence factors known as effectors inside the host cells (Figure 1.1) (Bozkurt and Kamoun, 2020; Fawke et al., 2015; Whisson et al., 2016).

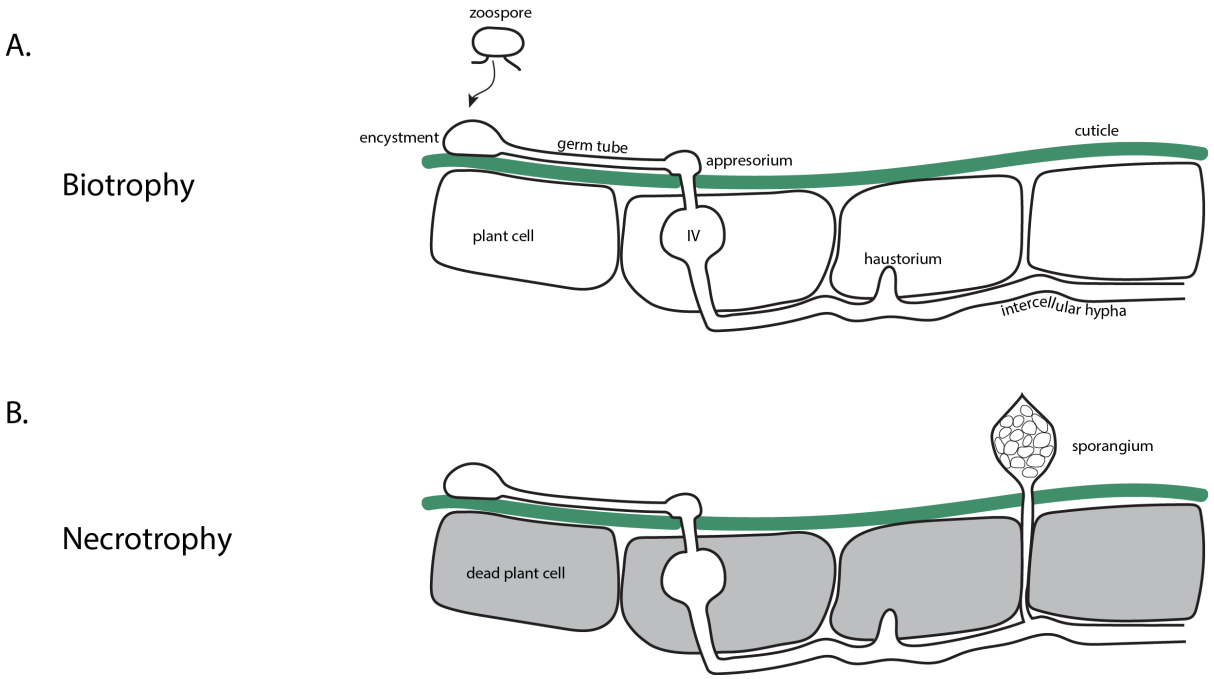


Figure 1.1: Infection of epidermal leaf cells by Phytophthora infestans.
Infection begins when a biflagellate motile zoospore, carried by water ends up on the cuticle of the plant epidermal tissue. The zoospore encysts and germinates to form an appressorium at the end of the germ tube. The appressorium is thought to apply pressure in order to penetrate into a cell underneath. Here it forms a spherical primary infection vesicle which, if it avoids the hypersensitive response, will form hyphal leaders that exit the cell to form intercellular hyphae. Hyphae produce digit-like perpendicular penetrations into cells known as haustoria, which are surrounded by a plant derived membrane known as the extrahaustorial membrane (EHM). *P. infestans* grows biotrophically initially (A), without killing the cells, but later these areas of infection become necrotrophic – that is the pathogen infected plant tissue is necrotic (B). Successful infection finishes with the growth of a fruiting bodies with sporangia for the release of zoospores, or zoosporangia for direct infection (not shown). Figure is not to scale. For reasons of simplicity, organelles, cytoplasm and membranes are not depicted.

Each haustorium is surrounded by a plant-derived membrane, known as the extra-haustorial membrane (EHM), which is continuous with the plant plasma membrane, but distinct in its protein and lipid composition (Bozkurt et al., 2015; Lu et al., 2012) (Figure 1.2). The matrix between the EHM and the pathogen known as the extra-haustorial matrix (EHMx), is thought to be the ultimate interface containing the secretome of both the pathogen and the plant. Although the mechanisms of EHM biogenesis and its origin are poorly understood, it is believed that the EHM is initially formed as part of a cell polarization response to pathogen attack. Possibly, at later stages, effectors secreted by the pathogen remodel the EHM properties. Consistent

with this, several secreted *P. infestans* effectors including AVRblb2 have been shown to accumulate at the EHM, when expressed inside the plant cells (Bozkurt et al., 2015, 2011; Saunders et al., 2012) (Bozkurt, unpublished).

One group transformed *P. infestans* with an RFP tagged effector, AVR3a, and showed its accumulation in the EHMx and subsequent translocation into plant cells (Whisson et al., 2007). However, how effectors translocate into host cells was the topic of debate for some time. To settle this, the same group identified a nucleus and nucleolus localised effector Pi04314, transformed *P. infestans* with an RFP fusion and found it accumulated to these sites – eliminating any question of signal originating from autofluorescence. They also transformed an RFP tagged apoplastic effector in *P. infestans*, EPIC1-mRFP (Wang et al., 2017a). Extracellular protease inhibitors of cysteine proteases (EPICs) are secreted by *P. infestans* to inhibit plant apoplastic defence proteases like C14, the secretion of which is also inhibited by cytoplasmic effector AVRblb2 (Bozkurt et al., 2011). The demonstration that EPIC1-mRFP accumulates in the EHMx experimentally verifies that haustoria are indeed sites of effector secretion (Wang et al., 2017a). Plant secreted apoplastic proteins are excluded from the EHMx in a similar fashion to how plasma membrane proteins are excluded from the EHM. An example of the latter includes the surface immune receptor, FLS2 which recognises flg22 from bacteria but is excluded from the EHM of *P. infestans* (Bozkurt et al., 2015).

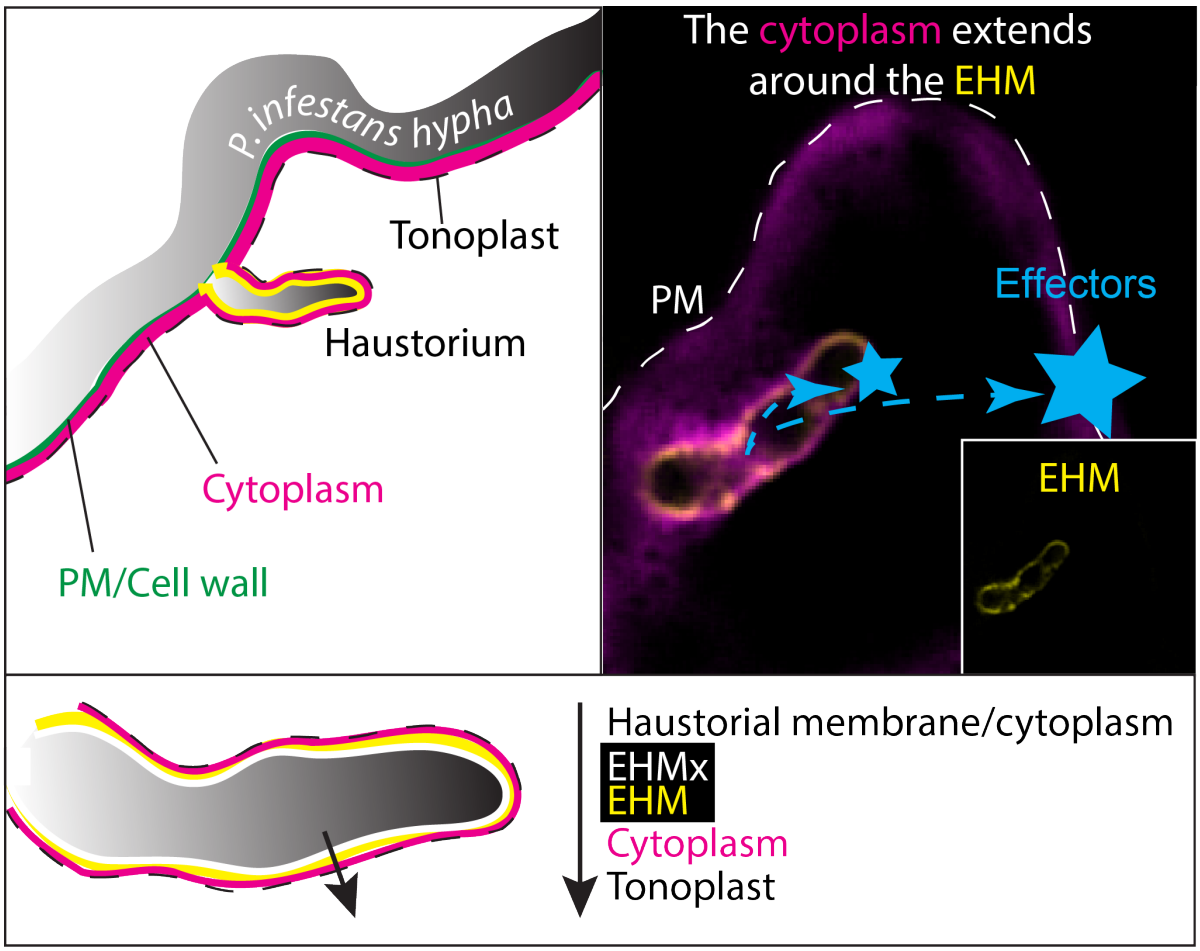


Figure 1.2: Cellular compartments surrounding the haustorium.
Each haustorium is thought to secrete effector proteins into the Extrahaustorial matrix (EHMx), the space between the haustorium and the Extrahaustorial membrane (EHM) that is a plant derived membrane continuous with the plasma membrane and enclosing the haustorium. Many of these effector proteins are translocated to the cytoplasm by an unknown mechanism and can be recognised, directly or indirectly, by a cognate NLR. If this occurs, the hypersensitive response (HR) is usually triggered in order to kill/starve the invading pathogen.

1.1. Surface immunity

Surface immune receptors, such as FLS2, are known as pattern recognition receptors (PRRs) and are responsible for recognising pathogen-associated molecular patterns (PAMPs); endogenous signals produced by pathogen infection, known as damage-associated molecular patterns (DAMPs); or apoplastic effectors. PAMPs are more correctly now known as Microbe Associated Molecular Patterns (MAMPs), as most are also found in non-pathogenic microbes. PRRs can be either Receptor Like Kinases (RLKs) or Receptor Like Proteins (RLPs), depending on the presence of a cytosolic

kinase domain. To activate downstream signalling, and ultimately PRR-triggered immunity (PTI), many PRRs require another cell-surface receptor known as BAK1 (Chinchilla et al., 2007; Roux et al., 2011). PTI, the first layer of plant innate immunity, aims to detect the pathogen in the apoplast, block pathogen entry by deposition of cell wall components such as callose and pectins, and kill the pathogen by secreting antimicrobial compounds like ROS. Occasionally build-up of the cell wall at sites of attempted pathogen ingress leads to production of a structure known as a papilla (Figure 1.3) (Schmelzer, 2002). Additionally, apoplastic effector recognition or recognition of conserved molecules known as elicitins, such as *Phytophthora* INF1, can lead to programmed cell death.

A.

Surface-mediated immunity /
PRR-Triggered Immunity (PTI)

B.

NLR triggered immunity (NTI) /
Effector Triggered Immunity (ETI)

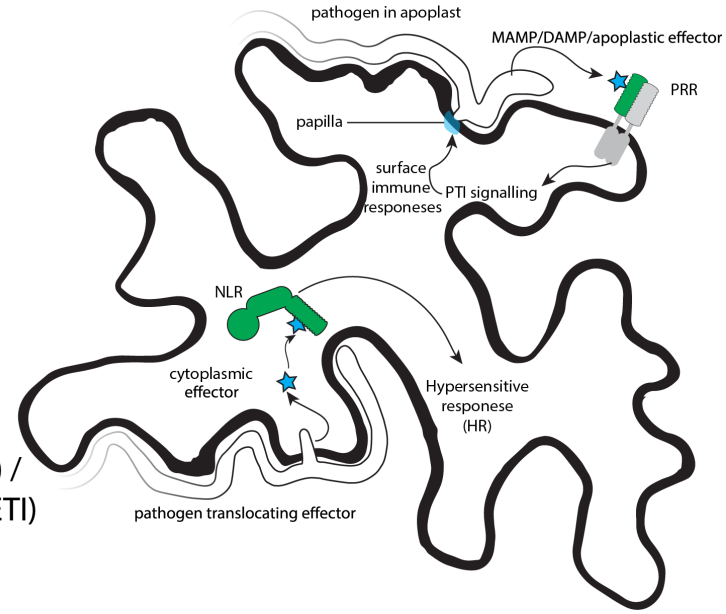


Figure 1.3: Pathogens are detected on the plant cell surface by PRRs and in the cell by NLRs.
(A) Pathogens are detected on the plant cell surface by Pattern Recognition Receptors (PRRs). PRRs recognise conserved Microbe Associated Molecular Patterns (MAMPs) that are shed in the apoplast by the microbe, or apoplastic effectors that are secreted here. Alternatively, they can recognise Danger Associated Molecular Patterns (DAMPs), which are released from the plant cell upon pathogen colonisation. The immune signal is transduced into the host cell and results in: an immediate burst of ROS; focal deployment of organelles and antimicrobial compounds; and deposition of cell wall compounds to form papilla that aim to block microbes penetrating the cell. Surface recognition of effectors or elicitins such as INF1 can also lead to the hypersensitive response (HR)-like programmed cell death. (B) Pathogens secrete effector proteins into the plant cell to subvert immune signalling and enable feeding. These cytoplasmic effectors can be recognised, directly or indirectly, by specialised immune receptors known as nucleotide-binding, leucine-rich repeat proteins (NLRs). NLRs then usually directly or indirectly elicit HR – however, in some cases a HR is not seen, but this may be microscopic and thus not noticed by researchers.

1.2. Effector triggered immunity

However, adapted pathogens are capable of subverting PTI. To this end, many pathogens including *P. infestans*, secrete effector proteins across the EHM to block this initial layer of defence and enable nutrient acquisition (Jones and Dangl, 2006). The mode of host translocation remains unknown and has long been highly debated within the field of plant-microbe interactions (Wang et al., 2017a). Many oomycete effector proteins contain a RXLR motif which is required for uptake by the host cells, however, it is unclear if the function of this motif is for translocation from the EHMx across the EHM, or provides another function such as a signal for non-conventional protein secretion, as was recently reported at IS-MPMI 2019 (Boevink et al., 2019). Additionally, it was shown by another group using mass spectrometry that the RXLR motif of the *P. infestans* effector AVR3a is cleaved before secretion, providing evidence this motif is not for host translocation but probably for secretion form the pathogen. Interestingly, the virulence proteins of the malaria parasite *Plasmodium falciparum* require a similar RXLXE/D/Q motif for host targeting, which when introduced to a *P. infestans* effector, enables translocation (Grouffaud et al., 2008; Hiller et al., 2004; Marti et al., 2004). However, while translocation of effector proteins can be successful for suppressing PTI, as is the case with Avr3a which suppresses cell death triggered by the apoplastic oomycete elicitor INF1 (Bos et al., 2010), plants have evolved intracellular receptors to sense effectors. These sensors, coded as resistance (R-) genes are mainly nucleotide-binding, leucine-rich repeat proteins (NLRs) - immune receptors which directly or indirectly detect pathogen effector proteins and trigger an immune response known as Effector Triggered Immunity (ETI). One such NLR, R3a, has evolved to recognise *P. infestans* RXLR effector Avr3a and triggers cell death (Bos et al., 2010). ETI usually culminates in a plant-specific form of programmed cell death, known as the Hypersensitive Response (HR) at the site of effector recognition. HR is the attempt by plant cells to limit the spread of the pathogen to non-infected neighbour cells (Jones and Dangl, 2006).

1.3. Types of NLRs

NLR's broadly follow a similar structure with one of three N-terminal domains; an Nucleotide Binding (NB) domain shared with APAF-1, various R-proteins and CED-4 (ARC) domains; and Leucine Rich Repeat (LRR) domains. There is also sometimes an N or C terminal extension. NLRs are subdivided into three different classes based on the structure of their N-terminal domain. These are coiled-coil (CC) NLRs (CNLs), Toll/Interleukin 1 Receptor (TIR) NLRs, or RPW8-like coiled NLRs (RNLs). The N-terminal domains are reportedly for oligomerisation and cell death signalling (Bentham et al., 2018). In fact, overexpression of some CC or RPW8-like CC domains alone results in an HR. This 'autoactivity' of the CC domain is highly dependent on where the truncation is made in the fourth alpha helix/linker region between the CC and nucleotide binding domain, and the HR phenotype can be lost altogether by removal of just one too many amino acids (Casey et al., 2016; Cesari et al., 2016; Maekawa et al., 2011; Wróblewski et al., 2018).

The NB-ARC domains determine the 'OFF/ON' state of the NLR. NLRs are believed to be in their 'ON' or 'Active' state when they have bound ATP in the nucleotide binding pocket of the NB, and 'Off' or 'Inactive' state when they have bound ADP (Takken et al., 2006; Takken and Goverse, 2012; Wang et al., 2019b). The p-loop motif of the NB domain is essential for ATP binding and hydrolysis, and mutations of this motif render many NLRs inactive (Takken et al., 2006). Following the NB domain is the ARC1 and ARC2 domains that contribute to activation and signal regulation. ARC2 contains the MHD motif which is essential in determining many NLR's activated state (Van Ooijen et al., 2008). In fact one or two amino acid changes in this motif is often sufficient to render an NLR 'autoactive' – that is, 'always on', triggering HR in the absence of an effector. Normally NLRs are thought to activate when a ligand is perceived. This perception usually occurs via the C-terminal, LRR domain. These domains are usually involved in protein-protein binding and ligand perception, but can also mediate regulation of the other domains (Cesari, 2017; Padmanabhan et al., 2009).

1.4. Models for NLR mode of action

How effector proteins elicit an immune response during recognition by NLRs is largely unclear, however a number of models have been suggested which fit well with

observations in the literature. Some effector proteins are thought to be directly recognised by a cognate NLR (Direct recognition). However, this gene-for-gene strategy requires the plant to maintain a large repertoire of NLRs recognising one effector each and for these NLRs to co-evolve with their cognate to ensure they have successful recognition of that effector. It could be for this reason that very few examples of this strategy have been found (Jones et al., 2016). More commonly, a smaller number of NLRs guard plant proteins, termed 'guardees'. In this model, the NLR 'guard' recognises the state of its guardee (effector target) and triggers an immune response if it is modified. The guard can recognise the natural state of the guardee, or in theory, the state modified by the pathogen. In the presence of a guarding NLR, it is favourable for the guardee to evolve to better bind to the effector protein, yet it might lose its native function in this process. Occasionally the guardee is duplicated and modified such that it does not carry out its cellular function, but instead becomes neofunctionalised into a specialized 'decoy' for the effector. This decoy is recognised by the pathogen effector and the guard NLR detects the effector-manipulation of the decoy (The Decoy Model) (Jones et al., 2016). In recent years it has been discovered that occasionally plants have incorporated these decoys as a new domain into the NLR which guards them – forming a so-called 'integrated decoy' (Cesari et al., 2014; Le Roux et al., 2015; Sarris et al., 2015).

An emerging model of NLR action is that not all NLRs sense the effector ('Sensor NLRs'). Some NLRs are thought to recognise the activated state of a sensor and pass this signal to downstream ETI elicitors. These NLRs are termed 'Helpers' (Jones et al., 2016). Sensor-Helper pairs can function in two ways: positive regulation and negative regulation. Positive regulation implies that upon pathogen perception, the sensor NLR activates the helper NLR. Negative regulation implies the helper NLR is already activated, but the sensor inhibits it from triggering cell death until a pathogen is perceived (Wu et al., 2017).

What happens after effector detection by sensor NLRs has been a topic of great discovery recently. For years, TIR NLR (TNL) sensors were known to signal through a lipase-like EDS1/SAG101/PAD4 protein (ENHANCED DISEASE SUSCEPTIBILITY 1/SENESCENCE ASSOCIATED GENE101/PHYTOALEXIN DEFICIENT4) (Lapin et al., 2019). Recently it was reported that NRG1 and ADR1 are RNL helpers required

for multiple TNL sensors and function downstream of EDS1/SAG101/PAD4 for HR and resistance (Castel et al., 2019a; Qi et al., 2018). It is unclear to date exactly how EDS1/SAG101/PAD4 transmit the HR/immune signal from the upstream TNLs to the downstream helpers NRG1 and ADR1.

A network of NLRs has been discovered in the solanaceous plant family, which includes many economically important crops, such as potato, tomato, aubergine, pepper and tobacco. In the wild relative of tobacco, *N. benthamiana*, the NRC (NB-LRR protein required for HR-associated cell death) family of CNLs has been investigated functionally. Silencing NRC members revealed that a large, and incomplete repertoire of sensor NLRs require them for immune signalling, meaning they act as a signalling hub (
Figure 1.3) (Brendolise et al., 2017; Wu et al., 2017). These results have since been reproduced with CRISPR/Cas9 induced mutations of NRC2, NRC4 and NRC4 in *N. benthamiana* and NRC4 knockout in tomato (Adachi et al., 2019; Wu et al., 2020). In general, each NRC helper is functionally redundant for some of sensors, meaning silencing of one NRC is often not sufficient to lose immune signalling from the upstream sensor.

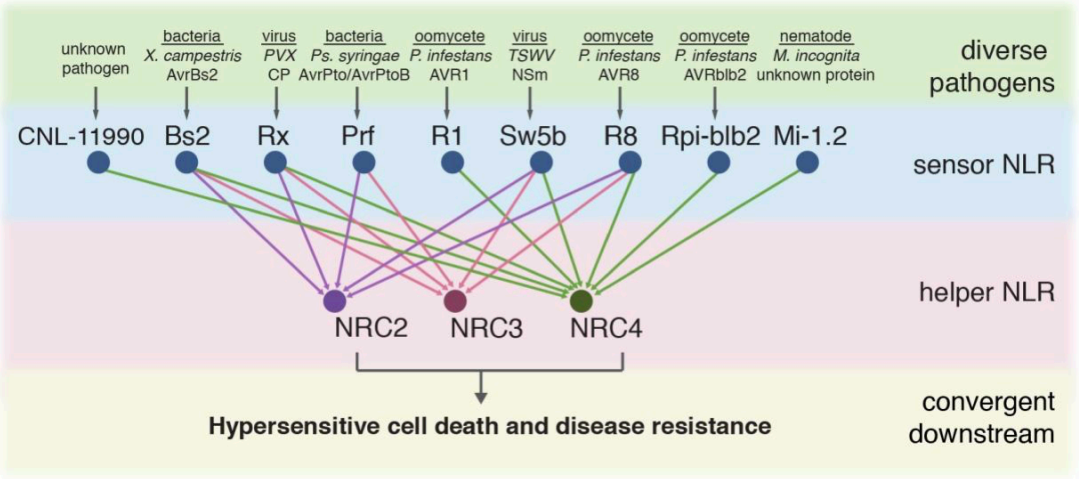


Figure 1.4: [Fig. S15 An NRC-dependent NLR immune signalling network confers resistance to diverse pathogens.
A schematic view of the identified NRC-dependent NLR immune signalling network. Several NLR that confer resistance to diverse pathogens, including virus, bacteria, oomycete, nematodes and insects converge on the three NRC proteins. These three NRC proteins are functionally redundant but also display specificity towards different some of the NLR. Similar to other plant NLR, the downstream signalling remains largely unknown.**]** **NOTE:** Figure and Figure legend copied from Wu et al., (2016) BioRxiv, (Fig S15) under CC-BY 4.0: http://creativecommons.org/licenses/by/4.0/

While a good deal is known about effector recognition and HR signal transduction, very little is known about the actual execution of cell death. Recently however, the first full structure of a plant NLR was published in two back-to-back papers by the same research group (Wang et al., 2019a, 2019b). These ground-breaking papers suggested that the *Arabidopsis* singleton NLR, ZAR1, binds ATP (or dATP preferentially in their assays) upon activation, as previously thought for NLRs. When this happens, the NLR changes conformation and in particular re-arranges the α-helices in its CC domain, such that the first alpha helix, α1, protrudes outwards. This relies on a region in the second half of the CC domain to switch secondary structure. Specifically, α4 changes length and position. The structural conformation change is coupled to an oligomerisation of the NLR into a pentamer structure, similar to the mammalian inflammasome. The pentamer has been named the “resistosome” and is believed to then associate with membrane(s) and perhaps elicit cell death by forming pores in the membrane. As ZAR1 is a CNL and therefore related to the NRCs, previously we were able to use Phyre2 homology modelling to generate a structural

model of NRC4 using ZAR1 in its inactive monomeric state, active monomeric state and active pentameric state (Figure 1.5) (Adachi et al., 2019).

We discovered that α1 overlaps a motif found in 20% of plant CNLs. This motif, nicknamed the "MADA motif" due to its consensus beginning M-A-D-A, is required for cell death and resistance. Generally it has been functionally conserved in the helper CNLs but not in the sensor CNLs (Adachi et al., 2019). This motif may be the elicitor of cell death for many AVR-R pairs. Our model for how NRC4 elicits an HR, is based on the model for ZAR1. Inactive NRC4 (in monomeric or some other low order complex) gets activated by an activated sensor NLR by stimulating the exchange of ADP for ATP (Figure 1.5A-B). When this happens, the first alpha helix is believed to 'flip out', becoming exposed (Figure 1.5B). NRC4 is thought to oligomerise into a pentameric resistosome, and this may insert into membrane(s) leading to cell death by forming pores which either directly lyse the cells or allow flux of ions or molecules and stimulate cell death (Figure 1.5C) (Adachi et al., 2019).

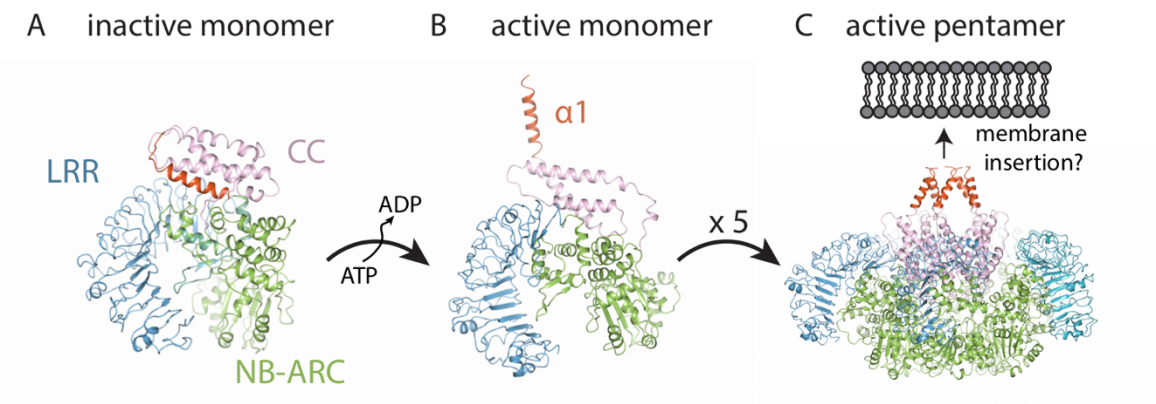


Figure 1.5: α1 helix of NRC4 is predicted to protrude out upon activation and form a pentameric resistosome.
(A) Inactive monomer, (B) active monomer and (C) active pentamer homology modelled by Phyre2. The α1 helix is highlighted in red, the rest of the CC domain is in pink, NB-ARC domains are in green and the LRR is in blue. (C) was published in Adachi et al., 2019 but this high-resolution image was given to me by Dr Abbas Maqbool who also produced (A) and (B) – unpublished.

1.5. Aims & summary of chapters

The primary aim of this thesis is to understand the mechanism of NRC4-mediated immunity to *P. infestans*, in particular that mediated by the sensor NLR Rpi-blb2. To investigate the timing of Rpi-blb2/NRC4-mediated immunity and the precise subcellular localisation where immune recognition and the immune response occurs, I performed a series of cell biology experiments, cell death assays or *P. infestans* infection assays. This revealed the spatio-temporal dynamics of this sensor-helper pair. Resistance probably occurs in the haustoria-forming stages of infection, where Rpi-blb2/NRC4 detect AVRblb2 most likely at an EHM microdomain (**Chapter 3**). In **Chapter 4** I examined the roles of NRC4 domains in mediating HR and disease resistance. I found that an extended c-terminal 'tail' is required for EHM localisation and disease resistance but not sufficient. The N-terminal CC domain meanwhile, is required and alone forms bright puncta, many of which associate with the EHM, but the CC domain is not sufficient for the same degree of focal accumulation and EHM labelling as the full length. Instead, this relies on fine tuning and regulation by the other domains of the NLR. I next investigated the involvement of the N-terminal MADA motif in NRC4-mediated resistance. This region does not determine the EHM focal accumulation, but likely executes NRC4's HR-related function there. In other words, the MADA motif may be forming pores in the EHM leading cell death and resistance to *P. infestans.* This indicates that Rpi-blb2/NRC4 may recognise AVRblb2 at the EHM, where NRC4 forms resistosomes which execute their cell death function, leading to resistance. I end **Chapter 4** by providing evidence that when NRC4 triggers HR, this is not sufficient for resistance to *P. infestans*. EHM localisation with a HR-functional NRC4 variant, NRC4 "autoactive" mutant, was necessary for disease resistance, indicating, execution of cell-death at the right place at the right time, is essential to provide full disease resistance mediated by NRC4. Finally, I screened candidate interactors of NRC4 identified by mass spectrometry to find regulators of NRC4 immunity and explore the mechanism by which NRC4 localises to the EHM. I conclude that NRC4 probably accumulates at the EHM via an endomembrane transport pathway however its identity remains obscure (**Chapter 5**).

2. Materials & Methods

2.1. Summary

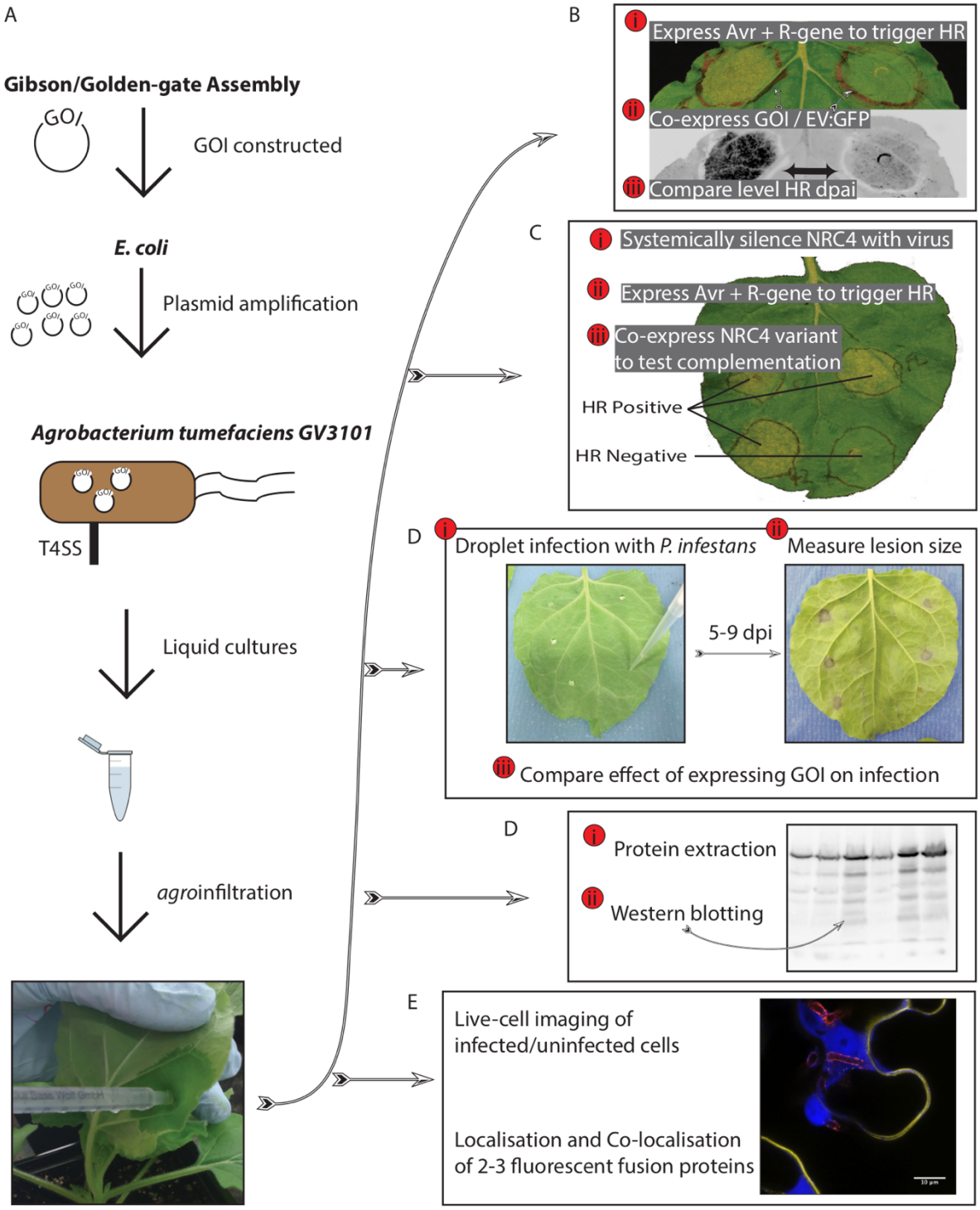


Figure 2.1: Summary of methods. GOI = gene of interest.

2.2. Cloning

2.2.1. Molecular cloning techniques

Molecular cloning was carried out as described previously (Dagdas et al., 2016). Briefly, plasmids were constructed with Gibson Assembly using the primers in Table 6 (end of chapter), transformed into DH5α chemically competent *E. coli* cells by heat shock. This involved firstly determining the melting temperatures of the primers using NEB Tm calculator (http://tmcalculator.neb.com/). The lower Tm of the primer pair was usually chosen as the annealing temperature, but if there was a problem with specificity, this was raised higher in subsequent attempts. The final annealing temperature used is recorded in Table 6. High-fidelity PCR was carried out with Phusion polymerase (pPCR). 50µl reactions were made up of 10 µl HF buffer (10x) [ThermoFisher], 1 µl Forward primer (100 pmol/µl), 1µl Reverse primer (100pmol/ul), 1 µl template DNA (1ng/µl plasmid details in Table 6), 0.5 µl Phusion polymerase (2U/µl) [ThermoFisher], 1 µl dNTPs (40mM) [Promega]. The size of the PCR product was predicted and the extension time was rounded up to the nearest 15 s per 1 kb product. 10 µl PCR products was mixed with 2 µl of TriTrack DNA loading dye (6x) [ThermoFisher]. This was loaded into 1% Agarose gels made with 1x TBE and 0.5 µl SyberSafe stain per 40 ml gel. Electrophoresis was carried out in 1x TBE at 100V for 40 m. Gels were imaged using a Syngene blue light transillumminator. Those PCR products that were correctly amplified were purified with Promega PCR purification kits. Next Gibson assembly was carried out with 5 µl home-made Gibson assembly mix (2µL of 5x ISO Buffer, 4nL 10U/µL T5 exonuclease [NEB], 0.1µL of 2 U/µL Phusion polymerase [ThermoFisher], 0.6 µL of 40U/µL Taq DNA ligase [NEB] and 0.6µL of nuclease free water)), 50 ng PK7 vectors linearised by *Eco*RV [*Eco*32I ThermoFisher Fast Digest], 2:1 molar ratio of insert(s) to vector. 5x isothermal (ISO) buffer is 3mL of 1M Tris-HCl pH 7.5150 µl, 2M $MgCl_2$, 240µL of 100mM dNTPs, 300 µl of 1M DTT, 1.5g PEG-8000, 300 µl of 100mM NAD – nuclease free water to 6mL. The reaction was topped up to 10 µl with nuclease free water and incubated at 50˚C for 1 h. The whole reaction was added to 10 µl 1x KCM, 30 µl dH2O and carefully added to 50 µl DH5α. This tube was mixed by flicking gently once. The cells were incubated on ice for 5-30 min and then heat shocked by transferring to a 42˚C heat block for 45 s. The tubes were briefly transferred to ice and 400 µl LB broth added to recover the cells. The cells were incubated at 37˚C on a shaking heat block at 400rpm for 1-1.5 h.

100 µl was plated on half a LB agar plate supplemented 100 µg/µl Spectinomycin. The rest of the cells were concentrated by centrifugation at 1500 *g* for 3 min. All but 50µl supernatant was discarded and the rest used to resuspend the cells carefully before plating on the rest of the plate. Plates were incubated upside down for 18 h before inspection. Colonies were screened by touching a sterile toothpick to them and inoculating 10 µl colony PCR (cPCR) master mix: 2 µl green buffer (5x) [Promega], 0.2 µl Forward primer (GA 35S F), 0.2 µl Reverse primer (PK7 Term Rev2), 0.2 µl dNTPs (40mM) [Promega], 0.04 GoTaq [Promega], 7.36 µl dH2O. All PCR product was loaded on gel and electrophoresed as before and analysed with the transilluminator. Colonies determined to be positive were grown at 37˚C shaking at 200rpm in culture tubes of 4 ml LB broth supplemented with 100 µg/ml Spectinomycin. Cultures were extracted by Promega Wizard Miniprep columns before being electroporated into *Agrobacterium tumefaciens* GV3101 electrocompetent cells. Electroporation was carried out by adding 1 µl plasmid to 50 µl electrocompetent cells and transferring this to a electorcuvette (2 mm gap) and then electroporated with a BioRad electroporator. LB agar supplemented with Gentamycin (25 µg/ml) and Spectinomycin (100 µg/ml) was used to grow cultures carrying pk7WGF2/pH7WGR2, while Gentamycin and Kanamycin (25 µg/ml) was used to select for cultures carrying TRV/pICH86966/pRNAiGG plasmids. Sequencing was provided by Eurofins. I domesticated the Gibson Assembly vectors further by introducing a *ccdB* selection, which is excised by *Eco*RV during vector linearisation. Figure 2.2 shows how these vectors were generated. The purpose of the *ccdB* was to kill DH5α chemically competent *E. coli* transformed by non-linearised plasmids. Golden gate assembly was carried out in the same ways as Gibson assembly with the following exceptions: the reaction was 100 ng/µl vector, 12-33 ng insert, 0.5 µl *Bsa*I [ThermoFisher *Eco*31I], 0.5 µl T4 DNA ligase [ThermoFisher] 1 µl ligase buffer (10x) [ThermoFisher], topped up to 10 µl with nuclease free water; incubated at 37˚C for 2 h; bacteria were grown with Kanamycin (25 µg/ml) instead of Spectinomycin for selection of plasmid and pRNAiGG cultures were supplemented with Chloroamphenicol (5µg/ml) to retain the intron.

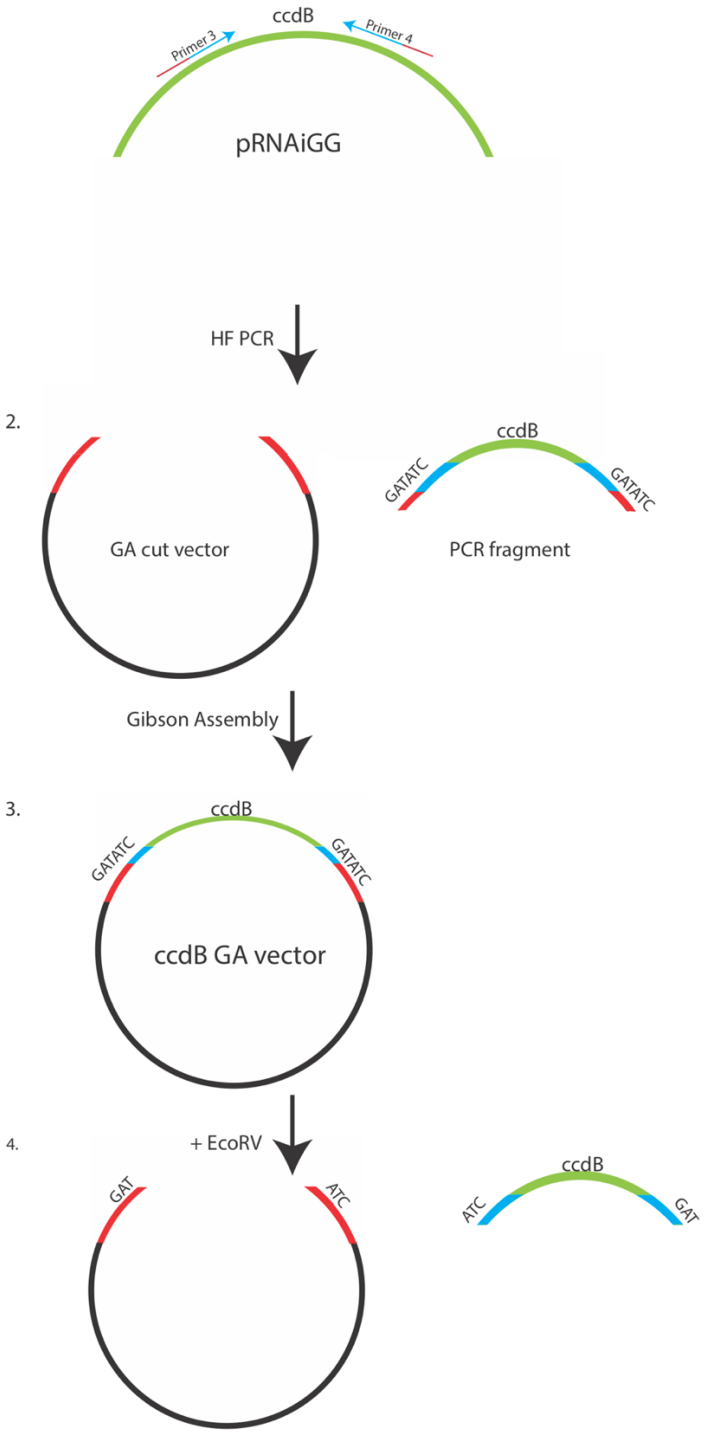


Figure 2.2: *ccdB* Gibson Assembly vector generation for fluorescent tagging. 1. I amplified the *ccdB* from pRNAiGG vector using "Primer 3" and "Primer 4". *CTGGATCTGGAGAATTTGATA*TCGGAGTGAGACCAATTCTCGACTAA (Forward) and *TAGCATGGCCGCGGGATA*TCTCGTTGAGACCGTCGACCTGT (Reverse) for N-terminal fusions respectively and *CAGGCGGCCGCACTAGTGATA*TCGGAGTGAGACCAATTCTCGACTAA (Forward) and *GCAGATCCAGCAGATCCGATA*TCTCGTTGAGACCGTCGACCTGT (Reverse) for C-terminal fusions respectively, where Red is destination vector overhangs, Blue is *Eco*RV cutting site and Green is *ccdB* fragment primers 2. PK7WGF2/PK7GWF2

had previously been domesticated with a long flexible linker and several new vectors had been produced by changing the fluorescent tag. These vectors were linearised with *Eco*RV. 3. The *ccdB* fragment was inserted by Gibson Assembly (GA). This led to a GA compatible vector that with new *Eco*RV restriction sites either side of the *ccdB*, and the vector was amplified in DB3.1 *ccdA* containing cells (*ccdB* resistant). 4. Digestion with *Eco*RV led to a linearised plasmid for inserting constructs of interest, or death of DH5α cells by the *ccdB*.

2.2.2. Fluorescent-tagging

To increase efficiency of cloning fluorescently tagged proteins, I introduced *ccdB* selection into our Gibson Assembly vectors (Figure 2.2). This was achieved by amplifying the *ccdB* selection cassette from pRNAi-GG and using Gibson assembly to insert into the *Eco*RV linearised plasmids, either N- or C-terminally to the fluorescent marker. In the PCR fragment of the *ccdB* cassette I included an *Eco*RV cutting site (GATATC), so that when the vector was re-linearised it would remove the *ccdB* or a *ccdB*-susceptible competent *E. coli* strain such as DH5α.

2.3. Growth, maintenance and experimental conditions with plants and Phytophthora infestans

2.3.1. Growth of plants

Nicotiana benthamiana plants were grown on a 3:1 mixture of soil and vermiculite at 25°C for 4 weeks before experimentation. Lighting was under 16 h days, 8 h night conditions.

2.3.2. Transient gene expression in Nicotiana benthamiana

Agrobacterium-mediated transient gene expression of epidermal leaf tissue by *agro*infiltration, also known as agroexpression, was carried out as previously described (Bozkurt et al., 2011). Briefly, cultures of *A. tumefaciens* GV3101 strain with genes for transient expression within the transfer DNA (T-DNA) were prepared for *agro*infiltration as follows. Cultures were suspended in 1.5 ml autoclaved dH_2O, spun at 1500 *g* for 5 min in a microcentrifuge, before removal of supernatant and repetition of this step. Upon completion of the second wash, the cell pellets were resuspended in 1 ml of *agro*infiltration buffer (10mM MES hydrate, 10mM $MgCl_2$, pH 5.7). Depending on the experiment, the OD_{600} of cell solutions were adjusted to the desired levels and

mixed with the appropriate solutions for co-expression. OD_{600} for each experiment are shown in Table 6. For experiments where plants were infected with *P. infestans*, after *agro*infiltration, leaves were allowed to incubate under standard growth conditions for 3-24 h prior to infection with *P. infestans.*

2.3.3. Cell Death Assays

Cell death assays were conducted by co-expression a cell death elicitor with either a a treatment of interest or a control (details in figure legends) on opposite sides of the leaf in ~20 mm diameter circles. Cell-death elicitors used were an AVRblb2 weak allele (in order to prevent HR saturation) (PITG_4085 from Dr Khaoula Belhaj, unpublished) in Rpi-blb2 transgenics; an autoactive NLR, or culture filtrate. At 3-4 dpai, lesions were imaged by white light photography and with a blue light from a transilluminator (λ*=420nm*), 1 s exposure. HR was quantified by comparing patches expressing the treatment vs control as I described previously (Dagvadorj et al., 2017), and the average grey value (pixel intensity) per patch was plotted opposite the control. Gray values were collected in ImageJ/FIJI by drawing an circular region of interest in the HR region and measuring. For HR assays where blue light imaging was not carried out, a HR index was used to 'score' the category of HR intensity, as per Wu *et al*., (2017) (Figure 2.3).

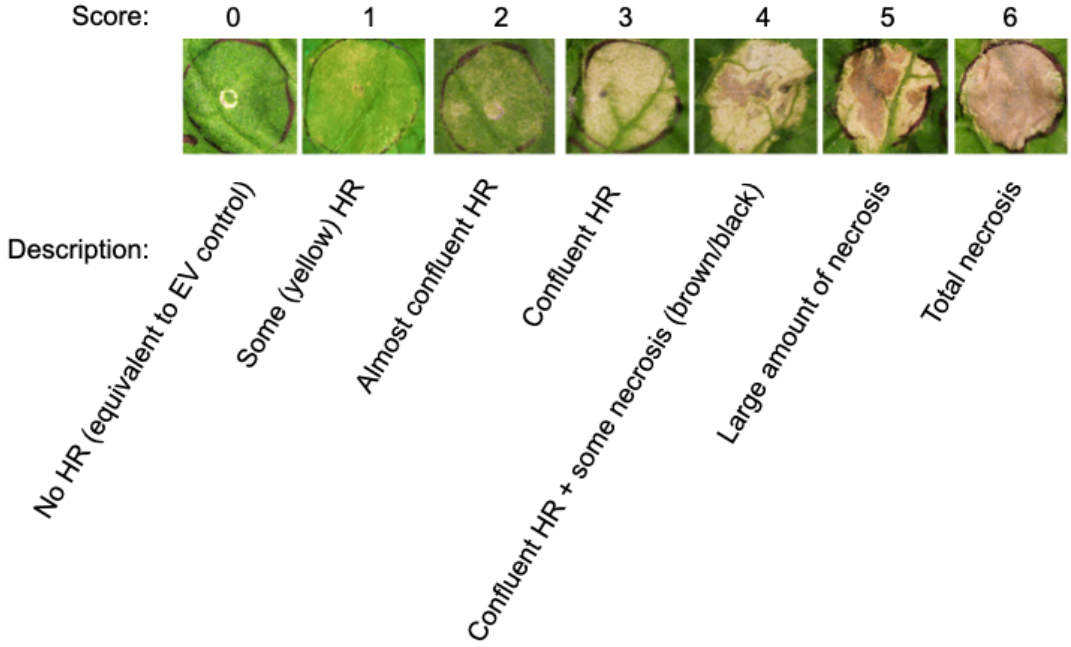


Figure 2.3: HR index used for some experiments.

2.3.4. Phytophthora infestans maintenance and infection of plant leaves

P. infestans 88069 isolate was grown on rye sucrose agar (RSA) media in the dark at 18°C for 8-21 days as previously described and described again below (Song et al., 2009). Experiments assessing the susceptibility of leaf tissue under certain gene expression conditions, i.e. infection assays, were carried out on the abaxial (underside) of detached leaves as described previously and described hereafter (Saunders et al., 2012; Song et al., 2009). Leaves were detached and placed on two layers of wet blue roll tissue paper in a 500 cm^2 Corning cell culture dish. These were parafilmed and placed at 18˚C in long-day conditions until the specified timepoint on each experiment. Infection of leaf material for the purpose of microscopy was carried out on the adaxial (topside) of leaves intact to the body of the plant, at 18°C, with a propagator cover on the tray to build up humidity. For all experiments, approximately 700 motile zoospores were used to inoculate the leaves, in cold water droplets of 10µl per infection spots. RSA was made as follows for 5 L: 300 g rye grains were surface sterilised in 10% chlorite solution for 4 min on an orbital shaker 100 rpm (15 ml of 10% chlorite in 600 ml = 0.25% final concentration). Grain was rinsed in dH2O and then washed three times on an orbital shaker in dH2O for 4 min each time. Once no chlorite could be smelled, the grain was put into large flat cell culture dishes in a single layer with approximately half the surface covered in water, i.e. the grain was not completely submerged. These dishes were then covered with aluminium foil and holes created for air exchange. The grain was germinated at 25˚C for 24 h. If ~50% or more of the grain had visible shoots, the next steps were conducted. Grain was homogenised with a blender in batches, such that every rye grain was at least halved but none were completely macerated – the grain should not fit through a flour sieve. The mash was then added to a beaker and topped off with 3 L dH2O, cooked at 55˚C for 3 h covered. The mixture was then stirred and sieved through a flour sieve. The filtrate was split in five and added to bottles with 20 g sucrose and 15 g agar before topping off to 1 L and autoclaving under standard media conditions. The autoclaved media was mixed by inversion and poured as soon as was comfortable to do so (i.e. it was never allowed to solidify or incubated). RSA plates were cultured by passing a two chunks of a fully grown plate onto a fresh plate and after 2 weeks of growth in the dark at 18˚C these plates were ready for use.

2.3.5. Virus Induced Gene Silencing (VIGS)

Agrobacterium cultures carrying Tobacco Rattle Virus (TRV) 1 (OD_{600} = 0.4) and gene specific TRV2 (OD_{600} = 0.2) were prepared as before, but *agro*infiltration buffer with 100 μM acetosyringone and cultures were left in the dark for 2 h prior to infiltration, to stimulate virulence. Seedlings approximately 10 days old were infiltrated. Both cotyledons and any true leaves that had emerged were infiltrated. Plants were left to grow under normal conditions until experiments could be performed 4 weeks later. New TRV2 constructs were cloned into a new vector which I domesticated to be compatible with golden gate assembly, TRV2gg. The generation of this vector is discussed below in Figure 2.4.

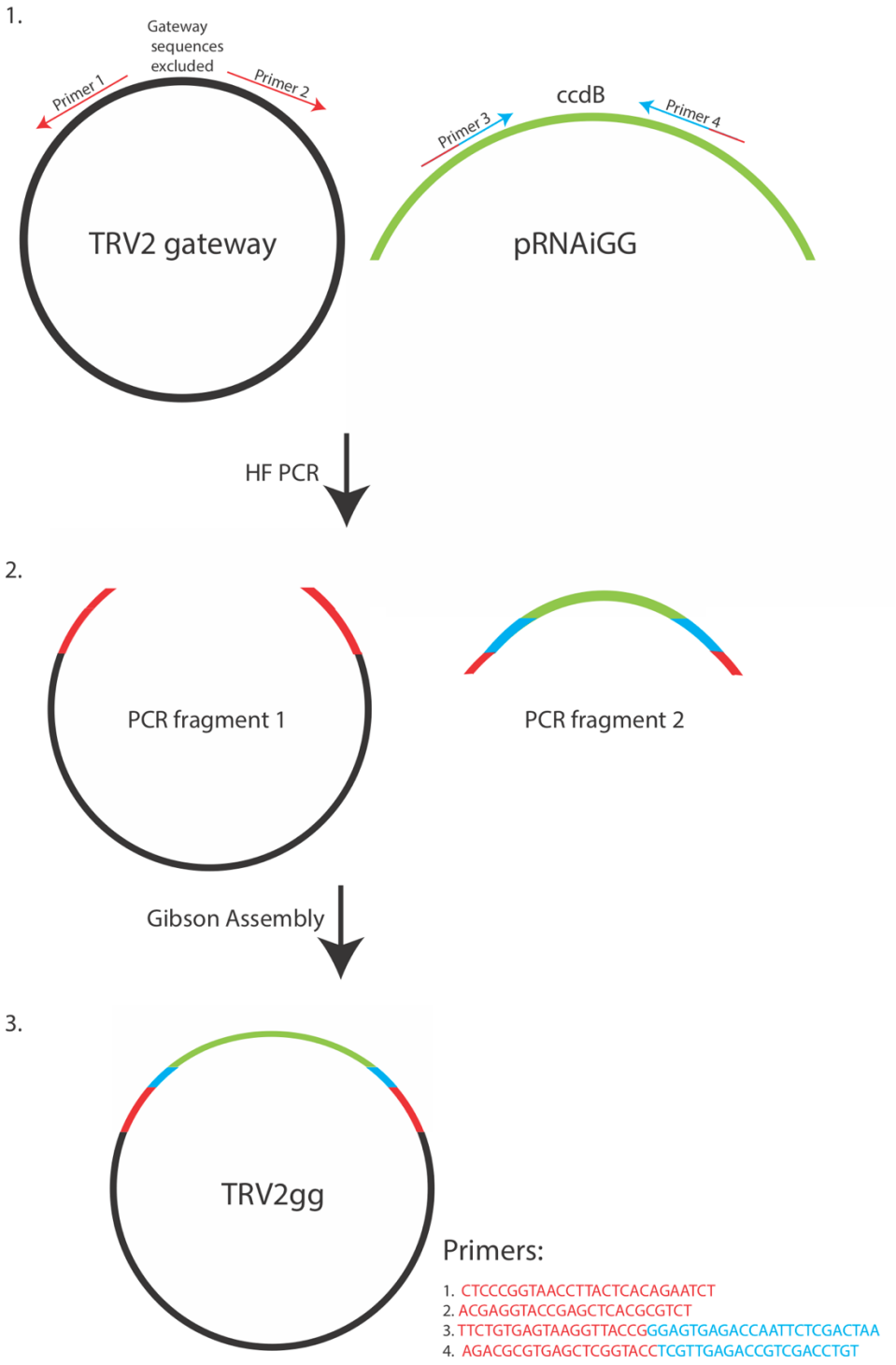


Figure 2.4: Generation of pTRV2gg vector for compatibility with PCR fragments produced for pRNAiGG vector.
pTRV2-GATEWAY (YL279) vector was linearised (PCR fragment 1) and gateway 'att' sites removed by high fidelity (HF) inverse PCR with primers 1 & 2, and the *ccdB* and golden-gate compatibility sites were amplified (PCR fragment 2) by primers 3 & 4 containing overhangs to fragment 1 for Gibson Assembly that circularised the plasmid. This was grown in *ccdB*-resistant cells (db3.1 competent E. coli) and plasmids extracted by miniprep kit for golden-gate and transformation into *ccdB*-susceptible DH5α competent *E. coli*.

2.3.6. Gene silencing by RNAi

Hairpin RNAi constructs were infiltrated in patches or half leaves, depending on the experiment, opposite hpGUS control. One day after infiltration leaves were ready to be infected as usual. For the Potato Virus X (PVX) infection assay, PVX was inoculated in a second infiltration in the same patches, to mimic the timing of *P. infestans* infections.

2.3.7. Suppression of Rpi-blb2 resistance

Rpi-blb2 transgenics were allowed to *agro*express for 24 h before infection with *P. infestans.* A spreading necrotic lesion was considered infected and that Rpi-blb2 resistance had been broken. Lesion sizes were also measured with the open source image analysis program ImageJ/FIJI in some experiments where there may have been a subtle difference between two constructs, but mostly a binary measure was sufficient to determine resistance was broken. In this case, the number of successful infections was counted and reported as a fraction of total infection sites.

2.3.8. Complementation of Rpi-blb2/NRC4-mediated resistance or HR

Either *nrc4a/b* mutant plants, or plants silenced by VIGS for *NRC4*, *NRC2/3*, *NRC2/3/4* and controls were agro-infiltrated 24 h before infection with *P. infestans*. For HR assays, the gene of interest was co-expressed with AVRblb2 to trigger HR. Lesion sizes were also measured with ImageJ in some resistance experiments where there may have been a subtle difference between two constructs, but mostly a binary measure was sufficient to determine resistance was broken. In this case, the number of successful infections was counted as a fraction of total infection sites.

2.3.9. Generation of transgenic 35S::NRC4-GFP plants

Five week old WT *N. benthamiana* were infiltrated with *Agrobacterium* expressing NRC4-GFP supplemented with acetosyringone. At 3 days post agroinfiltration (dpai) leaves were collected and cut into 1-2 cm^2 squares with a sterile scalpel. The largest veins were discarded. Leaf patches were surface sterilised in 70% EtOH for 30 s

followed by 1.5% sodium hypochlorite solution with 5 drops of Tween20 surfactant per 500 mL solution. After this, the leaf patches were washed in sterile water 4 times. Each leaf square was placed adaxial side up in selective media (Table 1) and gently pressed to increase surface contact with the media. These plates were sealed with micropore tape and incubated in a plant transgenesis room at 22˚C. Every two weeks patches were transferred to fresh plates. After 1 to 2 months shoots formed and were transferred to rooting media. After 4 weeks roots had formed and plantlets were transferred to soil in a high humidity chamber. Each day a little humidity was released until the T_0 plantlets had adjusted to the standard growth chamber conditions. Plants were screened using confocal microscopy after a few weeks and those with GFP fluorescence were kept for seed. T_1 seed was collected separately from their T_0 parent. T_1 lines with the best fluorescence were kept. T_2 seed was collected from individual parent plants separately. A T_2 line was selected for experiments as being the best expression (tNRC4-GFP #1.3).

Table 1: Composition of shooting and rooting media

Selection medium	**Rooting medium**
1x Murashige and Skoog medium with Gamborg's B5 vitamins	0.5x Murashige and Skoog basal salt
1% Sucrose	0.5% Sucrose
0.59 g/L MES	0.25% Gelrite
0.4% Agargel [Sigma]	0.05 mg/L NAA
2 mg/L BAP	500 mg/L Cefotaxime or 320 mg/L Timentin
0.05 mg/L NAA	100 mg/L Kanamycin
500 mg/L Cefotaxime or 320 mg/L Timentin	pH 5.8
100 mg/L Kanamycin	
pH 5.	

2.4. Protein-based and biochemical experiments

2.4.1. Crude protein extraction and western blotting

Protein extraction, SDS-PAGE and western blotting was conducted as previously described (Dagdas et al., 2016). Whole or half-leaves were *Agro*-Infiltrated. Plants were incubated for 3 days at standard growth conditions to allow protein expression. Leaves were detached and 6 leaf disks were cut using cork borer tool size 4, and snap-frozen in 1.5 ml Eppendorf tubes in liquid nitrogen. Disks were stored at -80˚C until protein extraction. *SDS-PAGE gel preparation:* Bio-Rad gel moulds were assembled and 1 mL autoclaved dH_2O added to determine if there were any leaks. Water was removed by carefully tipping and air drying. The separating gel of desired percentage (depending on experiment) was prepared using the recipe in Table 2.

The separating gel was carefully pipetted into the mould, leaving 2-2.5cm space for the stacking gel. Isopropanol (0.5 ml) was added to remove any bubbles and the gel left to polymerise for an hour and before removing the isopropanol by carefully pouring and air drying. For gradient gels, 2.2 ml of 4% gel was aspirated into a 5 ml serological pipette followed by 2.2 ml of 16% gel. An air bubble was drawn up through the two gels and the mixture quickly pipetted into the glass mould. The stacking gel was then prepared using the following recipe for two gels: 1.25 ml 0.5 M Tris pH 6.8, 0.375 ml 40% acrylamide, 3.3 ml glass distilled water, 0.05 ml 10% SDS, 0.05 ml 10% APS, 0.005 ml TEMED. The stacking gel was pipetted up to the top of the glass plates and the combs were added, taking care not to allow any bubbles to be trapped in the wells/under the combs. This was allowed to solidify, and after the proteins were extracted the gel was assembled into the gel tank with 1x SDS running buffer (Table 4) **.**

Protein extraction: Tubes were kept in liquid nitrogen and not allowed to defrost throughout the process, until the step where extraction buffer was added. Leaf disks were ground to a fine powder evenly with a grinding tool and 120 µl extraction buffer added (30 µl Laemmeli sample buffer 4x [Bio-Rad], 24 µl DTT 1 M, 66 µl dH_2O). Tubes were vigorously vortexed for 90 seconds, ensuring the buffer had reached all the tissue.

Tubes were centrifuged for the minimum amount of time possible in a microcentrifuge to bring tissue down from the sides, followed by denaturation of extracts at 80˚C in preparation for SDS-PAGE. The tubes were centrifuged at 16,000 *g* for 5-10 minutes to pellet the tissue and allow the crude protein extract to remain in the supernatant. This supernatant was carefully removed to new tubes, avoiding leaf material and frozen at -20˚C or left on ice until gel loading. The volume of protein extract to load depended on the experiment – unless otherwise stated in the figure legend, 19 µl was loaded from a 20µl master mix in order to account for pipetting error and evaporation. PageRuler Prestained Protein Ladder (4 µl) [Thermo Fisher] was added to one lane. Protein samples are carefully loaded and run in Bio-Rad Mini-PROTEAN Tetra Vertical Electrophoresis Cell using Bio-Rad PowerPac basic at 150 V constant until the proteins entered the separating gel, at which point the gel was run at 180 V until the ladder was separated enough to resolve the proteins of interest. *Western blotting:* PVDF membranes were activated in methanol for 60 seconds before equilibrating in 1X semi-dry transfer buffer [Bio-Rad] with the gel and transfer stacks (two stacks of 6-ply Wypall X60). The Trans-Blot Turbo Transfer System [Bio-Rad] was assembled (transfer stack -> membrane -> gel -> transfer stack) and the transfer machine set at 1.3 A, 25 V for 13 minutes to ensure transfer of low expressed, high-molecular weight proteins. *Detection:* Membranes were blocked for 1 hour shaking in 3% BSA blocking solution (in TBS), to prevent the primary antibody binding non-specifically. Appropriate primary antibody (Table 3) was added to in antibody solution (3% BSA solution in TBS supplemented with 0.1% Tween) and incubated shaking at 4˚C overnight. Membranes were then washed with TBS (Table 4) supplemented with 1% Tween 5 times for 5 minutes per wash, before adding the appropriate secondary antibody (Table 3) for 90 minutes. Blots were then washed as before. Luminol was then added for detection by chemiluminescence [ThermoFisher], or 5-bromo-4-chloro-3-indolyl phosphate (BCIP) and nitroblue tetrazolium (NBT) for colourimetric detection [Bio-Rad], depending on the conjugation to the particular secondary antibody, Horseradish Peroxidase (HRP) or Alkaline Phosphatase (AP) respectively. Chemiluminescence was recorded by a cooled CCD camera and colour was visualised with a light camera. Some western blots (indicated in respective figure legends) were imaged with the quantitative western blot machine, LI-COR Odyseey Fx.

Table 2: Recipe for SDS-PAGE Separating Gels

Final % Acrylamide	**4% (for gradient)**	**7.5%**	**10%**	**12%**	**16% (for gradient**
Glass Distilled Water	1588 µl	2738 µl	2425 µl	2175 µl	838 µl
1.5M Tris pH 8.8	625 µl	1250 µl	1250 µl	1250 µl	625 µl
40% BIS-acrylamide	250 µl	938 µl	1250 µl	1500 µl	1000 µl
10% SDS	25 µl	50 µl	50 µl	50 µl	25 µl
10% APS	10 µl	20 µl	20 µl	20 µl	10 µl
TEMED	2.5 µl	5 µl	5 µl	5 µl	2.5 µl

Table 3: Antibodies used for western blotting

Primary	**Anti-**	**GFP**	**tagBFP***	**GFP**	**HA**	**Myc**	**RFP**	**FLAG**
	Made in	Rabbit	Rabbit	Rat	Rat	Rat	Mouse	Mouse
	-Clonal	Poly	Poly	Mono	Mono	Mono	Mono	Mono
	Produce r	Chromotek	evrogen	Chromotek	Chromotek	Chromotek	Chromotek	Sigma-Aldrich
	Product code	PABG1	AB233	3H9	7C9	9E1	6G6	F3165
	Lot number	70828032AB	23301300366	80626001AB	71708012AB	70117003AB	51020014AB	SLBT6752
	Storage	4	-20	4	4	4	4	-20
	Dilution	5 µl/15 ml	3µl/15 ml	7µl/15 ml	7 µl/15 ml	5 µl/15 ml	5 µl/15 ml	5 µl/15 ml
Secondary with HRP (Chemiluminescence detection)	**Anti-**	**Rabbit**		**Rat**			**Mouse**	
	Made in	Goat		Goat			Goat	
	-Clonal	Poly		Poly			Poly	
	Produce r	Sigma-Aldrich		Sigma-Aldrich			Sigma-Aldrich	
	Product code	A9169		A9037			SAB3700986	
	Lot #	023M4757		-			RI318289	
	Storage	-20		-20			4	
	Dilution	1 µl/10 ml		4 µl/10 ml			1µl/10 ml	
Secondary with AP (Colour detection)	**Anti-**	**Rabbit**		**Rat**				
	Made in	Goat		Goat				
	-Clonal	Poly		Poly				
	Produce r	Sigma-Aldrich		Sigma-Aldrich				
	Product code	SAB3700834		SAB3700542				
	Lot #	RI1756		RI29963				
	Storage	4		4				
	Dilution	1 µl/10 ml		1 µl/10 ml				
Secondary with fluorescence Note: use low fluorescence	**Anti-**			**Rat (DyLight 800 nm)**				
	Made in			Donkey				
	-Clonal			Poly				
	Produce r			ThermoFisher				
	Product code			SA5-10032				
	Lot #			TL2687931				
	Storage			4				
	Dilution			1 µl/10 ml or 1 µl/20 ml				

*this antibody is designed for tagRFP but can be used to detect tagBFP as there is no specific antibody for tagBFP. tagRFP is not the same other RFP which is mRFP1 or TD-Tomato. This antibody detects many native proteins and so was not very useful.

2.4.2. Co-immunoprecipitation

Constructs were expressed in 3-4 whole leaves of *N. benthamiana* by *agro*expression, for 3 days before being frozen. This was achieved by first cleaning and drying the leaves, followed by removing the main vasculature with a clean scalpel. Leaf samples were taken, weighed and trimmed to the weight of the smallest sample (2-4 g). These were stored in 50 ml centrifuge tubes were frozen immediately in liquid nitrogen and stored at -80˚C until needed. A clean mortar & pestle was then chilled with liquid nitrogen for each sample and leaves were carefully ground to a fine powder without defrosting (nitrogen was added to the mortar to keep the leaves frozen during this process). The powder was poured back into the centrifuge tubes and ice-cold extraction buffer (Table 4) twice the weight of the leaves was added. Samples were vortexed until the samples defrosted, became completely liquid-like (normally the samples will 'jump' up and down the tubes when vortexed) and came in contact with the extraction buffer (normally 3-6 minutes). Tubes were centrifuged at maximum speed for 20 min at 4 °C. The 5-6 ml of supernatant was then filtered into 15 ml centrifuge through Miracloth (Merck Millipore) to remove the cell debris, taking care not to pour any PVPP powder in the pellet through the cloth. Tubes were centrifuged at 3220 *g* for 20 min at 4˚C. Around 50 µL of extract was frozen in a 1.5 ml tube as 'input' and a maximum of 4.8 ml of extract was added to a 5 ml tube and kept on ice. GFP-trap agarose beads were resuspended by tapping the side of the vial several times and pipetting the resin up and down using a 1 ml pipette with a cut tip. A master mix of beads was prepared with 12 µL per sample in 200 µL immunoprecipitation (IP) buffer per sample (Table 4), with a little extra to account for pipetting error. The bead mixture inverted before 200 µL of this mix was added to each sample and they were rotated end-over-end at 4 °C for 90 minutes. Tubes were centrifuged at 800 *g* for 30 s at 4 °C. The supernatant was discarded without removing the last 50 µl (to avoid aspirating the beads) and 1 ml of fresh IP buffer was added before inverting the tube 40 times. This was wash and spin step was repeated a further two times. On the last wash, a 1 ml syringe with a pointed needle was used to remove all of the IP buffer, without removing any beads. The beads were eluted by addition of 20 µl elution buffer and the proteins were denatured at 80°C for 5 min. The samples were centrifuged at 16,000 *g* for 5 minutes at room temperature and transferred to a new tube with syringe and needle, without aspirating the beads. Next, 10 µl of these immunoprecipitates

were added to SDS-PAGE gels made as described in the previous section. Inputs were prepared by taking 11 µl protein extract (stored in freezer), 5 µl of 4x Laemmli buffer and 4 µl of 1M DTT before denaturation at 80˚C and spinning with the immunoprecipitates.

Table 4: Common Buffers

GTEN:	10% glycerol, 25 mM Tris pH 8.4, 1 mM EDTA, 150 mM NaCl
Extraction buffer:	GTEN, 2% w/v PVPP, 10 mM DTT, 0.5% 1X protease inhibitor, 0.1% Tween 20 or Igepal
Immunoprecipitation (IP) buffer:	GTEN, 0.1% Igepal
Elution buffer:	50% of 4x Laemmli buffer, 20% of 1M DTT and 30% of glass distilled water
10x TBE (Electrophoresis buffer, Tris-Borate-EDTA):	Tris base 108 g, Boric Acid 55 g, EDTA 9.3 g, pH 8.3, top up to 1 L with dH_2O
10x TBS (Washing buffer, Tris-Buffered Saline):	Tris base (24 g), NaCl 88 g, pH 7.6, top up to 1 L with dH_2O
10x SDS Running Buffer:	Tris HCL 30 g, Glycine 114 g, SDS 10 g, top up to 1 L with dH_2O
10x Agroinfiltration buffer:	MES hydrate 4.8 g, $MgCl_26H_2O$ 5.1 g, pH 5.7, top up to 250 mL with dH_2O, autoclave

2.4.3. Membrane enrichment

Leaf tissue was collected and 600 mg per sample was frozen with liquid nitrogen then homogenised into a fine powder as with extraction for co-immunoprecipitation. Next, 2000 µl ice-cold sucrose extraction buffer was added (0.33 M sucrose, 20 mM Tris-HCL (pH 8), 1 mM EDTA) supplemented with 5 mM DTT, 1% Sigma Plant Protease Inhibitor and 0.5% PVPP. Samples were vortexed until they were liquid and well mixed. The lysate was cleared by centrifugation at 2000 x *g* for 5 min at 4˚C to remove debris. Supernatant was filtered with two layers of Miracloth (carefully ensuring not too much of the extract was lost to the Miracloth due to absorption). An aliquot of this (50 µl) of this was separated into a new tube as the total fraction (T). The rest was spun at 21,000 x *g* (unless otherwise stated) for 1 h at 4˚C, this was sufficient to enrich the membranes as despite popular belief, ultracentrifugation is not needed to enrich membranes if small sample volumes are used and the initial clearance is carried out at lower speeds than standard as to not pellet the heavy domains of membranes (Abas and Luschnig, 2010). The resulting supernatant was separated into a new tube and labelled as the soluble fraction (S). The pellet was resuspended with extraction buffer (minus the PVPP) in 3 times less volume than the soluble fraction (unless otherwise stated). The resulting fraction was labelled as the 3x membrane-enriched/microsomal fraction (M). Proteins fractions were run on SDS-PAGE gels as with western blotting, but with no water added to the loading buffer.

2.4.4. Callose stain

Callose staining was performed with Aniline blue as previously described (Bozkurt et al., 2011). First ‘buffer A’ of 0.07 M $NaH_2PO_4•H_2O$ was prepared by dissolving 0.483 g in 50 mL dH_2O. Then Sodium Phosphate ‘buffer B’ of 0.07 M pH 9.0 was prepared by dissolving 10.766 g of $Na_2HPO_4•2H_2O$ in 900 mL of dH_2O. This was adjusted to pH 9.0 using buffer A. Leaf disks of *P. infestans* infected material was collected and rinsed with 50% EtOH twice, i.e. placed into culture tubes with approximately 5 mL ethanol, inverted, removed and placed in a new tube and repeated. Disks were rinsed with buffer B once, then placed into fresh buffer B for 30 min incubating at room temperature. The buffer was replaced with 0.05% alanine blue (first 0.5% wt/vol analine blue was prepared using phosphate 0.07 M buffer B, then this solution was used to prepare aniline blue solution of 0.05% using buffer B as the diluting agent).

Samples were incubated in the stain for 60 min in the dark at room temperature. They were then mounted in the stain on microscopy slides and imaged using the UV laser.

2.4.5. RT-PCR

Total RNA was extracted from 6 size 4 leaf disks of plant tissue 5dpi from 4-week old leaves using the Agilent Plant RNA isolation Mini Kit (Agilent Technologies) according to the manufacturers protocol. RNA (1 µg) was reverse transcribed using the Ominiscript RT Kit (Qiagen) in order to produce cDNA. GAPDH was used as an internal loading control. Regions targeted in by hpRabE1 and amplified in the RT-PCR are detailed in Table 10 an Figure 2.5.

2.5. Microscopy, Imaging and Image analysis

2.5.1. Confocal microscopy

Leaf tissue was prepared for imaging by sectioning of desired area surrounding an infection spot using a cork borer size 4, and was mounted, live, in wells containing dH_2O made in Carolina Observation Gel to enable diffusion of gasses. The underside of the leaf tissue was imaged, where stated, using a 63x water immersion objective lens on a Leica TCS SP5 resonant inverted confocal microscope or, where stated, a Leica SP8 with 40x water immersion objective. Laser excitations for fluorescent proteins on SP5 and SP8 are presented in Table 5 below. Z-stack and single plane images were later exported to Fiji (ImageJ) image analysis software (Schindelin et al., 2012) for image analysis and processing of contrast & brightness. Images shown are representative of more than one experiment and observations are from multiple cells and more than one leaf.

Table 5: Laser excitations on Leica SP5 and SP8 microscopes

	SP8 (40x water objective)	SP5 (63x water objective)
GFP	488 nm (Argon)	488 nm (Argon)
RFP	561/594 nm (Diode)	543 nm (He-Ne)
BFP	405 nm (Diode)	405 nm (Diode)
mKOk	514 nm (Argon)	543 nm (He-Ne)
YFP	514 nm (Argon)	n/a

2.5.2. UV imaging of infection assays

Leaves were placed under direct illumination of two strong UV lamps as evenly as possible, in a dark room. A yellow coloured filter was attached to the camera lens and images were taken with long exposure of 2 seconds, F8.0 and ISO 400.

2.5.3. Quantification of focal accumulation

The focal accumulation of NRC4 and other proteins was determined in a number of ways. Firstly the distribution was investigated manually and by comparing to cytoplasmic and/or PM/EHM markers. Where signal was clearly much greater around haustoria vs the cytoplasm, it was considered focal accumulation. In some cases however, this was not sufficient to conclude focal accumulation or diffuse cytoplasmic localisation. In particular, determining focal accumulation was challenging as the shape of the cytoplasm around the EHM seems to affect how bright it is versus the cortical/peripheral cytoplasm. Quantification of the perihaustorial fluorescence was done in one of two ways, either absolute perihaustorial fluorescence or as a focal accumulation index. The former was achieved by making a freehand line region of interest (ImageJ) along the EHM when a marker was available and measuring the signal in the NRC4 (or other variable) channel. When an EHM marker wasn't available, the perihaustorial signal of the NRC4 channel was measured by drawing the region of interest directly on the brightest points of NRC4 signal. The focal accumulation index is a ratio between the perihaustorial signal (as before) versus the signal from the cytoplasm measured by drawing a region of interest on the cytoplasm using the marker available to define a short stretch of the cytoplasm.

2.5.4. Fluorescence recovery after photobleaching (FRAP) assay

A 'before' image was taken 5 minutes prior to photobleaching. Photobleaching was carried out by zooming into the haustorium to be bleached and raising Argon laser power to 80% for 5-10 s. An image was taken immediately after bleaching, and then in a sequence as outlined in the individual experiment. I left large gaps between time points (specified in graphs) to reduce the chances of bleaching the field of view during image acquisition.

2.6. Details of constructs

Table 6: Details of constructs cloned in this study

Name of construct	Forward Primer Name(pPCR)	Forward Primer Sequence	Reverse Primer Name(pPCR)	Reverse Primer Sequence	Template (pPCR)	Vector cloned into	OD_{600} infiltrated
hpGUS	GUS-RNAi-F	accaggtctcaggagTAAAGAGCTGATAGCGCGTGAC	GUS-RNAi-R	accaggtctcatcgtTGTCGGTGTACATTGAGTGCAG	pENTR-GUS	pRNAi-GG	0.3
hpRabE1	RABE1_3UTR_RNAi_FWD	accaggtctcaggagGCTTGCTGTGGTTCGTAAAAATGGT	RABE1_3UTR_RNAi_REV	accaggtctcatcgtTTCAGTCGCACCCAAACACAATG	cDNA	pRNAi-GG	0.3
hpNRC4	NRC4_nat_RNAi_F	accaggtctcaggagATGGCAGATGCAGTAGTGAATTTTCTGG	NRC4_nat_RNAi_R	accaggtctcatcgtTTTGTGCAGCTTCGCCTGAAC	cDNA	pRNAi-GG	0.3
hpExo70A1	hpExo70A1-F	accaggtctcaggagCAGGGATACACGTTCTCCTGTCCT	hpExo70A1-R	accaggtctcatcgtAGCAGCATGGCGACACTCGT	cDNA	pRNAi-GG	0.3
hpVPS18	hpVPS18-F	accaggtctcaggagAATGAGGATCCTGGCGTTCAC	hpVPS18-R	accaggtctcatcgtTTCCTGCTCAATGACATGC	cDNA	pRNAi-GG	0.3
hpVPS41	hpVPS41_new-F	accaggtctcaggagGCCCTTGCAGTTATCATAAATAA	hpVPS41_new-R	accaggtctcatcgtGACCTCCATGGATTTCATACTC	cDNA	pRNAi-GG	0.3

hpVPS8	hpVPS8-F	accaggtctcaggagGAAAACGATTCTCTAAATGATG	hpVPS8-R	accaggtctcatcgtGATGTGGAGAGTATCTGCTTG	cDNA	pRNAi-GG	0.3
NRC4-FL	NRB1synFWD	AGGCGGCCGCACTAGTGATCACCATGGCTGACGCTGTTGTTAACTT	NRB1synRev-new	GCGGACTCTAGCATGGCCGCGGGATTTACTGTGTGGCCTTGGATCCAG	pICH86988 synNRC4	pK7WGF2 cut w/ *Eco*RV	0.3
	GA35S-F	CGTTCCAACCACGTCTTCAAAGCAAG	35s_REV_NRB1_syn	AGTTAACAACAGCGTCAGCCATGGTGATCACTAGTGCGGCCGCC			
NRC4Δtail	NRB1_syn_FWD	AGGCGGCCGCACTAGTGATCACCATGGCTGACGCTGTTGTTAACTT	NRB1_syn_delC_RE V-NEW	CGGACTCTAGCATGGCCGCGGGATTTAGTTTTCCAGCCGCATCTCA T	pICH86988 synNRC4	pK7WGF2 cut w/ *Eco*RV	0.3
	GA35S-F	CGTTCCAACCACGTCTTCAAAGCAAG	35s_REV_NRB1_syn	AGTTAACAACAGCGTCAGCCATGGTGATCACTAGTGCGGCCGCC			
NRC4-GFP	GA 35S F	CGTTCCAACCACGTCTTCAAAGCAAG	NRC4 Cterm Rev	CGCCCTTGCTCACCATTGATCCCTGTGTGGCCTTGGATCCAGCTT		pK7FWG2 cut w/ *Eco*RV	0.3
NRC4-link-GFP	GA35S-F	CGTTCCAACCACGTCTTCAAAGCAAG	NRC4 Cterm linker R	GCAGATCCAGCAGATCCGATCTGTGTGGCCTTGGATCCAGCTT	NRC4-FL	pK7FWG2 2nd gen cut w/ *Eco*RV	0.3

NRC4-link-mKOk	n/a (used fragment from above)	n/a	n/a	n/a		pK7 mKOk cterm cut w/ *Eco*RV	0.3
NRC4-link-BFP	n/a (used fragment from above)	n/a	n/a	n/a		pK7 BFP cterm w/ *Eco*RV	0.3
NRC4-link-3xHA	n/a (used fragment from above)	n/a	n/a	n/a		pK7 3xHA cterm w/ *Eco*RV	0.3
NRC4Δtail-link-GFP	NRB1-syn-fwd	AGGCGGCCGCACTAGTGATCACCATGGCTGACGCTGTTGTTAACT	NRC4deltaC-GFP-R	GCAGATCCAGCAGATCCGATGTTTTCCAGCCGCATCTCAT	pICH86988 synNRC4	pK7FWG2 2nd gen cut w/ *Eco*RV	0.5
NRC4ΔC-link-HA	n/a (used fragment from above)					pK7 3xHA cterm w/ *Eco*RV	0.3
NRC4-GFP-HDEL	GA35S-F	CGTTCCAACCACGTCTTCAAAGCAAG	GFP-HDEL-R	TAGCATGGCCGCGGGATTTAAAGTTCATCATGCTTGTACAAG	*Agrobacterium* plasmid miniprep of NRC4-GFP	pK7WGF2 cut w/ *Eco*RV	0.3
NRC4 FL D478V	GA35S-F	CGTTCCAACCACGTCTTCAAAGCAAG	R1-seq-new	CGGACTCTAGCATGGCCGCGGGATTTAGTTTTCCAGCCGCATCTCAT	NRC4-FL	pK7WGF2 cut w/ *Eco*RV	0.08

	F1_Seq_new	TGGCGTCCATTGGGTTTACGTC	NRB1_syn_Rev	TCATGACTCGATGTCCCTTTTCG	pICH86988 NRC4-D478V		
NRC4ΔC D478V	n/a (used fragment from above)					pK7WGF2 cut w/ *Eco*RV	0.08
	F1_Seq_new	TGGCGTCCATTGGGTTTACGTC	NRB1synΔC-Rev	CGGACTCTAGCATGGCCGCGGGATTTAGTTTTCCAGCCGCATCTCAT			
NRC4-link-7KA-GFP	NRB1-syn-fwd	AGGCGGCCGCACTAGTGATCACCATGGCTGACGCTGTTGTTAACT	NRB1-delta-R	GTTTTCCAGCCGCATCTCATAAAG	pICH86988 synNRC4	pK7FWG2 2nd gen cut w/ *Eco*RV	0.3
NRC42	GA35S-F	CGTTCCAACCACGTCTTCAAAGCAAG	Chim_NRC4R_new	TTGCTGCTGTTTTGGTTGAGTTTTCCAGCCGCATCTCAT		pK7WGF2 cut w/ *Eco*RV	0.3
	Chim_4to2CterF_new	ATGAGATGCGGCTGGAAAACTCAACCAAAACAGCAGCAA	Chim_4to2CterR	TAGCATGGCCGCGGGATTTAGAGATCGGGAGGGAATATAGAG			
NRC42-link-GFP	NRB1-syn-fwd	AGGCGGCCGCACTAGTGATCACCATGGCTGACGCTGTTGTTAACT	NRC2 rev 1	GCAGATCCAGCAGATCCGATGAGATCGGGAGGGAATATAGAGAGC	NRC42		0.3

GFP-4Tail	NRB1_Cterm_F	CACCACAAGCAAAGCGGTCAAATCTGC	NRB1_Cterm_R	TCAGAAAACATGAGTAGCACCATATCC	GFP-NRC4	pK7WGF2 (using Gateway)	0.3
RFP-4Tail	NRB1_Cterm_F		NRB1_Cterm_R		cDNA	pK7WRF2 (using Gateway)	0.3
4Tail-GFP	Tail-GFP-F	CAGGCGGCCGCACTAGTGATGACAAGCAAAGCGGTCAAATC	CT-Linker-R	ATTCTCCAGATCCAGCAGCAGATCCA	NRC4-link-GFP (p14)	pK7FWG2 2nd gen cut w/ *Eco*RV	0.3
4Tail-mKOk	n/a (used fragment from above)					pK7 mKOk cterm cut w/ *Eco*RV	0.3
4Tail-BFP	n/a (used fragment from above)					pK7 BFP cterm w/ *Eco*RV	0.3
4Tail-7KA-GFP	Tail-7KA-GFP-F	CAGGCGGCCGCACTAGTGATGACAAGCGCAGCGGTCGCATC	CT-Linker-R	ATTCTCCAGATCCAGCAGCAGATCCA	NRC4-link-7KA-GFP (P13a)	pK7FWG2 2nd gen cut w/ *Eco*RV	0.3
2Tail-mKOk	2Tail-F	CAGGCGGCCGCACTAGTGATGTCAACCAAAACAGCAGCAA	NRC2CtermRev1	GCAGATCCAGCAGATCCGATGAGATCGGGAGGGAATATAGAGAGC	cDNA	pK7 mKOk cterm cut w/ *Eco*RV	0.3
Sec3a-GFP	Sec3a_F	CAGGCGGCCGCACTAGTGATGGCGAAA	Sec3a_R	GCAGATCCAGCAGATCCGATCATGGATGCCAA		pK7FWG2 2nd gen cut w/ *Eco*RV	0.3

		TCGAGTGCGGAT		AAGATCTCGC			
Sec3a-BFP	n/a (used fragment from above)	-	-	-	-	pK7 BFP cterm w/ *Eco*RV	0.3
Exo70B1-GFP	Exo70B1-GFP-F	CAGGCGGCCGCACTAGTGATGGCGAAGAAAAACTCATAG	Exo70B1-GFP-R	GCAGATCCAGCAGATCCGATCTTCCTGCCACCACCTGAT	cDNA	pK7FWG2 2nd gen cut w/ *Eco*RV	0.3
Exo70A1-GFP	Exo70A1-GFP-F	CAGGCGGCCGCACTAGTGATATGGGTATACCAAGAAACACAG	Exo70A1-GFP-R	GCAGATCCAGCAGATCCGATCCGTTTGGGCTCATTTAAC	cDNA	pK7FWG2 3nd gen cut w/ *Eco*RV	0.3
StVPS18-GFP	StVPS18F1-GFP	CAGGCGGCCGCACTAGTGATGGAAAGAAGACATCACGTT	StVPS18R1-GFP	GCAGATCCAGCAGATCCGATCACAGCTAAAGAAAGGCTTCTCTG	St cDNA	pK7FWG2 2nd gen cut w/ *Eco*RV	0.3
VPS41-GFP	VPS41-GFP-F	CAGGCGGCCGCACTAGTGATGTCACGGAATCTATCAG	VPS41-GFP-R	GCAGATCCAGCAGATCCGATACCTGCTGCCGTAGTACATA	cDNA	pK7FWG2 2nd gen cut w/ *Eco*RV	0.3
BFP-AVRblb2	n/a used synthetic sequence of PITG_20300 minus RXLR and Signal peptide					pK7 BFP Nterm w/ *Eco*RV	0.1

RFP-AVRblb2	n/a used synthetic sequence of PITG_20300 minus RXLR and Signal peptide	-	-	-		N term RFP *CCDB*	0.1
Luciferase-3xHA	GALucF	CAGGCGGCCGCACTAGTGATGGAAGACGCCAAAAACATAAAG	GALucR	GCAGATCCAGCAGATCCGATCAATTTGGACTTTCCGCCC	pGEM-LUC		0.2
Luc-3Myc	n/a (used fragment from above)					C term myc *CCDB*	0.2
NRC4-2CC-GFP	NRC2-F	CAGGCGGCCGCACTAGTGATGGCTAATGTGGCTGTTGAGTTCC	NRC2_CC-R_4oh_reorder	tcatcatcctccaatgcaggCGGAGGCTTTCTCTCCTGCA	pICH NRC2	*CCDB* C term GFP	0.3
	NRC4_CC-GFP-NB-F	CCTGCATTGGAGGATGATGA	Pk7 GFP Rev	AAGTCGTGCTGCTTCATGTG	synNRC4-linker-GFP		
NRC2-4CC-GFP	GA35SF	CGTTCCAACCACGTCTTCAAAGCAAG	NRC4_CC-GFP-NB_R	ACCCTGCTGAGTTGTTTCC	NRC4-GFP	pK7FWG2 2nd gen cut w/ *Eco*RV	0.3
	NRC2_NBD-F_4oh	cggaaacaactcagcagggtGTGGTAGAGGAAGATGATGTGG	NRC2 Cterm Rev1	gcagatccagcagatccgatGAGATCGGGAGGGAATATAGAGAGC	pICH NRC2		

NRC4-2CC83n-GFP	NRC2-F	caggcggccgcactagtgATGGCTAATGTGGCTGTTGAGTTCC	NRC2_cc.249_R	aaattacataaggaaaagTGCTTCGATAACGAATTTGTCG		pK7FWG2 2nd gen cut w/ *Eco*RV	0.3
	NRC4_cc.249_F_new	AAATTACATAAGGAAAAGAACAAAATGGCA	GA_TERM_REW2	GCAGGTCACTGGATTTTGGT	NRC4-GFP		
NRC4-2CC83c-GFP	NRC2_cc.249_F	aaattcgttgtgcaagctAAATTGCATAAAGATAAGGGCG	pK7 GFP-R	AAGTCGTGCTGCTTCATGTG	NRC4-2CC-GFP (V8)	*CCDB* C term GFP	0.3
	GA35S-F	CGTTCCAACCACGTCTTCAAAGCAAG	NRC4_cc.249-R	AGCTTGCACAACGAATTTGTCC	NRC2-4CC		
NRC2-4CC83n-GFP	GA_35S_F	CGTTCCAACCACGTCTTCAAAGCAAG	NRC4_cc.249_R	AGCTTGCACAACGAATTTGTCC	NRC4-GFP		0.3
	NRC2_cc.249_F	aaattcgttgtgcaagctAAATTGCATAAAGATAAGGGCG	NRC2 Cterm Rev1	gcagatccagcagatccgatGAGATCGGGAGGGAATATAGAGAGC	pICH NRC2		
NRC2-4CC83c-GFP	NRC2-NBD-F4oh	cggaaacaactcagcagggtGTGGTAGAGGAAGATGATGTGG	Pk7GFP R	AAGTCGTGCTGCTTCATGTG	NRC2-4CC83n-GFP	*CCDB* C term GFP	0.3
	GA35SF	CGTTCCAACCACGTCTTCAAAGCAAG	NRC4_CC-GFP-NBD_R	ACCCTGCTGAGTTGTTTCC	NRC4-2CC83n-GFP		

ZAR1_4CC17n_GFP	n/a used synthetic sequence	-	-	-	-	-	0.3
	ZAR1_17_F	GAAGAAAAAGGCCGAACCGTATCGG	ZAR1_R_ohlnkr	gcagatccagcagatccgatGGTTCTGTGCAATGGTGTTTTCATCC	WTZAR1	GA_3rd Gen C-term GFP	
ZAR1_4CC83c_GFP	n/a used synthetic sequence	-	-	-	-	-	0.3
	ZAR1_NBD_F	GAAGAGATAATGGAACTGATCGGTGGAG	ZAR1_R_ohlnkr	gcagatccagcagatccgatGGTTCTGTGCAATGGTGTTTTCATCC	WTZAR1	GA_3rd Gen C-term GFP	
NRC4_Z1CC83c_GFP	n/a used synthetic sequence	-	-	-	-	-	0.3
	NRC4_CC-GFP-NB-F	CCTGCATTGGAGGATGATGA	NRC4_Cterminkr_R	GCAGATCCAGCAGATCCGATCTGTGTGGCCTTGGATCCAGCTT	pICH86988 synNRC4	GA_3rd Gen C-term GFP	
ZAR1_4CC_GFP	n/a used synthetic sequence	-	-	-	-	-	0.3
	ZAR1_NBD_F	GAAGAGATAATGGAACTGATCGGTGGAG	ZAR1_R_ohlnkr	gcagatccagcagatccgatGGTTCTGTGCAATGGTGTTTTCATCC	WTZAR1	GA_3rd Gen C-term GFP	

Rpiblb2-MYC	Rpi-blb2-cfusion-F	CAGGCGGCCGCACTAGTGATGGAAAAACGAAAAGATAATG	Rpi-blb2-cfusion-R	GCAGATCCAGCAGATCCGATCTTAAATAACGGGATATCCTTCTGG	RFP-Rpi-bl2b	GA_3rd Gen C-term MYC	0.5
RPW8.2-mKOK	RPW82-mKOk-F	CAGGCGGCCGCACTAGTGATGATTGCTGAGGTTGCCG	RPW82-mKOk-R	GCAGATCCAGCAGATCCGATAGAATCATCACTGCAGAACGTAAA	RPW8.2-YFP (Wang et al 2009)	pK7 mKOk cterm cut w/ *Eco*RV	0.2
RPW8-BFP	n/a (used fragment from above)					pK7 BFP cterm w/ *Eco*RV	0.2
NRC4-2CC	GA35SF	CGTTCCAACCACGTCTTCAAAGCAAG	NRB1-term-Rew	TCAGAAAACATGAGTAGCACCATATCC	NRC4-2CC-GFP (V8)	first gen Nterm GFP	0.3
NRC4-2CC83n	GA35SF	CGTTCCAACCACGTCTTCAAAGCAAG	NRB1-syn-Rev	GCGGACTCTAGCATGGCCGCGGGATTTACTGTGTGGCCTTGGATCCAG		first gen Nterm GFP	0.3
NRC4-2CC83c	GA35SF	CGTTCCAACCACGTCTTCAAAGCAAG	NRB1-term-Rew	TCAGAAAACATGAGTAGCACCATATCC	NRC4-2CC83c-GFP	first gen Nterm GFP	0.3
NRC42-iGFP	NRB1-syn-fwd	AGGCGGCCGCACTAGTGATCACCATGGCTGACGCTGTTGTTAACT	NRC4_CC-GFP-NB_R	ACCCTGCTGAGTTGTTTCC	PICH86988 synNRC4	first gen Nterm GFP	0.3

	NRC4_CC-GFP_F	cggaaacaactcagcaggtATGGTGAGCAAGGGCGAGGAGC	NRC4_NBD-GFP_R	tcatcatcctccaatgcaggCTTGTACAGCTCGTCCAT	PK7WGF2		
	NRC4_CC-GFP-NB-F	CCTGCATTGGAGGATGATGA	Chim_4to2CterR	TAGCATGGCCGCGGGATTTAGAGATCGGGAGGGAATATAGAG	NRC42		
NRC4-iGFP	NRB1-syn-fwd	AGGCGGCCGCACTAGTGATCACCATGGCTGACGCTGTTGTTAACTT	NRC4_CC-GFP-NB_R	ACCCTGCTGAGTTGTTTCC	PICH86988 synNRC4	first gen Nterm GFP	0.3
	NRC4_CC-GFP_F	cggaaacaactcagcaggtATGGTGAGCAAGGGCGAGGAGC	NRC4_NBD-GFP_R	tcatcatcctccaatgcaggCTTGTACAGCTCGTCCAT	PK7WGF2		
	NRC4_CC-GFP-NB-F	CCTGCATTGGAGGATGATGA	NRB1synRev	GCGGACTCTAGCATGGCCGCGGGATTTACTGTGTGGCCTTGGATCCAG	PICH86988 synNRC4		

Table 7: Pre-existing constructs

Name of construct	Vector	Reference	OD_{600} infiltrated
RFP-Rpi-blb2	PH7WGR2	(Wu et al., 2017)	0.5
GFP-Rpi-blb2	PK7WGF2	(Wu et al., 2017)	0.5
RFP-NRC4	PK7WGR2	Unpublished (Gift from Tolga Bozkurt)	0.3
GFP-NRC4	PK7WGF2	Unpublished (Bozkurt Gift)	0.3
GFP-AVRblb2	PK7WGF2	(Bozkurt et al., 2011)	0.1
RFP-AVRblb2 (PITG_4085)	PK7WGR2	Unpublished (Gift from Khaoula Belhaj)	0.1
RFP-Rem1.3	PK7WGR2	(Bozkurt et al., 2014)	0.2
YFP-Rem1.3	PH7WGY2	(Perraki et al., 2012)	0.2
BFP-3xHA	PK7 derivative	Unpublished (Gift from Yasin Tumtas)	0.1
EV:BFP	PK7 derivative	Unpublished (Gift from Tolga Bozkurt)	0.1
GFP-SYT1	PK7WGF2	(Bozkurt et al., 2014)	0.2
EV-mKOk	PK7 derivative	Unpublished (Gift from Tolga Bozkurt)	0.1
EV-RFP	PK7WGR2	(Dagdas et al., 2018)	0.1
EV-GFP	PK7WGF2	(Dagdas et al., 2016)	0.1

EV-3xHA	PK7 derivative	(Dagdas et a., 2018)	0.1
RFP-RabD2a^{N128I}	pH7WGR2	Unpublished (Gift from Tolga Bozkurt)	0.2
RFP-GFP (pHlorin – pH sensitive GFP)	PK7WGR2	Unpublished (Gift from Tolga Bozkurt)	0.05
RFP-GUS	PK7WGR2	(Dagdas et al., 2016)	0.1
GFP-GUS	PK7WGF2	(Dagdas et al., 2016)	0.1
RFP8.2-YFP	pPZPYFP	(Wang et al., 2009)	0.2
SP-RFP-HDEL	Unknown (Kan selection in bacteria)	(Pain et al., 2019)	0.2
Actin-YFP	PB7YWG2	(Rocchetti et al., 2014)	0.2
PVX	pGR106	(Lu et al., 2003)	0.005
RFP-PI4P	PIPline	(Simon et al., 2014)	0.3
RFP-PI3P	PIPline	(Simon et al., 2014)	0.3
RFP-PIP_2	PIPline	(Simon et al., 2014)	0.3
hpGUS	pRNAiGG	(Dagdas et al., 2018)	0.3
TRV1	pYL155	(Liu et al., 2002)	0.4
TRV2:NRC2/3/4	pYL279	(Wu et al., 2017)	0.2
R3a	pCB302-3	(Segretin et al., 2014)	0.1
AVR3a	pGWB12	(Yaeno et al., 2011)	0.2

FLS2-GFP	pFLS2::FLS2	(Beck et al., 2012)	0.3
$I2^{N330Y}$	pGBKT7/pK7WG2	(Giannakopoulou et al., 2015)	0.05
AtExo84b-GFP		Unpublished (Gift from Yasin Dagdas)	0.3
$NRC3^{D480V}$	PICH86988	Unpublished (Gift from Chih-Hang Wu	0.2
NRC2-GFP	PICH86988	Unpublished (Gift from Chih-Hang Wu	0.3
NRC2-GFP	pICH47742	Unpublished (Gift from Hiroaki Adachi)	0.3
ZAR1-GFP	pICH47742	Unpublished (Gift from Hiroaki Adachi)	0.3
$NRC4^{ZAR1\alpha1}$-GFP	pICH47742	Unpublished (Gift from Hiroaki Adachi)	0.3
GUS-GFP	pICH47742	Unpublished (Gift from Hiroaki Adachi)	0.3
$NRC4^{L9E}$-GFP	pICH47742	Unpublished (Gift from Hiroaki Adachi)	0.3
$NRC4^{3A}$-GFP	pICH47742	Unpublished (Gift from Hiroaki Adachi)	0.3
$NRC4^{L9E/D478V}$-GFP	pICH47742	Unpublished (Gift from Hiroaki Adachi)	0.3

CC^{NRC4}-YFP	pICH47742	Unpublished (Gift from Hiroaki Adachi)	0.05
CC^{NRC2}-YFP	pICH47742	Unpublished (Gift from Hiroaki Adachi)	0.05
$NbZAR1^{L17E}$-GFP	pICH47742	Unpublished (Gift from Hiroaki Adachi)	0.3
$NbZAR1^{L17E/DV}$-GFP	pICH47742	Unpublished (Gift from Hiroaki Adachi)	0.3

Table 8: PK7 vectors and their derivatives

Name of vector	Tag	Tag fused to N or C term of protein of interest	Derivative	Change from derivative
PK7WGF2 (Gen 0)	GFP	N	n/a	n/a
PK7GWF2 (Gen 0)	GFP	C	n/a	n/a
PK7WGF2 (Gen 1)	GFP	N	PK7WGF2 (Gen 0)	Cut with *Eco*RV and ligated (att sites/*ccdB* gone)
PK7GWF2 (Gen 1)	GFP	C	PK7GWF2 (Gen 0)	Cut with *Eco*RV and ligated (att sites/*ccdB* gone /promoter piece missing)
PK7WGF2 (Gen 2)	GFP	N	PK7WGF2 (Gen 1)	Long linker inserted (GGATCTGCTGGATCTGCTGCTGGATCTGGAGAATTTGAT)
PK7GWF2 (Gen 2)	GFP	C	PK7GWF2 (Gen 1)	EcoRV cut site in promoter removed + Long linker inserted (ATCGGATCTGCTGGATCTGCTGCTGGATCTGGAGAATTTGGATCA)
PK7WGF2 (Gen 3)	GFP	N	PK7WGF2 (Gen 2)	*ccdB* inserted into *Eco*RV site, and new sites created either side of *ccdB*

PK7GWF2 (Gen 3)	GFP	C	PK7GWF2 (Gen 2)	*ccdB* inserted into *Eco*RV site, and new sites created either side of *ccdB*
PK7WGR2 (Gen 0)	RFP	N	n/a	n/a
PK7GWR2 (Gen 0)	RFP	C	n/a	n/a
PK7 RFP-Nterm (Gen 3)	RFP	N		Linker added and *ccdB* inserted into *Eco*RV site, and new sites created either side of *ccdB*
PK7 Cterm-RFP (Gen 3)	RFP	C		Linker added and *ccdB* inserted into *Eco*RV site, and new sites created either side of *ccdB*
PK7 BFP-Nterm (Gen 3)	BFP	N		Linker added and *ccdB* inserted into *Eco*RV site, and new sites created either side of *ccdB*
PK7 Cterm-BFP (Gen 3)	BFP	C		Linker added and *ccdB* inserted into *Eco*RV site, and new sites created either side of *ccdB*
PK7 HA-Nterm (Gen 3)	HA	N		Linker added and *ccdB* inserted into *Eco*RV site, and new sites created either side of *ccdB*
PK7 Cterm-3xHA (Gen 3)	HA	C		Linker added and *ccdB* inserted into *Eco*RV site, and new sites created either side of *ccdB*
PK7 Cterm-3xMYC	MYC	C		Linker added and *ccdB* inserted into *Eco*RV site, and new sites created either side of *ccdB*
PK7 Cterm-mKOk (Gen 2)	mKOk	C	PK7WGF2	GFP removed, mKOk added onto c-terminal site, linker in between start codon and mKOk

Table 9: Constructs created by gene synthesis (GeneWiz)

Construct Name	Sequence Ordered	Vector Cloned into	Accession number of gene
GOLD	accaggtctcaggagGGGATGTACAAGTTCTGTTTTAAGAATCCTTATTCAACACCAGAAACAGTCTCTTTCTAC ATACATATTGGACACATTCCCAATGAGCACGACCTTGCTAAAGATGAACATTTGGACCCCATTAATGTCAAAATTGCTGAACTAAGAGAGGCATTGGAGTCAGTTACTTCAGAGCAGAAGTACCTAAGAGCACGTGATGCTCGTCATCGTCATACTAATGAAAGCACAAGGAAGCGTGTTATATTTTACACAATTGGAGAGTATCTGTTGCTTATATTGGCAAGCGGGCTTCAAGTTCTATATATCCGACAACTATTCAGacgatgagacctggt	TRV2GG	NICBE_309786
EFhand	accaggtctcaggagCTACTTGTCTACAATGATATAAACAAGCTTTTGCCTGGTCCTCACTTTGATCCTCCTCCT AAAGAAGAAGTTAGAGCCTTGATGCAGGAGTGTGACATGAATCTTGACGGGGAACTGGATCATGGAGAATTCGTCAAGTTTATTAAAAAATTAACAAAGGATACATTCATCACTGTCAGTCAGGGACTGATTATTACATTGGCAGTAGCACCAACAGTTGCTCTTGTAACAAAAAGGACAACAGAAGGAGTTCCTGGTGTTGGGAAAGTGGTGCAGAAGATCCCAAATGCTGTTTATGCTTCCCTTGTCACCCTAACGATacgatgagacctggt	TRV2GG	NbS00010383g0004
CaCl	accaggtctcaggagATGAACTTTGCAGTTGTATCAAGGGAACTTTTTTCACCTTCTCCACAACCCCTTAGTCTA AGCTCATGGAAAAGAAGGGGAAGCCATTTCAGAATTTCTGCAAAATTAGGGGGAGGAGAG AGTGATGTCAAGAAAGACAAGAAGAAATTCATCACTAAAGAACAAGAACCTGAACAGTATTGGCAGACAGCAGGAGAAAGAGCAGGAGAGAACCCTATGATGACACCCCTTCCCTATATA ATCATATTTGGAATGTCAGCACCATTTGTGATCTTGGCTATTGCTTTTGCTAATGGTTGGATTAAGGTTCCAATAAGATGacgatgagacctggt	TRV2GG	NICBE_366990
PLAT	accaggtctcaggagTTCCCTCTCATTATCATCCTCTTCTCCATCACCATTTCTTCTACTTCTGGAACTGAATCA AATTGTGTGTACACAGCTTACATTCGGACTGGGCCATTCATGGAGGATGCAACTGACTCAAAAATAAGCTTGACTCTCTACGATGCGAGTGGCTATGGAATTAGAATCAAGAACCTAGTGGCTTGGGGTGGGCTTATGGGATCAGGGTACAACTACTTTGAAACGGACCACTCGGATATG TTCAGTGGCCATGGACCATGTTTGACTGGGCCGATCTGCAAAATGGTCTTGACTTCTGATGGTACAGGCCGACACTCAGCacgatgagacctggt	TRV2GG	NICBE_226268
DUF1295	accaggtctcaggagTTTGGCGAGATCCTTCTGTGGTGGGGAATATTTGTGGCTTCAACACCAGTGCTCGAGGGA GCTGAATGGCTCGTTATTCTTGGACCAGTATTCTTAACATTACTGCTTCTTTTTGTTAGTGGCATACCCCTGCTTGAGGAATCAGCAGACAAGAAACATGGAAATGTTTCTGAATATAGAGTATATAAGAGGACAACAAGCCCTCTCATTTTGCTGCCCCCTGGATTATACGGAAAGCTTCCTCCGTGGTTCAAAACTGTATTCCTTTTTGAGTTTCCTTTATACAGTCGCAATCTTGCCCAAGACGAGTTAAGCTGGTAacgatgagacctggt	TRV2GG	NbS00008935g0002
DUF2304	accaggtctcaggagACTCATCTTGCAGTCCTTATCTGGCCGTAGTTATTTTACAACAGAAATGGGGATTGACCA TGGAGTTGACTCTCTTATTGTTGTATTTCTACTGATTTCAATGGTTTCCACTTGTGTGGCCTACCGCCCCGGTGACATCGTTCCAATGAGCAAAATGGGTCAATACCACTCTTCGAGGAC	TRV2GG	NICBE_290487

	TGTTTGGCATGATATGATTGGAAAACACTGTCCCATTTTTGGGGTTAATCGTGAGGTGTT GATACCGATTCCAAAACCAACTGGTTACACTGGAGCTGATCCGTACAAGATATCATTCCA AGTTGGAAGAGAAAAATATCacgatgagacctggt		
Vesicle Fusing ATPase	accaggtctcaggagGATGCAATCTGTAAGTCTAGAGGATCAACTAGAGATGGAACTGGTGTAC ATGACAGCATT GTTAACCAGCTTCTCACTAAGATAGATGGGGTTGAATCACTGAATAATGTTTTGCTCATT GGAATGACAAATAGGAAAGATCTGCTTGATGAAGCACTTATGAGGCCAGGACGACTAGAA GTCCAAGTGGAGATAAGCCTTCCTGATGAAAATGGTCGACTGCAAATTCTCCAGATTCAT ACAAACCAGATGAAAGAGAATTCCTTTCTTTCCCCAGATGTGAACTTGCAAGAACTTGCC GCAAGGACAAAAAATTATAGacgatgagacctggt	pRNAiGG + TRV2GG	NbS0001 1575g00 12
Sec6	accaggtctcaggagGAAGATCTTGGCGTTCAGGCTAAGGAAGCCTCCGTTCGTGAGGTCGCTA AGCTTTTGCCT TTACCGGAGCTTTTACAGTCTATTTCGTCAATCAAAGCCGATTACATTGCTCGTCAACAG GCAAATGATGCACAACTTAGTACGATGGTCGCCGAACAGGTTGAACAAGCACAAGCTGGT CTGCAATCACTTAACTTATCTCAGAAGACTATAAACCAGCTCCGAGAAAACTTCCTTTCT ATTGAAAAGCTTTGTCAAGAGTGCCAAAACTTAATCGAAAATCATGACCAGATAAAGCTT CTCAGCAACACCAGGAATAAacgatgagacctggt	TRV2GG	NICBE_2 98622
Sec15	accaggtctcaggagCCAAGCAATGCAGATGGCAGCTAATATGGCTGTGTTTGAACGTGCATGT GACTTTTTCTT TCGTCATGCTGCACAGCTTTCAGGGATTCCATTGAGAATGGCAGAGAGGGGGAGGAGAC T GTTTCCTTTGACTAAAGCCCGTGATGCTGCTGAAGAGATGCTTTCTGGTCTGCTTAAGCA AAAGGTTGACGGGTTCCTTTTGCTGATTGAAACTGTGAATTGGATGGTGGATGATCCTCC GCAGGGTGGAAATGAGTATGTGCATGAGGTGACCATATTTCTTGAAACTCTAGTTTCTAC TGCCCAGCAGATCTTGCCTGacgatgagacctggt	TRV2GG	NICBE_2 39296
TRAPB	accaggtctcaggagAAGATGTATTTACCATCGTCGCTGGTAACACATCCATGTCATGGGAAAG GCTGGACGCTG GGGCCGCTCTCTCCCATTCCTTTGAGTTGGAGGCTACGAAAAAAACAGTATTGTATGGTG CACCAGCGGTTATAACATTCCGCATTCCCACAAAGGCTGCTCTACAGGAGGCATACTCAA CTCCAATCCTCCCACTTGACATACTAGCTGATAGGCCTCCGGAGAAGAAGTTCGACTGGA GGTTGATGGCAAAATATGGCTCCTTGGTTTCTGTGATCTCAATCGTGGTTCTATTTGTCT ACCTGATCGCGAGTCCTTCAacgatgagacctggt	TRV2GG	NICBE_0 61264
ER3	accaggtctcaggagGACCCAAACATGGCTATGGATATGATGAAGAAGAACTTGTCGATGATAAT TCCTCAGACT CTTACATTTGCATGGGTCAACTTCTTCTTCTCTGGTTTTGTAGCAGCGAAGATACCTTTT CCATTAACTCAGAGGTTCAGGGCCATGTTGCAAAATGGCATTGATCTAAGCACAGTCGAT GTCAATTATGTCAGCAGTCGCTCATGGTATTTTCTCAATCTGTTTGGATTAAGGGGATTG TTCAGTCTCATTCTTGGAGAAGAAAATGCAACCGATGATACTCAGCGTATGATGCAGATG AGCGGATTTGGTTTTGACCCacgatgagacctggt	TRV2GG	NICBE_3 40892_E R3
ER4	accaggtctcaggagATGGGTATGGGCCGTAGATGGGCAGTGGACTTCTCCGATAATTCCACTT CTCCTTCCTCC CGCGATATTCCTGATCCCCTTGGCTTCACTCGCGCTTCTCAAGATCAGGATGATTCAACA CTCAGTCGCGAAAAGAAGAATGCGGAAGCTAATTGGAAAAGCCAGAAAGCGTGGGAAGT G GCACAAGCACCTGCCAAGAATTTGATGATGATGGGTTTCATGATGTGGATGGCCGGAAGC ACAGTGCATTTATTTAGCATTGGTATCACAGTTTCAGCTCTATGGCAACCTCTTAGTGCT CTTCAAGGAGTTGGGAAAGTacgatgagacctggt	TRV2GG	NICBE_1 70029

VPS16	accaggtctcaggagGATGCAGCAGGTCATGAATTTGATGTTTCATTGCAATCAACGCTTTTAAGAGCAGCAAAC TACGGACAAGCCTTTTGCAGCCATTTTCGACGGGACCGCATTCAAGAGATGTGTAAAACCTTACGAGTCCTAAATGCTGTACGTCACCCAGATATTGGAATTCCTCTCAGTATTCAGCAGTATAAGTTGCTTACGCCTGCTGTTCTGATTGCTCGTCTTATTAATGCTCATCGCCACCTTCTTGCGCTACAAATATCAGAATATCTTGGAATGAATCAGGAAGTTGTAGTCATGCATTGGACATGTAGAAAGATCACAGCacgatgagacctggt	TRV2GG	NICBE_236764
VSR3	accaggtctcaggagGCCCTTATTGAGAAAAGCTTTGCAGAGAAGTTGAAGAAAGCTGTGAGTGCAGGAGAAATG GTTAATGTGAATCTTGATTGGAGAGAAGCTGTGCCCCACCCAGATGATCGTGTGGAGTATGAGCTGTGGACTAGTAGCAATGATGAATGTGGGTTCAAATGTGACATGTTGATGAAATATGTCAAAGATTTTAAGGGTGCAGCACAAATTCTTGAGAAAGGTGGATATACGCAATTCACACCCCACTATATTACTTGGTATTGCCCTCAGGCATTCACTGTAAGCAAGCAGTGCAAGTCTCAATGTATCAACCACGGAAGacgatgagacctggt	pRNAiGG + TRV2GG	NICBE_083936
VSR6	accaggtctcaggagGATGTTCAATGAAGCAAAAGAGATACAGCAAAGAATGTGCTGAGGAGGTCATGAAATCAC TCGATTTACCTGTTGAGAAGATAAAGGAATGCATGGGTGATCCAGAGGCTAATGTAGAAAATGCAGTGCTAAAGACTGAGCAAGATCTCCAGGTCGGCCGAGGACCTCGTGGTGATGTGA CAATCTTACCAACAATGGTCGTCAATGATGTTCAATATCGAGGAAAATTGGAGAGGGCTGCTGTTTTGAAGGCCATATGTGCTGGATTTAAGGAAACAACTGAACCTTCAATATGTTTAAGTGGAGATCTTGAAACAAATacgatgagacctggt	TRV2GG	NICBE_031939
COG2	accaggtctcaggagCATCCCGCAAAATCCATCTGGAGTTGTTGGTGGATCATCTGGAGATGAACTTGAGCAGGA CTATGCAAAGATCAAGCAATATATAGAGGATGACTGTAAATTTCTATTGGACATATCCTCTATCGAGGTTCACTCTGCCATCCAGAAAGTAAAACCAGTGGTATTCTCCCCTGGAAGGCCTACGGTGTTCCTCAAAAATTACAAAGCAAGCTTGGATTTCTTGGCACATTTAGAAGGTTATTGTCCCTCGCGATCTGAAGTAGTCAAGTTTCGCTCTGAAGCTGCATATATTGACTTCATGAAACAATGGAATGTCGGTGacgatgagacctggt	TRV2GG	NICBE_396062
RabD2a	accaggtctcaggagCAGTGGCTGAGTGAAATTGATCGTTATGCTAGTGACAATGTTAACAAAATTCTTGTCGGGAACAAGTCCGATCTTACTGCAAATAGAGTCGTCTCATATGAAACAGCTAAGGCATTTGCTGATGAAATTGGTATTCCATTCTTGGACACCAGTGCTAAAGATGCTACGAATGTAGAACAGGCTTTTATGGCTATGACTTCTGCTATCAAAAATAGGATGGCAAGCCAACCAACCAATAATTCCGCTAAGCCTCCAACGGTGAATATCCGTGGACAGCCGGTGACACAGAGTGGTGGCTGTTGCTCATCTTAGacgatgagacctggt	TRV2GG	NICBE_110965
TPR	accaggtctcaggagGGATTACTCGTCTTAATCGTTGTGATGTTGATCAGATAAAGAAGGAAATAGGTGAGACTG ATGTACCATTGTCTTATTCTGGTGGTGTACCTGAAAAGTCAATACGCAAGGCTTCACTGGAGGAGATTCTGCACAGATTGCTTAAATTCTTGAAGCCAGAGACATTTATAGGAGCTGTTAAAGCCATTAACCAGAAAATTCTCTCTGTTTTAGATGAGTCAGAATCAGGTAGGGTGGATCTAGGCATGTTTTTTGCCGTTCTTGCTCCTGTCTGTGGAGGACCACCGGACAAAAGAAAACGCATTGCATATGAGGCGCTTacgatgagacctggt	pRNAiGG + TRV2GG	NICBE_208402
TM	accaggtctcaggagATGGCAACTCCTGAAGAAAACATTGCACCTGCAGCTCCACCACCGCCGGCGGCAGAACCA TCAGCGGTGGAGGCTTTAGTGACCACTATTGAAACAGCGACCAAACAGGTTGAAACACCGAAGGAAGTCAAGGAGGAGAAGAAAGGAGGAGCACAGGATCTCAAGTTAACCCTTTTGATTCCAGGGGCTGTAGTAGCTGTTGTTGGAGTAGTTCTTGCCATTGTCAAGAAGGTGAAAGAGTCGGCTAATTGAacgatgagacctggt	pRNAiGG + TRV2GG	NICBE_361827

PITP	accaggtctcaggagGCGGAGGTAAAAAGACCACATTCAGTATCAGTGCATCCACAGGTAAGAA TCTCACTGGAG GAAAGCTGGTGATTGATGTCAACTATTTATTCTTCCATGTCCACCACGAGGCCATCGACC TTTGTAAAGAGACATCTTGCCCTGCTTCCGGTGATTTCCTGATTTCCCACTCACAAGAGT TGCCTGGATTTACTCCACCTGGATCATACACTCTTACAATGAAGATGGTGGATGACAAGA ATCAGCAACTGTCCTGCATAAGTTTTGGCTTCAGCATTGGGTTTATAGCCGAGTCCCAGG CGTTAGCAGCAGATAGCTAGacgatgagacctggt	TRV2GG	NICBE_216370
LRR	accaggtctcaggagCTTTCTGGTAGGATCCCTCGTTCCTTAACCAATTTATCATCTTTAATGCAT TTAGATCTA CGTAACAACCGAATTTTCGGAACCCTACCAACAAATTTTGGAAAATTAAGGATGTTAAGT CGAGCTTTATTAAGTGGAAACCGTTTAATTGGAAAAATTCCATATTCTATTTCCTATATT TATAGACTTTCCGATTTGGATCTTTCTTTAAATAAACTATCTGGTACAATTCCACCATCT CTAGGCAAAATGCGCGTTCTTGCTACATTAAATCTTGATGGTAACAATATTTCTGGTACC ATACCACCAACGTTAATTAAacgatgagacctggt	pRNAiGG + TRV2GG	NICBE_028866
NDPK1	accaggtctcaggagGCCTTCGCTGAAAAGCATTACGCAGACTTGTCTGCTAAGCCTTTCTTTAG TGGTCTTGTT GATTATATTATCTCTGGCCCCGTTGTTGCAATGGTCTGGGAAGGTAAGGGTGTAGTTACC ACTGGCAGGAAGATCATTGGAGCAACAAACCCATTGGAGTCTGCTCCTGGTACAATCCGT GGTGATTATGCTATTGACATTGGCAGGAACGTTATTCATGGAAGTGATGCAGTCGAGAGT GCAAGGAAGGAAATTGCTCTTTGGTTCCCCGAAGGAGTTGCAGAGTGGCAGAGCAGCCT T CACTCTTGGATCTATGAGTAacgatgagacctggt	TRV2GG	NICBE_048921
TROP	accaggtctcaggagGGTTCAGTATATGGAGCAACAAAAGGGGCAATGAATCAGCTCACGCGAA ATCTGGCTTGT GAATGGGCAAAAGATAGCATTCGAGTTAATGGTGTTGCCCCGTGGTATATAAGGACGTCT TTGGTAGAACATTTGCTCGAAAATAAAACATTTTTGGATGGAGTAATATCTAGAACTCCC CTTAGACGCCCTGGAGAGTCTCAAGAAGTTTCATCCCTGGTAGCTTATCTTTGTCTACCT GGAGCATCGTACATCACCGGGCAAGTTATAGCAGTTGATGGAGGTTTCACAGTCAATGGG TTCGAAATGACAAGCTACTGacgatgagacctggt	TRV2GG	NICBE_060415
USPa	accaggtctcaggagAAATCTGGTTCTCCTTTAATTCCGTTGGTGGAGTTTAGGGAGCCTGAAGT GATGAAGAAA TATGATGTGGAGACTGATATTGATGTTCTTGATTTGCTTGATACTGCTACTAGGCAGAAA GAGATAACAGTTGTGACCAAATTATACTGGGGAGATGCTAGGGAGAAACTCATAGATGCT ACTGAAGATCTGAAGTTGGATTCTTTGGTTATGGGTAGCAGAGGTCTTGTTGTGACCAAA TTATACTGGGGAGATGCTAGGGAGAAACTCATAGATGCTACTGAACATCTGAAGTTGGAT TCTTTGGTTATGGGTAGCAGacgatgagacctggt	TRV2GG	NbS00016898g0005
Brain	accaggtctcaggagACTGCCAAACCTATATTCTAGGAATTTATTAAATTACCAAATTGAAAATTC TTTTGATAA CCAAAAGTCAATAAAACACCACACTAATACTAATACGAGAGATATTATACAGAGAAAAGT CAGATACAAAATTTTACCTTTCATGGCGACTTCAAAACTCCAGGCTCTATGGAATCACCC TGCTGGTCCAAAGACCATTCATTTCTGGGCACCAACCTTCAAGTGGGGCATCAGTATAGC AAATATCGCTGACTTTGCTAAGCCTCCTGAAAAGATTTCATTACCCCAGCAAATAGCTGT TACAGCTACTGGACTTATCTacgatgagacctggt	TRV2GG	NbS00017703g0007

Table 10: RT-PCR primers

Name of Primer	Sequence
GFP_RABE1_FWD_new	ACGAGCTGTACAAGGGTGGAAGCATGGCAGCACCACCGGCAAGAG
DN_RabE1_R1	CATGTCAGCCTTGATCCCTACAAGTATTTTGTTGA
NbRab8aRTF1-2	GTGTGGGTAAGAGTTGCCTT
NbRab8aRTR1	TGATTTTTGAGCGCTTTGAC
NbRab8aRTR2	GGTTGATTTATCCTGATAGTCTGT
NbRab8a3F	AAATTTGGGATACTGCTGGC
NbRab8a3R	GGATGTAGGAACAGCCCG
NbRab8a4F	GACTCGTCCGTGACATCG
NbRab8a4R	GCAGCTCCACCAGCTAGG
NRC4_seq_F2	AAGTGATTCGCTTGTGGATAG
NRC4_seq_R2	TCCAGGCACTTAAGCTCTAC
GAPDH-F	ATGGCTTCTCATGCAGCTTT
GAPDH-R	ATCCTGTGGTCTTGGGAGTG



Figure 2.5: Alignment of RabE family proteins tested for silencing by hpRabE1a.

3. Results Chapter I: Where and when does NRC4-mediated resistance against *P. infestans* occur?

3.1. Chapter Summary

NLRs are described as intracellular immune receptors. A few examples of plant NLRs are known to localise to the nucleus, plasma membrane, endosomes and tonoplast (Qi and Innes, 2013), but the localisation of plant NLRs during infection is unknown. Since *N. benthamiana* can be successfully infected with *P. infestans*, it lacks sensor NLRs for this pathogen and can therefore be used to study the cell biology of helper NLRs against *P. infestans.* This enabled us to study the localisation of one such helper, NRC4. We made an unprecedented discovery that NRC4 alters its localisation upon infection with *P. infestans.* When the finger-like pathogen appendages known as haustoria form, in the plant cell, NRC4 focally accumulates to a microdomain in the plant membrane surrounding the haustoria. To study the localisation of the sensor NLR Rpi-blb2 that provides resistance to *P. infestans* and blocks 100% of infections in an NRC4-dependant manner, we first disarmed the plant by mutating NRC4 with CRISPR/Cas9 mutagenesis. We were able to transiently express an N-terminal fusion of NRC4 and rescue the focal accumulation of NRC4, but not the HR cell death. Thus we could study the localisation of NRC4 with the sensor NLR during infection with *P. infestans* without triggering HR cell death. We were surprised to find that Rpi-blb2 did not accumulate at the EHM with NRC4, but instead remained cytoplasmic. Rpi-blb2 either recognises AVRblb2 and activates NRC4 transiently at the EHM (‘kiss-and-run’ process), or AVRblb2 recognition and/or NRC4 activation occurs indirectly. Finally, I present evidence that Rpi-blb2/NRC4 resistance is active at the haustoria-forming stages of infection and does not prevent the initial penetration of *P. infestans*.

3.2. Introduction

One of the pertinent questions of the NLR field is to decipher where in the cell resistance proteins recognise effectors and execute defense activation (Engelhardt et al., 2012). The localisation of NLRs and their cognate effectors gives us an insight into how recognition takes place, and also how the NLR raises an immune response. Despite this, the localisation of NLRs with or without infection is rather understudied. This is partially due to the low abundance of NLRs (van Wersch et al., 2020), and in the presence of the pathogen it is normally not possible to carry out cell biology due

to the cell death initiated upon effector perception. Although technically challenging, studying NLR localisation during pathogen infection is biologically much more relevant than studying NLRs solely in the absence of infection.

Most studied NLRs are cytoplasmic in uninfected cells. But many NLRs have predicted nuclear localisation signals (NLS) (Shen and Schulze-Lefert, 2007). Some of these localisations have been experimentally validated with biochemistry or microscopy (Rx1, SNC1, RPS1, RPS4, RRS1, N), however the localisations are not exclusively nuclear (Chiang and Coaker, 2015). The recognition and/or elicitation of an immune response is believed to occur in the nucleus for these NLRs. However, it is somewhat questionable whether these findings would be consistent with the scenario in which the immune-recognised pathogen is present.

In contrast, many studies have revealed the localisations of pathogen effector proteins. These studies mostly rely on heterologous expression of effector proteins directly in the plant cells, a highly useful strategy that overcomes the difficulties of pathogen transformation and the low levels of effector expressed from pathogens (Bozkurt et al., 2012). It has been found that *P. infestans* RXLR effectors target a wide variety of host compartments (Wang et al., 2018a). Some of these were investigated during infection with the *P. infestans*. Others were not, and effectors can have different localisations during infection (Bozkurt et al., 2011). One advantage of the transient expression system via *Agrobacterium* is that the cell-to-cell variation in expression can be used to a microscopist's advantage by selecting examples of low and high expression to image and see if they correlate.

3.3. Aims

Effector localisation studies raised an interesting question: where are the R-proteins that detect them? In this chapter, I explore this question in two parts – (1) Considering AVRblb2 localises to the EHM during infection (Bozkurt et al., 2014, 2011), does its cognate R-protein, Rpi-blb2, also localise there? (Section 3.4.1.3); (2) What is the localisation of its helper NLR, NRC4? (Sections 3.4.1.1 & 3.4.1.2).

3.4. Results & Discussion

3.4.1. NRC4, but not Rpi-blb2, accumulates at an EHM microdomain, co-localising with AVRblb2

3.4.1.1. Unlike other NLRs, NRC4 accumulates around haustoria

How does Rpi-blb2 recognise AVRblb2, considering that this effector localises to the EHM and how does Rpi-blb2/NRC4 trigger disease resistance? Unfortunately, imaging NLRs against *P.* infestans during infection is ordinarily not possible due to the HR cell death they produce upon effector recognition. However, since *N. benthamiana* can be infected by *P. infestans*, it naturally lacks sensor NLRs effective against *P. infestans*. This therefore enabled me to investigate the *N. benthamiana* helper NLR NRC4 during infection.

Firstly, to determine which fluorescent tag was most suitable for live cell imaging, I generated N- and C-terminally tagged fusion proteins of NRC4 with GFP. We performed genetic complementation assays using these fusion proteins in Rpi-blb2 transgenic plants that had NRC4a/b mutated (Rpi-blb2$^{nrc4a/b}$) by CRISPR/Cas9 genome editing (unpublished gift from Dr Hiroaki Adachi). While the N-terminal fusions failed to complement HR or resistance to *P. infestans*, like the negative control EV:GFP, the C-terminal fusions were functional for both HR and resistance (Figure 3.1A-E). In fact, expression of GFP-NRC4 in Rpi-blb2 transgenics was sufficient to break Rpi-blb2 resistance, indicating that it acts as a dominant-negative mutant (S1 Figure 3.19). We therefore generated stable transgenics expressing NRC4-GFP under the 35S constitutive promoter (see Materials & Methods) (hereafter *35S::NRC4-GFP*). I found that during infection with *P. infestans*, NRC4-GFP and GFP-NRC4 showed an accumulation of NRC4-GFP signal (Figure 3.1F-G), similar to that seen for AVRblb2 (Bozkurt et al., 2011), whereas EV-GFP remained diffuse throughout the cytoplasm, which also surrounded the haustorium (Figure 3.1H). This was confirmed with stable, constitutive expression of NRC4-GFP (Figure 3.1I). In contrast, prior to infection NRC4-GFP, GFP-NRC4 and EV-GFP were all similarly localised to the cytoplasm, but EV-GFP also diffused into the nucleus due to its small size (Figure 3.1J-L). The cytoplasmic localisation of NRC4 prior to infection was confirmed with stable, constitutive expression of NRC4-GFP (Figure 3.1M). To determine if other NLRs accumulate around haustoria, or if this could be specific to NRC4's mode of action, I

investigated the localisation of GFP-tagged paralogue of NRC4, NRC2 and the model CNL, AtZAR1 (hereafter ZAR1), with NRC4-mKOk (red/orange coloured fluorescent fusion). NRC2-GFP formed filaments throughout the cell, some of which associated with the EHM, but did not focally accumulate (Figure 3.1N-Q). ZAR1-GFP was also distributed throughout the cytoplasm with some possible membrane association (Figure 3.1R-U). All the studied NLRs produced expected band sizes during western blot analysis (Figure 3.2).

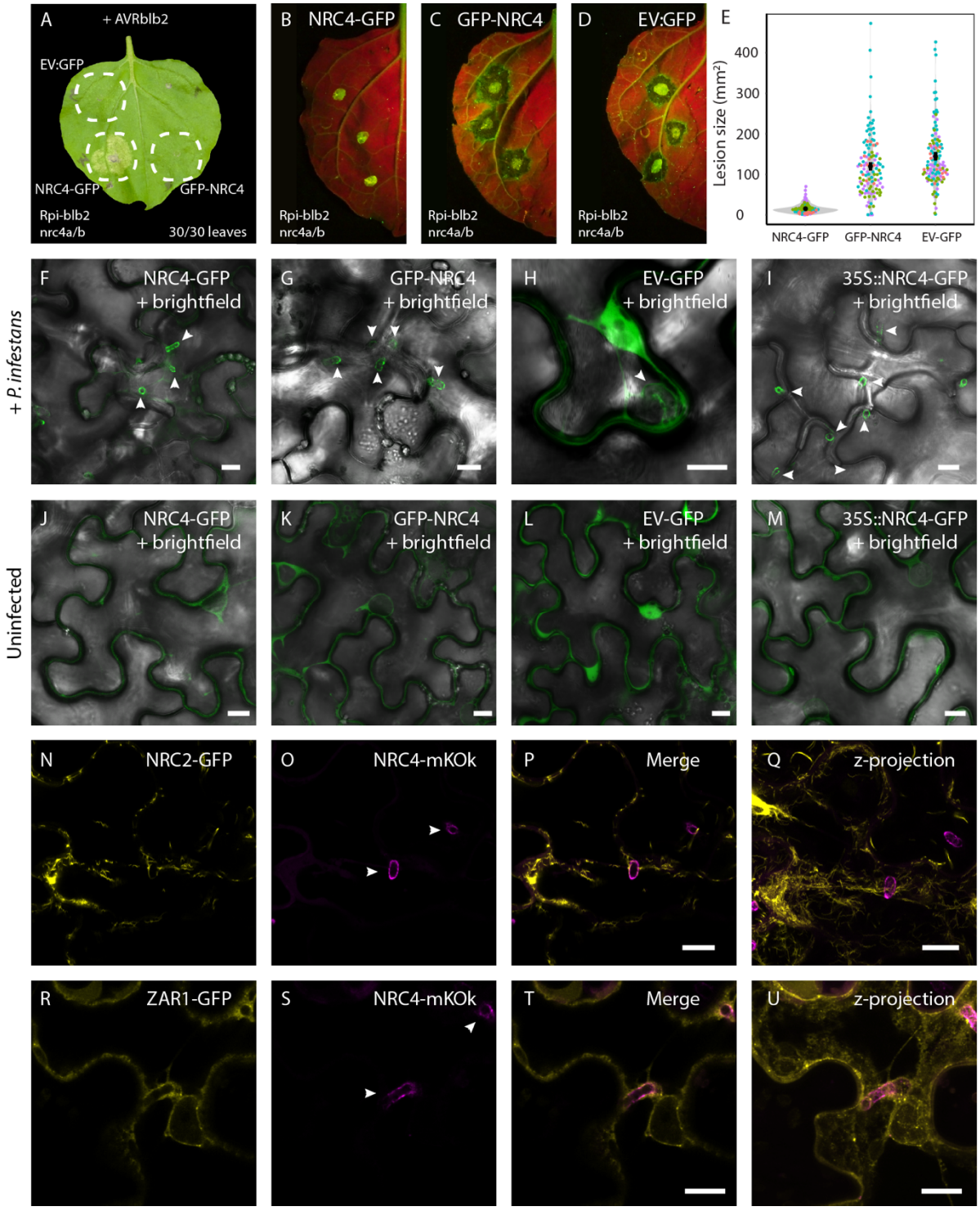


Figure 3.1: NRC4, but not NRC2 or ZAR1, accumulates at the EHM.
NRC4-GFP but not GFP-NRC4 or EV-GFP genetically complement CRISPR/Cas mutation of NRC4a/b in Rpi-blb2 transgenic background by triggering (A) HR when co-expressed with AVRblb2 and (B-E) resistance when expressed alone. (A) AVRblb2 was co-expressed with EV:GFP, NRC4-GFP or GFP-NRC4 in Rpi-blb2 nrc4a/b plants and after 8 days leaves were detached and photographed. The result was replicated in 30 leaves, over three independent biological reps where $N > 6$ leaves per rep. The result shown was seen in all leaves, i.e. yellowish HR cell death in NRC4-GFP patches, no HR cell death in EV:GFP or GFP-NRC4. (B-E) NRC4-GFP, GFP-NRC4

or EV:GFP were expressed separately in Rpi-blb2 nrc4a/b plants on half leaves. After one day these were detached and infected with *P. infestans.* After 8 days leaves were imaged with UV (shown) and white light, and the latter was used to quantify the lesion size. Points in scatter violin plot (E) represent the area (mm^2) occupied by infection spots measured on white light images, where each construct had $N > 116$ infection spots. Four independent biological reps were conducted. (F-H) Single plane confocal micrographs showing *Agrobacterium* mediated expression of NRC4-GFP and GFP-NRC4 but not EV-GFP, accumulates around *P. infestans* haustorium. (I) Transgenic *35S::NRC4-GFP* focally accumulates around pathogen haustoria. (J-L) *Agrobacterium* mediated expression of NRC4-GFP, GFP-NRC4 and EV-GFP all localise to the cytoplasm in uninfected cells. (M) Transgenic *35S::NRC4-GFP* also cytoplasmic in uninfected cells. (N-P) Single plane images transiently expressing NRC2-GFP with NRC4-mKOk during infection with *P. infestans* showing NRC2 does not focally accumulate around haustoria but localises to disperse filaments. (Q) Z-projection of 10 z-slices. (R-T) Single plane images transiently expressing ZAR1-GFP with NRC4-mKOk during infection with *P. infestans* showing ZAR1 does not focally accumulate around haustoria, but is diffuse in the cytoplasm. (U) Z-projection of 11 z-slices. All scale bars are 10 µm.

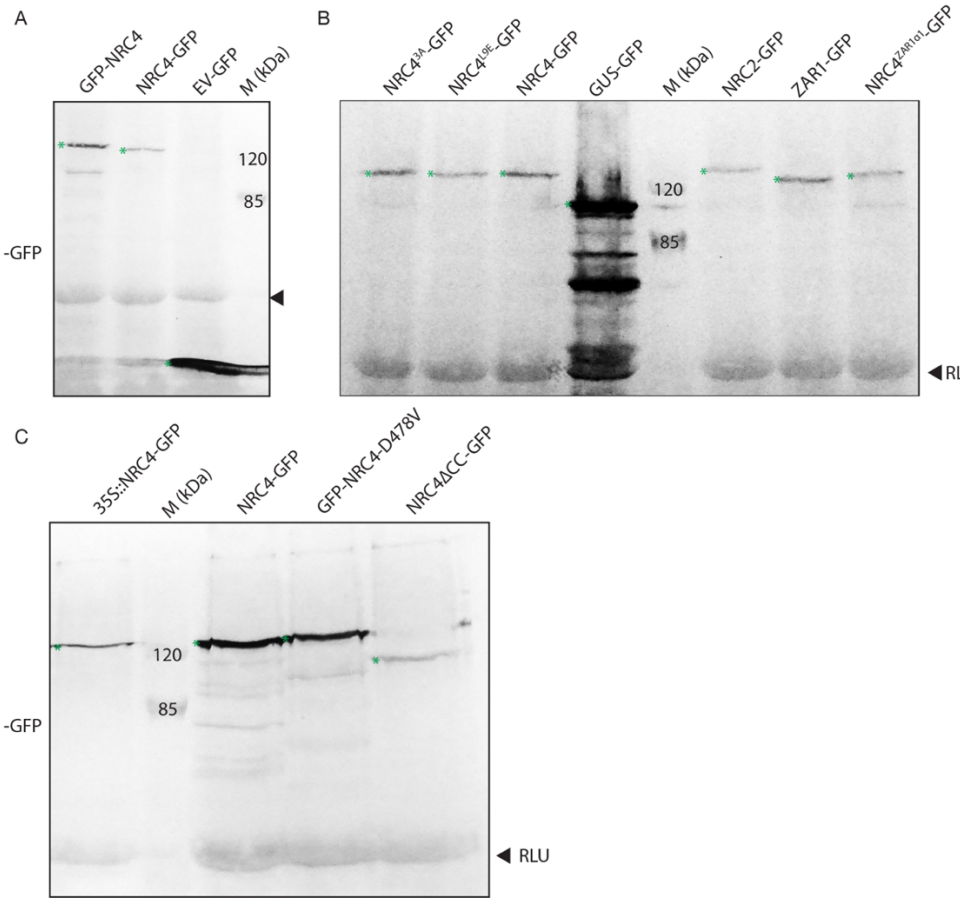


Figure 3.2: Western blot analysis shows studied NLRs stably produced.
(A) Constructs used in Figure 1A-E. (B) Constructs used in Figure 1N-U and Chapter 4. (C) Constructs used in Figure 1I & M and Chapter 4. RLU = Rubisco Large Subunit (loading control). For each lane, the expected band is highlighted with green star. M = Marker, kDa = kilodaltons.

3.4.1.2. NRC4 accumulates to an EHM microdomain

Sometimes during imaging, it is possible to monitor cells where the central vacuole shrinks, making it clearly distinguishable from the cytoplasm and the plasma membrane. This allowed me to observe some instances where NRC4-GFP signal was localised at the plasma membrane as well as the cytoplasm, in uninfected tissue (Figure 3.3A). Note that in Cell 1, NRC4 has little to no PM localisation, whereas in Cell 2, NRC4 shows strong PM localisation. NRC4 seems to vary in its PM association from cell to cell and most of time seemed to be cytoplasmic, not PM localised. Therefore I decided to determine the average localisation by carrying out membrane enrichment by protein extraction in sucrose buffer lacking detergents, followed by centrifugation at 21,000 *g* for one hour. To determine the efficiency of enrichment, I used tissue expressing the plasma membrane marker AtFLS2-GFP with NRC4-3xHA and used rubisco large subunit or EV:RFP to mark the cytoplasm. Western blotting of the samples revealed that NRC4 is in both the membrane-enriched fraction and the soluble fraction (Figure 3.3B), consistent with the localisation in confocal micrographs. It's difficult to say whether NRC4 is more or less associated with one fraction as these enrichment experiments rely on the assumption that the membrane pellet is completely resuspended. Additionally, to ensure adequate signal was detected, 9 times enrichment was loaded in my experiments, i.e. the membrane pellet was not resuspended in the same volume as the soluble fraction, 9 times less (or 3 times less in future experiments) was used to concentrate the sample.

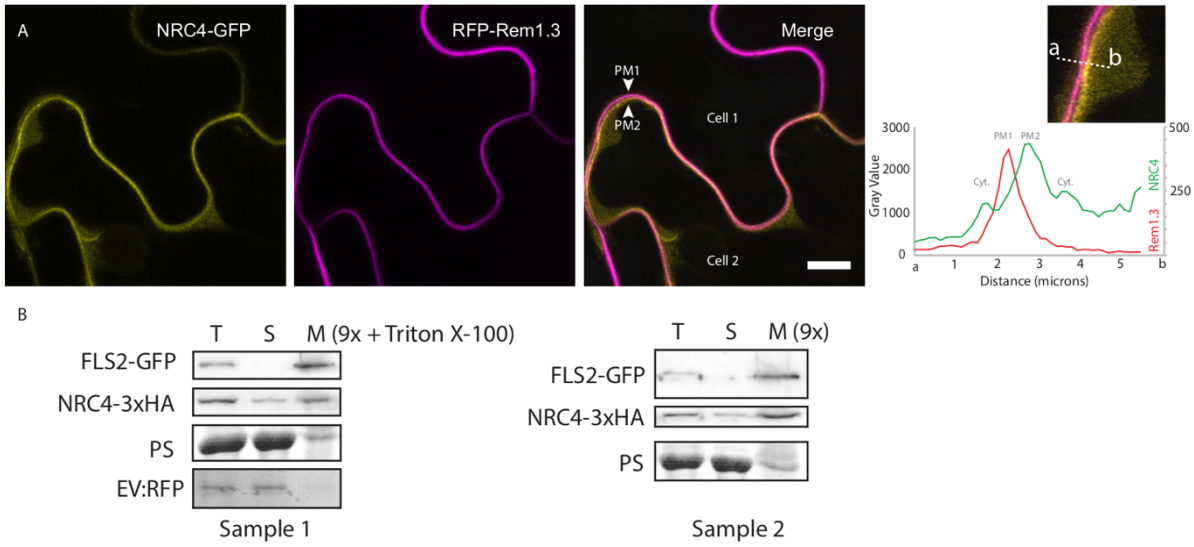


Figure 3.3: NRC4 associates with the plasma membrane as well as being cytoplasmic.
(A) NRC4-GFP was co-expressed with RFP-Rem1.3 in WT *N. benthamiana* leaves and imaged 3 dpai. Confocal imaging revealed instances where NRC4 localised to the plasma membrane. Here plasma membrane 2 (PM2) lacks PM marker Rem1.3 expression, but clearly peaks close to the cell periphery relative to the cytoplasmic signal. Scale bar is 10 µm (B) Membrane enrichment confirms NRC4 localises to soluble (cytoplasm) and membrane fractions. FLS2-GFP was used as a plasma membrane marker, rubisco large subunit (PS) was used as a cytoplasmic marker and in sample one EV:RFP was also included as cytoplasmic control (the blot for sample two was lost). NRC4-3xHA, FLS2-GFP and EV:RFP were co-expressed in WT *N. benthamiana* leaves for 3 days. Leaves were frozen in liquid nitrogen and extracted in sucrose buffer lacking detergents and after clearing the debris the Total fraction (T) was taken before the rest of the extract was centrifuged at 21,000 *g* for 1 h at 4˚C. The supernatant was taken as the Soluble (S) sample and the pellet was taken as the Membrane-enriched (M) sample, which was resuspended in 9 times less buffer than the S sample. Triton X-100 detergent was added to sample one membrane fraction. Ponceau stain (PS) was used to determine protein loading and cytoplasmic protein levels.

To determine if this is the localisation of NRC4 during basal conditions (in the absence of infection or *Agrobacterium* challenge), we carried out the experiment with *35S::NRC4-GFP* transgenics, in the absence of any challenge with *Agrobacterium* (Figure 3.4). Interestingly, the resulting western blot showed strong signal of NRC4 in the soluble fraction. Note that the loading in this experiment was 1X and 3X for the membrane enriched sample, and that the total fraction appears to have less loading than the soluble fraction – this could be due to protein degradation of this fraction during the spin cycle of the Soluble/Membrane fractions. In conclusion from these

experiments, NRC4 appears to be mostly cytoplasmic in absence of any pathogen challenge, but certainly also associates with membranes to a lesser extent.

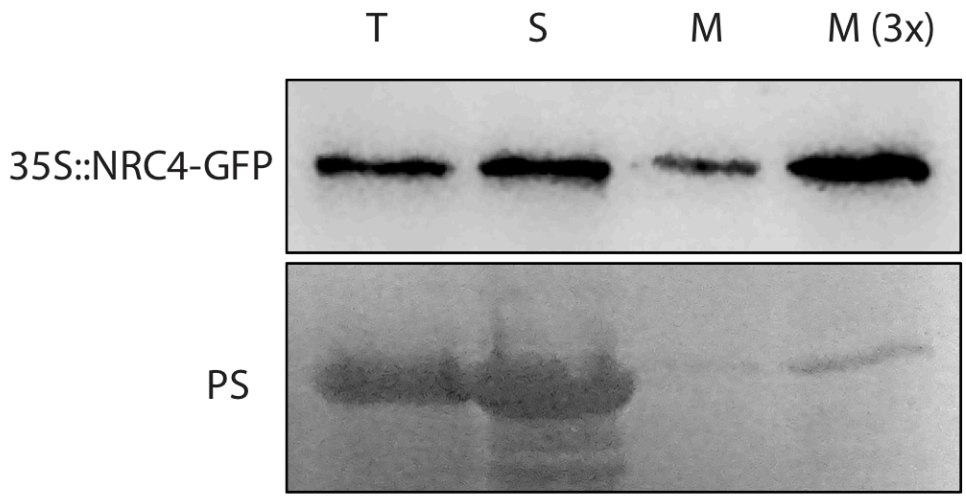


Figure 3.4: Membrane enrichment of transgenically expressed NRC4-GFP, in the absence of *Agrobacterium* or pathogen challenge, shows NRC4 is more cytoplasmic than membrane localised.
Transgenic 35S::NRC4-GFP plants were frozen and extracted under non-denaturing conditions in sucrose buffer, then soluble and crude membrane fractions were generated by centrifugation at 21,000 *g* for one hour. Membrane pellet was resuspended to three times less volume of extraction buffer as the soluble fraction to concentrate it (3x) and with the same volume. No membrane marker was included as the antibody for H^+ ATPase was not functional. Membrane fraction was included in 1x and 3x dilutions. T = Total fraction, S = Soluble fraction, M = Membrane fraction. Ponceau stain (PS) was used to determine protein loading and cytoplasmic protein levels.

To exclude the possibility that perihaustorial signal of NRC4 was originating from the cytoplasmic strip surrounding the EHM, I co-expressed a cytoplasmic marker, free GFP (EV:GFP), with NRC4 during infection. This revealed distinct localisation patterns of both proteins, where NRC4 signal peaks closer to haustoria which is engulfed by the thin layer of adjacent cytoplasm (Figure 3.5A). I repeated this experiment with PM/EHM marker YFP-Rem1.3, cytoplasmic marker EV:BFP and NRC4-mKOk (Figure 3.5B). NRC4 and Rem1.3 partially co-localised at the EHM whereas EV:BFP signal peaked before the NRC4 and Rem1.3 peaks as before indicative of the cytoplasm surrounding the haustorium. Next, to determine if NRC4 changes its association for membranes during infection I carried out membrane enrichment of uninfected and infected tissue (Figure 3.5C). Interestingly, NRC4 appeared to be enriched in the soluble fraction during infection. However, the membrane fraction of the uninfected

sample was contaminated with soluble markers (BFP-3xHA and Rubisco LSU). Additionally, there was more overall signal of NRC4 in the infected tissue, which could have amplified the signal in the soluble fraction. This is a preliminary observation as the experiment hasn't been reproduced to date, but is interesting as the plants used in this experiment are constitutively expressed *35S::NRC4-GFP* transgenics, meaning if this increase in NRC4 protein levels upon infection is reproducible, it probably would be due to a stabilisation of the protein levels. It's important to note that the EHM constitutes a tiny proportion of membranes of infected tissue, and therefore it is in fact unlikely we would detect it with this experiment. Nevertheless, this experiment indicates that biochemically it is not easy to determine NRC4 distribution in *P. infestans* challenged tissue. We require discovery of a biochemical way of isolating or enriching the EHM to show NRC4 EHM association through biochemical means.

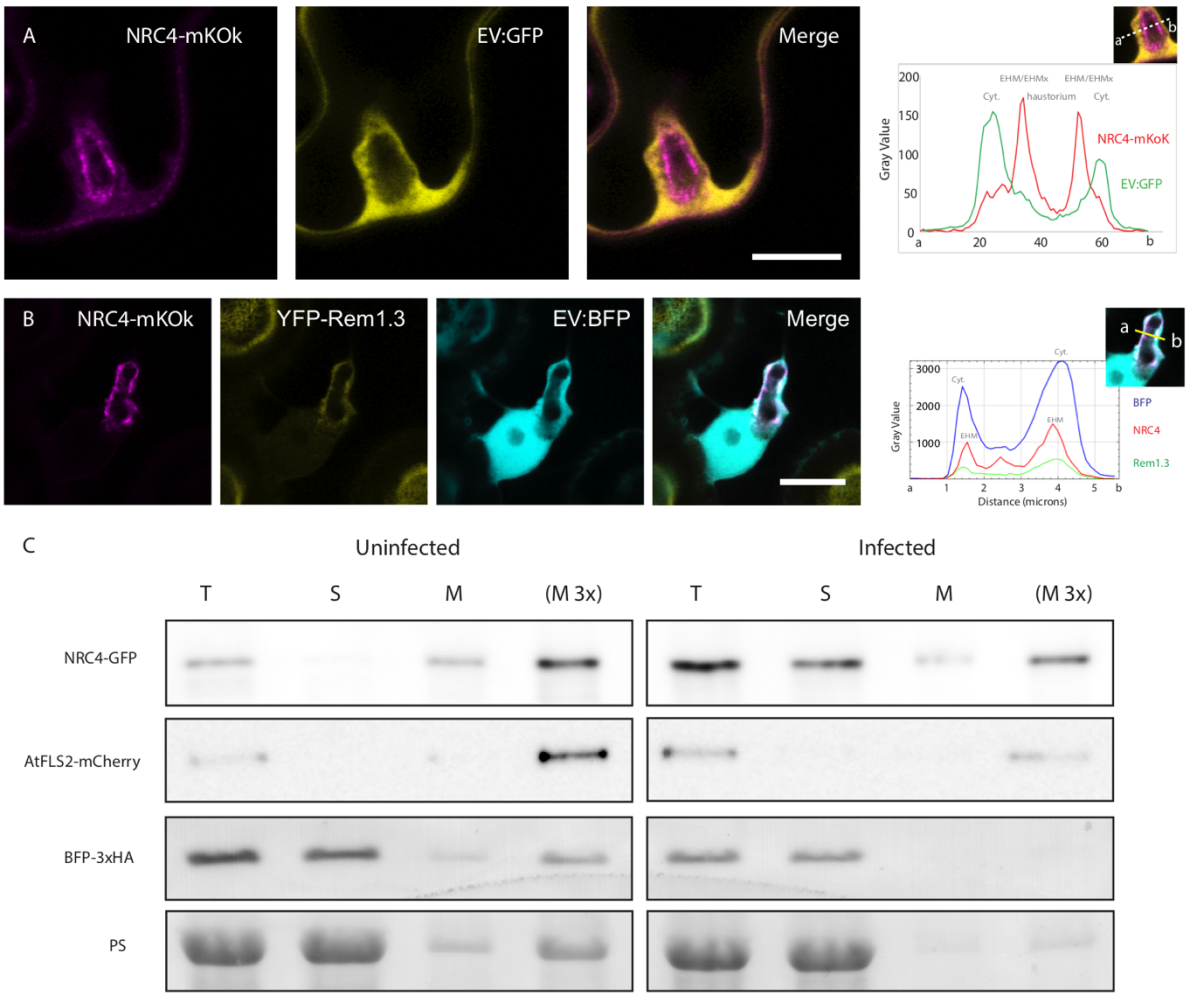


Figure 3.5: NRC4 accumulates at the EHM during infection with *P. infestans*. (A) NRC4-mKOk peak fluorescence is found internal (at EHM) to that of EV:GFP (cytoplasm) during infection with *P. infestans* 88069.(B) Peak fluorescence of NRC4 and EHM marker co-localise on the haustorial side of the cytoplasmic marker EV:BFP. Scale bars = 10µm (C) Membrane fractionation was inconclusive in revealing differential membrane association between infected and uninfected tissue. NRC4-GFP, AtFLS2-mCherry and BFP-3xHA were co-expressed in WT *N. benthamiana.* After 3 hours these were detached and one side of the leaves was infected with *P. infestans* spores, the other was treated with mock (water). These were left for 3 days and then #3 cork borer was used to take leaf disks centered on the infection droplets.. Disks were frozen in liquid nitrogen and extracted in sucrose buffer lacking detergents and after clearing the debris the Total fraction (T) was taken before the rest of the extract was centrifuged at 21,000 *g* for 1 h at 4˚C. The supernatant was taken as the Soluble (S) sample and the pellet was taken as the Membrane-enriched (M) sample, which was resuspended in 3 times less buffer than the S sample. Ponceau stain (PS) was used to determine protein loading and cytoplasmic protein levels.

It is important to determine the precise localisation of NRC4 during infection, as it is essential to find out how NRC4 is transported to these sites which could provide insights into activation of immunity. However, as illustrated earlier (Chapter 1, Figure 2) various sub-compartments engulf haustoria (perihaustorial compartments) and previous research revealed that even the EHM itself is not uniform (Bozkurt et al., 2014; Bozkurt and Kamoun, 2020). This makes it highly complicated to determine precisely to which perihaustorial compartment the protein of interest localizes, especially without using specific markers. To determine NRC4's localisation, I co-expressed fluorescent fusion proteins (FPs) of NRC4 in combination with well-established EHM markers.

Here, I show that the fluorescent signal of NRC4-FPs partially but not fully peak with the tested perihaustorial markers (Figure 3.6). The plasma membrane and EHM marker StRemorin1.3 fused to RFP (RFP-Rem1.3) produced signal that partially overlapped with NRC4-GFP signal, indicating imperfect colocalization of these proteins around haustoria (Figure 3.6A). Thereafter, I elected to use the peripheral membrane protein Synaptotagmin 1 (SYT1), which was previously shown to label ER in close contact with the EHM (Bozkurt unpublished) and discrete subdomains of the EHM that are not labelled by StRemorin1.3 (Bozkurt et al., 2014; Lu et al., 2012). When co-expressed, NbSYT1 partly but not fully colocalized with NRC4 around haustoria (Figure 3.6B).

I decided to perform colocalization experiments with AtRPW8.2 which has been extensively characterised as a marker for EHM of fungal pathogens in *Arabidopsis thaliana* (Castel et al., 2019b; Wang et al., 2013, 2009; Xiao et al., 2001; Zhang et al., 2015). Additionally, it has been reported to localise around haustoria during infection of *A. thaliana* with *Hyaloperonospora arabidopsidis* Noco2 (Wang et al., 2009). Therefore, I tested this atypical R-protein RPW8.2-YFP (Wang et al., 2009), kindly provided by Prof Shunyuan Xiao of the University of Maryland. Interestingly, not only did RPW8.2-YFP accumulate around haustoria of *P. infestans* in *N. benthamiana*, but it partially co-localised with NRC4-mKOk along the EHM (Figure 3.6C). However, NRC4 was not seen in vesicles which were reported to be involved transport of RPW8.2 (arrowheads) to the EHM (Kim et al., 2014). We cloned a BFP tagged RPW8.2 (RPW8.2-BFP) and co-expressed it with RFP-Rem1.3 and NRC4-GFP. I

found that Remorin and RPW8.2 display similar localisation patterns compared to NRC4, however there were some fluorescent peaks that overlapped between RPW8.2 and NRC4 (Figure 3.6D). Overall these data indicate NRC4 is present at an EHM subdomain of *P. infestans* 88069 haustoria.

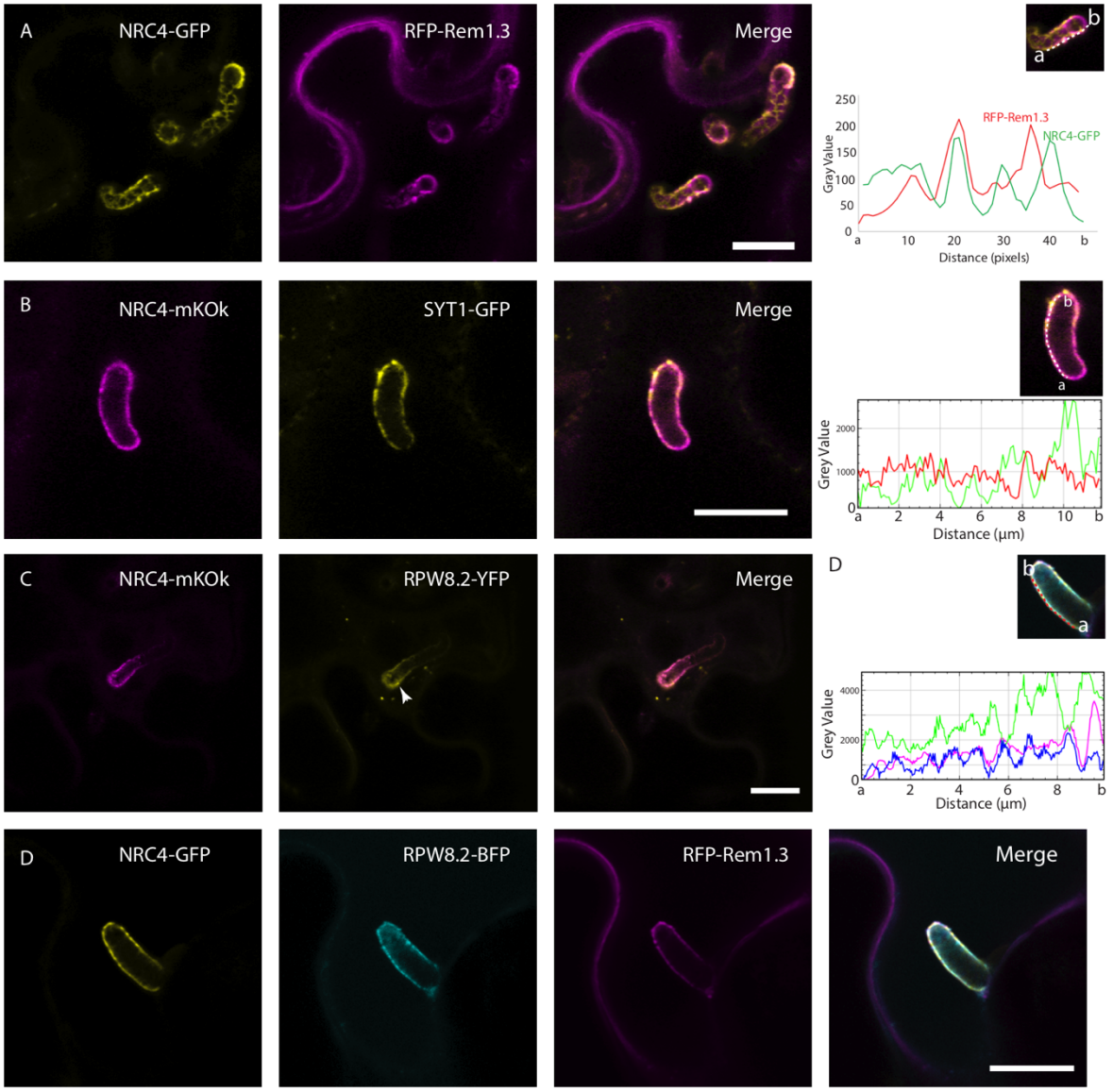


Figure 3.6: NRC4 localises to an EHM microdomain, partially but not fully co-localising with EHM markers.
NRC4-GFP or NRC4-mKOk (orange/red colour) were co-expressed with RFP-Rem1.3, SYT1-GFP, RPW8.2-YFP or RPW8.2-BFP in WT *N. benthamiana* leaves. After 3 hours the leaves were infected with *P. infestans* and images taken using SP5 confocal microscope (A-C) or SP8 confocal microscope (D) after 3 days. Line profiles drawn along the EHM show the peaks of the EHM localised proteins and whether they peak together or not demonstrates if they occupy the same niche. (A) NRC4- GFP shows a similar but not identical localisation to the EHM marker *Solanum tuberosum* StRFP-Remorin1.3 (RFP-Rem1.3). (B) NRC4-mKOk shows a perihaustorial localisation mostly exclusive to that of GFP-SYT1. (C) *A. thaliana* RPW8.2-YFP co-localises with NRC4-mKOk at haustoria. Some vesicles of YFP are not labelled by NRC4, including one at the EHM (arrowhead). (D) NRC4-GFP has a similar but different EHM localisation than RPW8.2-BFP and RFP-Rem1.3. Scale bars = 10µm.

Interestingly, NRC4 often displayed an ER-/cage-like distribution around haustoria (Figure 3.7A). This prompted me to test whether NRC4, despite lacking a signal peptide, was localising to the ER, which was previously found to surround haustoria (Bozkurt and Kamoun, 2020). Therefore, I co-expressed NRC4-GFP with secreted RFP containing an ER-retention signal (HDEL) on its C-terminus. The two FPs showed almost mutually exclusive localisation patterns around haustoria (Figure 3.7A). I also cloned an ER retention signal onto NRC4, NRC4-GFP-HDEL, and expressed this with the ER marker or WT NRC4, to determine if NRC4 was shuttling through the ER despite lacking a *predicted* signal peptide (**Error! Reference source not found.**B-C). Again, the peri-haustorial localisation patterns were mostly mutually exclusive, whereas WT NRC4-mKOk colocalised with NRC4-GFP-HDEL in the cytoplasm. I next investigated whether the cage-like NRC4 labelling was due to association with the cytoskeletal markers Actin-YFP or AtMAP4-GFP (Microtubule marker; Kindly provided by Dr Buschmann, Osnabrück). While both showed some perihaustorial association, neither co-localised with NRC4 in a cage-like manner (Figure 3.8A-B).

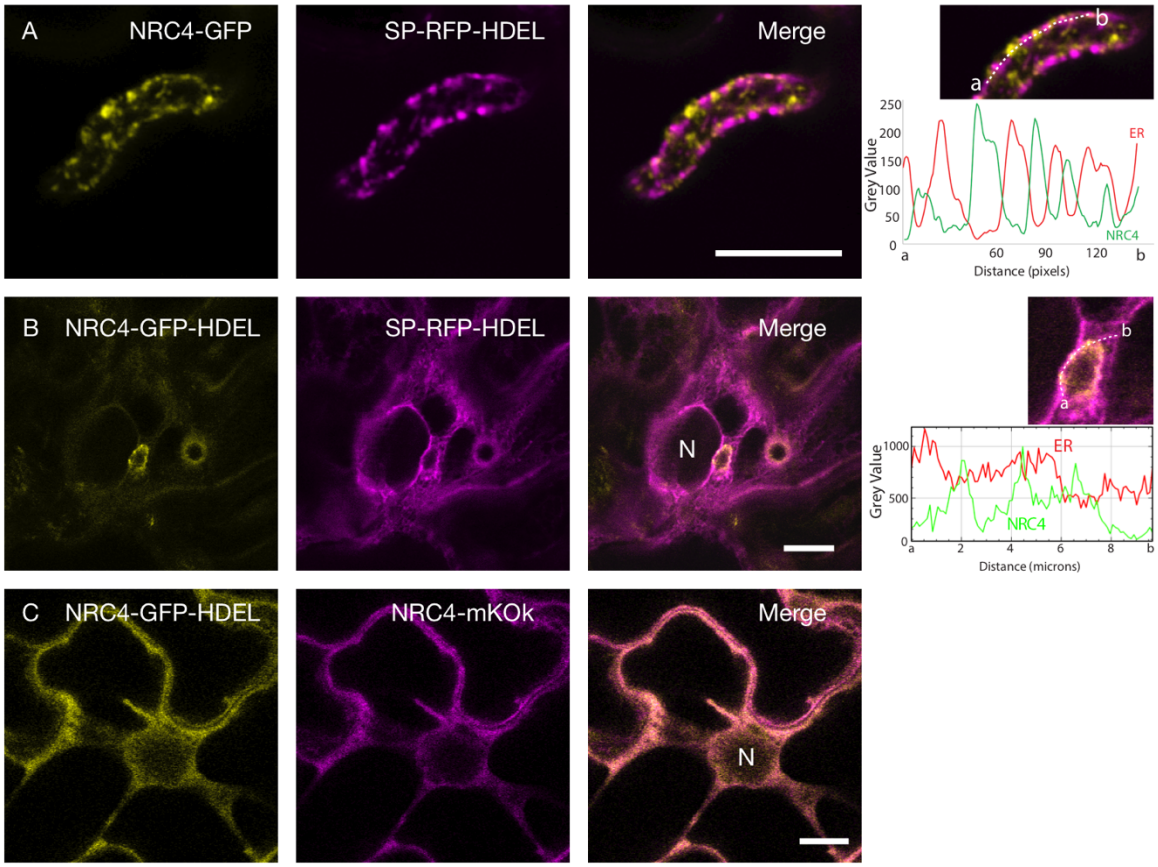


Figure 3.7: NRC4 cage-like haustorial structure is not due to localisation to ER surrounding the EHM.
NRC4-GFP or NRC4-GFP-HDEL were co-expressed with SP-RFP-HDEL or NRC4-mKOk in WT *N. benthamiana* leaves. After 3 hours the leaves for A-B were infected with *P. infestans.* Images were taken using SP5 confocal microscope (B-C) or SP8 confocal microscope (A) after 3 days. Line profiles drawn along the EHM show the peaks of the proteins here and that NRC4 does not peak in the same place as the ER marker. (A) NRC4-GFP shows perihaustorial localisation exclusive to that of secreted RFP tagged with an ER retention signal (SP-RFP-HDEL). (B) NRC4 cloned to have an ER-retention signal, NRC4-GFP-HDEL, does not co-localise with SP-RFP-HDEL in haustoriated cells (D) NRC4-GFP-HDEL co-localises with NRC4-mKOk in uninfected cells. N = Nucleus. Scale bars = 10μm

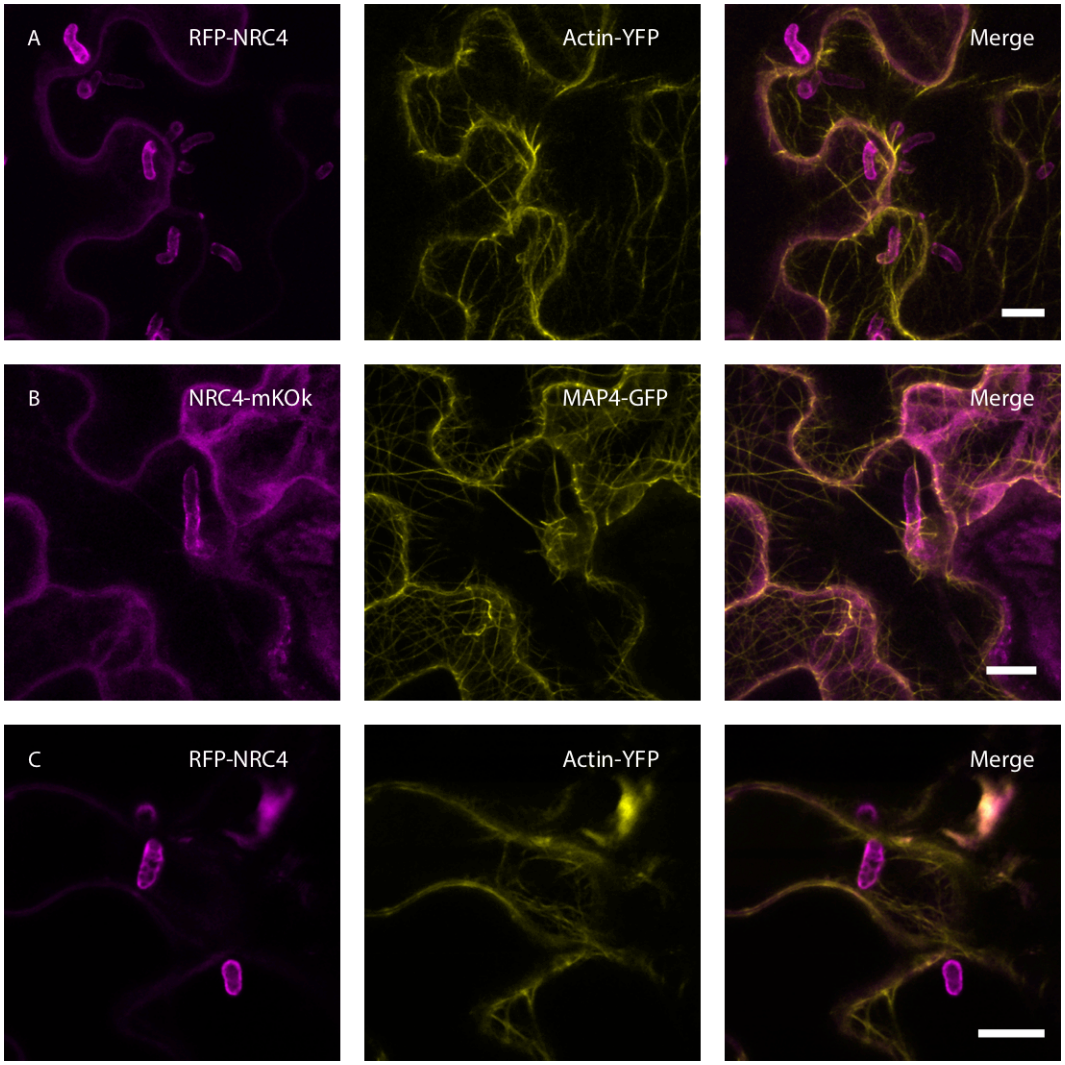


Figure 3.8: NRC4 perihaustorial cage-like localisation pattern does not co-localise with cytoskeletal markers.
RFP-NRC4 or NRC4-mKOk were co-expressed Actin-YFP or MAP4-GFP (microtubule marker) in WT *N. benthamiana* leaves. After 3 hours the leaves were infected with *P. infestans.* Images were taken using SP5 confocal microscope after 3 days. Maximum intensity z-projections of 12 and 15 slices respectively from *N. benthamiana* epidermal leaf cells co-expressing NRC4 with (A) Actin-YFP, which shows some association with haustoria but not co-localisation with NRC4; and (B) the microtubule marker MAP4-GFP, which shows some association with haustoria but not co-localisation with NRC4. Scale bars = 10μm

To determine whether the perihaustorial signal of NRC4 is originating from the matrix between the EHM and the pathogen haustorial membrane, i.e. the extrahaustorial matrix (EHMx), we established a collaboration with Shumei Wang and Paul Birch from James Hutton Institute, Scotland. They supplied us with a transgenic strain of *P. infestans* that expresses cytoplasmic GFP and an RFP tagged RXLR effector protein, which has the RXLR and EER motifs mutated to Alanine in every position, reducing the efficiency of translocation into host cells, effectively trapping it in the EHMx (personal communication with Dr Petra Boevink, James Hutton Institute). I infected tissue agro-expressing NRC4-BFP with this strain. This effector protein accumulates in the EHMx, whereas NRC4's signal peaks on the plant side, indicative of EHM localisation (Figure 3.9).

In conclusion, the results presented in this section demonstrate that NRC4 is dispersed throughout the periphery of the cell prior to infection with *P. infestans.* Upon infection, NRC4 accumulates at an EHM microdomain.

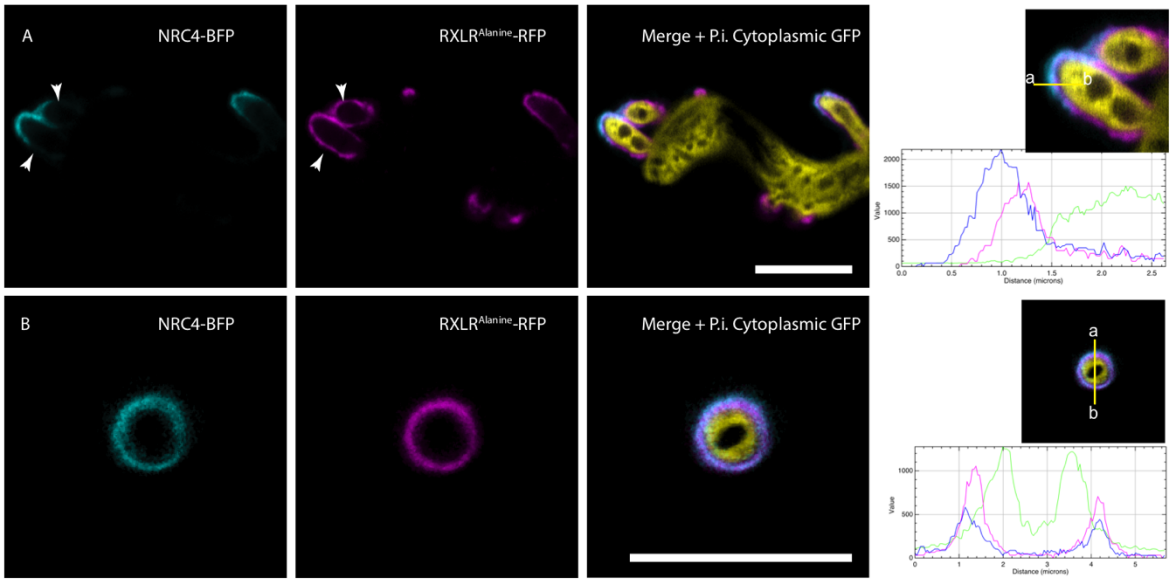


Figure 3.9: Fluorescent signal from NRC4 peaks on the host side of an EHMx marker.
NRC4-BFP was expressed WT *N. benthamiana* leaves and after 3 hours the leaves were infected with transgenic *P. infestans* expressing GFP in its cytoplasm (P.i. Cytoplasmic GFP) and secreting an RFP-tagged RXLR effector protein, that has the RXLR and EER motifs mutated to alanine to reduce the translocation into the host (RXLR^{Alanine}-RFP). Images were taken using SP8 confocal microscope after 3 days. Line profiles drawn from vacuole to pathogen cytoplasm show the peak localisations of the proteins. (A) is a side/sagittal/longitudinal view of haustoria and (B) is a top/transverse view.

Since phospholipids are major components of all cell membranes, I decided to employ several established phospholipid markers to investigate whether any of them label the EHM and colocalise with NRC4. In addition, ß-glucan callose is often deposited at the site of infection, resulting in the production of callosic-encasements that could entrap cytoplasm around the haustorium. These encasements were shown to fully engulf the haustoria of fungal or oomycete pathogens in *Arabidopsis*, whereas they are detected in only the neck of around 20% *P. infestans* haustoria in *N. benthamiana* (Ellinger and Voigt, 2014).

To assess whether NRC4 accumulation around the haustoria is due to callose encasements, I used a blue-dye stain and organic fluorophore, aniline blue which stains callose (Bozkurt et al., 2011). In addition to callose labelling, I also used phospholipid markers (phosphatidylinositol 4-phosphate-binding domain, PI4P; phosphatidylinositol 3-phosphate, PI3P; phosphatidylinositol 4,5-bisphosphate binding domain, PIP_2) (Simon et al., 2014) to further characterise the EHM and try to determine the phospholipid composition of the NRC4 microdomain. This revealed that callose deposits were restricted only to the neck of haustoria (Figure 3.10), which is in agreement with the findings of Bozkurt et al. (2014), whereas I did not detect any correlation with NRC4 and callose accumulation. Interestingly, although PI4P did not label most of the EHM, it showed a clear localization pattern to callose deposits (Figure 3.10A). PIP_2 and PI3P phospholipid markers did not show any colocalization with NRC4 or the callose deposits (Figure 3.10B-C). These experiments indicate that NRC4 perihaustorial fluorescence does not originate from callosic encasements but instead NRC4 localises to an EHM microdomain. Similar findings were recently published with the same PI4P and PIP_2 biosensors (Rausche et al., 2020). They found that the PI4P biosensor labelled the EHM in neck regions, but the PIP_2 marker did not – in fact it labelled the cytoplasm surrounding the EHM which correlates with my finding.

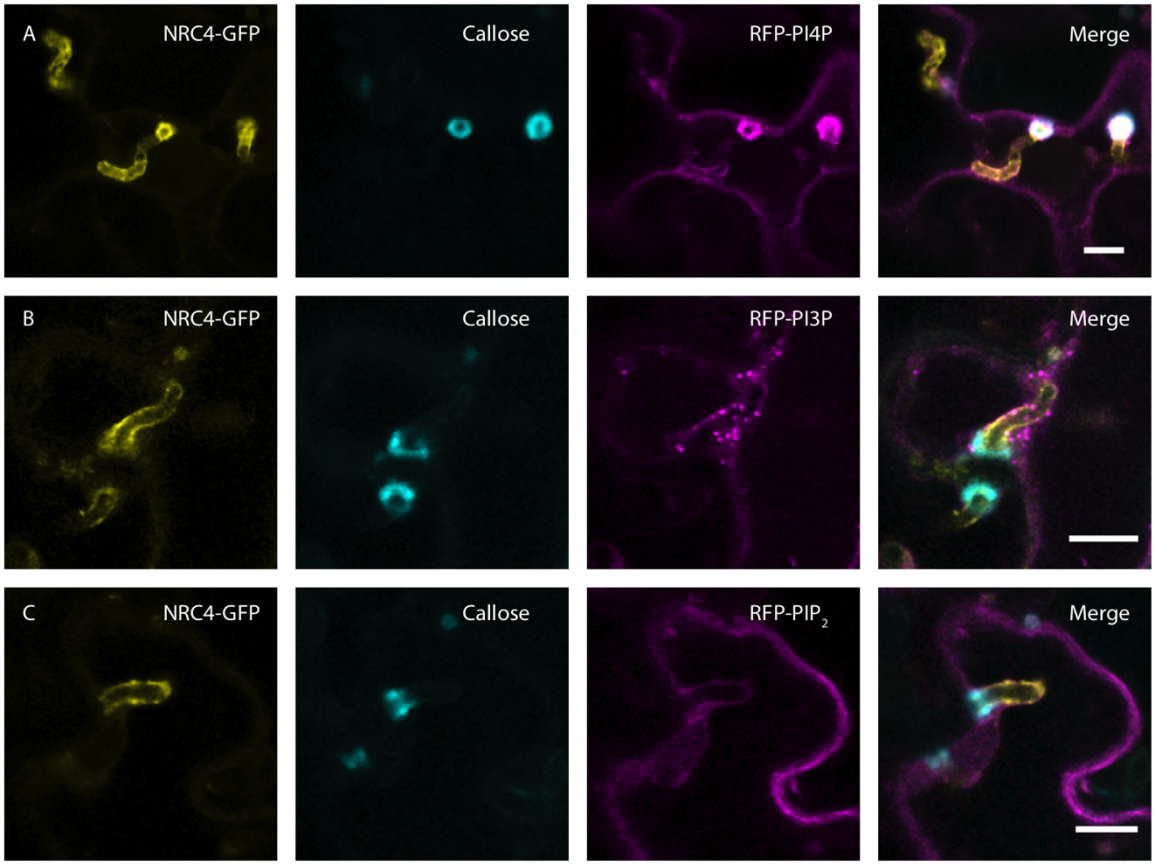


Figure 3.10: NRC4-GFP fluorescence does not originate from to callose deposits.
NRC4-GFP was co-expressed with either RFP-PI4P, RFP-PI3P or RFP-PIP_2 in WT *N. benthamiana* leaves. After 3 hours the leaves were infected with *P. infestans.* Alanine blue staining of haustoria, 1hr prior to imaging with UV lasers, revealed callose to be constrained to the neck of haustoria, when present. Images were taken using SP5 confocal microscope after 3 days. (A) PI4P binding domain fused to RFP showed highly similar localisation to the callose deposits at haustoria, as well as membrane localisation. (B) – (C) Binding domains for PI3P and PIP_2 fused to RFP did not show the same localisation. Scale bars = 10µm.

3.4.1.3. Rpi-blb2 does not accumulate at the EHM, but instead remains diffuse throughout the cytoplasm

For the Rpi-blb2 resistance pathway to be functional, AVRblb2, Rpi-blb2 and NRC4 are required (Wu et al., 2017). I therefore set out to investigate their localisation during infection. First, we cloned BFP-AVRblb2 and confirmed that AVRblb2 localizes to discrete EHM microdomains (i.e. not linearly labelled) labelled by StRemorin1.3 (Bozkurt et al., 2015, 2014, 2011), even in the absence of NRC4 and Rpi-blb2 (Figure 3.11A), when expressed in the NRC4 mutant *N. benthamiana* plants (nrc4a/b) kindly provided by Dr Chih-Hang Wu (TSL, Norwich, UK) (Adachi et al., 2019). AVRblb2 partially, but not fully, co-localised with GFP-NRC4 (Figure 3.11B).

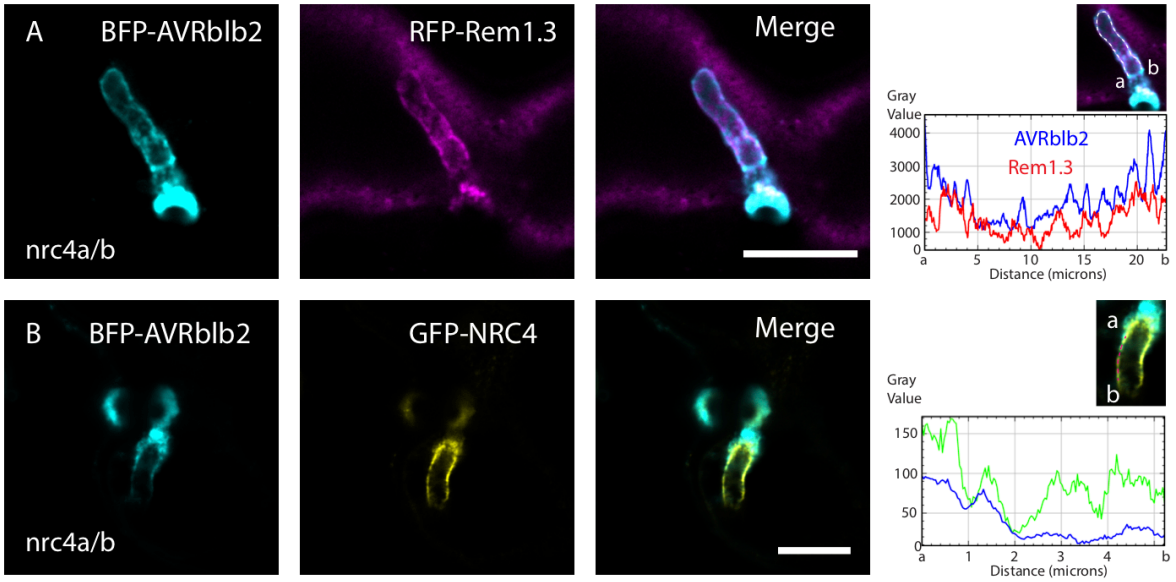


Figure 3.11: AVRblb2 localises to an EHM microdomain in the absence of NRC4 and in the presence of NRC4 partially co-localises with it.
BFP-AVRblb2 was co-expressed with either EHM/PM marker RFP-Rem1.3 or GFP-NRC4 in nrc4a/b mutant plants. After 3 hours, leaves were infected with *P. infestans* and after 3 days, imaged with SP8 confocal microscope. AVRblb2 accumulates at the EHM in the presence or absence of NRC4. Line profile along the EHM was used to determine the relative peaks of EHM localised proteins. The signal of AVRblb2 and NRC4 partially overlaps at the EHM. Scale bars are 10 µm.

For functional resistance, the model of helper-sensor immunity is that the helper and sensor directly interact (Cesari, 2017; Jubic et al., 2019). It is unknown if Rpi-blb2 and NRC4 directly interact as purification is extremely challenging and yeast two hybrid has not been attempted. I investigated the localisation of Rpi-blb2 with NRC4 during infection. I achieved this using N-terminally tagged NRC4 which is deficient in cell

death but functional in terms of its ability to accumulate at the EHM (Figure 3.1 & S1 Figure 3.19). Using the EHM marker RFP-Rem1.3, I found that in the absence of NRC4, like EV-GFP (Figure 3.12A), Rpi-blb2 did not accumulate at the EHM but instead remained cytoplasmic, including the cytoplasmic strip around the EHM (Figure 3.12B). Upon complementation with RFP-NRC4, Rpi-blb2 remained cytoplasmic in infected cells (Figure 3.12C). This was surprising as it raises the question of how and where AVRblb2 recognition takes place, and how activated Rpi-blb2 activates NRC4. There are two models for how these processes could occur. Firstly, Rpi-blb2 could transiently accumulate at the EHM, detect AVRblb2 and activate NRC4, before dissociating and diffusing throughout the cytoplasm. This so called 'kiss-and-run' model could explain why we did not see Rpi-blb2 accumulation. Alternatively, Rpi-blb2 may not require accumulation at the EHM for AVRblb2 detection and/or NRC4 activation. These processes could occur directly through contact of cytoplasm surrounding the EHM, or by an indirect mechanism.

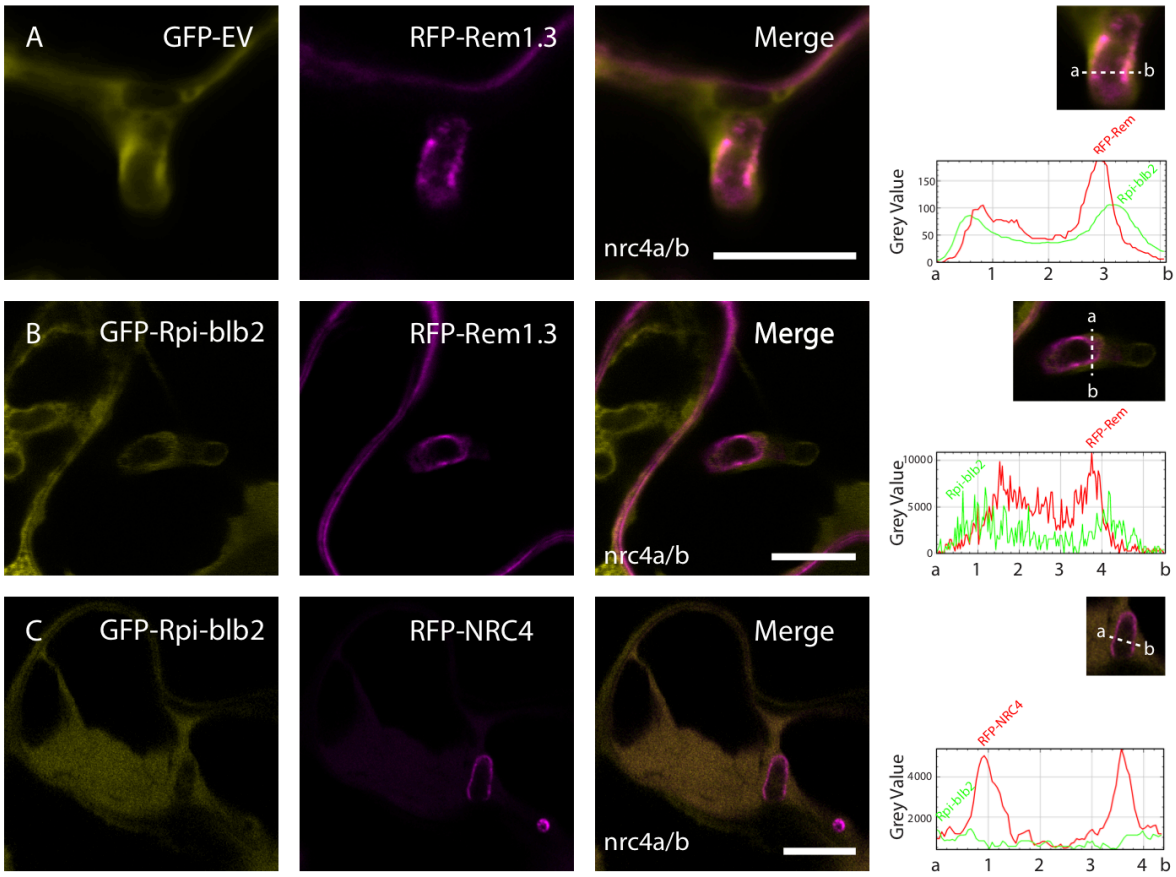


Figure 3.12: Rpi-blb2 is cytoplasmically distributed in the presence of haustoria. GFP-EV or GFP-Rpi-blb2 was co-expressed with either EHM/PM marker RFP-Rem1.3 or RFP-NRC4 in nrc4a/b mutant plants. After 3 hours, leaves were infected with *P. infestans* and after 3 days, imaged with SP8 confocal microscope. Line profile across the EHM, from the cytoplasm was used to determine the whether the GFP protein peaked in the cytoplasm or at the EHM. (A) EV-GFP does not focally accumulate, but is present around the EHM. (B) In the absence of NRC4, Rpi-blb2 does not focally accumulate but remains cytoplasmically distributed. (C) In the presence of HR deficient RFP-NRC4, Rpi-blb2 does not focally accumulate at the EHM but remains cytoplasmic. Scale bars are 10 μm.

3.4.1.4. Association between Rpi-blb2 and AVRblb2 was not detectable by in planta co-immunoprecipitation

To investigate whether Rpi-blb2 associates with AVRblb2, I carried out a series of co-immunoprecipitation experiments with Rpi-blb2 and AVRblb2 in the presence and absence of NRC4. First, I used an existing clone of RFP-AVRblb2 variant PITG_04085, which triggers weak HR compared to the RD40/PITG_20300 (Belhaj et al., unpublished). I pulled down GFP-Rpi-blb2 and was easily able to detect RFP-NRC4 in the IP, validating previous unpublished experiments by Dr Tolga Bozkurt and Dr Chih-Hang Wu. Some weak signal for RFP-PITG_04085 was detected in the IP but

it also came non-specifically with the EV:GFP pull-down, indicating RFP-PITG_04085 binds to the beads (Figure 3.13). This problem was previously reported for AVR3a (Engelhardt et al., 2012). Since the reciprocal pull-down would likely lead to saturation of the abundant effector on the beads and poor signal from the sensor NLR, I did not attempt this experiment. Instead I swapped the tags, and carried out an RFP pull down of RFP-Rpi-blb2 and attempted to detect association with the AVRblb2 allele PITG_20300 which was reported to trigger intense HR (Bozkurt et al., 2011; Oh et al., 2014). Unfortunately, the cleavage products of RFP-Rpi-blb2, which matched the size of GFP-AVRblb2, were also pulled down and may well have been detected in the GFP immunoblot (Figure 3.14). In conclusion, I was unable to confirm or deny an interaction between Rpi-blb2 and AVRblb2.

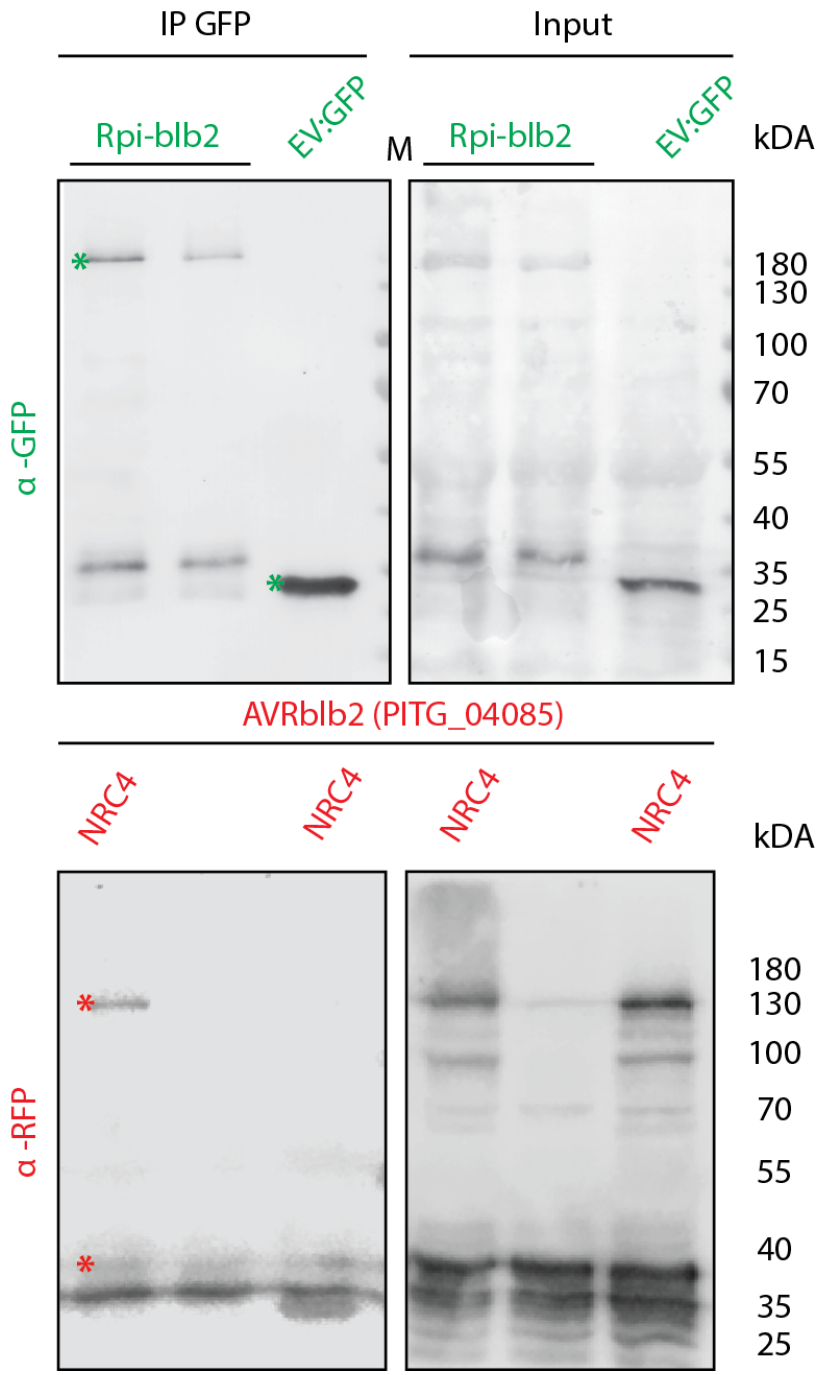


Figure 3.13: NRC4 co-immunoprecipitates with Rpi-blb2 but AVRblb2 pulls down non-specifically.
In planta co-immunoprecipitation or proteins extracted 3 dpai. RFP-AVRblb2 (PITG_04085) was transiently co-expressed with either GFP-Rpi-blb2 or EV-GFP and RFP-NRC4. IPs were obtained with GFP-trap agarose beads, and GFP and RFP was immunoblotted along with total protein extracts (input). Samples were separated on a 4-16% gradient SDS-PAGE gel and PageRuler Prestained Protein Ladder was used to determine approximate kilodaltons (kDa). Asterisks indicate expected band sizes for proteins in that sample. GFP-Rpi-blb2 was predicted to be ~175 kDa, RFP-NRC4 was predicted to be ~130 kDa, EV:GFP 27kDa and RFP-AVRblb2 was predicted to be ~ 35 kDA.

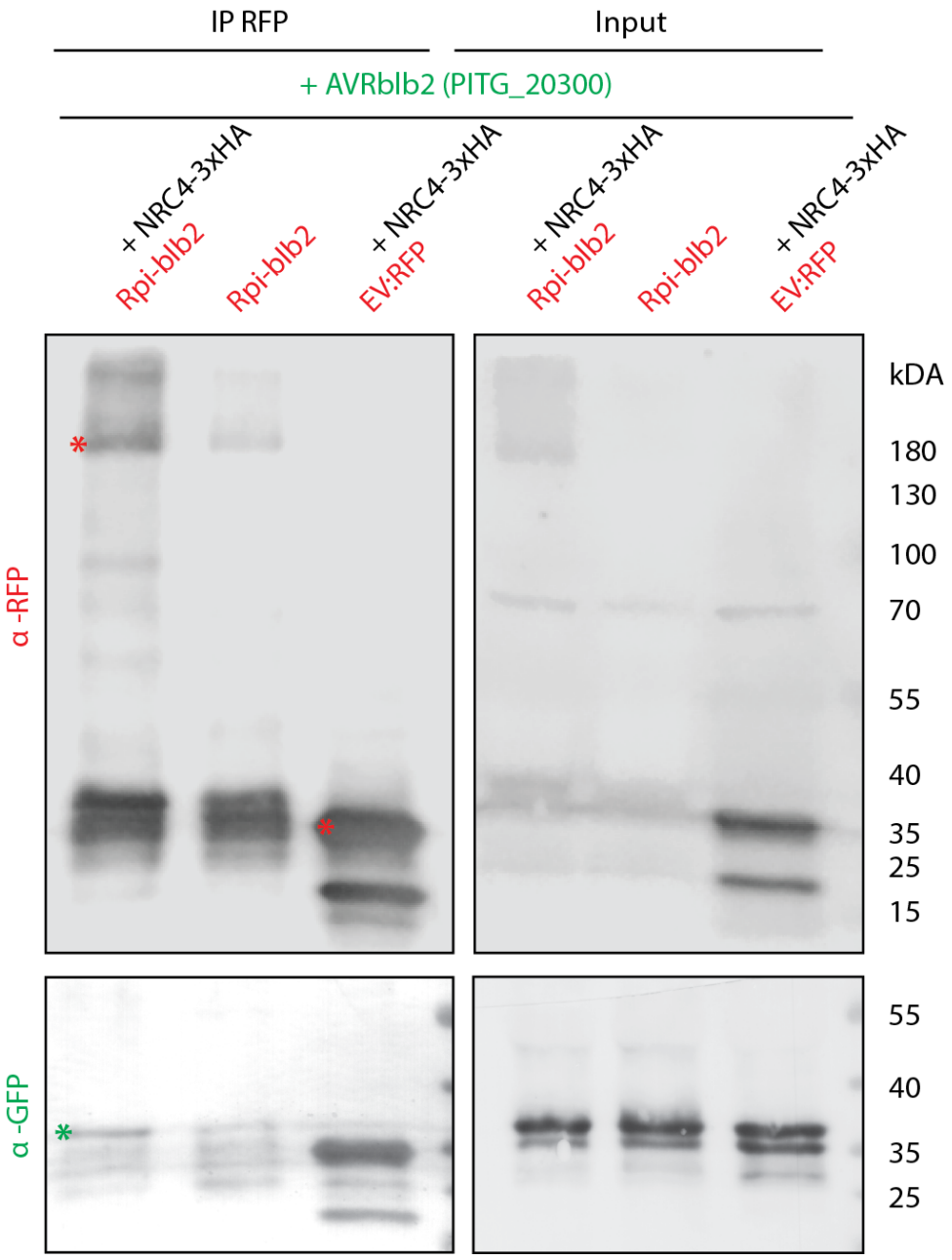


Figure 3.14: NRC4 co-immunoprecipitates with Rpi-blb2 but it is unclear if AVRblb2 CoIPs or not.
In planta co-immunoprecipitation or proteins extracted 3 dpai. GFP-AVRblb2 (PITG_20300) was transiently co-expressed with either RFP-Rpi-blb2 or EV-RFP and 3xHA-NRC4. IPs were obtained with GFP-trap agarose beads, and GFP and RFP was immunoblotted along with total protein extracts (input). Asterisks indicate expected band sizes for proteins in that sample as predicted with https://www.bioinformatics.org/sms/prot_mw.html . Note: anti-HA blot was never detected.

3.4.1.5. Rpi-blb2/NRC4-mediated immunity is active at the haustoria-producing stage of infection

Rpi-blb2-NRC4 immunity to *P. infestans* could occur during initial penetration of the first cell or later stages of invasive hyphal growth. To address this, I transiently silenced NRC4 in Rpi-blb2 stable transgenics and conducted a *P. infestans* immunity assay, with pathogen induced necrosis as the readout. I agro-expressed a hairpin RNAi construct in small patches one day before infecting the centre of the patch. On the opposite side of the leaf I included a hairpin RNAi construct targeting the GUS reporter construct as a negative control. Thus the RNAi-NRC4 patches would be silenced for NRC4 and RNAi-GUS would not be silenced. Wild-type *P. infestans* grew to and stopped at the border of the infiltration zone, even after 17 days of infection, indicating Rpi-blb2-mediated immunity was active in the non-silenced cells. Wild-type plants, naturally lacking Rpi-blb2, were infected far past the infiltration zone (Figure 3.15). This experiment was repeated, and 38/38 successful infections in the RNAi-NRC4 zone on Rpi-blb2 plants did not grow past the infiltration zone, versus 0/6 on the WT plants. However, I found that marking the infiltration zone with a marker pen was insufficient to accurately demarcate the agro-expressed zone. Additionally, leaving infections for 17 days makes it difficult distinguish necrosis associated with pathogen growth, and leaves decaying due to detachment.

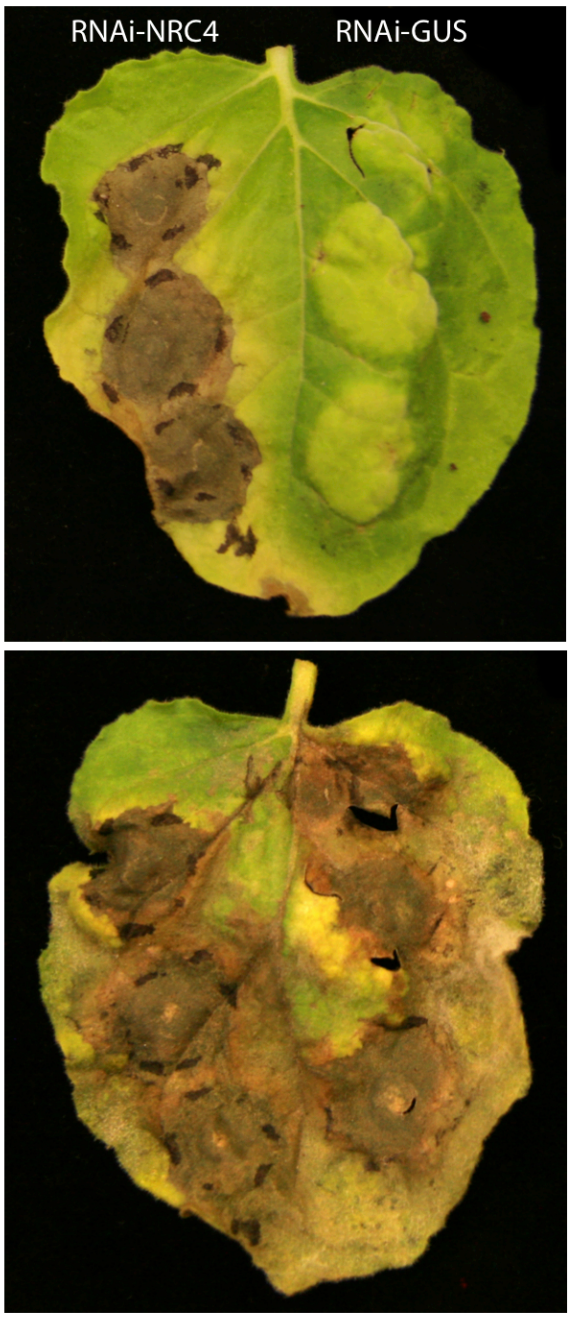


Figure 3.15: Hairpin RNAi of NRC4 compromises Rpi-blb2 resistance locally. Rpi-blb2 transgenic or WT *N. benthamiana* leaves were infiltrated in patches with hairpin RNAi constructs targeting either NRC4 or the reporter gene GUS, one day before infection with *P. infestans.* After 17 days the pathogen necrotic lesion had only extended to the NRC4-silenced zone of Rpi-blb2 plants, not infected in RNAi-GUS control and had extended out of both zones in WT plants. The experiment was repeated several times with similar results.

If Rpi-blb2/NRC4 are not active at the haustoria forming stages of infection, I would expect *P. infestans* and its associated necrosis to spread out beyond the infiltrated region, as was the case in the WT plants lacking the sensor Rpi-blb2. To confirm the precise zone where the pathogen was restricted, we co-agroexpressed an EV:GFP reporter with the RNAi constructs. We then infected with the red fluorescent TD-tomato 88069 *P. infestans* strain, hereafter referred to as TD Tomato, and used fluorescent stereo-microscopy to track the growth of the pathogen over time (Figure 3.16). We found that the growth of the pathogen on Rpi-blb2 plants in RNAi-NRC4 patches correlated with the infiltrated zone, confirming our previous observations. Therefore, we concluded that Rpi-blb2-NRC4 mediated resistance to *P. infestans* is active in the haustoria forming timepoint of infection.

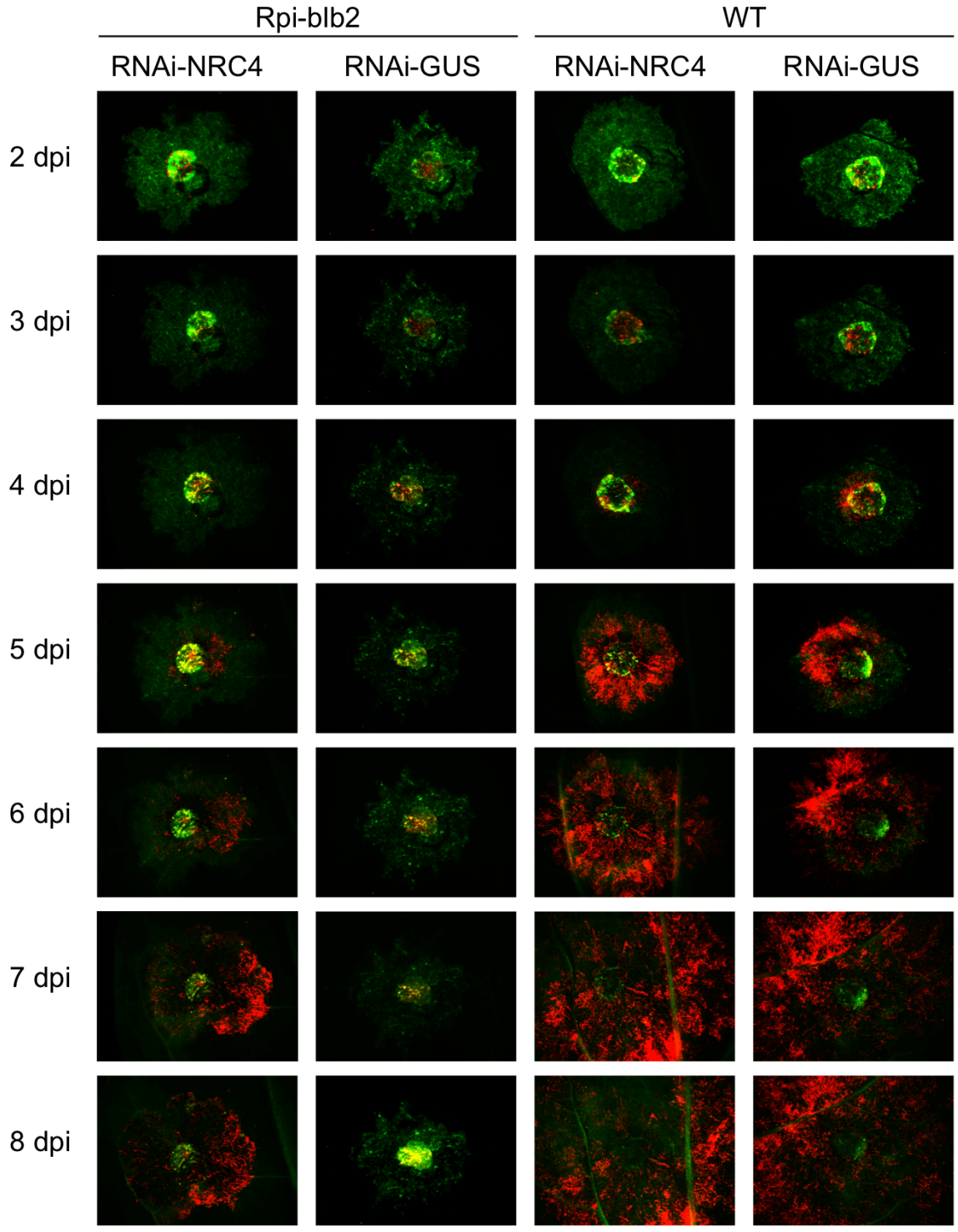


Figure 3.16: Hairpin RNAi of NRC4 compromises Rpi-blb2 resistance in the agro-infiltrated zone only.
Rpi-blb2 transgenic or WT *N. benthamiana* were infiltrated in patches with EV-GFP as an infiltration marker and hairpin RNAi constructs targeting either NRC4 or the reporter gene GUS, one day before infection with the red fluorescent strain of *P. infestans*, TD tomato. The progress of the pathogen was imaged with fluorescent stereomicroscopy and was found to be restricted to the GFP agro-expressing zone in the RNAi-NRC4 patches of Rpi-blb2 plants.

3.4.2. Rpi-blb2/NRC4 does not prevent the initial penetration

3.4.2.1. Infection vesicles form in WT and Rpi-blb2 transgenic plants

The previous experiments indicate that Rpi-blb2 resistance is functional at the haustoria-forming stages of *P. infestans* infection. However, whether this resistance is active in the very early stages of infection is unknown. Therefore I carried out confocal microscopy of TD tomato infections on WT and Rpi-blb2 transgenic *N. benthamiana.* Unsurprisingly, the initial penetration attempt by the spores was successful, however it was surprising to see the formation and growth of infection vesicles in the resistant Rpi-blb2 line (Figure 3.17). Leakage of RFP signal from the pathogen into the plant cell indicates pathogen cell death and is a failure of infection at this stage. The spores did not germinate synchronously, so it was possible to find non-germinated spores, infection vesicles and destroyed infection vesicles at all time points tested. This made quantifications difficult. I was therefore unable to quantify a comparison between WT and Rpi-blb2 plants as the image acquisition was at risk of having a sampling bias. Future experiments should quantify the RFP protein levels in multiple infected leaf disks during a time course experiment.

Nevertheless, I did witness more than 20 living infection vesicles in living plant cells, over the course of four independent experiments at various timepoints from 22-40 hpi. Therefore, considering the presence of living infection vesicles in Rpi-blb2 transgenics, it is likely that this resistance pathway isn't active at this stage. This finding could be due to lack of expression/secretion of AVRblb2 at this stage. Considering the non-synchronous germination of spores, it would be difficult to investigate the hypothesis because timepoints wont reflect the actual development of the pathogen. However, *in planta* expression analysis by RT-PCR of the natural host tomato infected with *P. infestans* 88069 or 43072 previously revealed that expression of AVRblb2 peaks at around 2-3 dpi (Lee et al., 2014; Oh et al., 2009). Therefore it is plausible that Rpi-blb2 mediated resistance does not take place at early stages of infection, purely due to lack of AVRblb2 expression and secretion. An alternative hypothesis would be the localisation of the sensor/helper and effector are different leading to lack of recognition or a delayed recognition in the first cell.

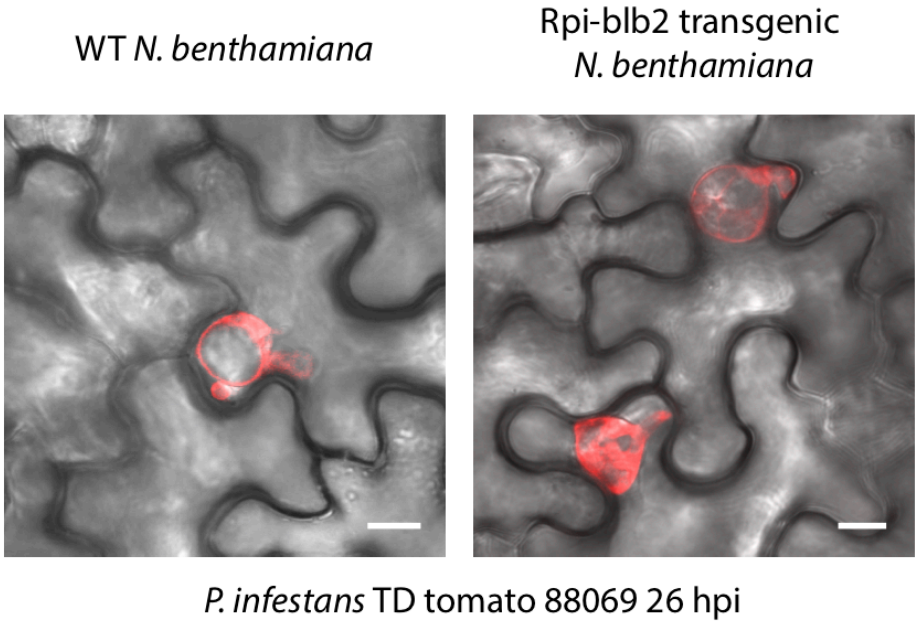


Figure 3.17: Infection vesicles form in both WT and Rpi-blb2 transgenic lines. WT and transgenic *N. benthamiana* constitutively expressing Rpi-blb2 were infected with the red fluorescent strain of *P. infestans*, TD tomato. After 26 hours the pathogen had formed many infection vesicles in both genotypes. This experiment was performed independently four times with the same results at 22-40 hpi timepoints. More than 20 intact infection vesicles in living plant cells were imaged for both WT and Rpi-blb2 transgenic lines.

3.4.2.2. NRC4 accumulates at membrane surrounding haustoria-like hyphal leaders emerging from Infection Vesicles

Lack of Rpi-blb2 resistance during the infection vesicle stage could be due to the expression patterns of AVRblb2 or the localisation patterns of the components of this immune pathway. To investigate, I analysed the distribution of NRC4 in infection-vesicle containing cells. I found NRC4-GFP generally does not accumulate at the membrane surrounding infection vesicles. However, it does accumulate at the haustoria-like hyphal leaders which emerge from the vesicle to penetrate neighbouring cells (Figure 3.18).

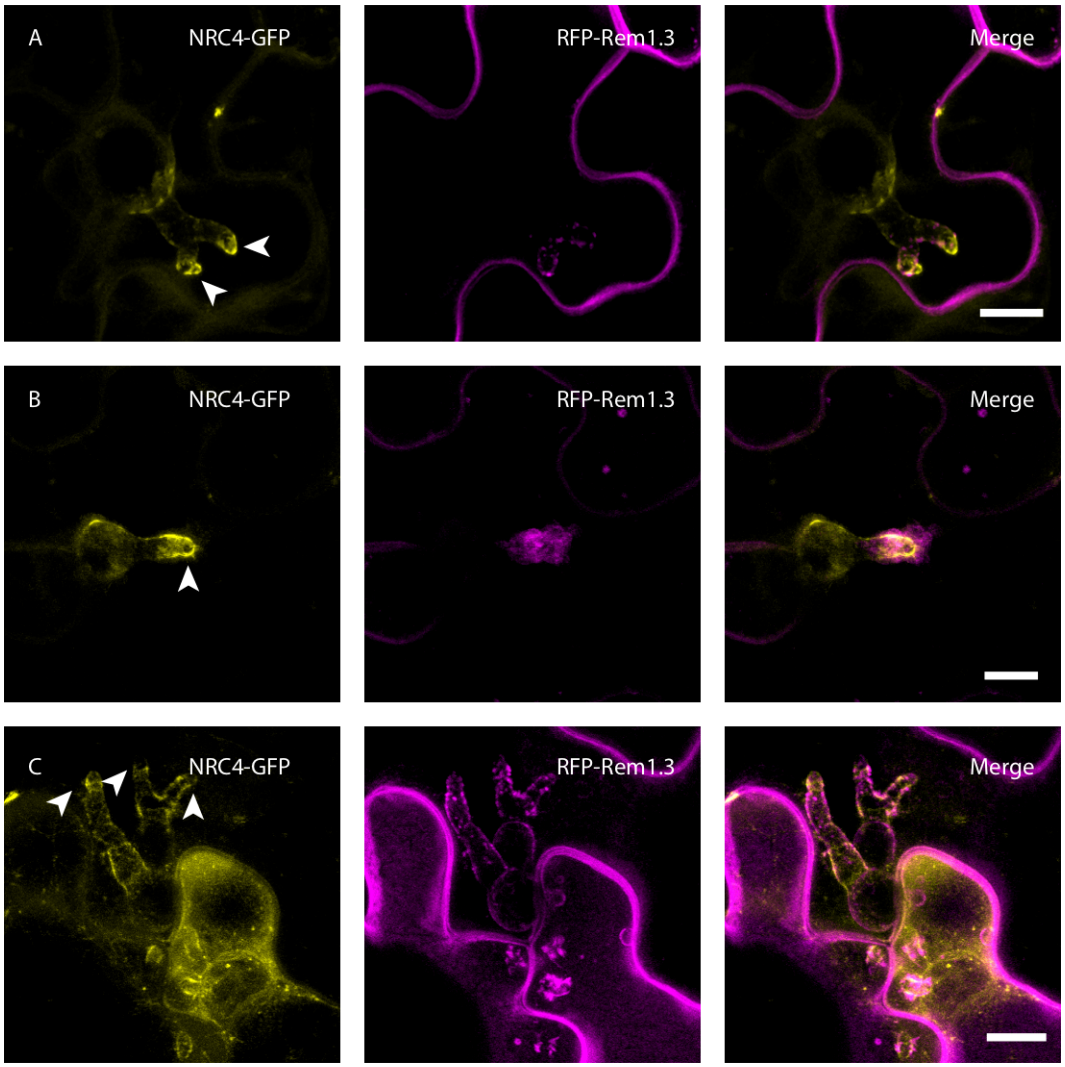


Figure 3.18: NRC4 accumulates at the tips of the membrane surrounding hyphal leaders that emerge from infection vesicles.
NRC4-GFP was co-expressed with plasma membrane and EHM marker RFP-Rem1.3 one day before leaves were detached and infected on the underside. After 24 hours, the leaves were imaged with the Leica SP5 microscope. Z-projections of stacks are displayed in order to contain hyphal leaders and infection vesicles in the same image. Arrowheads indicate the tip of hyphal leaders. Scale bars are 10 μm.

3.5. Chapter Conclusions

I have described the investigation of NRC4-Rpi-blb2's spatio-temporal mode of action. First, I demonstrated that NRC4 has an unusual distribution during infection with *P. infestans*, compared to other NLRs. I characterised this distribution extensively and determined that NRC4 localises to an EHM microdomain. I then showed that whereas AVRblb2 and NRC4 partially co-localise at the EHM, Rpi-blb2 does not accumulate to this site. Detection of AVRblb2 by Rpi-blb2 and activation of NRC4 by Rpi-blb2 could occur directly or indirectly. It's also possible Rpi-blb2 transiently associates with AVRblb2 or NRC4 to perform these functions.

It was previously shown that AVRblb2 blocks secretion of the defense protease C14 (Bozkurt et al., 2011). Additionally, without NRC4, Rpi-blb2 mediated resistance to *P. infestans* 88069 is broken, but with NRC4, resistance is absolute (Wu et al., 2017). Considering the importance of the EHM in facilitating effector translocation, and the secretion of defence compounds to the pathogen, it is not surprising that the pathogen would target it with effectors or that the plant would deploy NLRs to this site. It is unclear whether NRC4 is directly guarding defence related secretory pathways which are directed towards the EHM; or indirectly by screening for perihaustorial effectors whilst NRC4 is present at the EHM (see Chapter 6, general discussion and conclusions).

Finally, I provided evidence that Rpi-blb2/NRC4-mediated immunity is active during the haustoria-forming stage of infection. Since at this stage, NRC4 is EHM localised, NRC4 may be detecting the pathogen effectors at the EHM to provide resistance. I observed that Rpi-blb2 plants were successfully penetrated by *P. infestans*. NRC4 did not accumulate at the membrane surrounding infection vesicles, but did usually accumulate at the tips of hyphal leaders extending from them. I conclude that Rpi-blb2/NRC4 resistance probably does not occur in the first cell infected where *P. infestans* forms an infection vesicle, but it is likely that resistance occurs in the next cell, which is penetrated by a haustorium. However, whether resistance at these stages is determined by NRC4 localisation, or AVRblb2 expression, is not clear. Determining exactly when AVRblb2 is expressed and secreted is not an easy task as the firstly *Avrblb2* is a large family of effectors (Oliva et al., 2015); and secondly I found

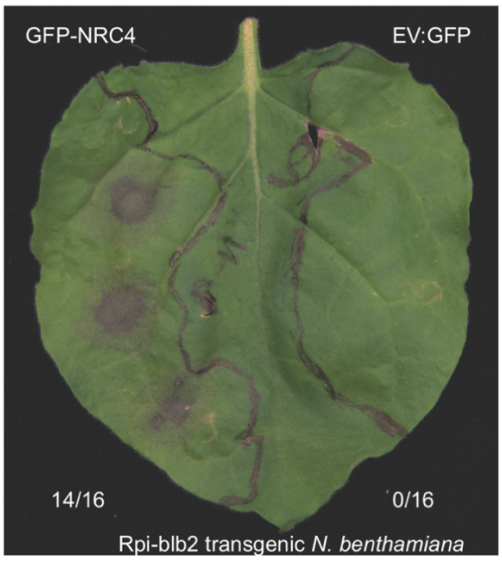
that during inoculation with *P. infestans* zoospores, the germination and penetration events are non-synchronous meaning that some zoospores will have penetrated into the first or second cells whilst others will still not have germinated. Therefore, a method of synchronising germination is required or infecting tissue with just a single zoospore and extracting RNA when the correct infection stage has been reached. Furthermore, closer observation of the early time points of infection is required. Do haustoria form in Rpi-blb2 transgenics or does the penetrated cell die before this can occur? While this is an outstanding question, in the next chapter I present my investigation of the intramolecular determinants of NRC4-mediated immunity and localisation at the EHM. In other words, what parts of NRC4 are required for EHM localisation and immunity, and what function do they provide in the context of the whole NLR?

Supplementary Figures:

A



B



S1 Figure 3.19: RFP-Rpi-blb2 is functional but GFP-NRC4 is not and causes a dominant negative effect.
(A) RFP-Rpi-blb2 provides resistance to *P. infestans* 88069. WT *N. benthamiana* leaves were infiltrated with *Agrobacterium* to express RFP-Rpi-blb2 on one side of the leaf and EV:GFP on the other side of the leaf. After 24 h, leaves were detached and infected as per methods section. (B) GFP-NRC4 compromises resistance mediated by Rpi-blb2 and endogenous NRC4. Rpi-blb2 transgenic *N. benthamiana* leaves were infiltrated with *Agrobacterium* to express GFP-NRC4 on one side of the leaf and EV:GFP on the other side of the leaf. After 24 h, leaves were detached and infected as per methods section. Numbers represent sum of successful infections per total inoculation spots.

4. Results Chapter II: What *intra*molecular properties of NRC4 determine immunity?

4.1. Chapter Summary

Plant NLRs consist of a conserved domain structure with generally conserved functions: CC or TIR N-terminal domain followed by the NB-ARC domains, followed by the LRR domain. As well as these domains, NRC4 has a non-canonical extended C-terminal domain of approximately 37 amino acids, or 'tail', with no annotated function. Additionally, focal accumulation of a plant immune receptor to pathogen contact sites has never been reported, so it is unclear what domain(s) are responsible for this phenomenon. In this chapter I show that NRC4's coiled-coil (CC) domain is sufficient for focal accumulation at the EHM. However, for efficient EHM targeting the entire structure of NRC4, including a tail is required. Moreover, expression of NRC4's tail interfered with NRC4-mediated resistance. The precise function of the tail is unclear, but is evidently required for NLR function. Finally, I provide evidence that the N-terminal α1 helix is acting to elicit HR cell death from the EHM niche. Overall, in this chapter I demonstrate that find roles for sub-domains of NRC4 and find that as expected, each domain and sub-domain co-operates to facilitate the immune response.

4.2. Introduction

Plant NLRs have a multidomain structure with fairly well annotated functions of each domain (Cesari, 2017). In general we know that the CC, TIR or RPW8-like N-terminal domain functions in NLR oligomerisation and signalling. The NB-ARC domain functions as a molecular switch that determines the OFF/ON state of the NLR, via ADP to ATP nucleotide exchange (Steele et al., 2019). The LRR domain is known to be involved in pathogen detection. There is evidence that this is true for NRC4 since the LRR domain encodes the sensor specificity (pathogen detection) (Wu, 2016). That is, the LRR domain determines which sensor NLRs NRC4 pairs with. Many NLRs have been found to contain integrated domains, i.e. non-canonical domains such as heavy metal associated (HMA) domains (Cesari et al., 2014). Others have extended N- or C-terminal domains of unknown function. A number of NLR extended C-termini have been discovered to provide unique functions (Cesari et al., 2014).

Recently we discovered that the CC domain of NRC4 is probably involved directly in HR elicitation via oligomerisation (Adachi et al., 2019). We showed that 20% of plant CNLs contain a motif on their N-terminus, with the consensus sequence 'M-A-D-A'. This so-called MADA-motif overlaps with the first alpha helix (α1) of the model CNL ZAR1, which is implicated in directly eliciting HR by forming pores in the plasma membrane. Upon activation, ZAR1 oligomerizes into a pentameric structure called the resistosome in which the α1 helices form a funnel shape that is predicted to cause membrane pores ('ZAR1 death switch model') (Wang et al., 2019a). Consistent with this notion, expression of the N-terminal 29 amino-acids (aa) of NRC4 (containing α1/MADA motif) fused to YFP, which can form pentamers (Kim et al., 2015), was sufficient to trigger an HR. We showed that the 29aa-YFP construct was dependent on the YFP in order to oligomerise and trigger HR. The YFP may have been mimicking the rest of the NLR and providing a scaffold for the 29aa construct to oligomerise into a pentamer for cell death. These results indicate that NRC4, and many other CNLs, may execute HR directly by the ZAR1-death switch model. Furthermore, we showed that NRC helpers have the MADA motif, but sensors do not – which instead show diversification in this region and some even have extended N-terminal domains inserted upstream of the ancestral degenerated MADA motif. This supports the notion that the NRCs helper-sensor pairs evolved from multifunctional singleton NLRs. However, the majority of the 20% of MADA-containing NLRs are yet to be experimentally validated to determine whether they are all indeed helper NLRs.

4.3. Aims

My goal was to understand how NRC4-mediated immunity is regulated in terms of the intrinsic properties of the protein. If I could comprehend how this worked, I should then be able to block peri-haustorial accumulation of NRC4 and determine the impact of this on immunity. This would also reveal a novel EHM trafficking domain or system which could be used to understand the biogenesis of the EHM. Understanding more about immunity against haustoria-forming pathogens could one day help us develop disease-resistant crops.

4.4. Results & Discussion

4.4.1. The extended C-terminal domain of NRC4 is required for EHM localisation, stability and immunity

Bioinformatic analysis with InterproScan (Jones et al., 2014) of NRC4 revealed an extended C-terminal region of approximately 37 amino acids that did not fit the Leucine Rich Repeat structural motif (Figure **4.1**).



Figure 4.1: InterProScan reveals c-terminal extension of NRC4 with no annotated domain or motif.
A scan of known domains was conducted by submitting NRC4b protein sequence to InterProScan (https://www.ebi.ac.uk/interpro/search/sequence/). This found a CC domain similar to Rx (2-122 amino acids), an NB-ARC domain (162-397), and a LRR (477-845). The region from amino acid 845 to the end, 881 was considered the C-terminal extension or 'Tail'.

4.4.1.1. Loss of NRC4 C-terminal 'tail' leads to disruption of NRC4's EHM accumulation and a dominant-negative immune phenotype

I generated a truncation of the extended C-terminal domain and named the resulting truncate NRC4Δtail (Figure 4.2A). I found NRC4Δtail-GFP failed to accumulate at the EHM and localizes to cytoplasm in *P. infestans* 88069 infected cells (Figure 4.2B).

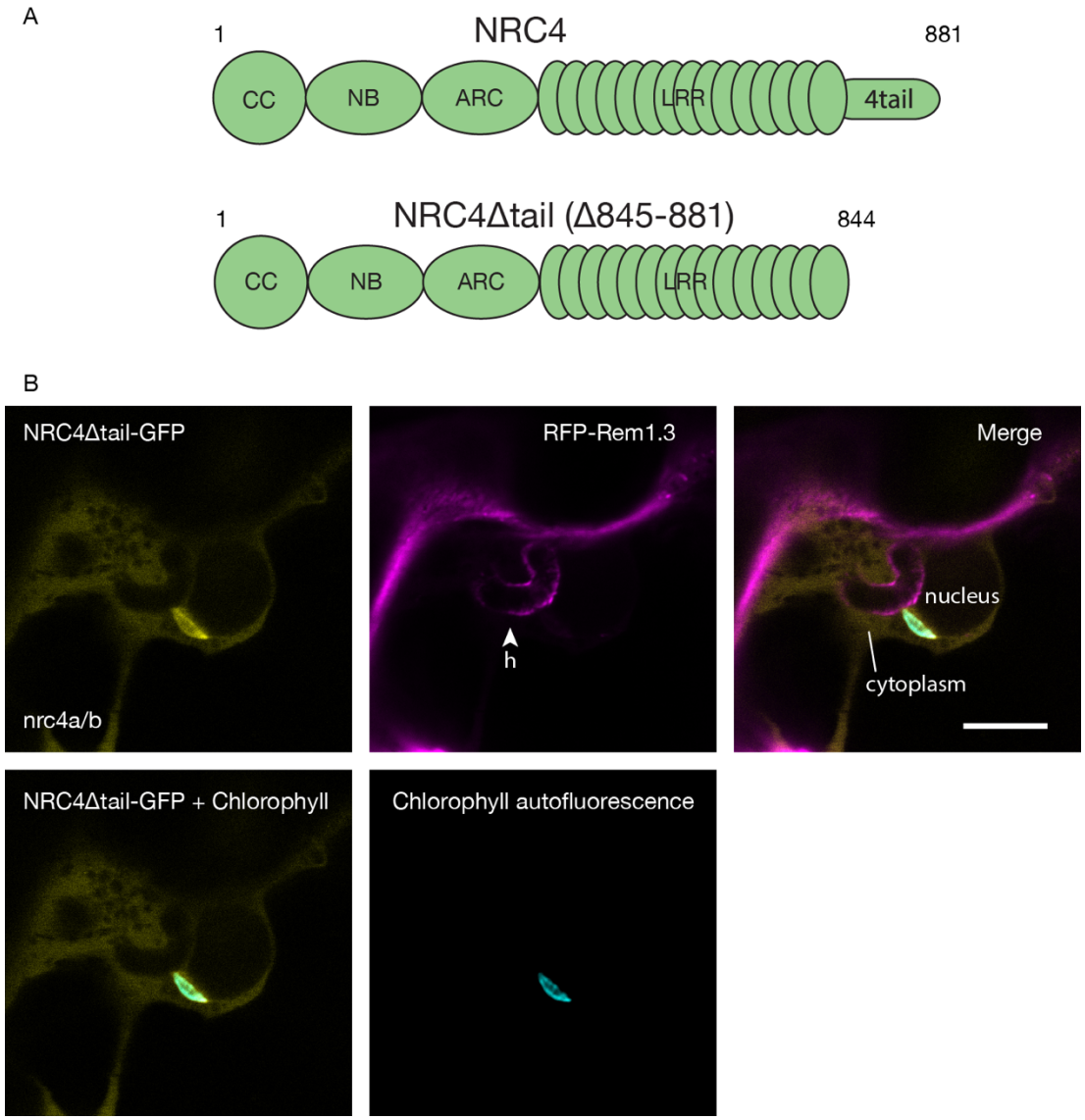


Figure 4.2: NRC4Δtail truncate does not accumulate at the EHM, but instead remains cytoplasmic
(A) A cartoon demonstrating that NRC4Δtail is c-terminally truncated to lack the tail. (B) NRC4Δtail-GFP fluorescence is not polarised to haustoria, but instead it remains cytoplasmic, including in the cytoplasm surrounding haustoria. RFP-Rem1.3 and NRC4Δtail-GFP and P19 silencing suppressor (to increase transgene expression) were transiently co-expressed in nrc4a/b *N. benthamiana* leaves, infected the same day with *P. infestans* and imaged 3dpi. h = haustorium labelled by RFP-Rem1.3. Chlorophyll autofluorescence (cyan) was overlayed due to it crossing into the GFP channel because of poor GFP signal. Scale bar 10μm.

As this truncate of NRC4 failed to target the haustorial interface, but instead remained diffusely localised to the cytoplasm, I reasoned it could be used to test if peri-haustorial accumulation of NRC4 was required for resistance. This would rely on NRC4Δtail retaining its functionality in terms of its ability to trigger HR when the corresponding AVRs are expressed ectopically. Therefore, I tested untagged NRC4Δtail for its ability

to rescue AVRblb2 triggered Rpi-blb2 mediated HR but found it to be non-functional (Figure 4.3A). First, I systemically silenced NRC2/3/4 in Rpi-Blb2 transgenic *N. benthamiana* with Virus Induced Gene Silencing (VIGS). Next, I transiently co-expressed AVRblb2 (also known as RD40 or PITG_20300) with EV:GFP ('no HR' control), silencing resilient (codon-shuffled) NRC4 (HR positive control) and silencing resilient NRC4∆tail and assayed their ability to rescue HR. Full-length NRC4 showed HR in 100% of infiltration patches, whereas NRC4∆tail only had HR in 15% of these repeats, similar to EV:GFP (Figure 4.3). This is consistent with the Wu *et al.,* (2017) finding that due to the variability in silencing efficiency by VIGS, some negative controls displayed HR symptoms. To validate these findings, I confirmed NRC4∆tail-GFP and NRC4∆tail-3xHA's HR inactivity in NRC4 Rpi-blb2 nrc4a/b mutant plants when they were available (Figure 4.31).

However, I observed during microscopy that NRC4∆tail-GFP had low fluorescence, meaning NRC4∆tail may lack the ability to rescue HR simply due to low stability of the truncate. To test this I reasoned that if NRC4∆tail was non-functional it would likely have a dominant negative effect on endogenous NRC4. Therefore I overexpressed NRC4∆tail, EV:GFP or NRC4 full-length opposite one another on half of a leaf of Rpi-blb2 transgenics after 24 h infected with *P. infestans* to assess whether Rpi-blb2 resistance was broken (Figure 4.3B). Indeed, a necrotic lesion larger than the inoculation droplet was found in 81% of inoculations, indicating resistance was broken. The EV:GFP control did not show such lesions, indicating intact resistance. Interestingly, in 14% of inoculations full-length NRC4 showed relatively large lesions, which could be due to spreading necrosis of an intense HR created by the increased load of helper NLR (LAI and Eulgem, 2017). This is possible considering that increasing the expression of NRC4 has been shown to increase resistance to *P. infestans* (Derevnina et al., 2019), presumably by amplifying the HR. The suppression of Rpi-blb2 resistance by NRC4∆tail is likely caused by suppression of HR. To confirm this, I expressed AVRblb2 in Rpi-blb2 transgenics to trigger HR and co-expressed NRC4∆tail or EV. I found a clear pattern of HR suppression by NRC4∆tail compared to the EV control (shown later with Figure 4.7). As removal of the tail seems to lead to destabilisation of NRC4 (low fluorescence witnessed during microscopy) and loss of immune function, it is possible it could disrupt the folding of NRC4 or NRC4∆tail may have been failing to respond to Rpi-blb2. To address this, I introduced a mutation into

the MHD motif in the NBD of NRC4Δtail, a mutation that is known to confer autoactivity. This D478V mutation renders NRC4 “always-on” in regards to HR (Wu et al., 2017). I cloned this mutation by site-directed mutagenesis, but no visible HR was produced by the tail truncate NRC4Δtail^{D478V} (Figure 4.3C). This indicates NRC4Δtail is indeed non-functional in terms of its ability to execute an HR. However, I was unable to confirm stability of these constructs as I did not include a tag in order to increase chances the protein would be functional.

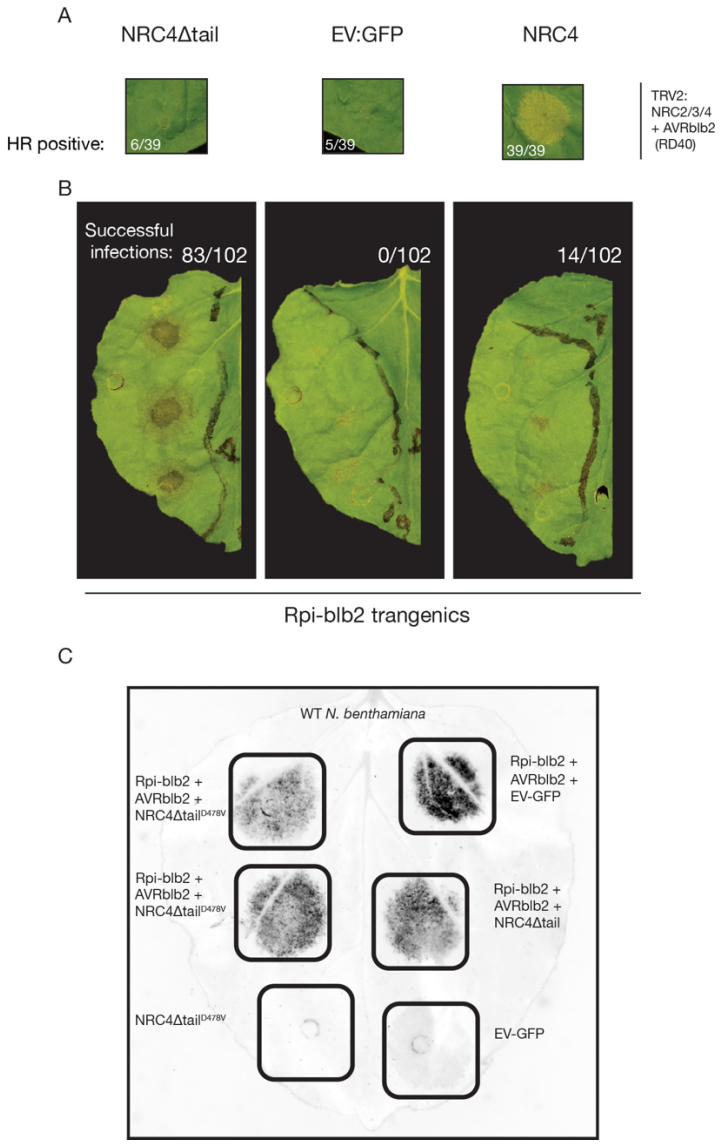


Figure 4.3: NRC4Δtail is non-functional and suppresses immunity.
(A) NRC4Δtail does not complement HR, like EV:GFP but unlike full-length NRC4. NRC2, NRC3 & NRC4 were silenced in Rpi-blb2 transgenics by VIGS and the ability to complement for HR was assayed, by co-expressing AVRblb2 (RD40) with silencing resistant NRC4Δtail, EV:GFP or NRC4. Numbers represent the sum of patches with HR per total number of infiltrations (one of each construct per leaf) from 3 independent experiments. Leaves imaged 3dpai. (B) NRC4Δtail expression suppresses resistance of Rpi-blb2 transgenics, but EV:GFP and NRC4 full-length do not. NRC4Δtail, EV:GFP or NRC4 were transiently expressed opposite one another and at one dpai they were infected with *P. infestans* and the number of spreading lesions were counted per total inoculations 7dpi, in 3 independent experiments. (C) Blue light imaging of HR showing NRC4Δtail^{D478V} suppresses HR compared to EV-GFP, does not increase HR compared to NRC4Δtail, and is not autoactive alone. WT plants were *agro*infiltrated with either Rpi-blb2, AVRblb2 and NRC4Δtail^{D478V}; Rpi-blb2, AVRblb2 and EV-GFP; Rpi-blb2, AVRblb2 and NRC4Δtail; NRC4Δtail^{D478V} alone or EV-GFP alone. After 4 days of expression, leaves were detached and imaged with blue-light transilluminator, 1 s exposure, λ = 420 nm.

4.4.1.2. C-terminal 'tail' does not focally accumulate around the haustoria and its overexpression compromises Rpi-blb2 resistance and weakly suppresses HR

Truncation of the NRC4 C-terminal 'tail' (4Tail) indicated it was required for NRC4 haustorial localisation. Therefore, I set out to determine whether 4Tail serves as a haustorial transport signal. Confocal microscopy of infected tissue showed GFP-4Tail mainly localizes to the cytoplasm (Figure 4.4A), including the cytoplasm surrounding the EHM. An example of this localisation can be seen with EV:GFP (Chapter 3, Figure 1H), and unlike NRC4, 4Tail does not accumulate around haustoria. I cloned the tail of the homologue NRC2 (Figure 4.5A), fused it to mKOk (mKusabira-Orange-kappa) (2tail-mKOk) and found it was also localised throughout the cytoplasm during infection (Figure 4.4B). These results, combined with the results from Figure 4.2 show that 4Tail is required for localisation, but not sufficient for localisation.

The loss of activity of NRC4∆tail truncate suggested that 4Tail plays an essential role in NRC4 function and prompted me to further investigate its mode of action in immunity. To test if 4Tail had any effect on Rpi-blb2/NRC4 mediated immunity, I expressed it in Rpi-blb2 transgenic *N. benthamiana* and performed infection assays after one day of expression. Surprisingly, these experiments revealed that Rpi-blb2 resistance was compromised in 88% of inoculations when GFP-4Tail is expressed, whereas only one infection appeared successful on the control GFP expressing leaf patches (Figure 4.4C). The same result was found for C-terminally tagged 4Tail-GFP (Figure 4.4D) and was also seen with other tags mKOk, RFP (Supplementary 1 = Figure 4.37A-B). The RFP-4Tail construct was cloned separately from cDNA and had two amino-acid differences to other 4Tail constructs used (Supplementary 1 = Figure 4.37C), which corresponded to the sequence of NRC4a (Niben044Scf00002971), but still compromised Rpi-blb2 immunity (Supplementary 1 = Figure 4.37B). All other NRC4 constructs in this thesis, including GFP-4Tail and 4Tail-GFP/mKOk-FLAG/BFP were cloned from a plasmid containing NRC4b (Niben044Scf00016103) provided by Dr Chih-Hang Wu (PICH87988 synNRC4). 4Tail has only 37 amino acid residues, so I investigated what aspect contributes to this immune suppression. 4Tail is highly positively charged (10/37 residues; Figure 4.5). Additionally, a few of the lysine residues found in 4Tail are conserved in NRC paralogues (Figure 4.5A), but they are better conserved in NRC4 orthologues (Figure 4.5B).

Therefore, I mutated the seven lysine residues to alanine in the 4Tail sequence to remove the positive charge as well as to interfere with a number of potential post-translational modifications. I named this mutant 4Tail-7KA and found its expression does not compromise Rpi-blb2 resistance (Figure 4.4E), despite being well expressed (Figure 4.9). Similarly, 2Tail (NRC2 tail) also has seven positively charged residues, but the positioning of these are different to 4Tail (Figure 4.5A). Expression of 2Tail did not compromise Rpi-blb2 resistance (Figure 4.4F), despite being well expressed. Both 4Tail-mKOk and 2Tail-mKOk produced higher-molecular weight bands above their predicted 32kDa molecular weight (Figure 4.6).

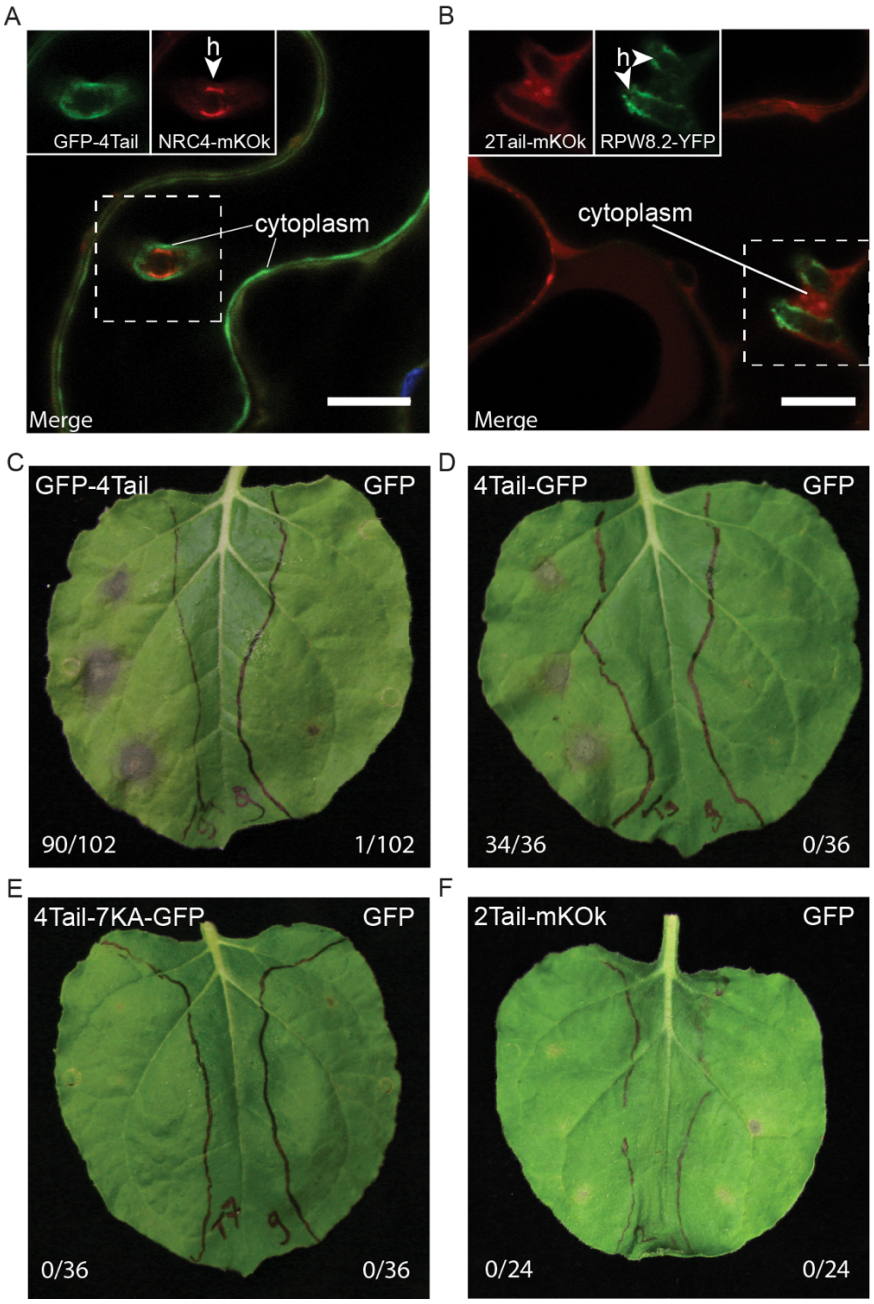


Figure 4.4: 4Tail suppresses Rpi-blb2 resistance (in a lysine dependent manner), but 2tail does not.

(A-B) GFP-4Tail or 2Tail-mKOk was co-expressed with either NRC4-mKOk or EHM/PM marker RPW8.2-YFP. After 3 hours, leaves were infected with *P. infestans* and after 3 days, imaged with SP5 confocal microscope. Neither (A) GFP-4Tail nor (B) 2Tail-mKOk accumulate at haustoria. Scale bars = 10µm (C-F) GFP-4Tail, 4Tail-GFP, 4Tail-7KA-GFP or 2Tail-mKOk were expressed on half leaves opposite EV GFP in Rpi-blb2 transgenic *N. benthamiana*. After 24 h, leaves were detached and infected with *P.* infestans. Eight days after infection, leaves were photographed. Expression of (C) GFP-4Tail leads to suppression of Rpi-blb2 resistance as well as (D) 4Tail-GFP, but not EV:GFP control. (E) The seven lysine residues on 4Tail were mutated to alanine and this lead to loss of Rpi-blb2 suppression. (F) 2tail-mKOk, the C-terminal extension of NRC2 was unable to suppress Rpi-blb2 resistance. Numbers refer to sum of successful infections (spreading lesions) per total innoculations.

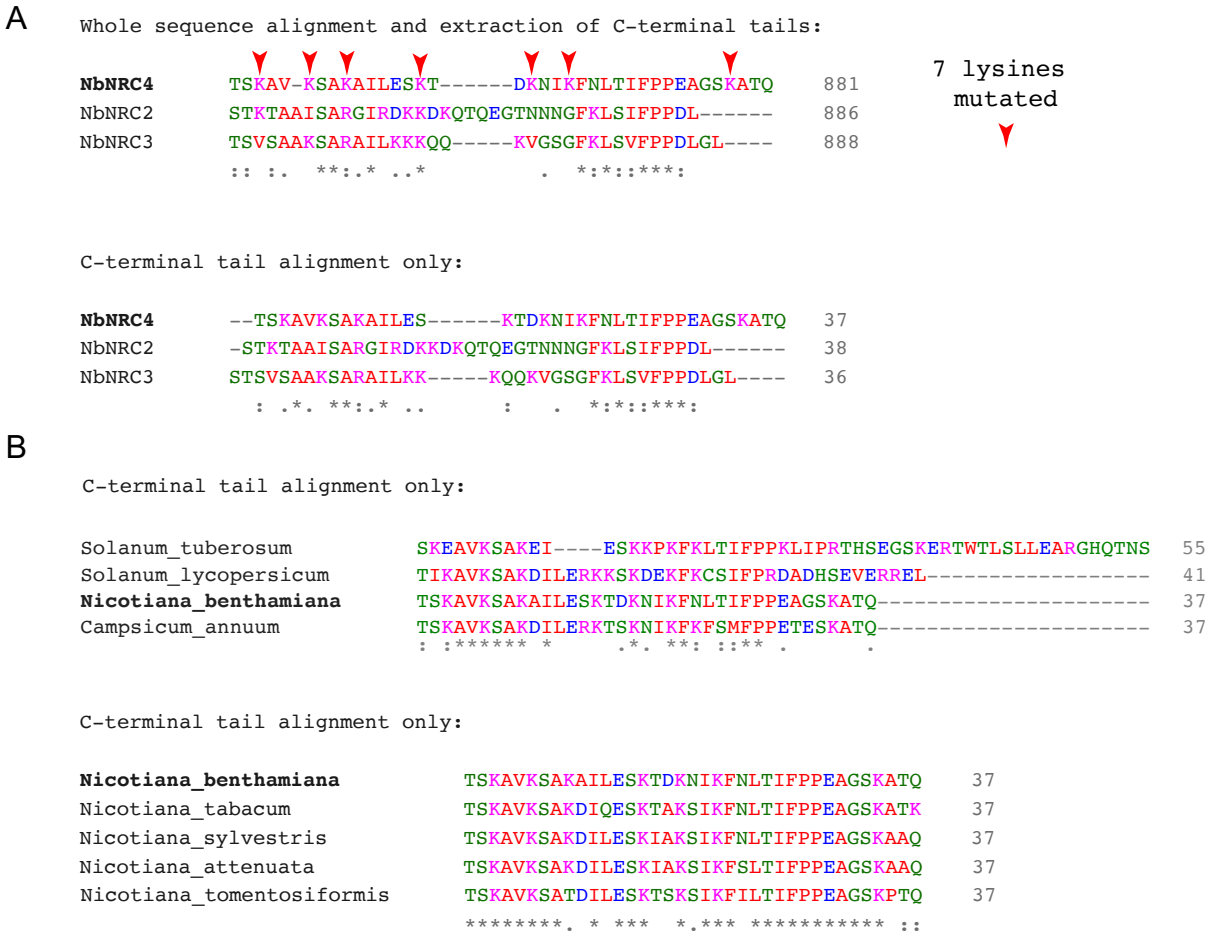


Figure 4.5: Multiple sequence alignment of NRC C-terminal extensions reveals conservation in charged amino acids.
Clustal Omega was used for multiple sequence alignment of either the C-terminal tail only, or the full sequence after which the c-terminal extensions were extracted, to improve the alignment. (A) Paralogues NRC2, NRC3 and NRC4 from *Nicotiana benthamiana* have some conserved residues in their C-termini. (B) Orthologues of NRC4 in solanaceous crops have conservation of lysines and orthologues from within *Nicotiana* have conservation of lysines and other amino acids. Accession numbers were as follows: *S. lycopersicum* XP_004236959, *S. tuberosum* XP_015161267, *C. annum* PHT61391, *N. tabacum* XP_016485826, *N. sylvestris* XP_009793040, *N. attenuata* XP_019236380, *N. tomentosiformis* XP_009594795, NbNRC4b NbS00002971g0007.1, *NbNRC2a* NbS00018282g0019.1, *NbNRC3* NbS00011087g0003.1.

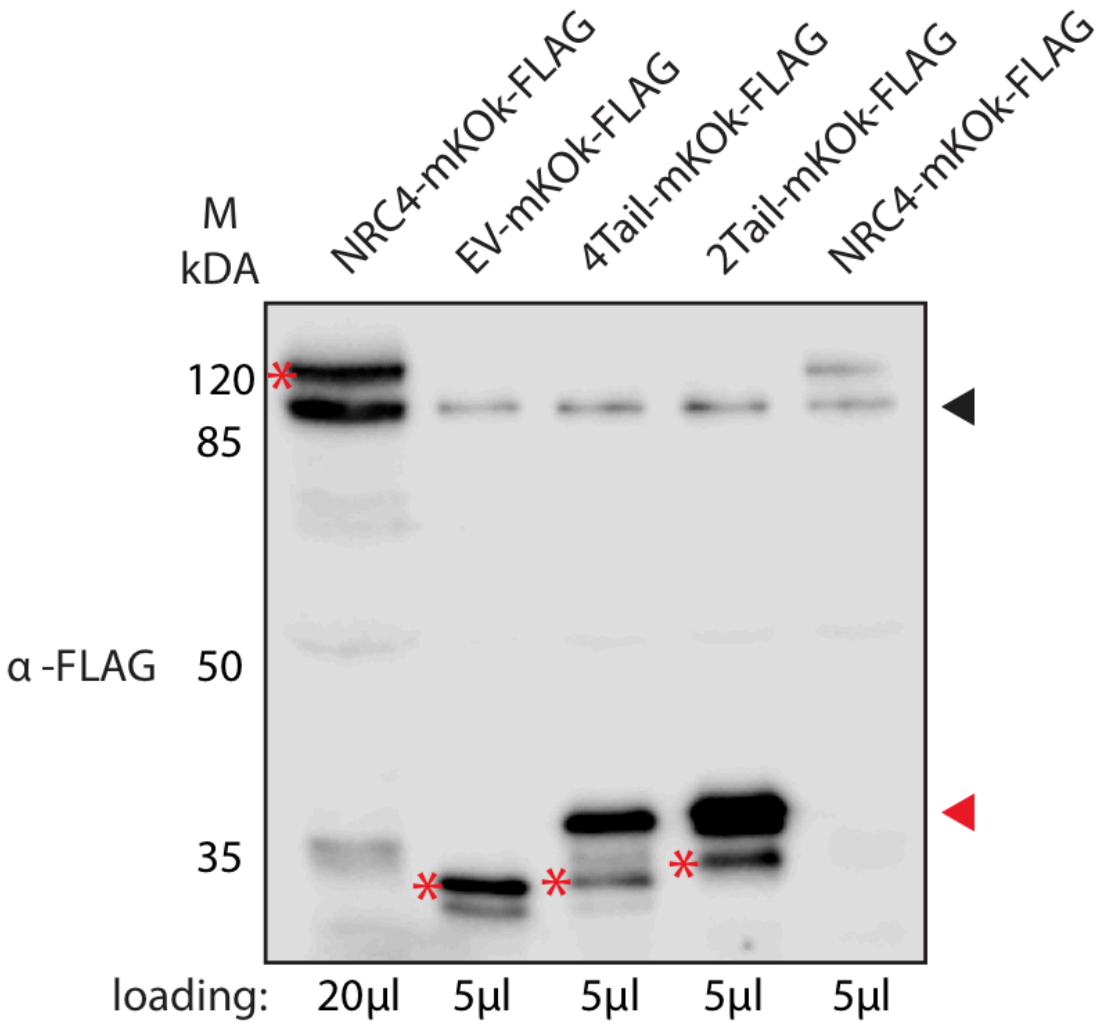


Figure 4.6: Western blot showing mKOk-FLAG proteins are correctly cloned and stably expressed.
NRC4 was loaded with a high volume (20 µl) to ensure good signal (left), and lower volume equal to the other constructs (5 µl; far right). These volumes correspond to 20 µl or 5 µl after four leaf disks taken by #4 cork borer and extracted in 120 µl crude extraction buffer. Red Arrowhead: Higher molecular weight bands probably corresponding to 4Tail and 2Tail were found, approximately 35-40 kDa, their predicted size is ~32 kDa with the mKOk-FLAG tag. Red Asterix: the predicted approximate size of the indicated proteins. 10% gel was used with chemiluminescence (HRP secondary) detection. Black arrowhead shows non-specific signal from plant protein detected by the anti-FLAG antibody.

4.4.2. 4Tail suppresses NRC4 immunity by an unknown mechanism

4.4.2.1. 4Tail expression weakly inhibits HR

To test if the suppression of Rpi-blb2 resistance by 4Tail is due to loss of HR, I tested the ability of RFP-4Tail to suppress endogenous NRC4-mediated HR. I co-expressed RFP-AVRblb2 and RFP-Rpi-blb2 to trigger HR, and treated the same patches with expression of either RFP-4Tail or EV:RFP (Figure 4.7). Previously, I developed a method of quantifying HR by proxy of the autofluorescent compounds produced during this programmed cell death (Dagvadorj et al., 2017). Thus, I quantified the mean grey value (pixel intensity) emitted during imaging with a blue light transilluminator for each HR patch (see Materials and Methods), and plotted this against that of the control EV:RFP. I found a small but statistically significant difference in HR in patches expressing 4Tail compared to patches expressing EV:RFP. However, the suppression of HR by expression of NRC4∆tail-3xHA was so strong that it was clear to the naked eye without quantification, whereas 4Tail suppression relied upon quantification. It is plausible that a small change in HR during infection could be more detrimental to immunity due to the accumulation of NRC4 at the EHM.

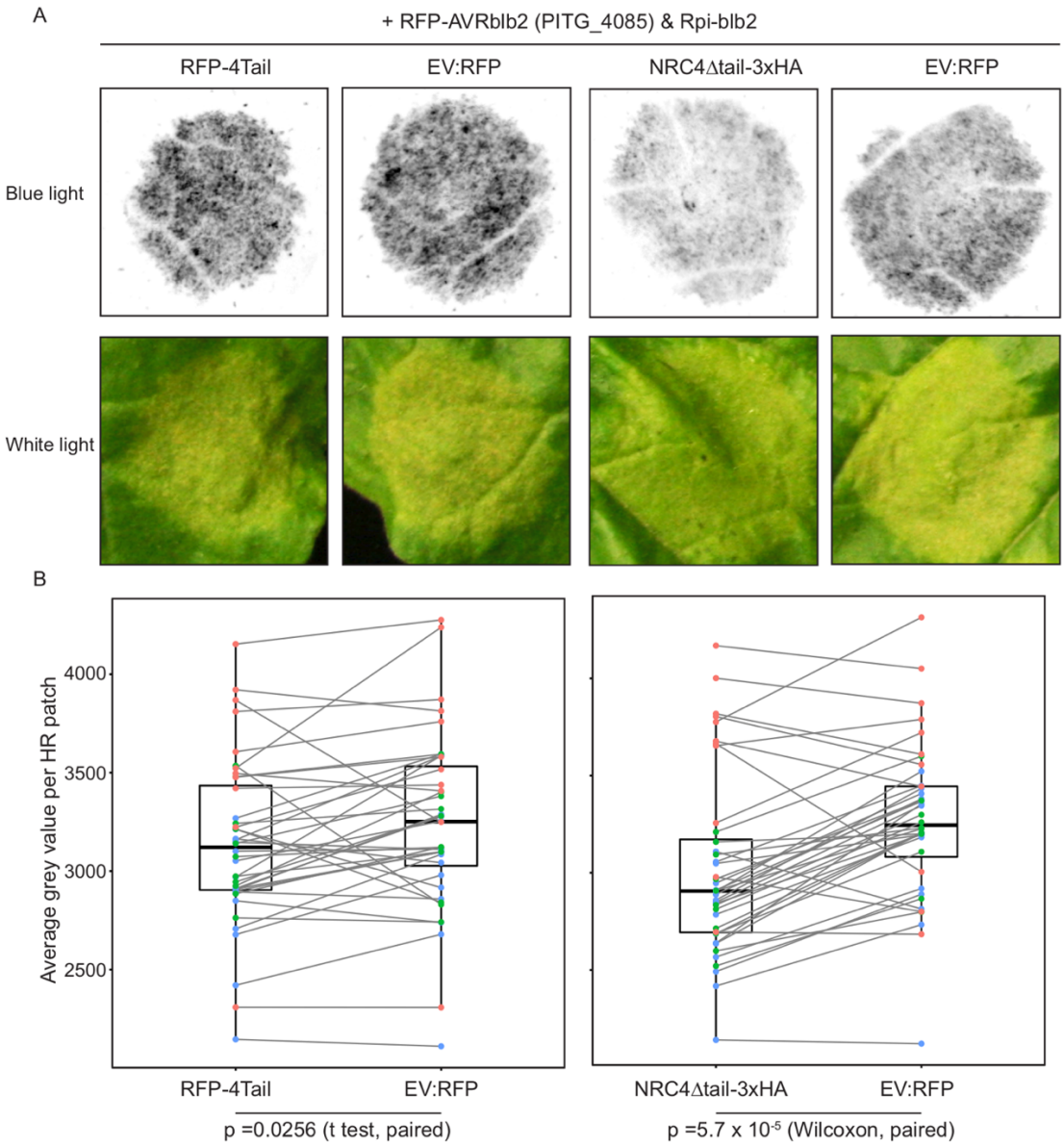


Figure 4.7: 4Tail weakly suppresses NRC4-mediated HR.
(A & B) RFP-AVRblb2 (PITG_4085) and Rpi-blb2 (transient RFP-Rpi-blb2, transgenic reps 2 & 3) were expressed to trigger HR. A treatment or control was co-expressed to judge the effect on HR after 3 days: Either treatment of 4Tail opposite control EV:RFP, or NRC4Δtail-3xHA treatment vs EV:RFP control. Blue light transilluminator with λ = 420 nm, exposure 1 second, was used to image HR by proxy of the phenolic compounds produced during HR. A circular region of interest was drawn on each patch and the mean grey value plotted as individual data points in (B). Whiskers in box plot represent Max and Min data points, centre represents median of all data points, top of box 1st quartile, the lower and upper hinges of the box correspond to the first and third quartiles respectively (the 25th and 75th percentiles). Shapiro-Wilk normality test determined the NRC4Δtail3xHA sample is non-normally distributed, so a paired Wilcoxon test was performed with p = 5.7x 10^{-5}. For RFP-4Tail and its corresponding EV:RFP control, they were both normally distributed so a paired t test was performed with p=0.0256, a paired Wilcoxon test would result in p=0.00826.

4.4.2.2. 4Tail expression does not interfere with NRC4 stability

Next, to test if 4Tail had any impact on NRC4 stability, I investigated whether 4Tail expression alters NRC4-3xHA protein levels (Figure 4.8). I used western blot analysis of total protein extracts to compare the protein levels of NRC4-3xHA in tissue co-expressing 4Tail-GFP versus EV:GFP. I found that expression of 4Tail had no visible effect on NRC4 levels – a conclusion strengthened by sequential dilutions of the extracts to reduce the chance of bias introduced due to protein saturation. I also co-expressed RFP-GUS in all samples as a control to better demonstrate equal protein extraction and loading between samples.

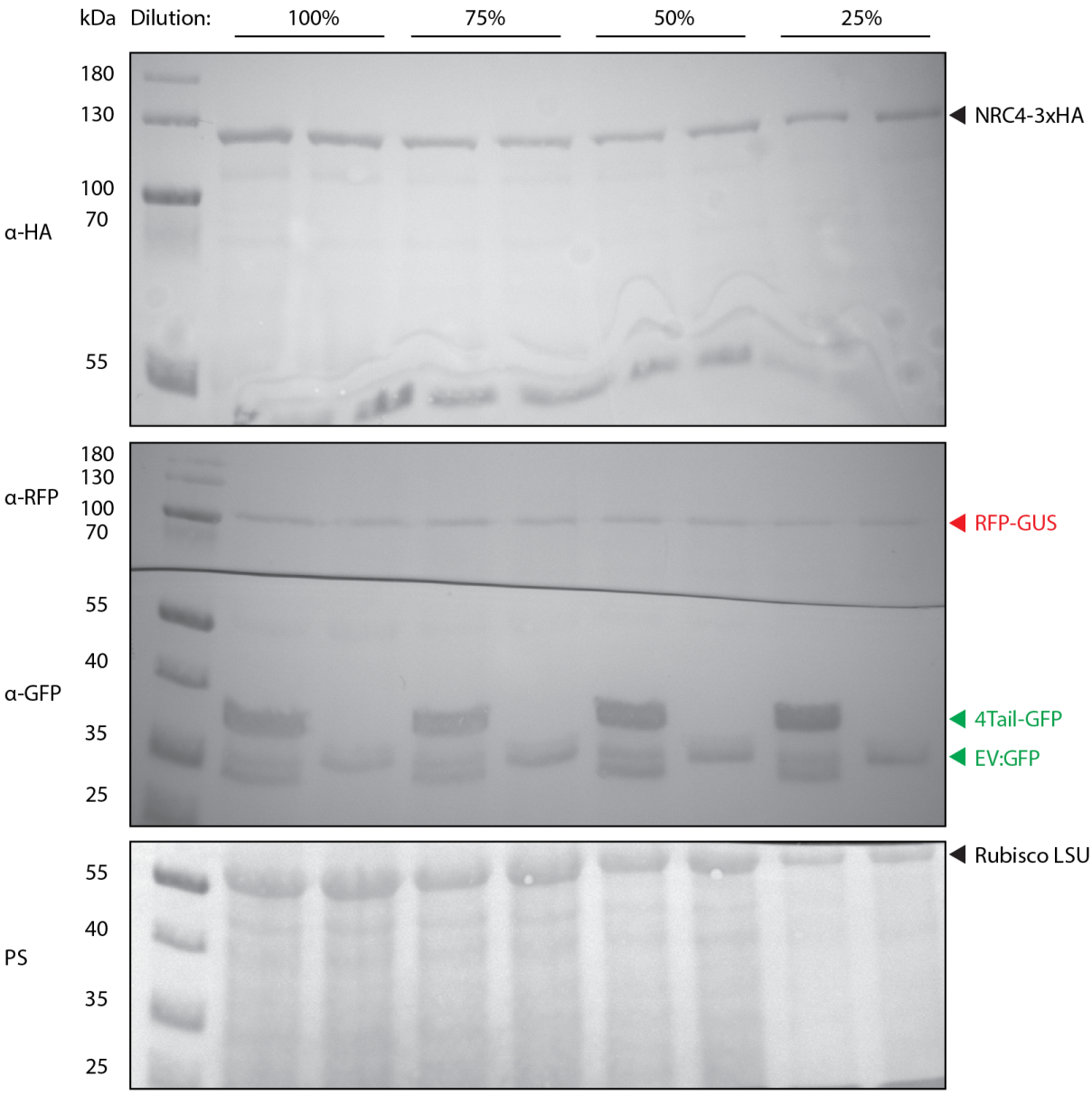


Figure 4.8: 4Tail expression does not lead to NRC4 degradation.
NRC4-3xHA and RFP-GUS were transiently co-expressed with 4Tail-GFP or EV:GFP in *N. benthamiana* leaves and protein levels were analysed 3dpai by SDS-PAGE and western blotting. Total protein extracts (100%) (4 leaf disks from #4 cork borer were extracted in 120 µl extraction buffer and 20 µl of this constituted 100% extract) were also diluted to 75%, 50% and 25% with 1x Laemmli buffer and loaded side-by-side to prevent bias by saturation of protein bands. 4Tail-GFP expression did not alter the protein levels of NRC4-3xHA or internal control for agroexpression and loading, RFP-GUS. Protein extraction and loading was approximately equal across samples as evidenced by the Ponceau Stain (PS) of rubisco large subunit (LSU) and the antibody detection of RFP-GUS. M = Marker. Proteins were run on a 7.5% polyacrylamide gel to detect NRC4-3xHA, and a 10% gel to resolve RFP-GUS, 4Tail-GFP and EV:GFP. The blot originating from the 10% gel was cut to allow RFP and GFP to be simultaneously probed.

4.4.2.3. 4Tail does not associate with NRC4 or Rpi-blb2

To test whether 4Tail expression was compromising Rpi-blb2/NRC4 resistance by interfering with NRC4 directly, I first investigated whether NRC4 binds to 4Tail *in planta* (Figure 4.9). I co-expressed NRC4-3xHA with wither NRC4-GFP, 4Tail-GFP, 4Tail-7KA-GFP or EV:GFP and immunoprecipitated the GFP-tagged proteins. I did not detect NRC4-3xHA in immunoprecipitates of 4Tail-GFP or 4Tail-7KA-GFP, whereas NRC4-3xHA showed clear co-immunoprecipitation (co-IP) with NRC4-GFP indicating that NRC4 could self-associate or even oligomerise. Therefore, pending further validation particularly completing the reverse co-IP, it is unlikely 4Tail is disrupting immunity by binding to full-length NRC4.

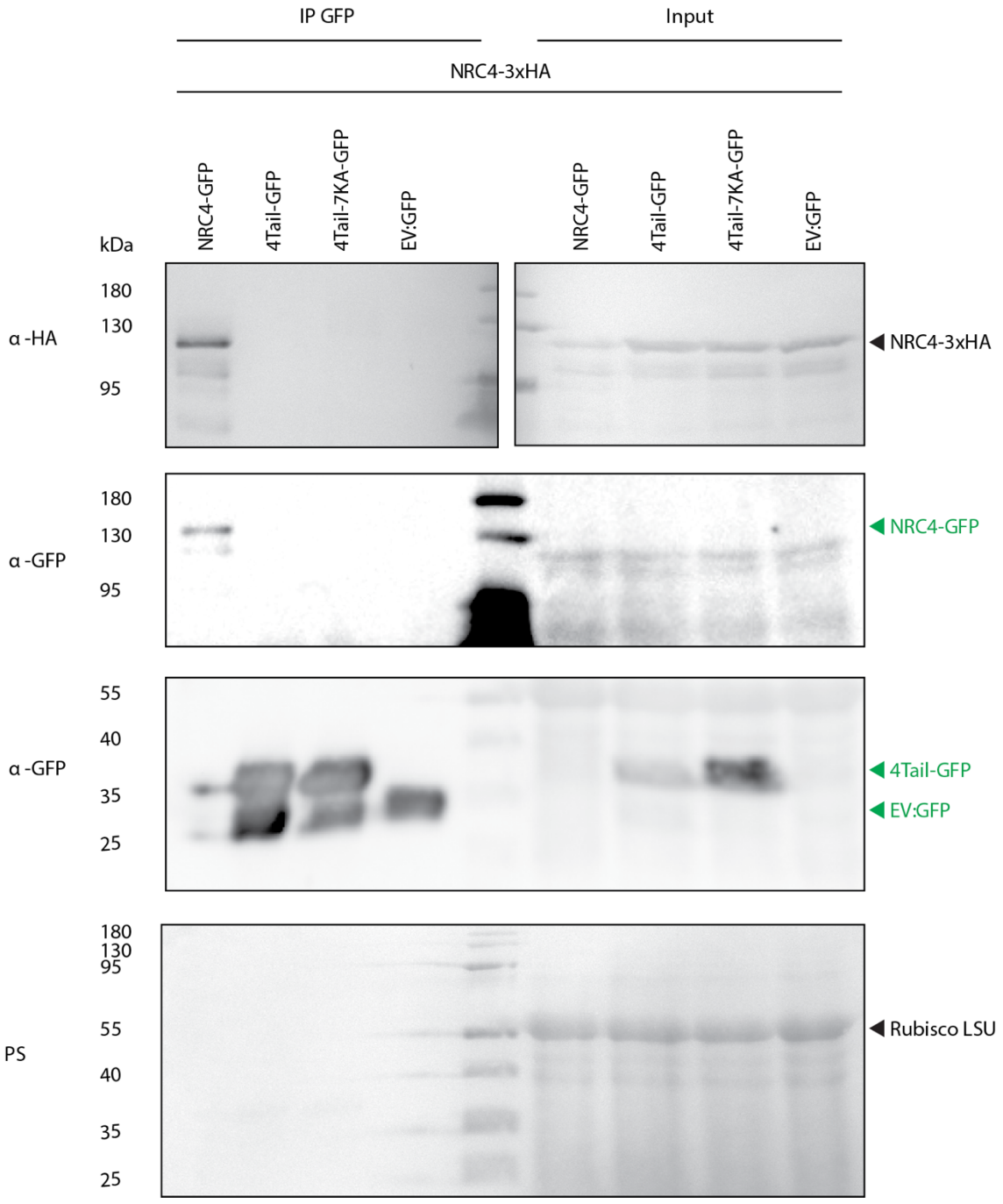


Figure 4.9: Full-length NRC4 does not coimmunoprecipitate with 4Tail.
NRC4-3xHA was transiently co-expressed with either NRC4-GFP, 4Tail-GFP, 4Tail-7KA-GFP or EV:GFP in *N. benthamiana* leaves and proteins were extracted after 3 days and immunoprecipitation (IP) experiments were carried out. Anti-GFP or anti-HA antisera were used to detect IPs (left) or total protein extracts (input, right) on immunoblots. NRC4-3xHA binds to NRC4-GFP as expected, but did not bind to 4Tail-GFP, 4Tail-7KA-GFP or EV:GFP. A 7.5% SDS-PAGE gel was used to separate the high molecular weight NRC4 proteins, whilst a 12% SDS-PAGE gel was used to separate the others, which were low molecular weight proteins. Protein extraction and loading was approximately equal across samples as evidenced by the Ponceau Stain (PS) of rubisco large subunit (LSU). Arrowheads indicate expected band for proteins indicated. kDa = kilodaltons

Another possibility is that 4Tail interferes with sensor NLR functions. To determine whether 4Tail interacts with Rpi-blb2, I performed an *in planta* co-immunoprecipitation experiment between Rpi-blb2 and 4Tail. Despite the controls indicating the experiment was successful, I did not detect an association between 4Tail and Rpi-blb2. Again NRC4 did co-immunoprecipitate with 4Tail, in this assay (Figure 4.10).

To test whether 4Tail associates with the sensor-helper complex, I performed a reciprocal co-IP between Rpi-blb2 and NRC4 in the presence or absence of 4Tail. I pulled down NRC4 (Figure 4.11) or Rpi-blb2 (Figure 4.12) and investigated if 4Tail associated with them. I performed two independent experiments. However, these experiments were inconclusive as I detected 4Tail-mKOk-FLAG signal in immunoprecipitates of both the test and negative control samples, suggesting that 4Tail-mKOk-FLAG may have affinity to the GFP-trap beads or GFP itself.

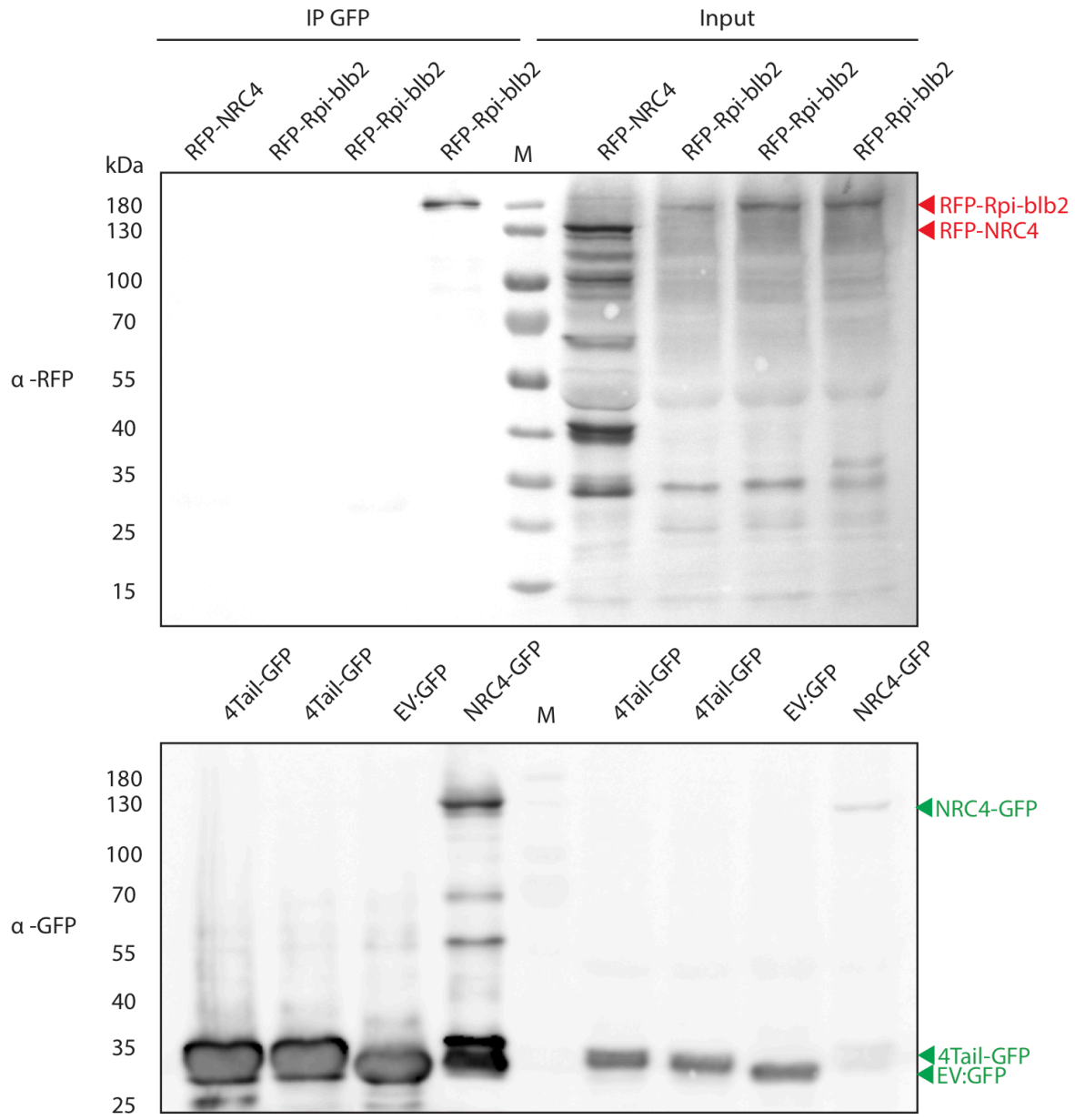


Figure 4.10: Rpi-blb2 or NRC4 does not coimmunoprecipitate with 4Tail. 4Tail-GFP, EV:GFP or NRC4-GFP were transiently co-expressed with RFP-Rpi-blb2 or RFP-NRC4. After 3 days proteins were extracted, and GFP-trap agarose beads were used to immunoprecipitate proteins. After washing off non-specific interactions, IPs and total inputs were separated by SDS-PAGE and immunoblotted. Despite the positive control NRC4-GFP pulling down RFP-Rpi-blb2, neither RFP-Rpi-blb2 or RFP-NRC4 coimmunoprecipitated with 4Tail-GFP. Arrowheads indicate the expected band of the indicated proteins. kDa = kilodaltons

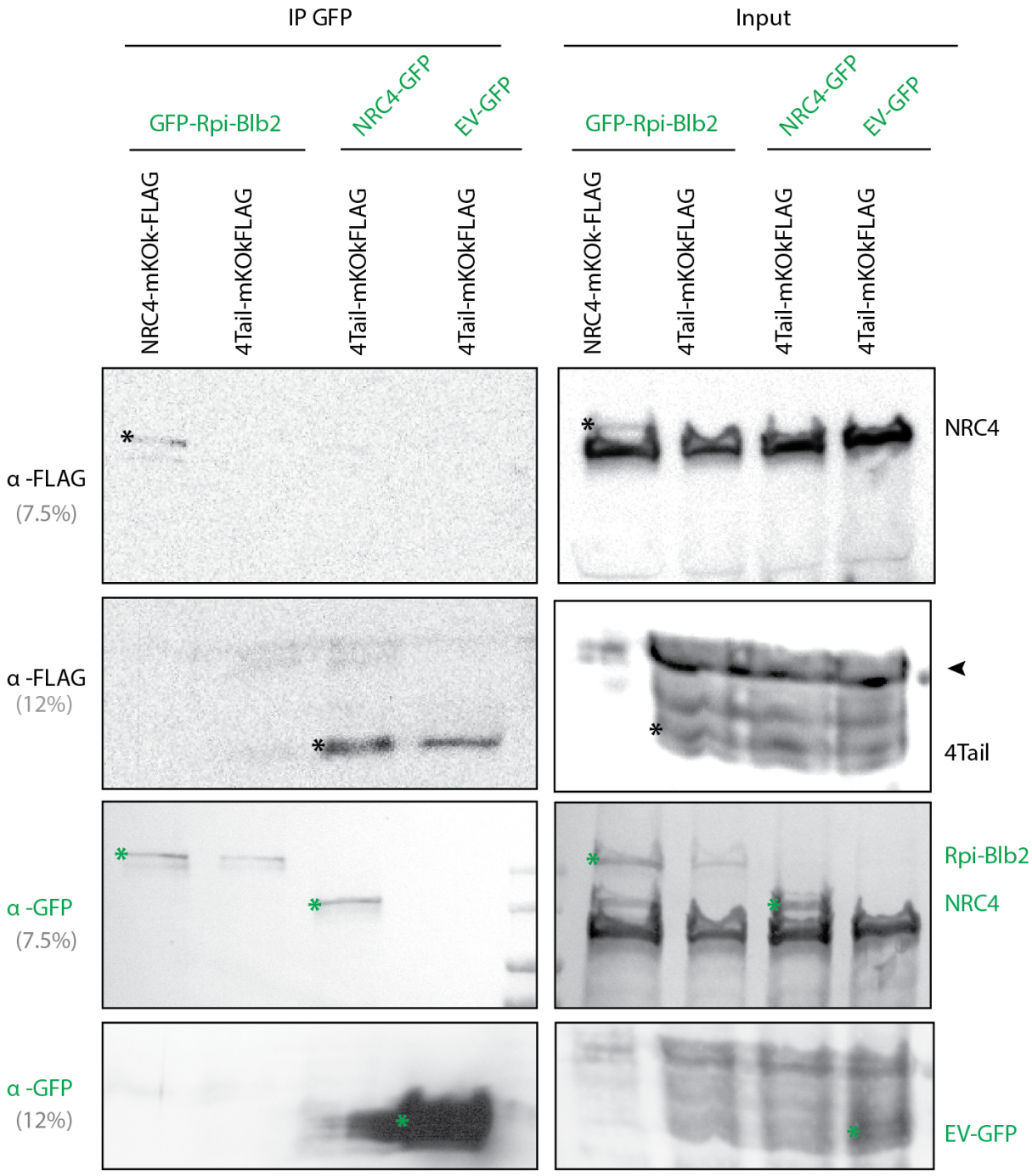


Figure 4.11: 4Tail co-immunoprecipitates with NRC4 but also the negative control EV:GFP.
4Tail-mKOk-FLAG or NRC4-mKOk-FLAG were transiently co-expressed with GFP-Rpi-blb2, NRC4-GFP or EV:GFP. After 3 days proteins were extracted and GFP-trap agarose beads were used to immunoprecipitate proteins. After washing off non-specific interactions, IPs and total inputs were separated by SDS-PAGE and immunoblotted. The positive control NRC4-mKOk pulled down with GFP-Rpi-blb2. 4Tail-mKOk-FLAG coimmunoprecipitated with NRC4-GFP but also the negative control EV:GFP. Asterisks indicate expected band sizes of proteins indicated on the right hand side. Arrowhead indicates higher molecular weight 4Tail-mKOk-FLAG-asssociated band, discussed with Figure 4.6. kDa = kilodaltons

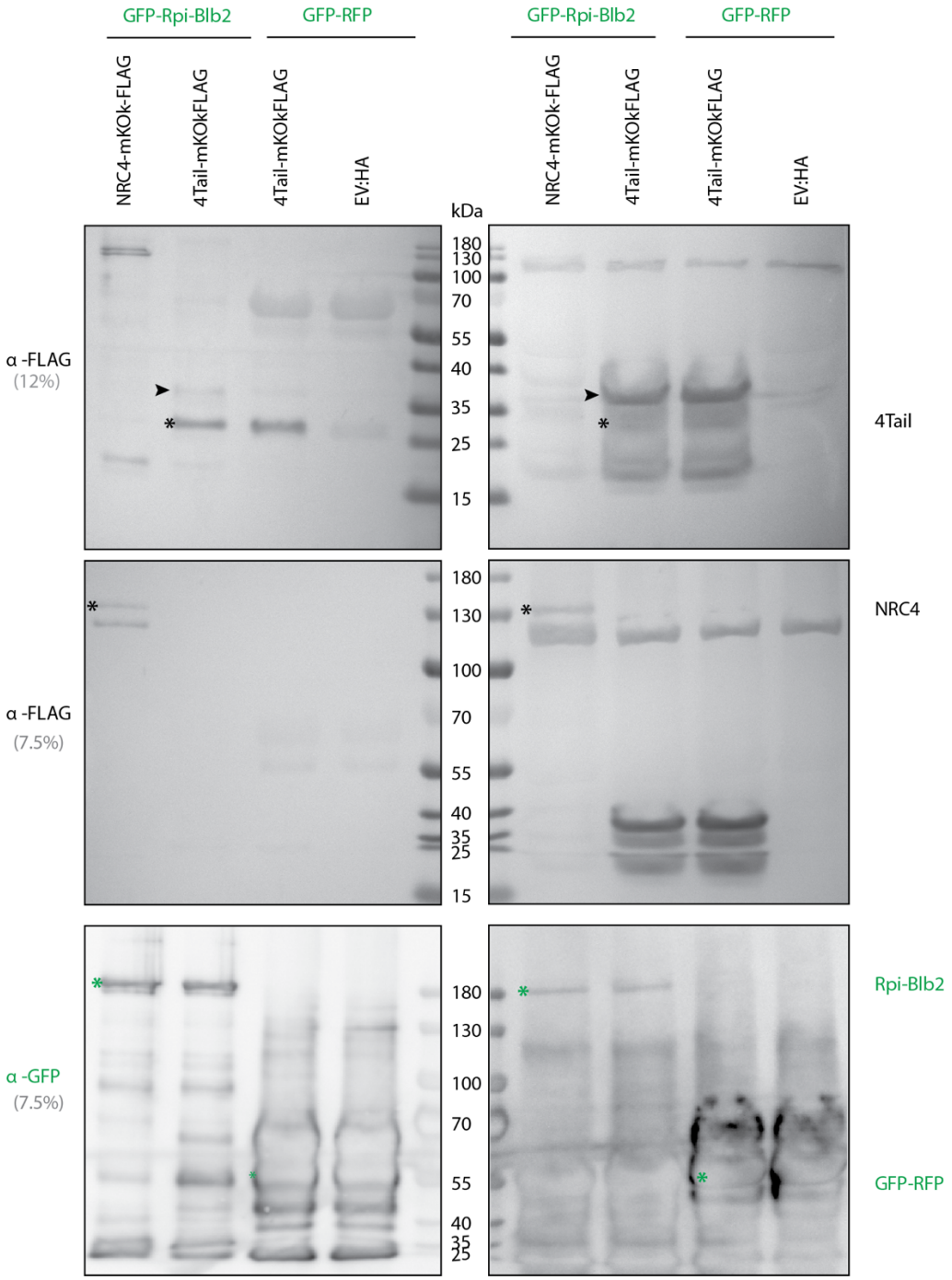


Figure 4.12: 4Tail co-immunoprecipitates with GFP-Rpi-blb2 but also the negative control GFP-RFP tandem.
4Tail-mKOk-FLAG, NRC4-mKOk-FLAG or EV:HA were transiently co-expressed with GFP-Rpi-blb2 or GFP-RFP tandem. After 3 days proteins were extracted and GFP-trap agarose beads were used to immunoprecipitate proteins. After washing off non-specific interactions, IPs and total inputs were separated by SDS-PAGE and immunoblotted. The positive control NRC4-mKOk pulled down with GFP-Rpi-blb2. 4Tail-mKOk-FLAG coimmunoprecipitated with GFP-Rpi-blb2 but also the negative control GFP-RFP tandem. Asterisks indicate expected band sizes for proteins indicated on the right hand side. Arrowhead indicates higher molecular weight 4Tail-mKOk-FLAG-asssociated band. kDa = kilodaltons.

4.4.2.4. 4Tail does not inhibit NRC4-NRC4 interaction or NRC4-Rpi-blb2 interaction

It is possible that the mechanism of 4Tail impairment of Rpi-blb2 resistance is by inhibiting oligomerisation of the NLRs. I therefore carried out a series of co-immunoprecipitation experiments to determine if the binding was impaired in the presence of 4Tail expression relative to EV expression. Firstly, I co-expressed two differentially tagged NRC4 full-length constructs in the presence and absence of 4Tail expression. I pulled down NRC4-GFP and assayed for relative differences in NRC4-3xHA levels. After taking into account the relative pull-down efficiency of NRC4-GFP, two independent experiments indicated no effect of 4Tail on NRC4 homo-oligomerisation (Figure 4.13 & Supplementary 2 = Figure 4.38). I then investigated Rpi-blb2-NRC4 hetero-oligomerisation. I carried out the same experiment with RFP-Rpi-blb2 instead of NRC4-3xHA and found no clear effect on association, after relative pull-down efficiencies were taken into consideration with quantitative western blotting, where the band intensities can be accurately measured by a new western blotting machine made available, the LI-COR Odyseey FX (Figure 4.14 & Supplementary 3 = Figure 4.39).

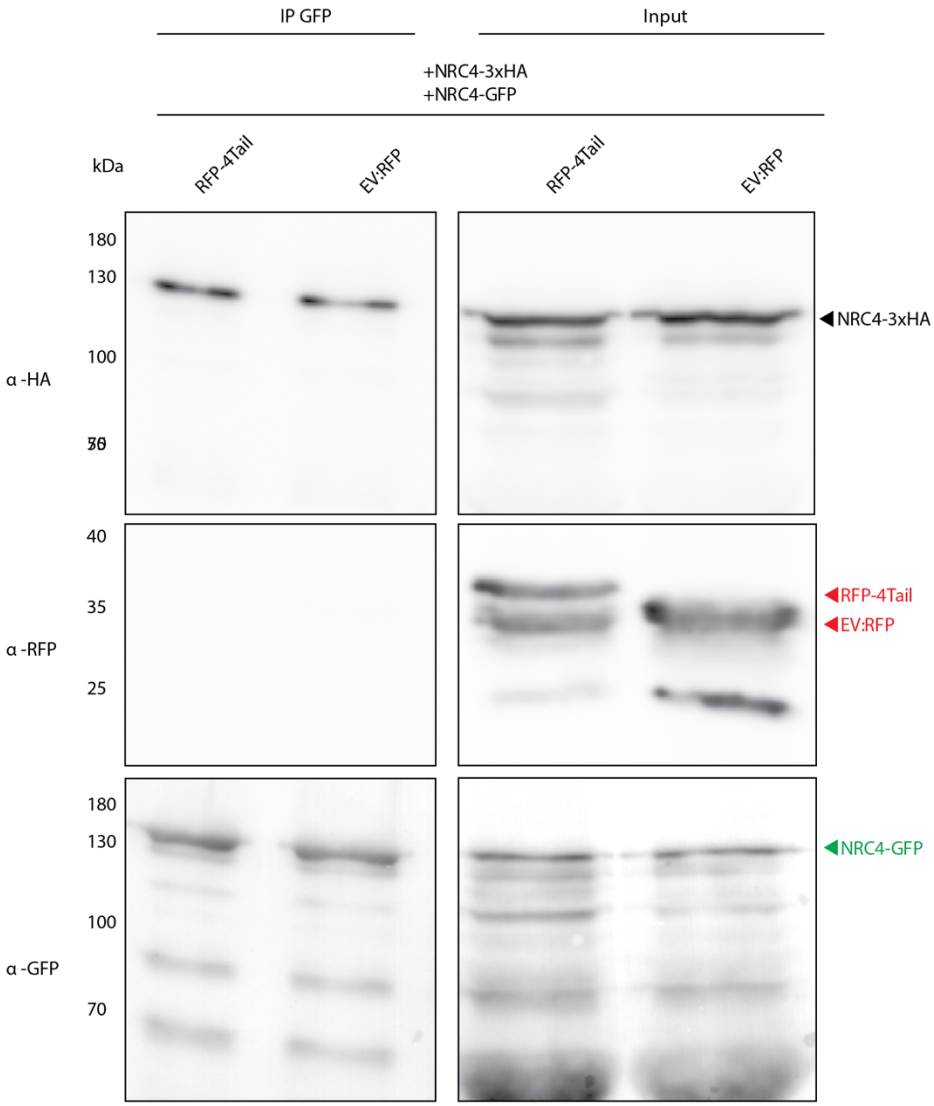


Figure 4.13: 4Tail expression does not seem to effect NRC4-NRC4 interaction. Differentially tagged NRC4, NRC4-GFP and NRC4-3xHA was co-expressed with RFP-4Tail or EV:RFP on opposite sides of *N. benthamiana* leaves to reduce variation in expressions. After 3 days proteins were extracted and GFP-trap agarose beads were used to immunoprecipitate proteins. After washing off non-specific interactions, IPs and total inputs were separated by SDS-PAGE and immunoblotted. The relative association of NRC4-3xHA with NRC4-GFP did not appear to be altered by 4Tail expression. Arrows indicate expected band sizes. kDa = kilodaltons.

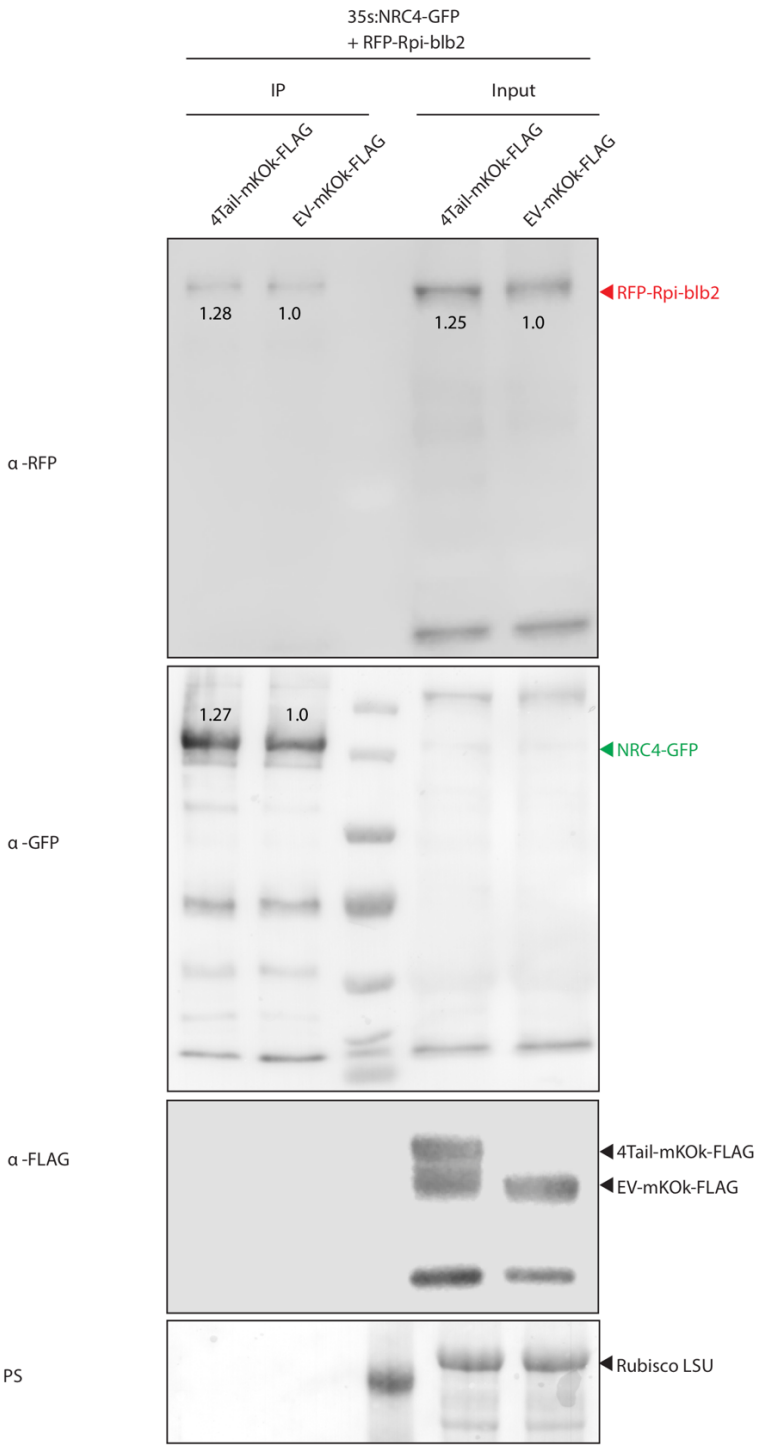


Figure 4.14: 4Tail expression does not seem to effect NRC4-Rpi-blb2 interaction. RFP-Rpi-blb2 was co-expressed with RFP-4Tail or EV:RFP on opposite sides of 35S:NRC4-GFP *N. benthamiana* leaves to reduce variation in expressions. After 3 days proteins were extracted and GFP-trap agarose beads were used to immunoprecipitate proteins. After washing off non-specific interactions, IPs and total inputs were separated by SDS-PAGE and immunoblotted. The relative association of RFP-Rpi-blb2 with NRC4-GFP did not appear to be altered by 4Tail expression. Numbers indicate the band 'Signal' as determined by LI-COR Odyseey FX quantitative western blotting. Arrows indicate expected band sizes. kDa = kilodaltons.

4.4.2.5. 4Tail suppressed NRC4's haustorial localisation, but doesn't have a noticeable effect on membrane association of NRC4

The most intriguing explanation for the effect of 4Tail would be on NRC4's localisation. Therefore I conducted confocal microscopy of full length NRC4 during infection of *P. infestans* in the presence and absence of 4Tail expression. In NRC4-GFP stable transgenic (*35S::NRC4-GFP*) plants, expression of RFP-4Tail did not appear to alter NRC4 accumulation around the haustoria when compared to expression of RFP-EV control. However, after quantifying the perihaustorial NRC4-GFP signal, I found a reduction in samples expressing 4Tail than samples expressing EV control (Figure 4.15). I then repeated the experiment in nrc4a/b plants transiently expressing NRC4-GFP, as I hoped removal of endogenous, untagged NRC4, would lead to a clearer effect. Cell-to-cell variation in expression means that this quantification method is not suitable to samples transiently expressing NRC4. Therefore I quantified the perihaustorial signal and the cytoplasmic signal (using EV-RFP or RFP-4Tail as a cytoplasmic marker) and plotted a ratio of the two to give the peri-haustorial NRC4 signal relative to the cytoplasm (i.e. focal accumulation index). This showed a strong decrease of NRC4-GFP accumulation at the EHM in 4Tail samples compared with EV samples. (Figure 4.16).

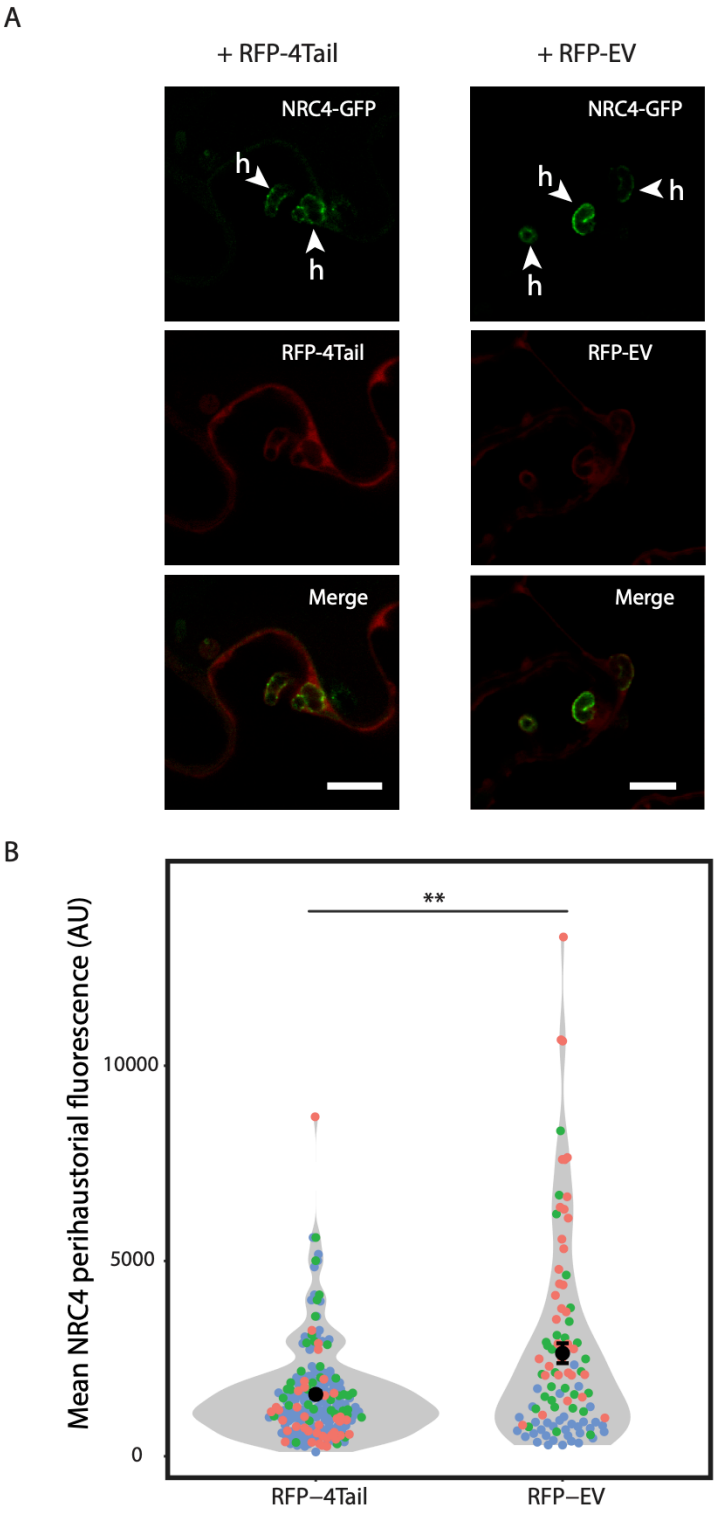


Figure 4.15: 4Tail expression reduces NRC4-GFP perihaustorial fluorescence. 35S:NRC4-GFP plants were treated with RFP-4Tail or RFP-EV expression during infection with *P. infestans.* (A) Representative single plane images. Scale bars are 10 µm. (B) The mean perihaustorial fluorescence or NRC4-GFP was measured with ImageJ using a freehand ROI line. These values are plotted in scatter violinplot. The total number of haustoria measured, *N* = 195 for RFP-4Tail, and *N* = 99 for RFP-EV. Three independent reps were carried out.

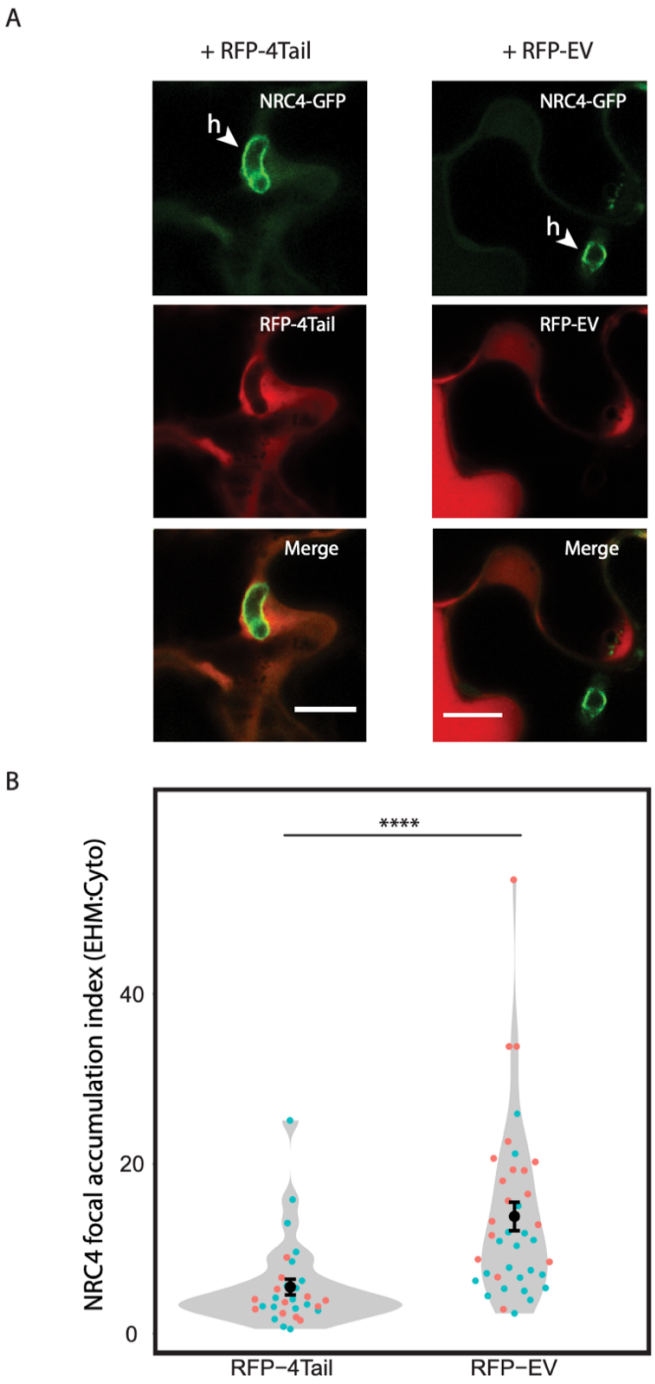


Figure 4.16: NRC4 focal accumulation is suppressed by 4Tail expression. nrc4a/b plants were transiently complemented with NRC4-GFP, co-expressed with either RFP-4Tail or RFP-EV during infection with *P. infestans.* Absolute perihaustorial signal of NRC4 seemed to be higher in RFP-4Tail expressing samples possibly due to too few cells being sampled. Therefore the mean NRC4 perihaustorial fluorescence was compared to the cytoplasmic signal. (A) Representative single plane images. Scale bars are 10 µm. (B) Scatter violinplot shows NRC4 focal accumulation is reduced in 4Tail expressing samples. Here the mean perihaustorial fluorescence sampled was divided by the mean cytoplasmic fluorescence sampled. The total number of haustoria:cytoplasmic measurements, *N* = 30 for RFP-4Tail, and *N* = 38 for RFP-EV. Just two reps were conducted.

However, the manual image acquisition and manual quantification in this experiment runs the risk of human bias. Additionally, it's unclear if the reduction of NRC4 EHM accumulation measured in these experiments, is sufficient to cause Rpi-blb2 resistance to be broken. Therefore, to gain biochemical evidence to support these findings, I investigated microsomal/membrane enrichment to determine whether 4Tail expression reduces NRC4 membrane association. I enriched membranes in samples expressing NRC4-GFP and RFP-Rem1.3 (PM marker) with either 4Tail-mKOk-FLAG or EV:mKOk-FLAG. The membrane marker RFP-Rem1.3 displayed strong signal in the soluble fraction of both samples and weak signal roughly comparable to that of the rubisco cytoplasmic control. Therefore the enrichment may have been ineffective, or RFP-Rem1.3's cytoplasmic pool was stronger than it's membrane associated pool in this experiment. This correlates with the strong rubisco signal in the membrane fractions of both samples which indicates the enrichment was not effective or the membrane fraction was 'contaminated' with cytoplasm. 4Tail-mKOk-FLAG and EV:mKOk-FLAG showed similar expression levels. NRC4 signals were poor possibly due to low expression or poor detection. Excluding the fact the enrichment was unsuccessful, it is possible to say there was no decrease in NRC4 membrane associated signal in the presence of 4Tail relative to EV expression (Figure 4.17). However, these results are not so surprising considering the very minor reduction of HR intensity in my pathogen independent HR assays. In contrast, the effect of 4Tail on Rpi-blb2 resistance to the pathogen is of a stronger magnitude.

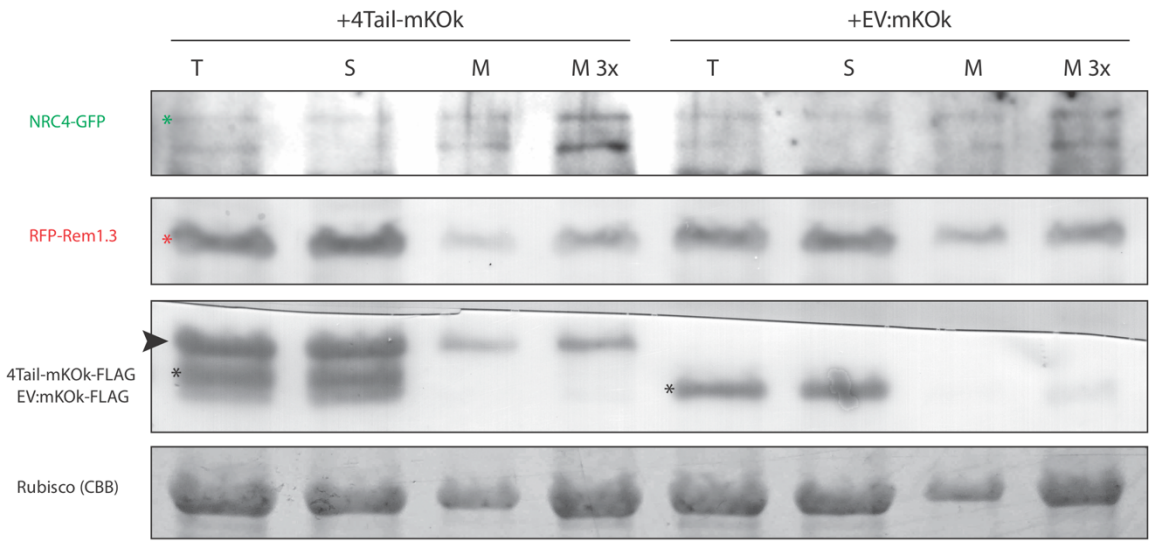


Figure 4.17: NRC4 membrane association is not altered by overexpression of 4Tail.
Membrane enrichment of transiently expressed NRC4-GFP tissue (nrc4a/b plants) shows similar membrane association of NRC4 in both conditions. RFP-Rem1.3 was co-expressed as a membrane marker. 4Tail-mKOk related higher molecular weight bands (arrowhead) appear to be membrane associated. Stars indicate expected band sizes. NRC4-GFP and RFP-Rem1.3 were co-expressed with either 4Tail-mKOk-FLAG or EV:mKOk-FLAG in nrc4a/b *N. benthamiana.* Leaves were frozen in liquid nitrogen after 3 days and extracted in sucrose buffer lacking detergents and after clearing the debris the Total fraction (T) was taken before the rest of the extract was centrifuged at 21,000 *g* for 1 h at 4˚C. The supernatant was taken as the Soluble (S) sample and the pellet was taken as the Membrane-enriched (M) sample, which was resuspended in 3 times less buffer than the S sample. Ponceau stain (PS) was used to determine protein loading and cytoplasmic protein levels.

4.4.2.6. Resistance to non-haustorial pathogen, Potato Virus X is compromised by 4Tail expression

As an alternative strategy to determine whether 4Tail compromised NRC4-mediated immunity via inhibiting focal deployment of NRC4, I investigated whether 4Tail could disrupt NRC4-mediated immunity to a non-haustoriated pathogen. Potato Virus X (PVX) is recognised by Rx1 sensor CNL, which requires NRC2, NRC3 or NRC4 redundantly (Wu et al., 2017). To investigate whether 4Tail could inhibit Rx1 resistance, we first expressed systemic silencing Virus Induced Gene Silencing (VIGS) constructs targeting NRC2/3 in transgenic Rx1-4xHA plants and compared it to positive control NRC2/3/4-targeted plants or non-silenced TRV2:EV plants (Figure 4.18).

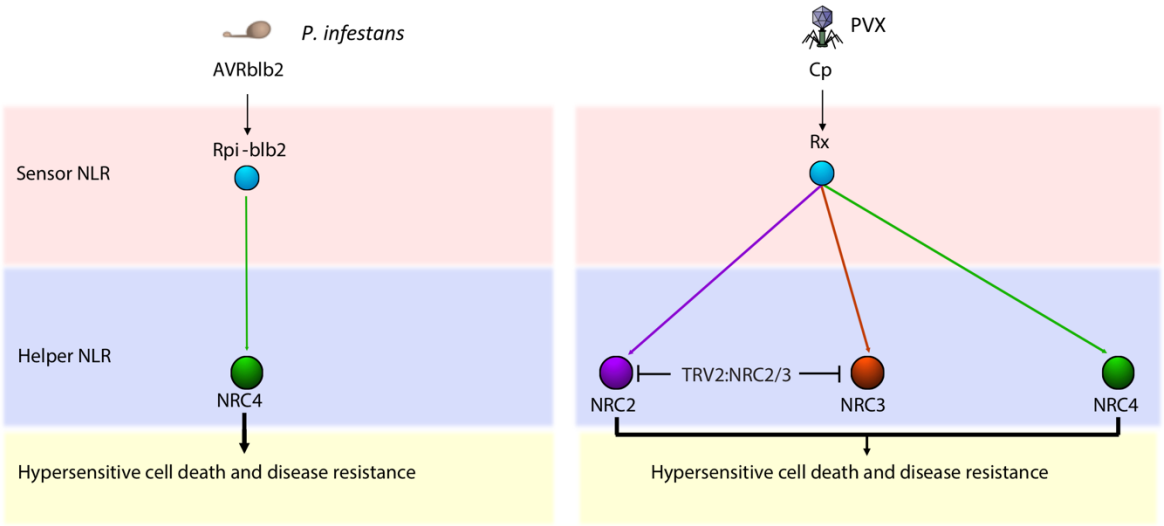


Figure 4.18: Model of Rpi-blb2 and Rx1 mediated resistances.
Adjusted from a model made by Jess Upson, which was based on Wu et al., 2017. Cartoon showing that *P. infestans* secretes an effector protein AVRblb2 which is recognised by the sensor NLR Rpi-blb2 that requires the helper NLR NRC4 for HR and disease resistance. Potato Virus X (PVX) is a plant pathogenic virus, not a bacteriophage (as shown for communication purposes only). The coat protein (Cp) of PVX is recognised by the sensor NLR Rx (Rx1) which is dependent on NRC2, NRC3 or NRC4 for HR and disease resistance. In the following experiment, TRV2:NRC2/3 was expressed in order to silence NRC2 and NRC3 to allow us to assay 4Tail effects on NRC4.

We transiently expressed patches of 4Tail on the opposite side of the leaf to EV negative control. As positive controls for breaking NRC4-mediated immunity, we expressed dominant-negative RFP-NRC4 opposite EV negative control and RNAi-

NRC4 opposite RNAi-GUS negative control. After one day we infected the patches with PVX by a low OD_{600} of *Agrobacterium* expressing the virus. At this OD_{600} the virus only infects a few cells and if immunity is compromised leads to the formation of necrotic lesions (Wu et al., 2017), similar to the hemi-biotrophy of *P. infestans.* In parallel, we conducted an identical experiment with Rpi-blb2 resistance to *P. infestans.* Necrotic lesions were visible in most patches containing RFP-NRC4 and RFP-4Tail and to a lesser extent RNAi-NRC4 expressing patches, on leaves infected with both pathogens. In the case of PVX infection, these necrotic lesions were not observed on TRV2:EV expressing plants but were observed on both TRV2:NRC2/3/4 (positive control) plants and TRV2:NRC2/3 plants. Necrotic lesions were seen in negative control RNAi-GUS or RFP-EV patches only in TRV2:NRC2/3/4 plants. This suggests that 4Tail and RFP-NRC4 compromised resistance to *P. infestans* and PVX, in an NRC4-dependent manner (Figure 4.19). The efficacy of the RNAi-NRC4 construct dropped in the latter reps, which could have been due to a temperature change in the infection rooms affecting RNAi efficiency or a contamination of the culture. Whilst it was unexpected that 4Tail expression would disrupt immunity to a non-haustorial pathogen, we cannot discount that 4Tail is inhibiting NRC4 focal accumulation in this situation also. It is possible that NRC4 accumulation to virus containing vesicles is required for immunity and 4Tail expression disrupts this. Expression of the constructs and silencing efficiencies were not confirmed in this experiment, but were previously shown in Wu et al., 2017 for VIGS constructs and in Figure 4.10 & Figure 4.13. RNAi-NRC4 was functionally validated in this experiment by compromising resistance in Rpi-blb2 transgenics.

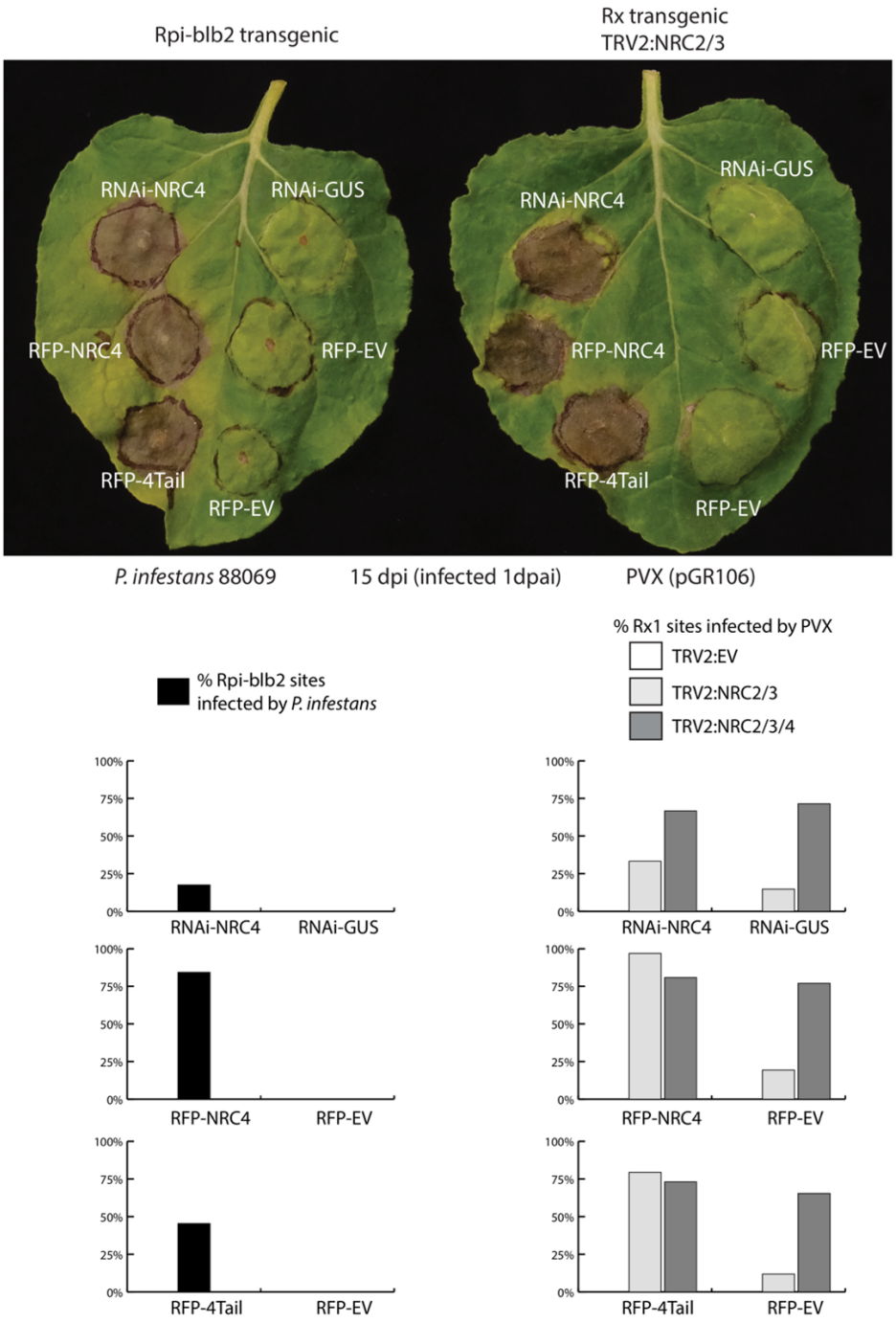


Figure 4.19: Rpi-blb2 and Rx1 resistance is broken by 4Tail.
Rx1 transgenic plants were systemically silenced with VIGS using TRV2:EV, TRV2:NRC2/3 or TRV2:NRC2/3/4. Non-silenced Rpi-blb2 plants, and silenced Rx1 plants were infiltrated with RNAi-NRC4, RFP-NRC4 or RFP-4Tail with their negative controls infiltrated on the opposite side of the leaf, RNAi-GUS, RFP-EV and RFP-EV respectively. One day after agroinfiltration, the patches were infected with either *P. infestans* spore droplets, or PVX *Agrobacterium* cultures (by infiltration of whole patch). Leaves were kept in the same condition for 8-9 days after infection before imaging and quantifying binary score of infected or non-infected. (B) The % of sites infected for all treatments are plotted, where 5 independent reps were performed with the total number of infiltration patches per treatment $N > 20$.

4.4.2.7. Swapping NRC4's tail with that of its paralogue NRC2 retains the immune function

Confocal microscopy of the NRC homologue, NRC2, revealed it does not localise to haustoria (Fig 19A). Considering 4Tail is required for localisation to haustoria, and that its removal results in loss of function and considering its assumed important role in immunity, I reasoned that swapping it with the tail from NRC2 (2Tail) might retain NRC4 HR function whilst losing EHM accumulation capabilities. Therefore, in order to determine the function of NRC4 localisation at haustoria, I generated a chimera between NRC4 and its homologue NRC2 that does not localise to haustoria (Figure 4.20A & Chapter 3, Figure 1). I annotated this construct as NRC4^{2Tail} and first tested its ability to complement resistance against *P. infestans 88069* in NRC4 silenced Rpi-blb2 transgenic plants. I found that leaf patches expressing this chimera were only infected in 45% inoculations, close to complementation by transiently expressing NRC4 (31%) and much lower than EV:GFP expressing patches (78%; Figure 4.20B). In accordance with this, those inoculation spots which were successfully infected displayed significantly smaller necrotic lesions in NRC4^{2Tail} expressing patches, compared to the EV:GFP expressing patches and did not show any difference in size between NRC4^{2Tail} and NRC4 expressing tissues (Figure 4.20C). Therefore, the NRC4^{2Tail} chimera rescues NRC4/Rpi-blb2 mediated resistance. This was further validated by confirmation that NRC4^{2Tail} rescues HR cell death (Figure 4.20D). I silenced NRC2/3/4 in Rpi-blb2 transgenics then transiently co-expressed AVRblb2 with EV:GFP (HR negative control), silencing resilient NRC4 (HR positive control) and silencing resilient NRC4^{2Tail} and assayed their ability to rescue HR. NRC4^{2Tail} rescued HR in 94% of infiltration patches like full-length NRC4 (89%). The charges of 2Tail are very similar to that of 4Tail (Figure 4.20A), and so it's possible that this is what enables NRC4^{2Tail} to rescue HR and resistance.

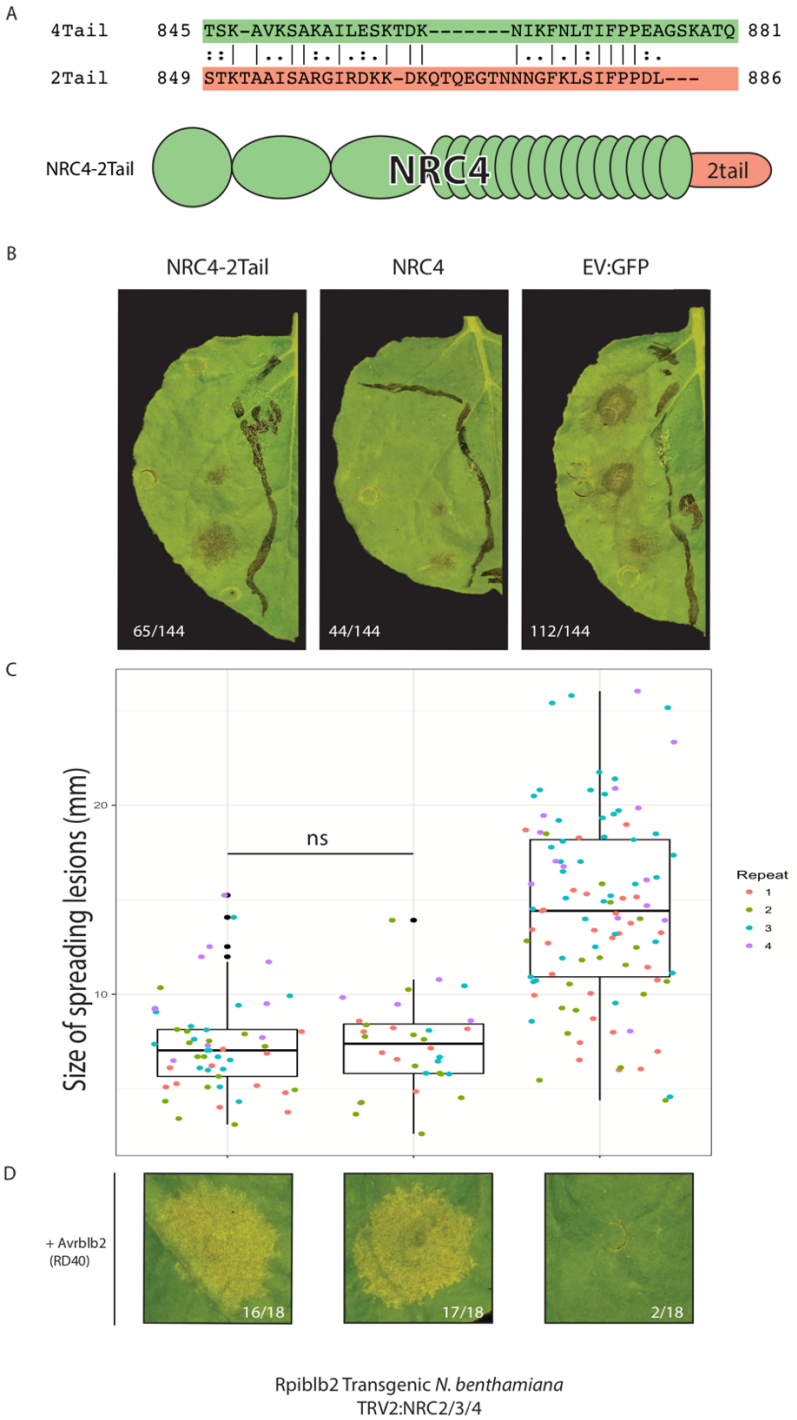


Figure 4.20: NRC4^{2Tail} chimera is functional for immunity.
(A) The C-terminal tail of NRC4 (4Tail), which lacks a leucine repeat, was swapped for that of NRC2 (2Tail) to form a chimera NRC4^{2Tail}. EMBOSS Needle pairwise sequence alignment (EMBL-EBI) was used to compare the tails. (C-D) NRC2, NRC3 & NRC4 were silenced in Rpi-blb2 transgenics by VIGS and the ability to complement for resistance (B-C) or HR (D) was assayed. (B) NRC4^{2Tail} complements resistance, like full length NRC4 (positive control), but unlike EV:GFP (negative control). The number of successful infections per sum of inoculations is recorded on bottom left of panel B. The lesion diameters were measured in millimetres. ns = non-significant (p= 0.94) at CI = 95%/99%. p-value < $2.2x10^{-16}$ for NRC4/Chimera & GFP at CI =99%.

As hypothesised, tagging of NRC4^{2Tail} with GFP conferred a non-polarised localisation in the cytoplasm during infection (Figure 4.21A; as does 2Tail-mKOk Figure 4.4B). However, fusion to GFP also resulted in loss of function as demonstrated by its inability to complement HR in NRC4-silenced Rpi-blb2 transgenics (Figure 4.21B). Since the GFP tag was interrupting its HR function, it could be interrupting its localisation also. Additionally, western blot analysis showed a very weak band approximately the correct size for NRC4^{2Tail}-GFP (Figure 4.22). However, this band appears to be present in all the lanes, meaning it could be due to non-specific binding of the antibody to a plant protein. As such, the localisation results of the NRC4^{2Tail}-GFP are unreliable. I cloned an N-terminal tagged version, GFP-NRC4^{2Tail} (Figure 4.22), but considering N-terminal tagging also leads to loss of function in NRC4 (Chapter 3, Figure 1), I decided this construct wasn't useful for investigating the relationship between NRC4's localisation and function. Therefore I decided to tag NRC4 internally. I reasoned that if GFP was inserted into the disordered region after the coiled-coil domain (Figure **4.1**), each domain of the NLR and GFP should fold independently, maintain their tertiary structure and the structure of the overall NLR and thus retain function. Indeed, internal tagging of NRC4 retained its EHM polarisation (Figure 4.21C). Remarkably, internal tagging of the chimera, NRC4^{2Tail}-iGFP also displayed EHM polarisation (Figure 4.21D). Therefore I concluded this was the true localisation of NRC4^{2Tail} chimera.

Since conducting this research, a greater understanding of the molecular mechanisms of CNLs has emerged. We now believe the CC domain of NRC4 executes the HR, and we also know the disordered region of CC domains, linking the CC and NBD domains is critical for HR (Wróblewski et al., 2018). In fact, this region is now thought to be required for the α1a to α1b conformational switch, i.e. 'the death switch' (Burdett et al., 2019; Wang et al., 2019a, 2019b). Considering this recent evidence, it is unsurprising that both NRC4-iGFP and NRC4^{2Tail}-iGFP could not elicit an HR (Figure 4.21E). The HR phenotypes of NRC4^{2Tail}-GFP, NRC4^{2Tail}-iGFP and NRC4-iGFP were confirmed in Rpi-blb2 nrc4a/b plants when they were available (Figure 4.31). Despite both NRC4^{2Tail}-GFP and NRC4^{2Tail}-iGFP having no HR functionality, I would argue it is more likely that the true localisation of untagged NRC4^{2Tail} at the EHM because this is an extra-ordinary localisation exhibited by NRC4^{2Tail}-iGFP, NRC4-iGFP and NRC4-

GFP, whereas the cytoplasmic localisation of NRC4^{2Tail}-GFP is a common localisation of proteins and is more likely to have been caused by loss of function due to tagging. Therefore, the NRC4^{2Tail} chimera is inappropriate for investigation of NRC4 haustorial function. However, NRC4^{2Tail} offers insights into this process in that 2Tail was sufficient to allow NRC4 function and localisation. Therefore, 4Tail and 2Tail appear to be functionally interchangeable for these purposes. In other words, NRC4 requires a 'Tail' but not specifically its own. Additionally, these results have highlighted that adding a bulky tag can disrupt functionality.

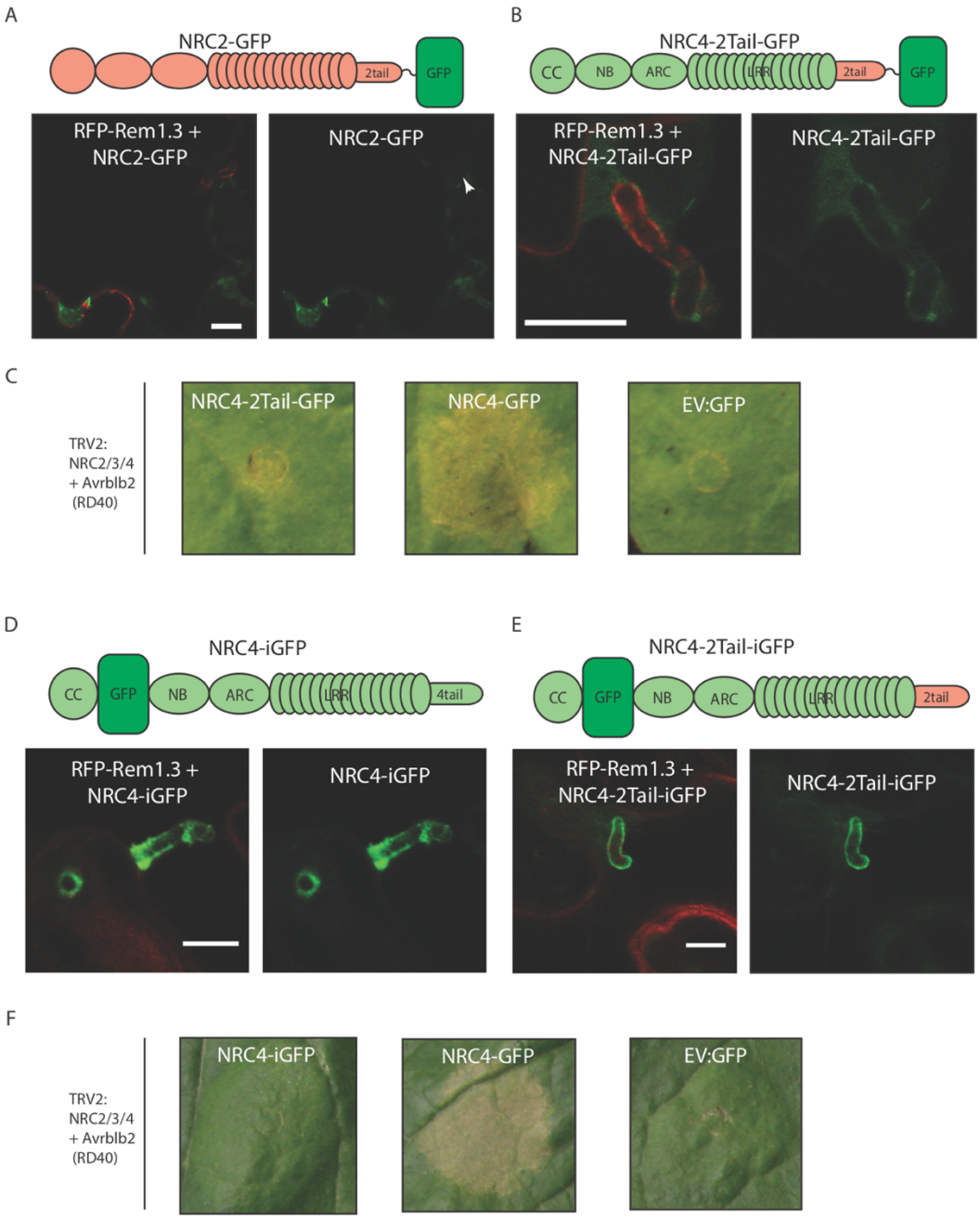


Figure 4.21: Internal tagging of NRC4^{2Tail} reveals it accumulates at haustoria. (A-B, D-E) RFP-Rem1.3 was co-expressed with either PICH89NRC2-GFP, NRC4-2Tail-GFP, NRC4-iGFP or NRC4-2Tail-iGFP. After 3 hours, leaves were infected with *P. infestans* and after 3 days, imaged with SP5 confocal microscope. Scale bars = 10µm. (C & F) Rpi-blb2 plants were silenced with TRV2:NRC2/3/4 and then AVRblb2 was co-expressed with either NRC4-2Tail-GFP, NRC4-iGFP, NRC4-2Tail-iGFP or EV:GFP. Yellowish colouration after 4 days was photographed as HR cell death. (A) NRC2-GFP and (B) NRC4^{2Tail}-GFP do not localise to haustoria, however the latter is non-functional in terms of HR (C). (D) NRC4 and (E) NRC4^{2Tail} were internally tagged after the CC domain and both localised to haustoria, but (F) NRC4-iGFP was HR non-functional. Arrowhead indicates location on unlabelled haustorium.

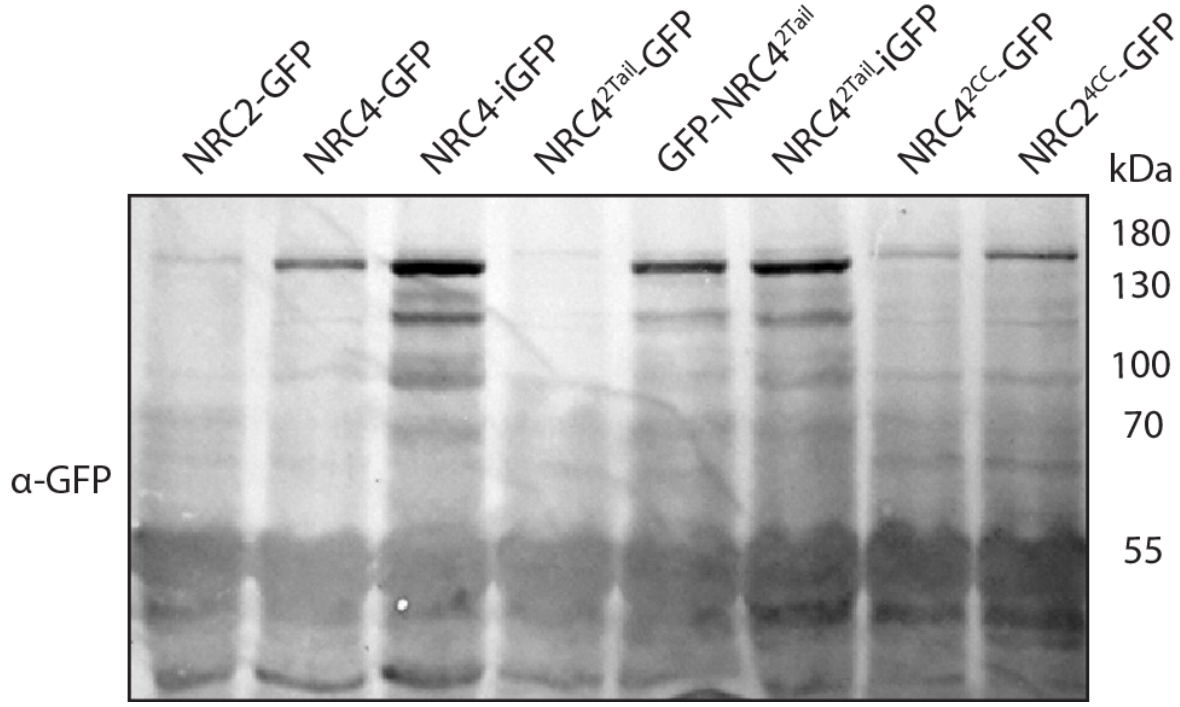


Figure 4.22: Western blotting shows NRC4-NRC2 chimeras are correctly cloned. Proteins were co-expressed at an OD_{600} = 0.3 with 0.1 of P19 to boost expression. NLRs are all expected to be approximately 130 kilodaltons (kDa). The western blot was detected by colour detection which also stains the Rubisco Large Subunit at approximately 55 kDa.

4.4.3. The CC domain of NRC4 mediates EHM accumulation and programmed cell death

In an effort to identify the true signal for haustorial localisation I selected the CC domain as a candidate due to the tendency for these domains to be involved in oligomerisation, and the cage-like accumulation of NRC4 at the EHM was reminiscent of an oligomeric structure. Additionally, ZAR1 CC domain is known to mediate membrane association (Wang et al., 2019a). The LRR domain is already annotated as containing the signal for sensor recognition (Wu, 2016), and the NBD is functionally constrained in nucleotide binding (Cesari, 2017; Qi and Innes, 2013).

4.4.3.1. CC domain is required for EHM localisation of NRC4

I N-terminally truncated NRC4 to remove the coiled-coil domain (Figure 4.23A). The InterProScan package determined that the region ending around amino acid 148 contained the full CC domain, and this region was predicted to be intrinsically disordered making it a good region to truncate (Figure **4**.**1**). Phyre2 modelling of NRC4 on the published structure of ZAR1 also corresponded with this finding (Adachi et al.,

2019). NRC4ΔCC-GFP displayed cytoplasmic localisation (Figure 4.23B), which sometimes appeared like accumulation but as the line profile in Figure 4.23B shows, this signal is external to the EHM labelled by RFP-Rem1.3. However, future work should quantify the degree to which this truncate accumulates, if at all, in comparison to the wild type. These results revealed that the CC domain is required for proper EHM accumulation.

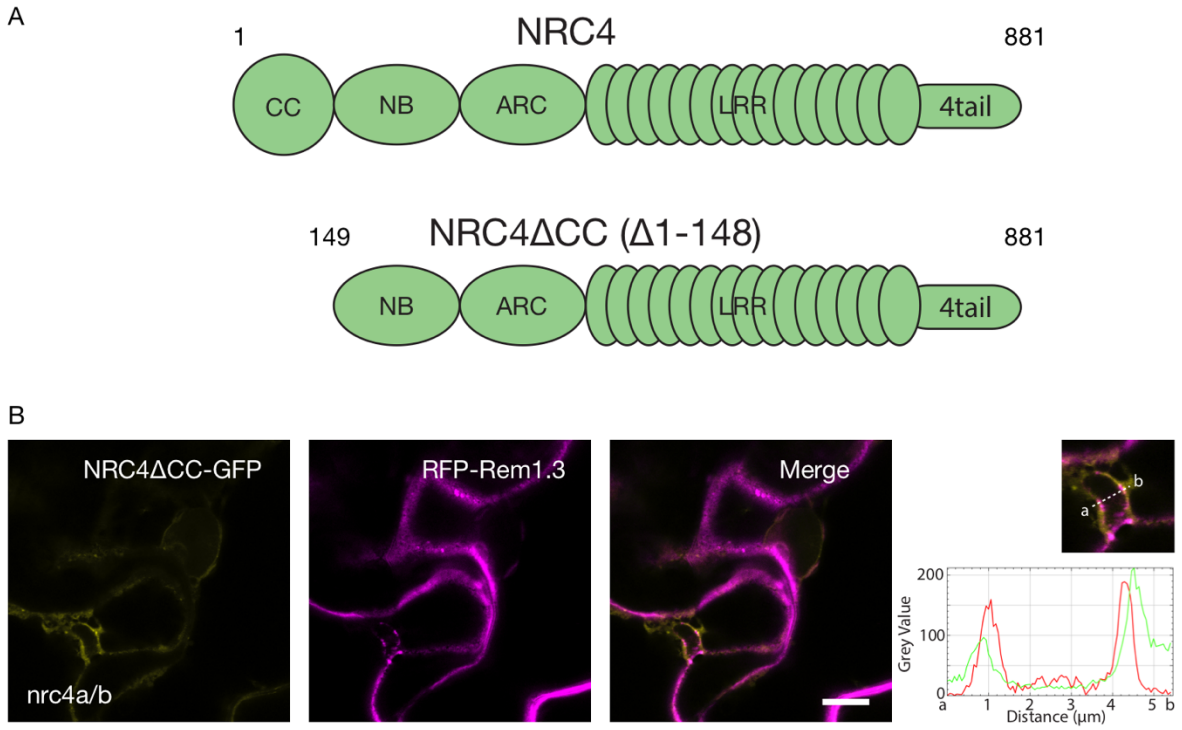


Figure 4.23: The CC domain of NRC4 is required for EHM accumulation.
(A) A cartoon demonstrating that NRC4ΔCC is N-terminally truncated to delete the CC domain. (B) NRC4ΔCC-GFP fluorescence is not polarised to haustoria. RFP-Rem1.3 and NRC4ΔCC-GFP and P19 silencing suppressor (to increase transgene expression) were transiently co-expressed in nrc4a/b *N. benthamiana* leaves, infected the same day with *P. infestans* and imaged 2dpi. Transect shows that NRC4ΔCC-GFP fluorescence is in the cytoplasm, external to the RFP-Rem1.3 EHM fluorescence. Scale bar 10μm.

4.4.3.2. NRC4's CC domain alone accumulates at the EHM

Having discovered that the CC domain of NRC4 is required for its perihaustorial localisation, the next step was to determine whether it was sufficient. I found that expression of CC^{NRC4}-YFP usually leads to aggregation and formation of high intensity puncta of all sizes up to ~5 μm in diameter (Figure 4.24). Many of these were associated with haustoria (Figure 4.24A-B). Some haustoria had focal accumulation of CC^{NRC4}-YFP at the EHM (Figure 4.24C). Other haustoria had diffuse CC^{NRC4}-YFP

signal that overlapped with the EHM and cytoplasm (Figure 4.24D). Of the 28 haustoria identified by Remorin or visible in the brightfield, 24 had either EHM focal accumulation of 4CC-YFP, high intensity 4CC-YFP puncta associated with the haustoria, or a concentration of cytoplasmic 4CC-YFP signal around the EHM. The differences in localisation were probably due to the expression levels in the cells, timing of haustorial penetration with regards to expression and even could be due to the size of the cell. NRC2's CC domain however did not show any haustorial association. It remained diffuse throughout the cytoplasm (Figure 4.24E).

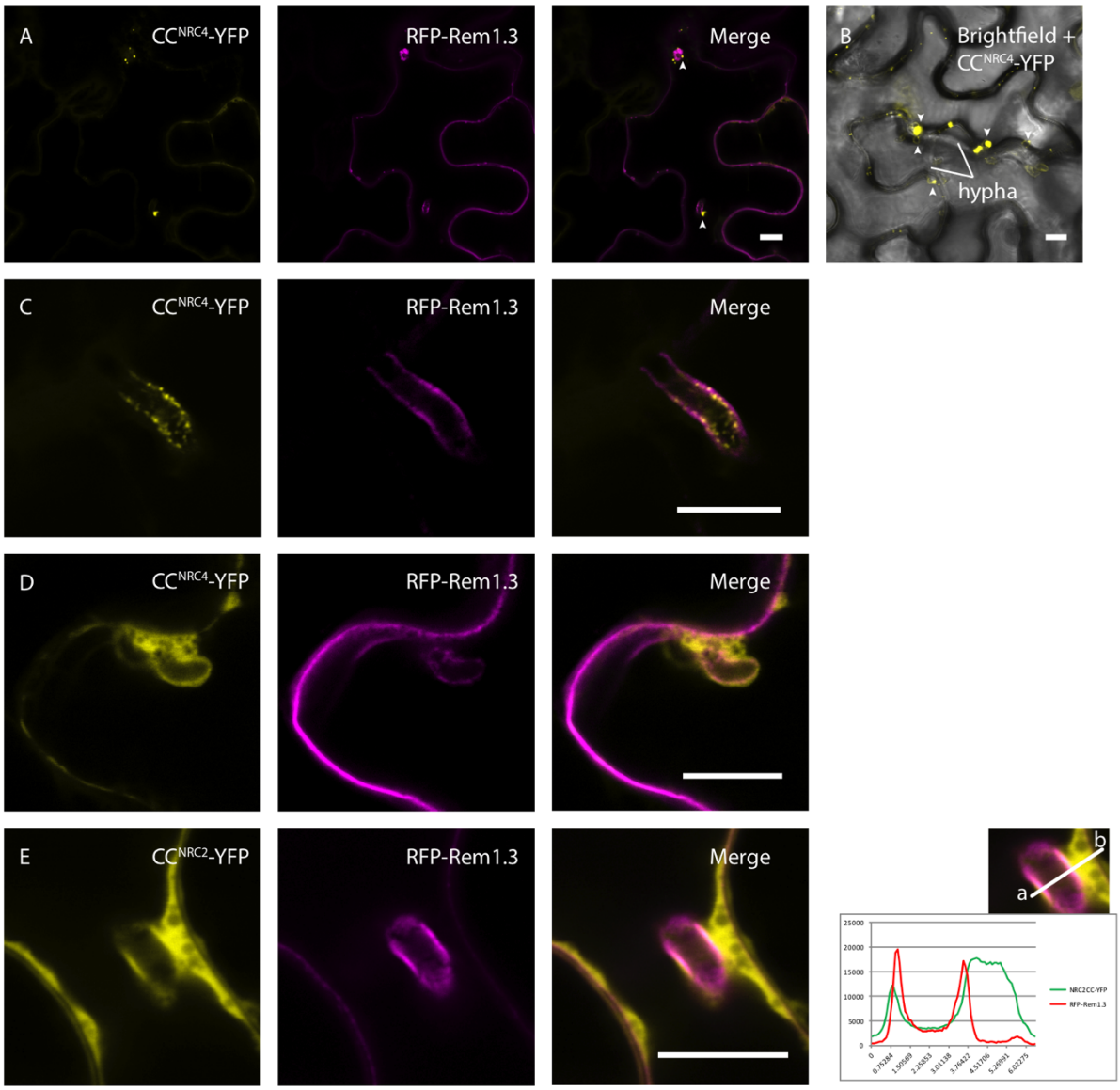


Figure 4.24: The CC domain of NRC4 can inefficiently focally accumulate to the EHM unlike NRC2.
CC^{NRC4}-YFP (A-D) or CC^{NRC2}-YFP was transiently co-expressed with RFP-Rem1.3 and infected on the same day. Three days after infiltration the images were collected on Leica SP8 confocal microscope (A-B) Single-plane confocal micrographs showing the CC domain of NRC4 (CC^{NRC4}) forms aggregate-like structures that often associate with haustoria (arrowheads). (C) Single-plane confocal micrographs showing CC^{NRC4} can focal accumulate, mostly in puncta. (D) Single-plane confocal micrographs showing CC^{NRC4} can be diffuse around haustoria. (E) Single-plane confocal micrographs showing CC^{NRC2} does not focally accumulate and remains diffuse throughout the cytoplasm. Scale bars are 10µm.

4.4.3.3. CC domain swap chimeras between NRC4, NRC2 and AtZAR1 implicate the CC domain in EHM targeting

Considering the CC domain of NRC4 is required and sufficient for at least partial perihaustorial focal accumulation, I decided to make a series of CC-swap chimeras. Surprisingly, NRC4 with NRC2's CC (NRC4^{2CC}) retained its focal localisation to the EHM (Figure 4.25). However, NRC2 with NRC4's CC (NRC2^{4CC}) gained focal EHM localisation (Figure 4.26). It sometimes displayed linear/continuous labelling, like RFP-Rem1.3, or punctate labelling of the plasma membrane, perhaps indicating 4CC facilitates membrane association. Despite 4CC being sufficient to at least partially accumulate at the EHM, ZAR1^{4CC} did not focally accumulate in most instances (Figure 4.27). However, ZAR1^{4CC} displayed some small filamentous aggregations that appear to be membrane associated and often these were localized at the EHM (12/31) (Figure 4.27B). It is plausible that folding of ZAR1's NBD-LRR on the CC domain of NRC4 inhibited the haustorial translocation machinery or system. Perhaps ZAR1^{4CC} even requires a C-terminal tail to accumulate at the EHM. Alternatively, ZAR1^{4CC} may be 'trigger-happy' in that it accumulates to membranes, prior to pathogen penetration or ETI (discussed in chapter 6). In the future, the degree to which ZAR1^{4CC}-GFP accumulates at the EHM should be quantified by image analysis.

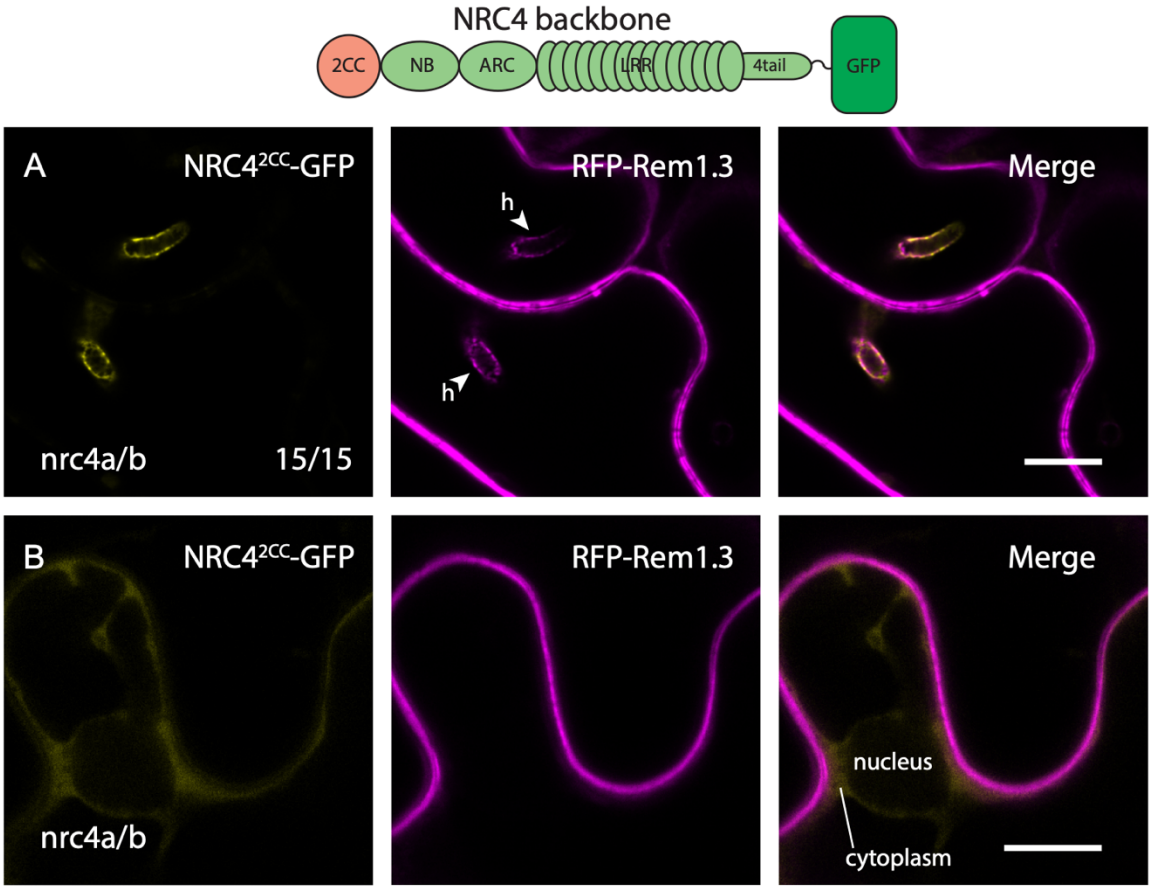


Figure 4.25: NRC4 does not lose perihaustorial focal accumulation when its CC domain is swapped with that of NRC2.
Domain boundaries were determined using an online disorder calculator. Cartoon of chimera shows NRC4 backbone in green and NRC2's CC domain in orange. NRC4^{2CC}-GFP was transiently co-expressed with RFP-Rem1.3 and silencing suppressor P19 in nrc4a/b mutant plants and infected on the same day for (A) and left uninfected for (B). Three days after infiltration the images were collected on Leica SP8 confocal microscope. (A) Single-plane confocal micrograph showing NRC4^{2CC}-GFP focally accumulates at the EHM. Numbers indicate the number of times RFP-Rem1.3 positive labelled haustoria were co-labelled by NRC4^{2CC}-GFP in a focal manner. (B) Single-plane confocal micrograph showing NRC4^{2CC}-GFP lacks membrane association in uninfected cells. Scale bars are 10 μm

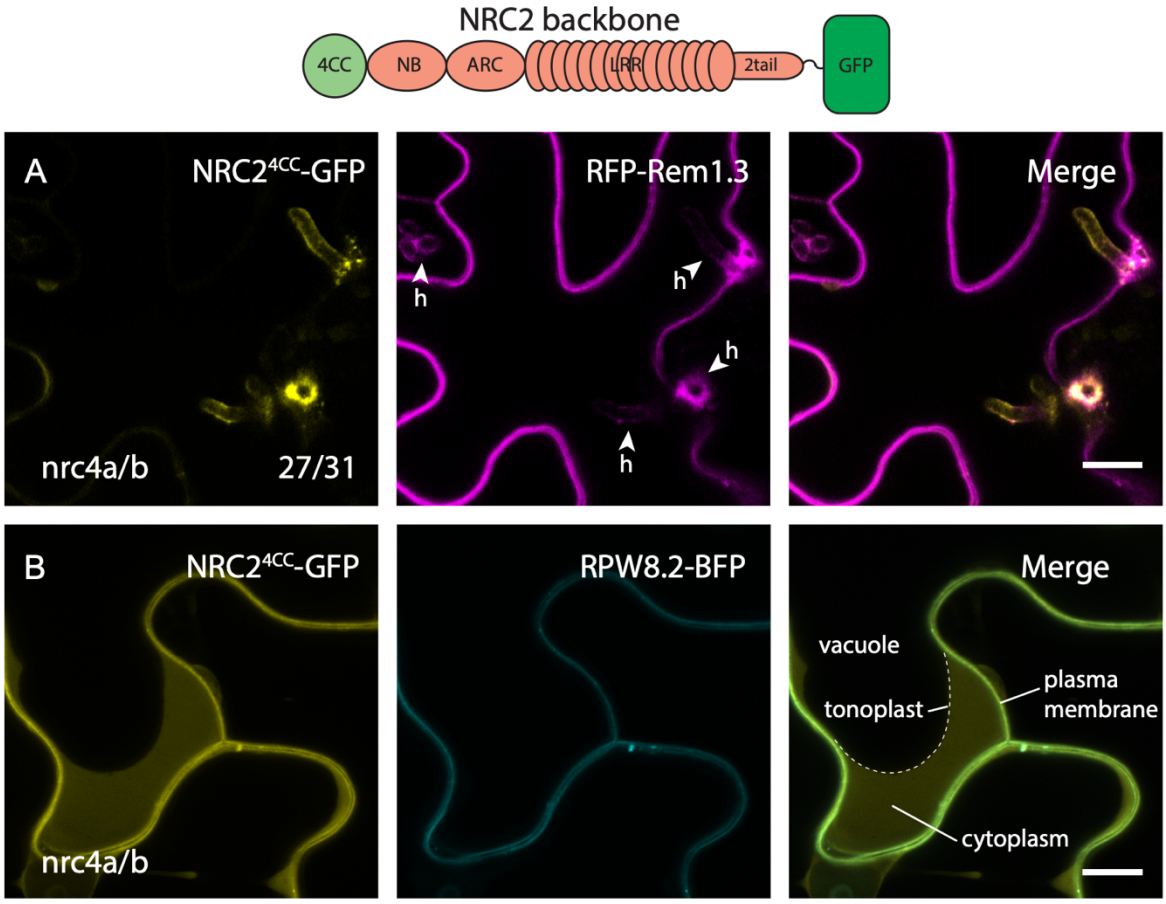


Figure 4.26: NRC2 gains perihaustorial focal accumulation when its CC domain is swapped with that of NRC4.
Domain boundaries were determined using an online disorder calculator. Cartoon of chimera shows NRC2 backbone in orange and NRC4's CC domain in green. NRC2^{4CC}-GFP was transiently co-expressed with RFP-Rem1.3 (A) or RPW8.2-BFP (B) and silencing suppressor P19 in nrc4a/b mutant plants and infected on the same day for (A) and left uninfected for (B). Three days after infiltration the images were collected on Leica SP8 confocal microscope. (A) Single-plane confocal micrograph showing NRC2^{4CC}-GFP focally accumulates to the EHM. Numbers indicate the number of times RFP-Rem1.3 positive labelled haustoria were co-labelled by NRC2^{4CC}-GFP in a focal manner. (B) Single-plane confocal micrograph showing NRC2^{4CC}-GFP membrane association in uninfected cells. Scale bars are 10 µm.

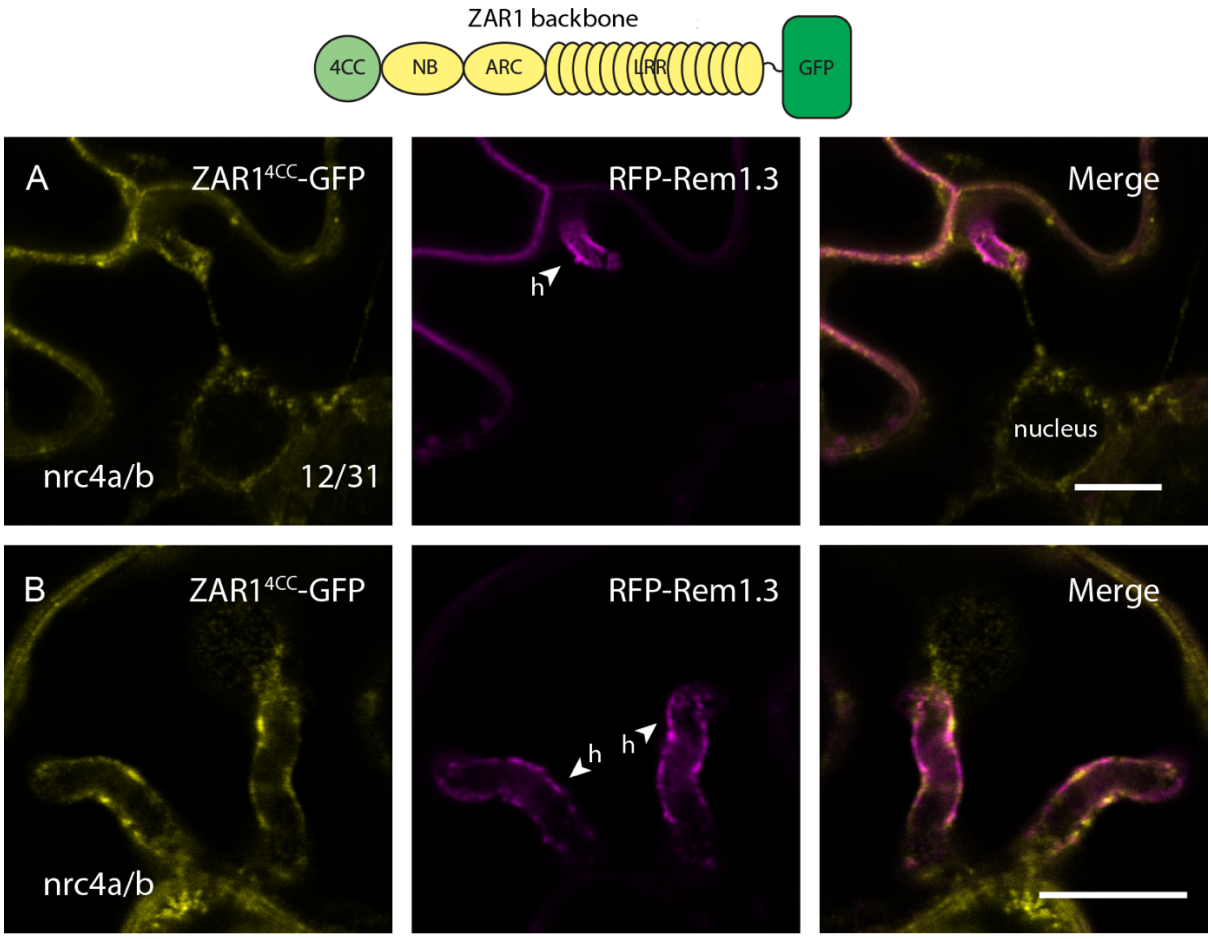


Figure 4.27: ZAR1 does not gain full perihaustorial focal accumulation when its CC is swapped with that of NRC4, but did show EHM labelling.
Domain boundaries were determined using an online disorder calculator for NRC4 to be consistent with the other NLRs and for ZAR1, the cryo-EM structure was used. Cartoon of chimera shows ZAR1 backbone in yellow and NRC4's CC domain in green. ZAR1^{4CC}-GFP was transiently co-expressed with RFP-Rem1.3 and silencing suppressor P19 in nrc4a/b mutant plants and infected on the same day. Three days after infiltration the images were collected on Leica SP8 confocal microscope. (A) Single-plane confocal micrograph showing ZAR1^{4CC}-GFP membrane association in infected cells, some of which associates with the EHM. (B) Single-plane confocal micrograph showing ZAR1^{4CC}-GFP does not focally accumulates to the EHM. Scale bars are 10 µm. Numbers indicate the number of times RFP-Rem1.3 positive labelled haustoria were co-labelled by ZAR1^{4CC}-GFP.

4.4.3.4. EHM targeting is determined by more than just the CC domain but the second half of NRC4's CC domain is positively contributing to focal accumulation

To narrow-down further the signal for haustorial focal accumulation, I designed a series of intra-domain CC swaps between NRC2 and NRC4. We identified secondary structure boundaries using a homology model of NRC4 built on the active/inactive state of ZAR1 (Adachi et al., 2019). The first 83 amino acids make up the first three α-helices or roughly half the CC domain and the second half of the CC domain is made up of a α4 helix in addition to a long, disordered region. For the chimeras, I named the swaps after the α1-3 helices or the α4 helices, but the latter also contained the disordered region. First, I swapped the N-terminal half of NRC2 onto NRC4 and the N-terminal half of NRC4 onto NRC2, NRC4$^{2CC\alpha1\text{-}3}$ and NRC2$^{4CC\alpha1\text{-}3}$, respectively. The chimera with NRC4 backbone, NRC4$^{2CC\alpha1\text{-}3}$-GFP, did not lose EHM focal accumulation (Figure 4.28A). Similarly, the chimera with NRC2 backbone, NRC2$^{4CC\alpha1\text{-}3}$-GFP, did not gain focal accumulation (Figure 4.28B). Together this indicates the first three alpha helices of NRC4 are not sufficient in an NRC2 backbone to facilitate focal accumulation. However, it is not possible to conclude which part of NRC4 determines its EHM accumulation without an NRC2 chimera that gains EHM accumulation or a truncation that is sufficient for EHM accumulation.

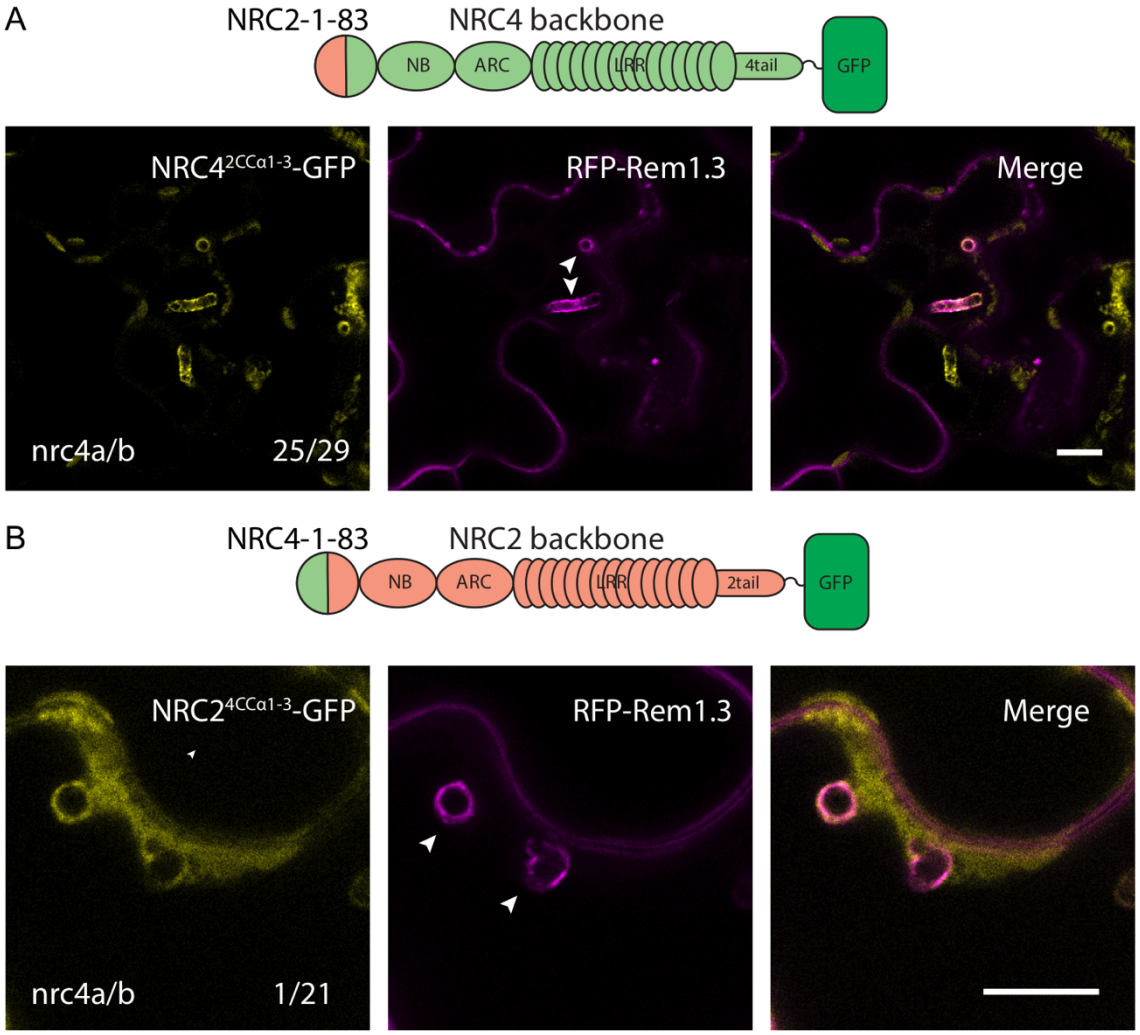


Figure 4.28: The first half of the CC domain of NRC4 does not appear to contain the signal for haustorial targeting.
Secondary structure boundaries were determined using an online disorder calculator for NRC4 and NRC2. NRC4's secondary structure was consistent with Phyre2 homology model of NRC4 based on ZAR1 cryo-EM structure. Cartoon of chimeras show NRC2 in orange and NRC4 in green. NRC4$^{2CC\alpha1-3}$-GFP (A) or was NRC2$^{4CC\alpha1-3}$-GFP was transiently co-expressed with RFP-Rem1.3 and silencing suppressor P19 in nrc4a/b mutant plants and infected on the same day. Three days after infiltration the images were collected on Leica SP8 confocal microscope. (A) Single-plane confocal micrograph showing NRC4$^{2CC\alpha1-3}$-GFP EHM focal accumulation. (B) Single-plane confocal micrograph showing NRC2$^{4CC\alpha1-3}$-GFP does not focally accumulate to the EHM. Scale bars are 10 µm. Numbers indicate the number of times RFP-Rem1.3 positive labelled haustoria (arrowheads) were co-labelled by chimeras in a focal manner.

I then made chimeras of the second half of the CC domains to determine whether the signal for perihaustorial accumulation is encoded in the NRC4's, α4 and disordered region. NRC4 with α4 of NRC2, NRC4$^{2CC\alpha4}$, remained focally accumulated around haustoria (Figure 4.29A). Interestingly it also displayed some association for the plasma membrane. However, it is plausible that NRC2 is too closely related to NRC4 to disrupt its localisation when performing intra-domain swaps such as these, because NRC2 may have some EHM association/accumulation properties which are not fully executed due to a dominant trait of cytoplasmic localisation or filament formation (Figure 3.1N-Q). That said, NRC4 with α4 of ZAR1, NRC4$^{Z1CC\alpha4}$, also retained its ability to focally accumulate (Figure 4.29).

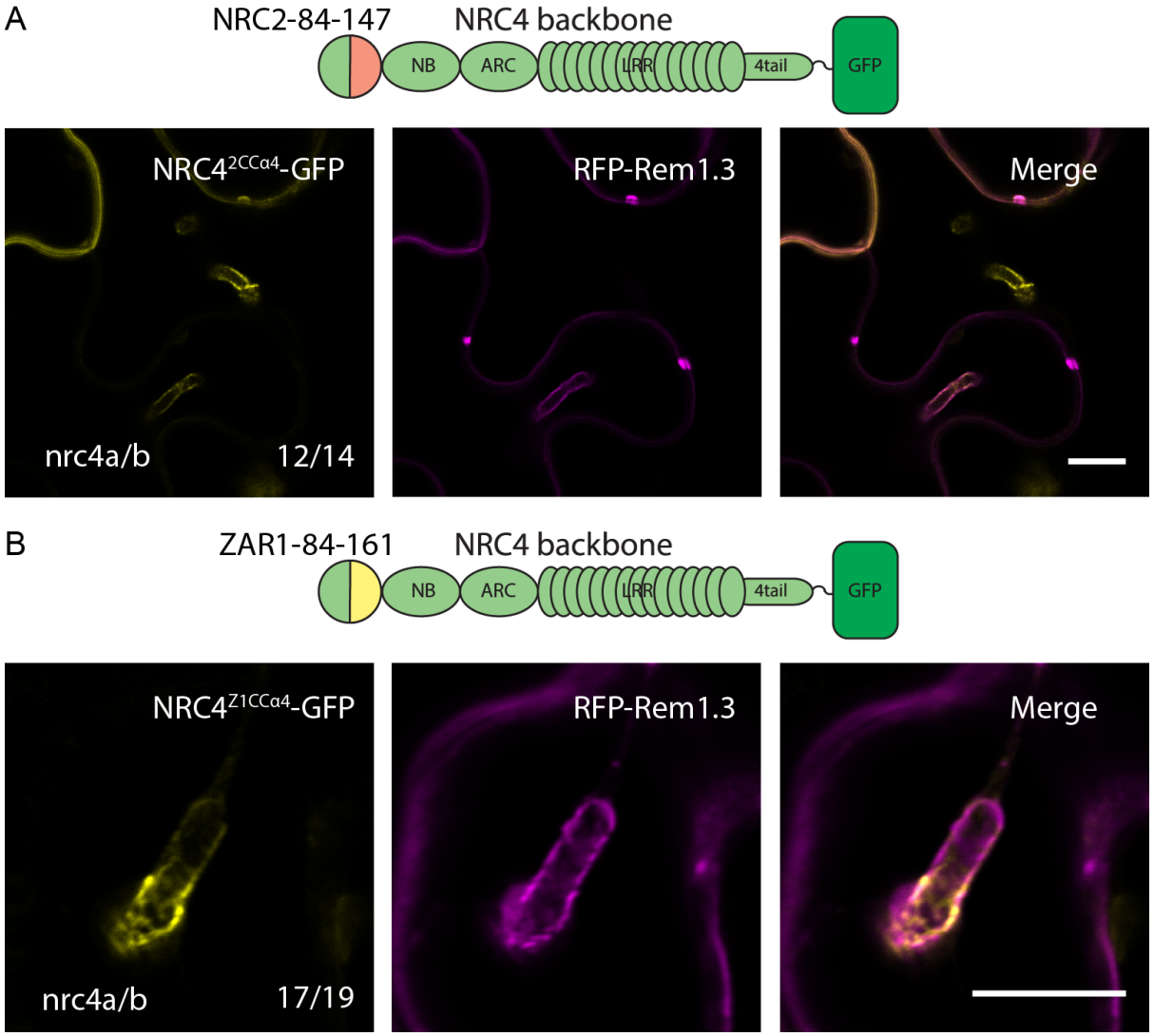


Figure 4.29: NRC4 with the second half of the CC domain from NRC2 or ZAR1 still accumulates at the EHM.
Secondary structure boundaries were determined using an online disorder calculator for NRC4 and NRC2. NRC4's secondary structure was consistent with Phyre2 homology model of NRC4 based on ZAR1 cryo-EM structure. Cartoon of chimeras show NRC2 in orange, NRC4 in green and ZAR1 in yellow. NRC4$^{2CC\alpha4}$-GFP (A) or was NRC2$^{Z1CC\alpha4}$-GFP was transiently co-expressed with RFP-Rem1.3 and silencing suppressor P19 in nrc4a/b mutant plants and infected on the same day. Three days after infiltration the images were collected on Leica SP8 confocal microscope. (A) Single-plane confocal micrograph showing NRC4$^{2CC\alpha4}$-GFP EHM association. The chimera focally accumulated at most haustoria (12/14), there was occasionally association with the plasma membrane also. (B) Single-plane confocal micrograph showing NRC2$^{Z1CC\alpha4}$-GFP focally accumulates at the EHM, however it is partially impaired and mostly present at the neck or young haustoria. Numbers indicate the number of times RFP-Rem1.3 positive labelled haustoria were co-labelled by chimeras in a focal manner. Scale bars are 10 μm.

These chimeras suggest that the fourth alpha helix does not encode the 'signal' for EHM focal accumulation. However, more than one component of the NLR could be facilitating interactions that allow this localisation. Therefore a gain of function is more reliable in terms of dissecting the component(s) of NRC4 required and sufficient for localisation. Strikingly, NRC2 with α4 of NRC4 gained focal accumulation at haustoria (NRC2$^{4CC\alpha4}$) (Figure 4.30A). However, this did not completely transfer focal accumulation to ZAR1 (ZAR1$^{4CC\alpha4}$) (Figure 4.30B), perhaps due to negative regulation from the NB-ARC and/or LRR domain. ZAR1$^{4CC\alpha4}$ often associated with membranes and I observed that one third of haustoria imaged did have some localisation at the EHM, however, it was unclear whether this localisation constitutes focal accumulation like the WT NRC4. The degree to which it accumulates should be investigated with image analysis and compared to that of NRC4 and ZAR1. The cytoplasmic localisation of ZAR1 may be mostly dominant over the EHM localisation facilitated by NRC4's CC domain or α4 (Figure 4.27 & Figure 4.30). Like ZAR1^{4CC}, with ZAR1$^{4CC\alpha4}$, I also visualised membrane association in puncta which could represent an autoactivated NLR associating with the membrane. However, no HR was seen with this chimera (Figure 4.31), which could be due to an inability to coordinate α4 and α1 conformational changes that are known to be required for HR (Wang et al., 2019a).

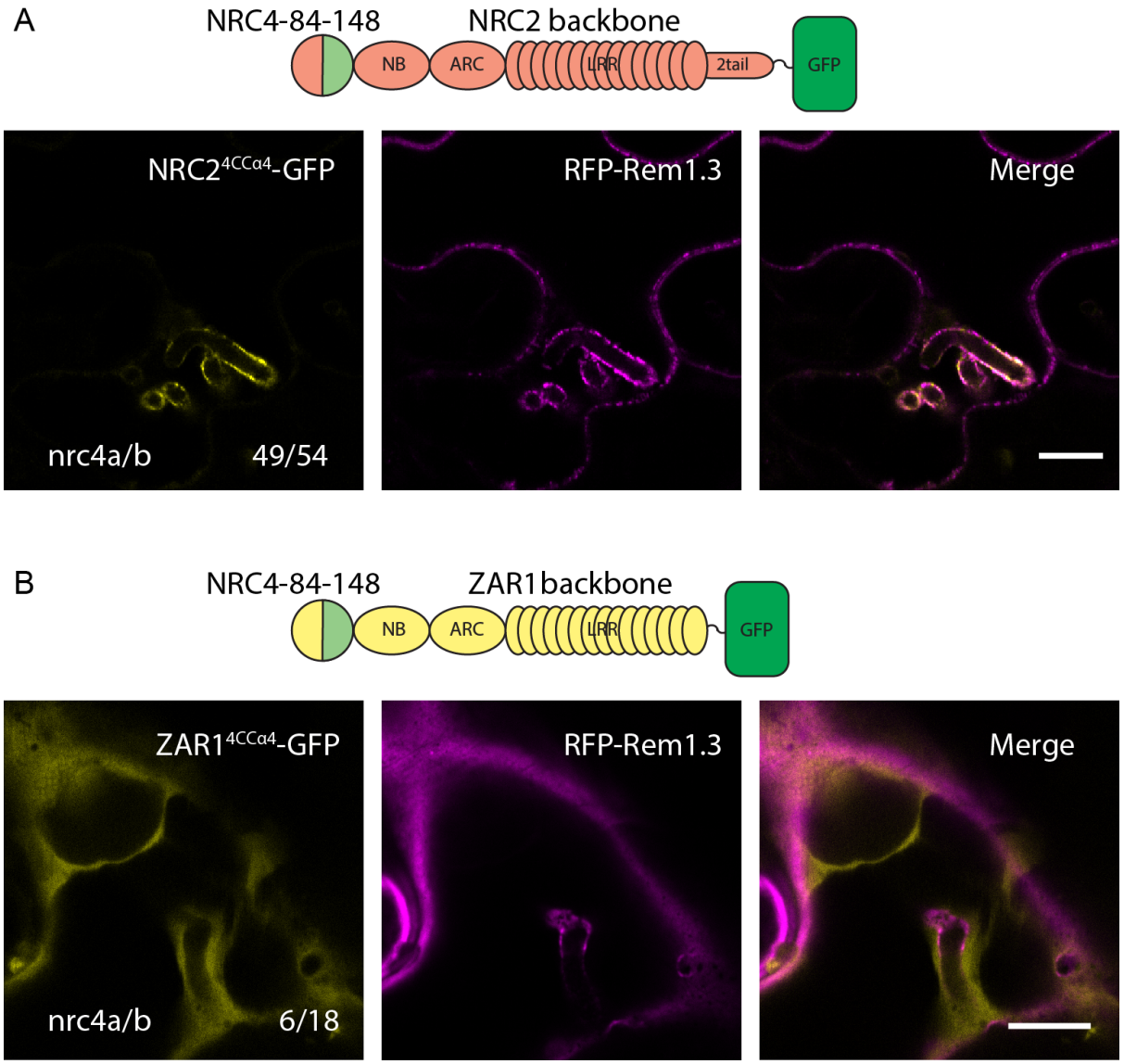


Figure 4.30: The second half of the CC domain of NRC4 permits haustorial targeting to NRC2 but not ZAR1.
Secondary structure boundaries were determined using an online disorder calculator for NRC4 and NRC2. NRC4's secondary structure was consistent with Phyre2 homology model of NRC4 based on ZAR1 cryo-EM structure. Cartoon of chimeras show NRC2 in orange, NRC4 in green and ZAR1 in yellow. NRC2$^{4CC\alpha4}$-GFP (A) or was ZAR1$^{4CC\alpha4}$-GFP was transiently co-expressed with RFP-Rem1.3 and silencing suppressor P19 in nrc4a/b mutant plants and infected on the same day. Three days after infiltration the images were collected on Leica SP8 confocal microscope. (A) Single-plane confocal micrograph showing NRC2$^{4CC\alpha4}$-GFP EHM accumulation. (B) Single-plane confocal micrograph showing ZAR1$^{4CC\alpha4}$-GFP diffuse, non-polar, localisation. In many cells this chimera was also found in the vacuole (not shown). Numbers indicate the number of times RFP-Rem1.3 positive labelled haustoria were co-labelled by chimeras in a focal manner. Scale bars are 10 µm.

Why NRC4 backbone chimeras still accumulate at the EHM is difficult to explain. The nrc4a/b mutant plants are not full knockouts. They express the first 123 amino acids of one copy of NRC4, in frame (Adachi et al., 2019). This represents the majority of the CC domain, which feasibly is sufficient for EHM targeting. The NRC4 backbone chimeras may be interacting with and carried to the EHM by the NRC4 truncates that are expressed in nrc4a/b plants. Another possibility regards NRC2's EHM localisation (Chapter 3, Figure 1). NRC4^{2CC}, NRC4$^{2CC\alpha1\text{-}3}$ and NRC4$^{2CC\alpha4}$ may associate with the EHM for the same reason as NRC2. Presumably NRC2 interacts with some other component localised at the EHM, perhaps another NLR. We cannot exclude the possibility that this is also true for NRC4.

Ultimately, the immune functionality of the aforementioned chimeras is critical for making strong conclusions. In particular, if any of the NRC4 backbone chimeras are still functional for HR-mediated by Rpi-blb2 and AVRblb2, it could facilitate dissection of this immune pathway. Chimeras which retain this function but lack the ability to focally accumulate at the EHM would allow us to determine if this localisation is required for immunity. To this end, I cloned NRC4 backbone chimeras without a tag, to remove the chance that it might inhibit HR function. I expressed the NRC4-2CC chimeras in Rpi-blb2 nrc4a/b plants with 3xHA-AVRblb2 to trigger HR. I included a positive control for complementation, NRC4-GFP and a negative control, EV-3xHA. Unfortunately, none of the chimeras retained the cell death capabilities, highlighting the fickleness of NLRs (Figure 4.31). However, the C-terminal GFP fusion proteins were correctly cloned (Figure 4.32). It is important to note that whilst these proteins did not retain their cell-death capabilities, many retained their focal accumulation function. Ultimately a more subtle approach, such as PCR mutagenesis, is warranted to determine the precise determinants of EHM targeting and to generate a mutant of NRC4 which cannot accumulate at the EHM but can produce a HR in pathogen independent HR assays.



Figure 4.31: HR complementation assay in Rpi-blb2 nrc4a/b plants shows that NRC4 varients which remove, swap or add a domain on NRC4 lead to loss of HR function, except for C-terminal fusions.
nrc4a/b plants were infiltrated with 3xHA-AVRblb2 to trigger HR and complemented with NRC4 fusion proteins or NRC4 variants tagged/untagged. Only those that retained the full sequence of NRC4 were HR functional. Numbers indicate the sum of HR positive sites per total infiltration sites. Leaves were imaged at 6 dpai.

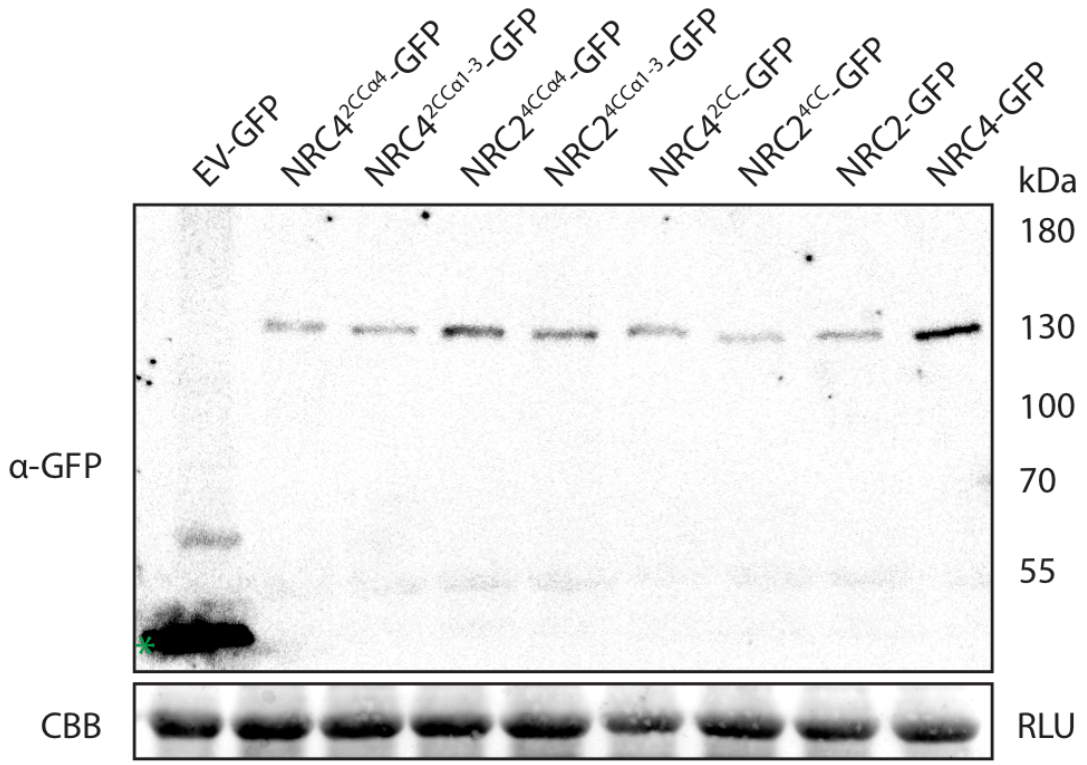


Figure 4.32: Western blot analysis confirms chimeras are cloned correctly and of expected molecular weight.
Proteins were co-expressed at an OD_{600} = 0.3 with 0.1 of P19 to boost expression. NLRs are all approximately 130 kilodaltons (kDa). CBB = Coomassie Brilliant Blue (loading control) of Rubisco Large Subunit (RLU). Star indicates expected size of EV-GFP.

4.4.3.5. The immune function of NRC4's MADA motif is probably executed at the EHM

The pore forming model of ZAR1 suggests a mode of action for Rpi-blb2/NRC4-mediated resistance to *P. infestans.* It is plausible that upon recognition of AVRblb2 by Rpi-blb2, NRC4 forms resistosomes associated with the EHM, leading to cell death and/or perturbation of the EHM. This is a challenging model to validate, however over the next few figures I provide some evidence suggesting that Rpi-blb2 triggers NRC4 to form resistosomes at the EHM, leading to resistance.

Recently we found that a motif exists in the very N-terminus of one fifth of all plant CNLs (Adachi et al., 2019). The consensus begins "M-A-D-A" and so is coined the "MADA motif". We provided data that implicates this motif in executing the hypersensitive response. Together with the findings by others (Wang et al., 2019a,

2019b), it is possible that the function of the MADA motif is for the N-terminal alpha helix (α1) to extend out from the CNL and into the membrane enabling pore-formation when the resistosome is formed. I first validate findings we published which showed α1 of ZAR1 could be transferred to NRC4 without loss of function. I used CRISPR/Cas9 mutants of NRC4 in the background of Rpi-blb2 (Rpi-blb2$^{nrc4a/b}$) to transiently complement the chimera of ZAR1 and NRC4, NRC4$^{\alpha1}$. I found that it fully rescued HR when co-expressed with AVRblb2, and rescued resistance to the same degree as WT NRC4-GFP (Figure 4.33A).

These findings in themselves are good evidence for the conservation of the MADA motif's function, but do not implicate its execution at the EHM. Therefore, I confirmed that NRC4$^{\alpha1}$-GFP still localises to the EHM (Figure 4.33B). Cloning the reciprocal chimera validated that α1's function isn't for EHM localisation (Figure 4.33C). Unfortunately ZAR1 is not functional in *N. benthamiana* (Harant et al., 2020), so it was not possible to validate the functionality of this chimera. In the future, cloning these chimeras with the endogenous NbZAR1, would be useful. The decision to use *Arabidopsis* ZAR1 was taken as this is the only full-length CC NLR structure available to date.

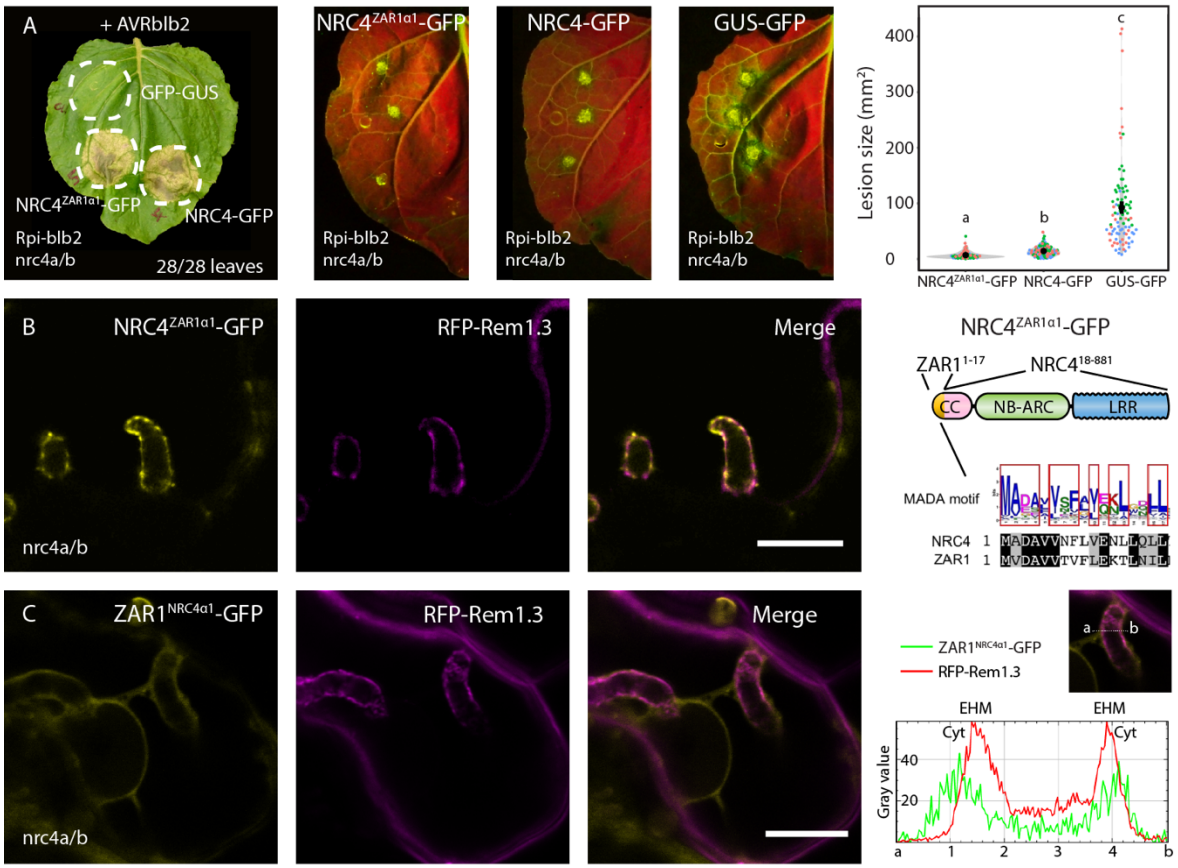


Figure 4.33: The first alpha helix of ZAR1 is functional in NRC4 and does not alter its localisation.

(A) NRC4 chimera with the N-terminal 17 amino acids from ZAR1, and NRC4-GFP but not EV-GFP genetically complements CRISPR/Cas mutation of NRC4a/b in Rpi-blb2 transgenic background by triggering HR when co-expressed with AVRblb2 and resistance when expressed alone and infected 1 dpai. The HR assay was repeated with the same results in 28 leaves, over two independent biological reps where *N* > 11. Images were taken at 8 dpai. Scattered points in scatter violin plot represent the area (mm^2) occupied by infection spots measured on white light images, where each construct had *N* > 88 infection spots. Three independent biological reps were conducted as indicated by colour of dots. UV (shown) and white light imaging was taken at 8 dpi. Significance grouping is indicated with letters a-c, as determined by unpaired Wilcoxon tests. (B) Single plane confocal micrograph showing $NRC4^{ZAR1\alpha1}$-GFP, also known as $NRC4^{ZAR1\text{-}1\text{-}17}$-GFP, focally accumulates at EHM with RFP-Rem1.3. Model depicts the chimera of $NRC4^{ZAR1\alpha1}$. (C) Single plane confocal micrograph showing $ZAR1^{NRC4\alpha1}$-GFP, also known as $ZAR1^{NRC4\text{-}1\text{-}17}$-GFP, which does not focally accumulate at EHM with RFP-Rem1.3. Scale bars are 10 µm.

To validate the function of the MADA motif we generated a series of point mutations and found two mutants that had total or partial loss of function, NRC4^{L9E} or NRC4$^{L9A/V10A/V14A}$ respectively (Adachi et al., 2019). I then validated these findings with the Rpi-blb2 nrc4a/b plants. I found that both were unable to rescue the HR phenotype and disease resistance to the same extent as the negative control, GUS-GFP. I found that NRC4$^{L9A/V10A/V14A}$ as reported was partially functional, produced a weak HR and gave resistance to intermediate extent compared to the negative control GUS-GFP and positive control NRC4-GFP (Figure 4.34A). I then investigated whether NRC4^{L9E} loss of resistance was due to failure to accumulate at the EHM. I saw efficient focal accumulation when co-expressed with RFP-Rem1.3 (Figure 4.34B). I found the same localisations with NRC4$^{L9A/V10A/V14A}$ (Figure 4.34C), whereas the EV-GFP control remained cytoplasmic (Figure 4.34D). Therefore these mutants could not rescue resistance because they cannot produce an HR instead their inability to localise to the EHM.

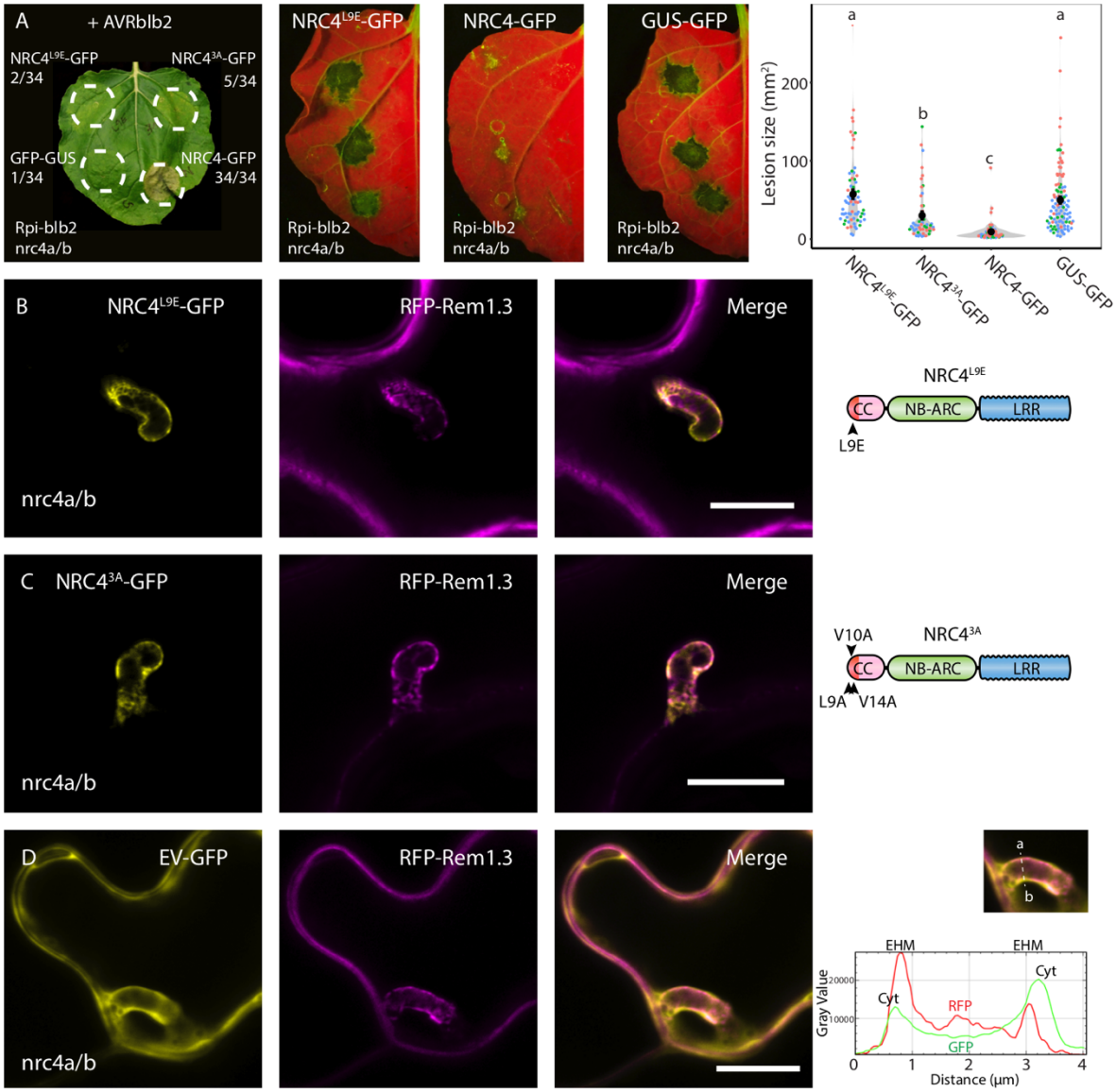


Figure 4.34: Mutations in the MADA motif of NRC4 lead to loss of immune function but do not alter localisation.

(A) NRC4-GFP, but not NRC4^{L9E} mutant, NRC4$^{L9A/V10A/V14A}$ mutant or EV-GFP genetically complements CRISPR/Cas mutation of NRC4a/b in Rpi-blb2 transgenic background by triggering HR when co-expressed with AVRblb2 and resistance when expressed alone and infected 1 dpai. The HR assay was repeated with the same results in 34 leaves, over two independent biological reps where $N > 11$. Images were taken at 3 dpai. Scattered points in scatter violin plot represent the area (mm^2) occupied by infection spots measured on white light images, where each construct had $N > 48$ infection spots. Three independent biological reps were conducted as indicated by colour of dots. Significance grouping is indicated with letters a-c, as determined by unpaired Wilcoxon tests. UV (representative images for three constructs) and white light imaging was taken at 8 dpi. (B-D) Single plane confocal micrographs showing NRC4^{L9E}-GFP or NRC4$^{L9A/V10A/V14A}$-GFP focally accumulates at EHM with RFP-Rem1.3, but not the EV-GFP control which remains cytoplasmic. Models depict the location of mutation in NRC4^{L9E} or NRC4$^{L9A/V10A/V14A}$. Scale bars are all 10 µm.

To understand whether NRC4 was capable of forming resistosomes like those reported for ZAR1, I decided to express the autoactive NRC4^{D478V} and view this in the absence of infection. However, due to the HR produced by this construct, I chose to disarm it with the L9E MADA mutation, thus generating an active, HR-suppressed NRC4 – NRC4$^{D478V/L9E}$-GFP. I found that this version of autoactive NRC4 formed puncta which were associated with the membrane sections of the cell labelled by RFP-Rem1.3 (Figure 4.35A-B). In contrast, the inactive form, NRC4^{L9E}-GFP, was diffuse in the cytoplasm and did not form puncta (Figure 4.35C-D). I next investigated what would happen with the puncta formed by autoactive NRC4 during infection. NRC4$^{L9E/D478V}$ remained associated with the PM and EHM, but with no visible polar localisation to the EHM (Figure 4.35E). This was unexpected and intriguing as perhaps this result could be used to dissect the function of NRC4's EHM localisation (discussed next). It is possible that autoactive NRC4 associates with the closest membrane source available, or alternatively oligomeric NRC4 cannot be recruited to the EHM in a focal manner.

I next wanted to determine if the NRC4 was capable of forming puncta when activated by a sensor NLR during infection, as this is the natural scenario for resistance to occur. To conduct this experiment, I expressed NRC4^{L9E}-GFP with RFP-Rpi-blb2 in nrc4a/b plants during infection. I found that NRC4^{L9E}-GFP sometimes (but not always) formed puncta which were associated with the EHM (Figure 4.35F). It is indeed possible that during Rpi-blb2-mediated immunity, NRC4 forms resistosomes associated with the EHM which elicit a HR or impair pathogenesis in some other way. For instance, NRC4 resistosomes could lead to pore formation which exposes the haustorium to plant defence compounds or lyse the EHM which may be required for pathogenesis.

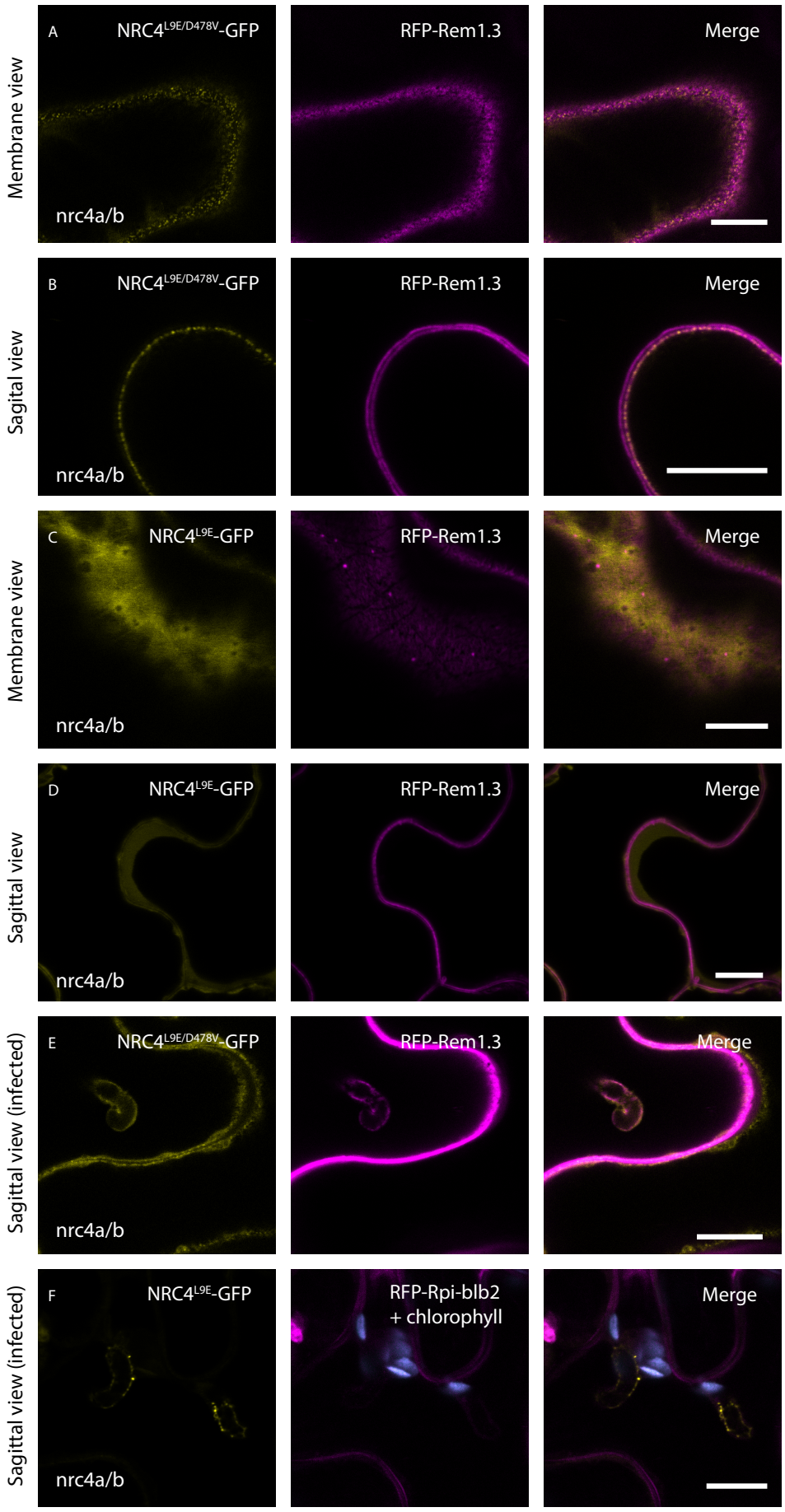

A
NRC4L9E/D478V-GFP
RFP-Rem1.3
Merge
nrc4a/b
Membrane view
B
NRC4L9E/D478V-GFP
RFP-Rem1.3
Merge
nrc4a/b
Sagital view
C
NRC4L9E-GFP
RFP-Rem1.3
Merge
nrc4a/b
Membrane view
D
NRC4L9E-GFP
RFP-Rem1.3
Merge
nrc4a/b
Sagittal view
E
NRC4L9E/D478V-GFP
RFP-Rem1.3
Merge
nrc4a/b
Sagittal view (infected)
F
NRC4L9E-GFP
RFP-Rpi-blb2
+ chlorophyll
Merge
nrc4a/b
Sagittal view (infected)

Figure 4.35: Activated NRC4 forms puncta which associate with the PM and/or EHM but is unable to focally accumulate.
NRC4^{L9E}-GFP or NRC4$^{L9E/D478V}$-GFP were co-expressed with RFP-Rem1.3 or RFP-Rpi-blb2 in nrc4a/b plants and imaged with a Leica SP8 confocal microscope after 3 days. For E-F, leaves were infected with *P. infestans* three hours after infiltration. (A-B) Autoactive NRC4, NRC4$^{L9E/D4378V}$, localises in puncta associated with the plasma membrane (PM) in non-haustoriated cells. (C-D) Non-active NRC4, NRC4^{L9E}, localises diffusely in the cytoplasm in non-haustoriated cells. (E) During haustorial penetration, the autoactive NRC4$^{L9E/D4378V}$ localises in puncta associated evenly with the plasma membrane and extra-haustorial membrane (EHM), and does not accumulate at the EHM. There is also some cytoplasmic signal. (F) During haustorial penetration, NRC4^{L9E} co-expressed with Rpi-blb2 to enable activation, focally accumulates at the EHM and forms puncta associating with the EHM. Overlay of chlorophyll autofluorescence in cyan for RFP-Rpi-blb2 and Merge channels was used because poor signal of Rpi-blb2 lead to non-specific autofluorescence from the chloroplasts. Scale bars are 10 μm.

Considering NRC4$^{D478V/L9E}$ localised to the PM and EHM linearly, i.e. the signal at the PM was approximately equal to that at the EHM, I wanted to determine what effect this misslocalisation would have on resistance to *P. infestans.* Therefore we expressed the HR functional autoactive NRC4^{D478V}-YFP, NRC4-YFP and EV-YFP (Adachi et al., 2019), in Rpi-blb2$^{nrc4a/b}$ plants opposite one another and after one day infected the leaves with *P. infestans.* The *P. infestans* associated necrotic lesion size was determined after 6-8 dpi. We expressed three different OD_{600}'s to try avoid saturation of NRC4^{D478V}'s HR. We determined that autoactive NRC4 does not provide resistance to *P. infestans*, despite causing HR. Due to the challenges with telling plant induced HR and pathogen induced necrosis apart, these results need to be replicated with an alternative quantification method, such as quantification of *P. infestans* TD tomato by western blotting, or qPCR of pathogen biomass. Additionally, it's prudent to determine if intercellular hyphae and haustoria are formed in the early stages of infection or if the pathogen is living saprophytically in the later stages. Trypan blue staining of the first 24-48 hours of infection and/or TD tomato imaging could be carried out to achieve this. However, with these results it appears as though NRC4^{D478V}'s lack of EHM accumulation may lead to loss of resistance to *P. infestans*, and therefore meaning WT NRC4's accumulation at the EHM is required for resistance.

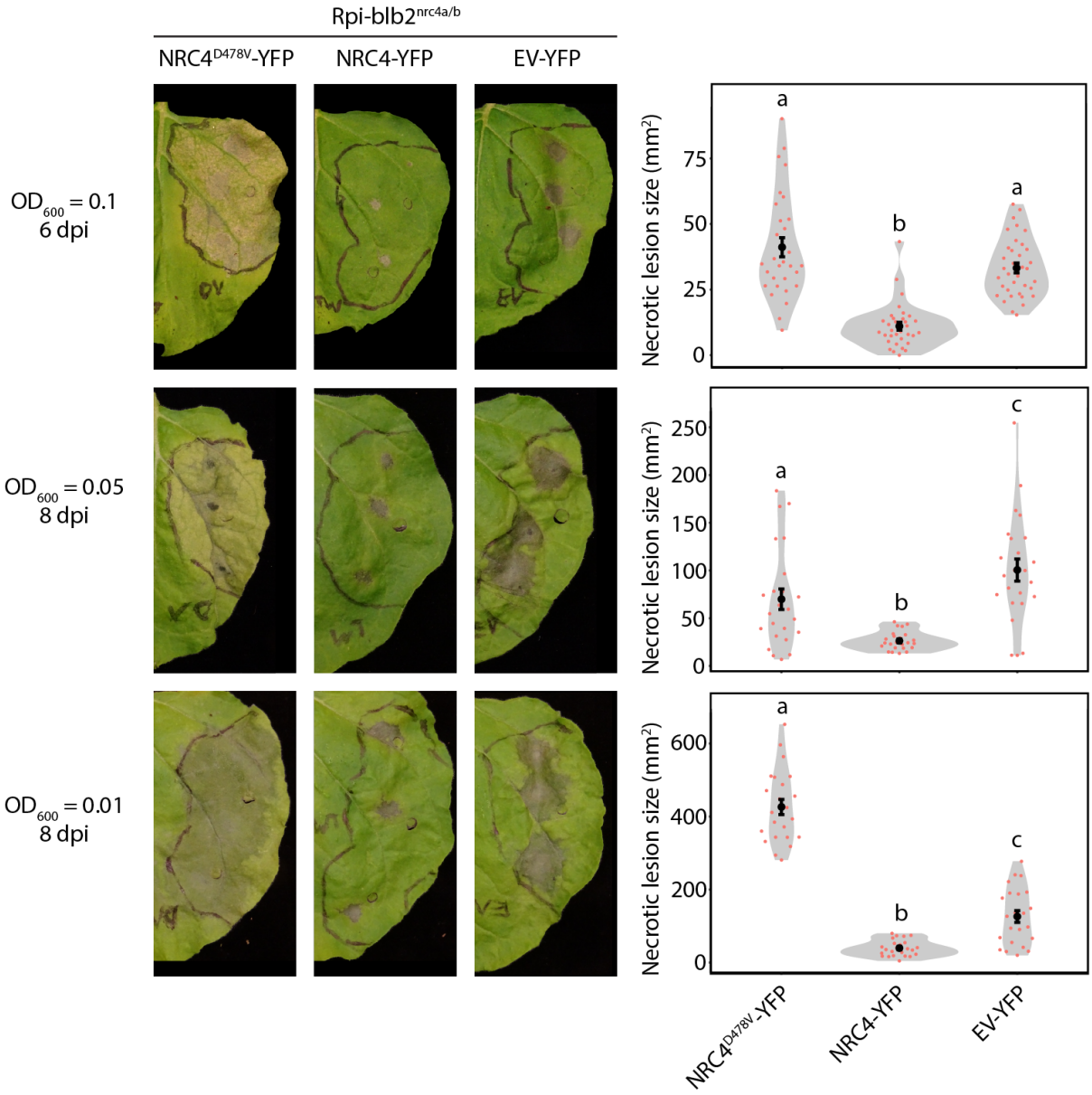


Figure 4.36: NRC4^{D478V} does not prevent necrotic lesion spread associated with *P. infestans* infection.
NRC4-YFP, but not NRC4^{D478V} autoactive mutant or EV-YFP genetically complements CRISPR/Cas mutation of NRC4a/b in Rpi-blb2 transgenic background by preventing necrotic lesion spread associated with *P. infestans infection.* Rpi-blb2$^{nrc4a/b}$ plants were agroinfiltrated with NRC4-YFP, NRC4^{D478V}-YFP or EV-YFP opposite one another, and after one day detached and infected with *P. infestans.* Lesions were imaged with white light photography after 6 or 8 dpi. Three experiments were conducted with variation in OD_{600} = 0.1, 0.05 and 0.01. At the highest OD_{600} the HR produced from the autoactive variant made it challenging to quantify the lesion size, but at the lower OD's it was clearer. Significance grouping is indicated with letters a-c, as determined by unpaired Wilcoxon tests – the grouping does not apply across experimental replicates. Note that for OD_{600} = 0.05, p = 0.032 for a-c.

4.5. Chapter Conclusions

In conclusion, I determined that both the N- and C-termini positively contribute to the immune function of NRC4. Both the CC domain and the tail are required for localisation. However, it seems the CC domain plays a more active role in EHM targeting, given that the CC alone can focally accumulate (Figure 4.24), whereas the tail cannot.

Assuming other NLRs target the EHM, it would be interesting to know whether any TIR NLRs are capable of this or if it is specific to CC domain containing resistance proteins. Removal of the CC domain of NRC4 caused loss of focal accumulation but swapping with NRC2's CC (or part of it), did not. It would be interesting to perform these swaps with ZAR1 to see if ZAR1's CC domain is sufficient to allow focal accumulation of NRC4. In which case the conclusion would be that NRC4 requires *a* CC domain. Currently it's premature to conclude that, as NRC2 is very closely related to NRC4 and NRC2 itself seems to have some EHM association - albeit not focal accumulation (Chapter 3, Figure 1). Indeed these results may be confounded by NRC2 interacting with another NLR which accumulates at the EHM. Removal of the residues which are leading to NRC2's filament formation (Figure 3.1N-Q) may result in the EHM accumulation.

It's clear that the CC domains of NLRs are key components in self-association and oligomerisation. It is possible then that focal accumulation is dependent on oligomerisation. The CC^{NRC4}-YFP was partially capable of focally accumulating at the EHM (Figure 4.24). Therefore, this CC domain has some inherent affinity for the EHM or the transport pathway targeting the EHM. The rest of the protein may be required to adopt a conformation that facilitates efficient labelling of the EHM. Interestingly, $ZAR1^{4CC}$-GFP did not focally accumulate (Figure 4.27). This could be due to inability of the rest of the protein to adopt the correct conformation/oligomer. Alternatively, ZAR1 may have high affinity for its dependent kinases that may associate with the plasma membrane, preventing its re-localisation upon haustoria formation. Also, as previously mentioned $ZAR1^{4CC}$ and $Zar^{4CC\alpha4}$ both showed PM association which could indicate it is autoactivated and accumulating at the plasma membrane prior to haustoria formation, like $NRC4^{D478V}$ (Figure 4.35E). Ultimately, to unravel the region(s)

of NRC4 which determine EHM accumulation, I first need to repeat the localisation assays in this chapter and quantify the degree to which the chimeras accumulate at the EHM, in non-binary terms. Secondly, I need to investigate whether the first 123 amino acids of NRC4 expressed in nrc4a/b plants (Adachi et al., 2019), could be carrying some of the chimeras to the EHM. Thirdly, I need to investigate whether an EHM localised NLR is associating with NRC2, to facilitate its EHM association and whether this could be affecting some of the NRC4-NRC2 chimera localisations.

The CC domain of NLRs are believed to be autoinhibited by the LRR domain (Burdett et al., 2019). NRC4 and the chimeras with NRC2, may adopt an intermediate activation state possibly similar to that proposed for ZAR1 after the loss of ADP but before ATP binding (Wang et al., 2019b). If this is the case for NRC4, it must not rely on AVR perception as NRC4 is recruited to the EHM in the absence of appropriate sensor NLRs (Chapter 3, Figure 1).

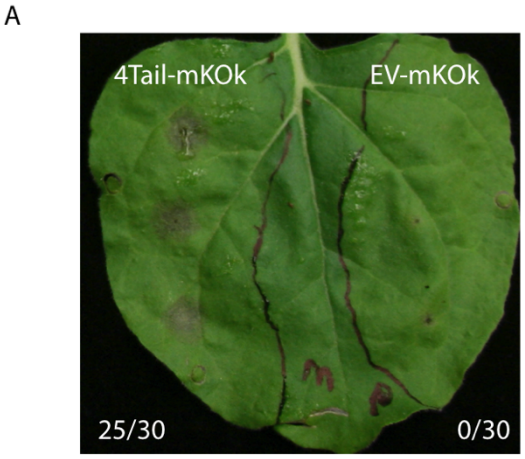
The function of the very N-terminus of NRC4 is likely for executing cell death, possibly directly by membrane insertion and pore formation (Adachi et al., 2019). I demonstrated that the function of this α1 helix is probably executed at the EHM, leading to an intriguing model of NRC4-mediated immunity against *P. infestans*. That being, NRC4 is activated by Rpi-blb2's perception of AVRblb2, and NRC4 forms resistosomes which perform their cell death function at the EHM.

In this chapter I showed that the C-terminal tail was required for immunity and HR. Recently an endogenous *N. benthamiana* TNL Roq1 was shown to require an extended C-terminal domain (PL domain) for HR (Martin et al., 2020). However, this PL domain is also involved in effector perception of this sensor NLR. The C-terminal tail of NRC4 may not play a direct role in targeting EHM, instead it may be for retaining stability or allowing a conformation that permits EHM targeting, considering its removal leads to instability of NRC4 and lack of perihaustorial accumulation (Figure 4.2). How 4Tail disrupts NRC4-mediated immunity is a mystery but could involve an indirect mechanism as CoIPs were unable to determine an association with NRC4. This could involve sequestration of a third party required for NRC4-mediated immunity. This could be a protein, lipid, or even a post-translational modification. For instance, if NRC4 and

4Tail were ubiquitinated, then overexpression of 4Tail could lead to the sequestration of the ubiquitin molecules required for NRC4 function. To determine whether any of the 7 lysines on 4Tail are post translationally modified, the 4Tail-GFP and 4Tail-7KA-GFP constructs should be separated on 12 or 16% gels. Following this, it would be prudent to analyse 4Tail purified from plants with mass spectrometry, and in particular perform co-immunoprecipitation followed by mass spectrometry with it to determine what its interactors are. One major issue with the 4Tail assays described in this chapter, is that they were performed with the 'inactive' state of NRC4, whereas the resistance breaking phenotype of 4Tail on Rpi-blb2 occurs with the activated state of NRC4. Therefore, the co-immunoprecipitation and NRC4 EHM accumulation assays should be conducted either with the autoactive NRC4, or Rpi-blb2 with AVRblb2 co-expression or *P. infestans* infection. Importantly, we can investigate if 4Tail inhibits the resistosome-like puncta witnessed in Figure 4.35.

Whether the puncta formed by activated NRC4 represent resistosomes, is unclear. The resolution of our microscope is approximately 200 nm and the ZAR1 resistosome is 24 nm in diameter (Wang et al., 2019a). The larger size of NRC4-GFP puncta does not mean they are not resistosomes, however. Activated NRC4 may form resistosomes with one or more copies of its sensor NLRs, unlike the singleton ZAR1. Considering the published resistosomes of TIR NLRs are tetramers, it's not implausible that NRC4 may form a resistosome with more than five copies. Additionally, diffraction of light may make a small group of proteins appear larger than they are in reality. The addition of GFP's increases the size of the resistosome and the orientation of the GFPs and conformation of NRC4's themselves may affect the size too. In the future, deconvolution should be carried out to ascertain an accurate sizing of the NRC4 resistosome-like puncta. Alternatively, super resolution microscopy such as PALM or STORM could be conducted.

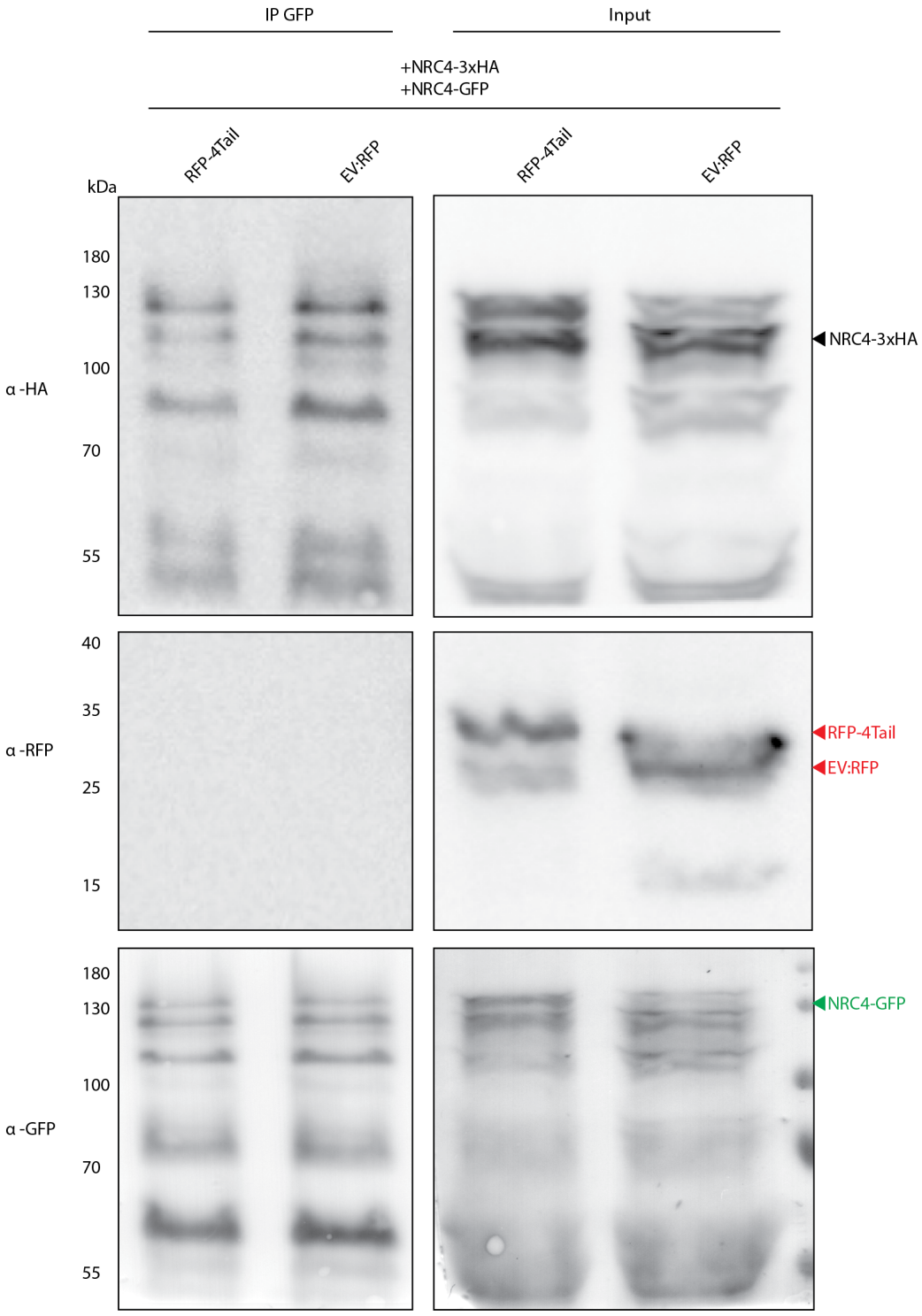
Supplementary Figures



C

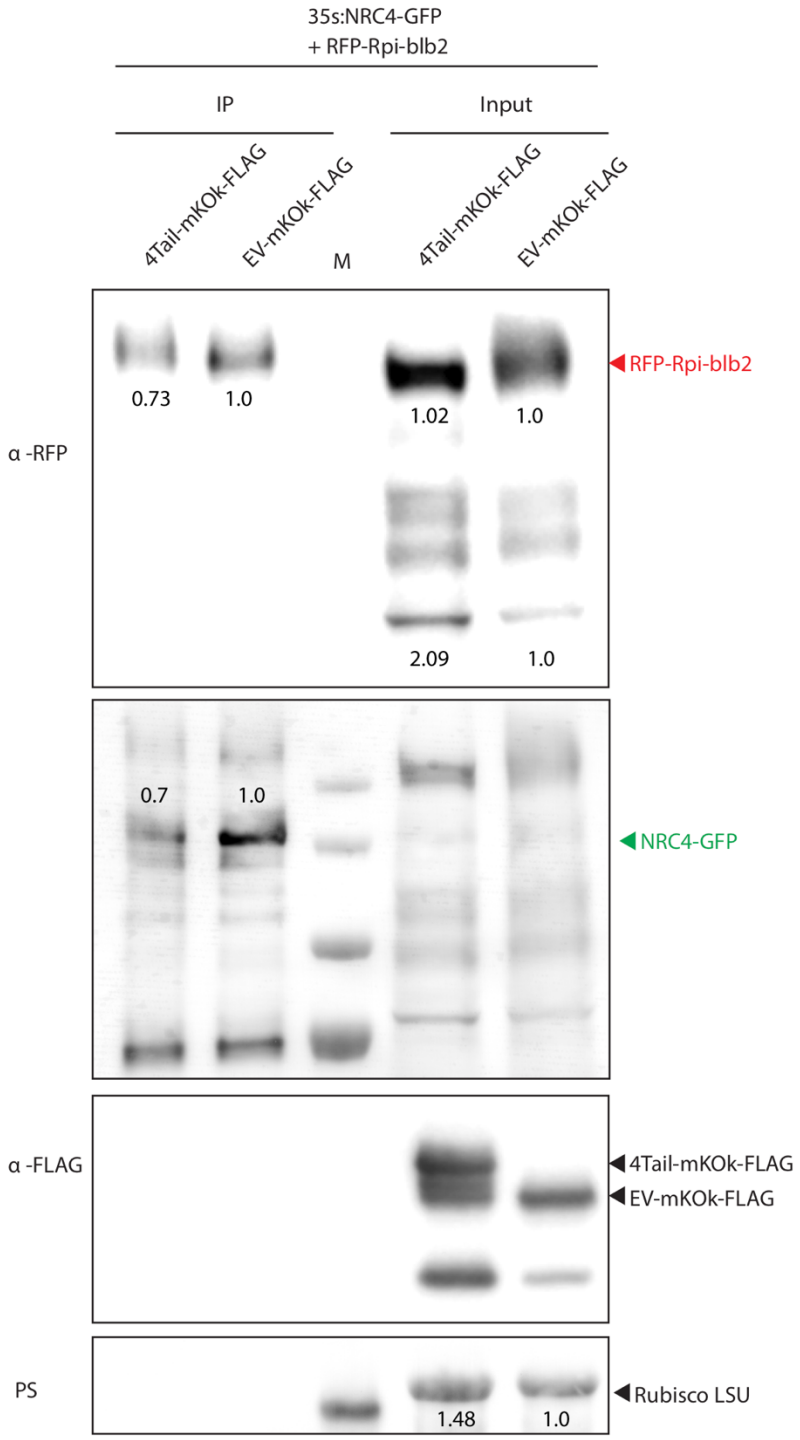
```
(RFP-) 4Tail                TSKAVKSAKAILESKTAKKIKFNLTIFPPEAGSKATQ
(GFP-) 4Tail (-GFP/mKOk)    TSKAVKSAKAILESKTDKNIKFNLTIFPPEAGSKATQ
                            ********************:*******************
```

Supplementary 1 = Figure 4.37: 4Tail-mKOk and RFP-4Tail suppress Rpi-blb2 immunity despite the latter having two amino-acid polymorphisms.
(A-B) Agro-expression of 4Tail-mKOk or RFP-4Tail opposite empty vector control, 1 day before infection with *P. infestans* was sufficient to break resistance in Rpi-blb2 transgenics for 4Tail but not EV. Numbers indicate the sum of successful infections per total infection sites. Leaves were imaged at 8 dpi. (B) Pairwise alignment of 4Tail from RFP-4Tail construct against 4Tail from GFP-4Tail, 4Tail-GFP or 4Tail-mKOk. Two amino acid changes were found, representing NRC4a's endogenous polymorphisms as RFP-4Tail was cloned from *N. benthamiana* cDNA and the others were cloned from a full-length NRC4b construct which had previously been cloned from *N. benthamiana* cDNA.



Supplementary 2 = Figure 4.38: 4Tail expression does not seem to effect NRC4-NRC4 interaction.

Differentially tagged NRC4, NRC4-GFP and NRC4-3xHA was co-expressed with RFP-4Tail or EV:RFP on opposite sides of *N. benthamiana* leaves to reduce variation in expressions. After 3 days proteins were extracted and GFP-trap agarose beads were used to immunoprecipitate proteins. After washing off non-specific interactions, IPs and total inputs were separated by SDS-PAGE and immunoblotted. The relative association of NRC4-3xHA with NRC4-GFP did not appear to be altered by 4Tail expression. Arrows indicate expected band sizes. kDa = kilodalton



Supplementary 3 = Figure 4.39: 4Tail expression does not seem to effect NRC4-Rpi-blb2 interaction.
RFP-Rpi-blb2 was co-expressed with RFP-4Tail or EV:RFP on opposite sides of 35S:NRC4-GFP *N. benthamiana* leaves to reduce variation in expressions. After 3 days proteins were extracted and GFP-trap agarose beads were used to immunoprecipitate proteins. After washing off non-specific interactions, IPs and total inputs were separated by SDS-PAGE and immunoblotted. The relative association of RFP-Rpi-blb2 with NRC4-GFP did not appear to be altered by 4Tail expression. Numbers indicate the band 'Signal' as determined by LI-COR Odyseey FX quantitative western blotting. Arrows indicate expected band sizes. kDa = kilodaltons.

5. Results Chapter III: Does an *inter*molecular system enable NRC4-mediated immunity?

5.1. Chapter Summary

NLRs are known to require a number of other components to enable resistance to disease. This is especially clear for helper NLRs like NRC4 that require sensors to detect specific pathogens. However, many other components are likely to be involved, but remain unknown. Here I describe an ongoing strategy for uncovering these components: 1) Co-immunoprecipitation of NRC4 followed by mass spectrometry to identify candidate interactors; 2) RNAi screen of a subset of these candidates to determine their role in NRC4-mediated HR, Rpi-blb2/NRC4-mediated immunity to *P. infestans*, and NRC4 trafficking to the EHM. I was unsuccessful in finding downstream components of NRC4-mediated immunity, which correlates with the current model for CC NLRs that they are the ultimate executer of cell death. However I did discover several proteins that when silenced resulted in altered *Agrobacterium* mediated transient expression levels and therefore may be important for immunity to bacteria. Additionally, I found several proteins that are candidate interactors of NRC4 and localise to the EHM.

5.2. Introduction

The emerging mechanism for how plant NLRs trigger immunity is that a helper (or singleton) NLR directly perturbs membrane homeostasis by forming pores, and this somehow leads to cell death by for instance enabling ion leakage inside the plant cells. This model fits with data from MADA CNLs like ZAR1, which has been shown to form resistosomes *in vitro* and *in vivo* and these are required for cell death (Hu et al., 2020; Wang et al., 2019a). This model also fits with the RNL helpers ADR1 and NRG1 (Jubic et al., 2019). HR could be caused directly by membrane lysis or the unregulated exchange of molecules across the membrane may lead to cell death. However, this model does not exclude the possibility of potential downstream, secondary signalling or parallel immune pathways, such as MAP kinase signalling cascades. For instance, recent work showed that the TIR domain of TNLs exert NADase activity to trigger cell death. However, TNLs still function through CNLRs ADR1 and/or NRG1. Could it be that the NADase activity is used to pass the signal through the lipase-like EDS1/PAD4/SAG101 components? These are known to be required for TNL mediated

HR. In fact NADase-mediated HR from TNLs was shown to be dependent on EDS1 in *N. benthamiana* (Horsefield et al., 2019). Knockout of *EDS1* recently enabled the determination of the first full length TNL structure – Roq1 of *N. benthamiana* (Martin et al., 2020). The authors found that upon activation, Roq1 forms a tetrameric resistosome, and the coming together of the four TIR domains activates their NADase function, which in the presence of EDS1 presumably leads to cell death. The same authors had previously shown that NRG1 is required for Roq1 HR (Qi et al., 2018), so activation of EDS1 somehow leads to activation of NRG1.

But other than the ZAR1 pore forming model, what is known about downstream signalling by CNLs? Many NLRs require SGT1, HSP90 and RAR1 ternary complex of chaperones for folding and stability (Kadota and Shirasu, 2012). For instance, silencing *SGT1* abolishes NRC4 mediated HR and resistance (Wu et al., 2017). However, so far the consensus is that there are no downstream components of the CNLRs as the chaperones act directly on the NLRs, not downstream (Adachi et al., 2019; Jubic et al., 2019; Wang et al., 2019a).

Given the perihaustorial accumulation of NRC4, we hypothesised that NRC4 might require ancillary components for its accumulation at the EHM and immune function. Additionally, NRC4 could form complexes with host components that are guarded by sensor NLRs such as Rpi-blb2. Here we use a co-immunoprecipitation/mass spectrometry list of candidate interactors of NRC4 to investigate what other proteins are involved in NRC4-mediated immunity. Considering the model that NRC4 is the executer of cell death, we did not expect to find any downstream components, but were anticipating proteins regulating its stability and, in particular, proteins involved in its transport or proteins guarded by NRC4-dependent sensor NLRs. Considering both NRC4 and AVRblb2 focally accumulate at the EHM, I was particularly focussed on finding candidates from the MS list that were reported to be involved in focal immunity (Kwon et al., 2008; Lipka et al., 2005). For instance, the atypical resistance protein RPW8.2 traffics to the EHM via VAMP labelled vesicles (Kim et al., 2014). I presented evidence in (Figure 3.6) that NRC4 is not carried by these same vesicles, so we predicted an alternative transport pathway may be involved in NRC4 EHM targeting. Here, I provide evidence that NRC4 accumulation at the EHM does not occur by passive diffusion through the cytoplasm. Instead, NRC4 focal accumulation appears

to be regulated by a dynamic process, i.e. it occurs slower than could be explained by passive diffusion. This could involve a transport mechanism to the EHM or passive diffusion through the cytoplasm, followed by a more time-consuming process of membrane association.

To investigate the putative transport of NRC4 to the EHM as well as any proteins regulating NRC4-mediated resistance to *P. infestans*, I chose to screen transgenic Rpi-blb2 plants. Constitutive expression of Rpi-blb2 in transgenic *N. benthamiana* renders these plants completely resistant to *P. infestans 88069* – that is, 100% of infections result in only a small HR lesion and no growth of the pathogen. It also provides resistance on potato and tomato (Bozkurt et al., 2011; Oh et al., 2014; Van Der Vossen et al., 2005; Wu et al., 2017). I found that systemic RNAi by Virus Induced Gene Silencing (VIGS) of 27 candidate immune regulators did not result in complete suppression of Rpi-blb2 mediated resistance. Many of the candidate interactors are delivered to the haustorial interface and some affected *Agrobacterium*-mediated transient gene expression. Overall this chapter is a preliminary investigation into the intermolecular regulation of NRC4-mediated immunity. The findings require following up and in most cases repetition.

5.3. Results & Discussion

5.3.1. NRC4 accumulation towards haustoria is unlikely to occur due to passive diffusion but instead by a dynamic process

NRC4 haustorial recruitment could be due to diffusion through the cytosol or via a regulated process including vesicle trafficking. I carried out Fluorescent Recovery After Photobleaching (FRAP) to analyse the dynamics of NRC4 fusion proteins. First, I co-expressed functional NRC4-GFP with RFP-Rem1.3 plasma membrane and EHM marker during infection. I focused on a cell where the pathogen had formed distantly separated haustoria allowing me to photobleach one, whilst comparing to an internal, non-photobleached control haustorium. This allowed me to normalise the signal so that any photobleaching during image acquisition of the recovery period was controlled for. I obtained a series of images 5 minutes before photobleaching (t =-5), immediately after photobleach (t=0), 5 minutes after (t=5), and then every 10 minutes until recovery had occurred (Figure 5.1). This revealed that NRC4-GFP signal restored in no less than 35 minutes. This was much slower than that of the atypical resistance protein RPW8.2 which was reported to transport to the EHM of fungal haustoria via vesicles, in 5-12 minutes (Kim et al., 2014; Wang et al., 2009). I used the time required for half of the observed recovery to occur ($t^{1/2}$) as a measure for the dynamics of a protein as previously reported (https://www.embl.de/eamnet/frap/html/halftime.html). I calculated that NRC4-GFP had a $t^{1/2}$ = 16.6 minutes, much slower than that calculated for RPW8.2, which took 3.3 minutes (Kim et al., 2014). It's important to note that the $t^{1/2}$ of NRC4-GFP represents a preliminary calculation that requires experimental replicates for strong conclusions to be drawn. RFP-Rem1.3, which has a very small cytoplasmic pool, did not recover during this imaging period. Because of this, I was unable to calculate the $t^{1/2}$ of RFP-Rem1.3. However, considering the shallow slope of the curve, the $t^{1/2}$ is presumably much larger than NRC4-GFP. This is in contrast to what has been previously shown for the *Arabidopsis* orthologue of Rem1.3 (At2g45820) which has a $t^{1/2}$ of 35 seconds on the plasma membrane (Jarsch et al., 2014). However, StRem1.3 may be different and previous FRAP experiments with GFP-StRem1.3 found a 23% recovery in 60 s but levelling off of the curve at that point (Martinière et al., 2012). Additionally, the impact of *P. infestans* on Remorin localisation has not been investigated.

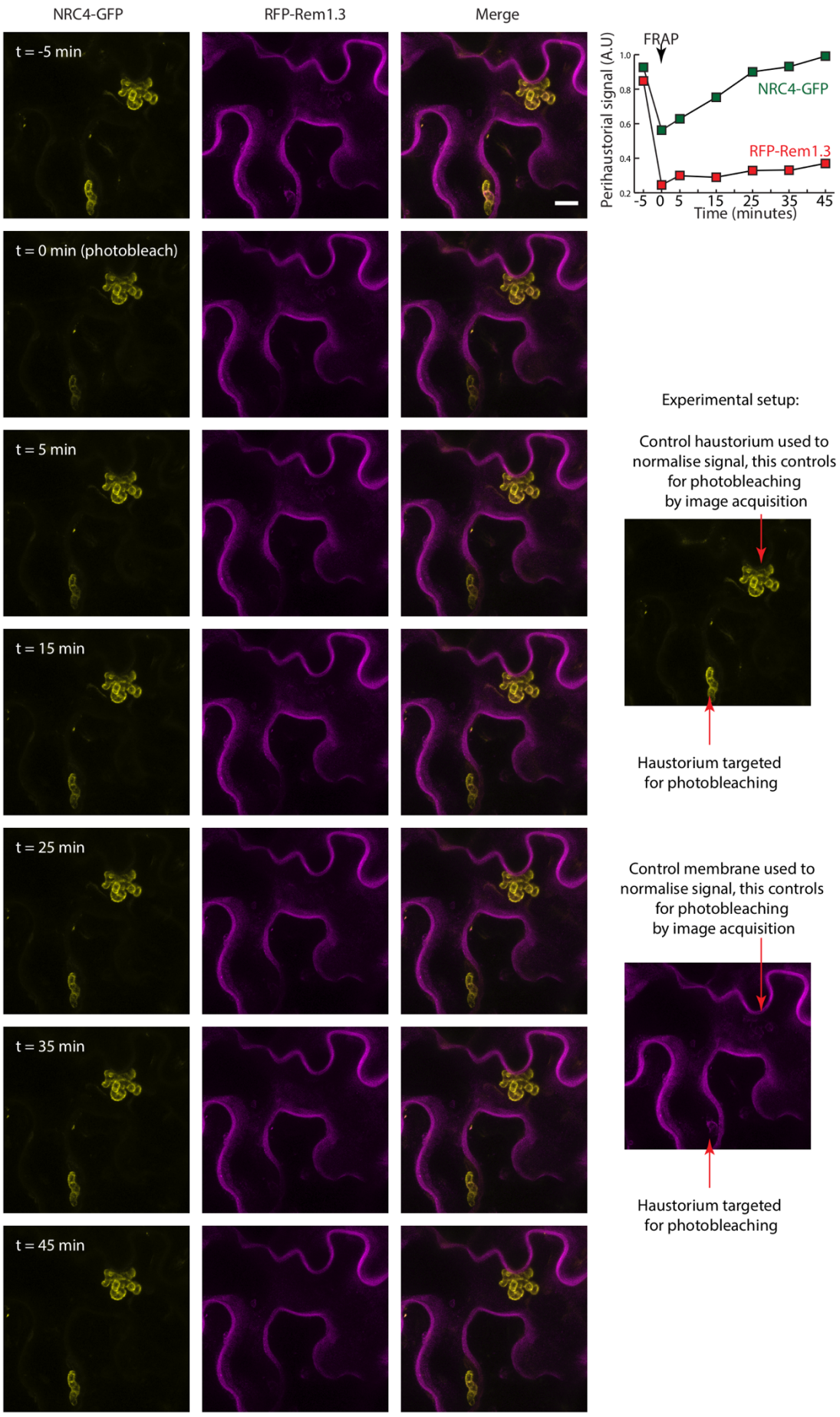

NRC4-GFP
RFP-Rem1.3
Merge
t = -5 min
t = 0 min (photobleach)
t = 5 min
t = 15 min
t = 25 min
t = 35 min
t = 45 min
FRAP
Perihaustorial signal (A.U)
1.0
0.8
0.6
0.4
0.2
NRC4-GFP
RFP-Rem1.3
-5 0 5 15 25 35 45
Time (minutes)
Experimental setup:
Control haustorium used to normalise signal, this controls for photobleaching by image acquisition
Haustorium targeted for photobleaching
Control membrane used to normalise signal, this controls for photobleaching by image acquisition
Haustorium targeted for photobleaching

Figure 5.1: Fluorescence Recovery After Photobleaching of NRC4-GFP recovers faster than RFP-Rem1.3.
Photobleaching of NRC4-GFP at haustoria and time lapse imaging revealed that NRC4 requires > 35 minutes for other NRC4 molecules to transit back to haustoria. An image was first taken 5 minutes before photobleaching (t = -5). At t = 0 488 nm laser was increased to 85% intensity and focused on the haustorium indicated by the arrow until the haustorium was photobleached. The recovery of NRC4-GFP fluorescence was monitored every 10 minutes until recovery, where perihaustorial signal normalised to a non-photobleached control haustorium in the same cell. RFP-Rem1.3 was also photobleached during this process and its recovery measured. It was normalised to fluorescence of membrane indicated because the control haustorium did not show sufficient Rem1.3 labelling. Scale bar = 10μm.

Next, to determine if NRC4 recovery time was consistent with diffusion, I co-expressed NRC4-mKOk with EV:GFP cytoplasmic marker (Figure 5.2). I measured a $t^{1/2}$ for NRC4-mKOk of 19 minutes, close to that of NRC4-GFP. Cytoplasmic GFP fluorescence recovered in between the photobleach step and the initial image acquisition after photobleaching (t=0). This is not surprising considering diffusion of cytoplasmic proteins in plants are known to occur in a matter of seconds, not minutes (Martinière et al., 2012). I concluded that NRC4 accumulation at the EHM probably does not occur by passive diffusion, at least not alone, and therefore is a dynamic, regulated process. NRC4 may require other proteins for this process or NRC4 may have an intrinsic ability to accumulate at the EHM, for instance via self-oligomerisation across the EHM.

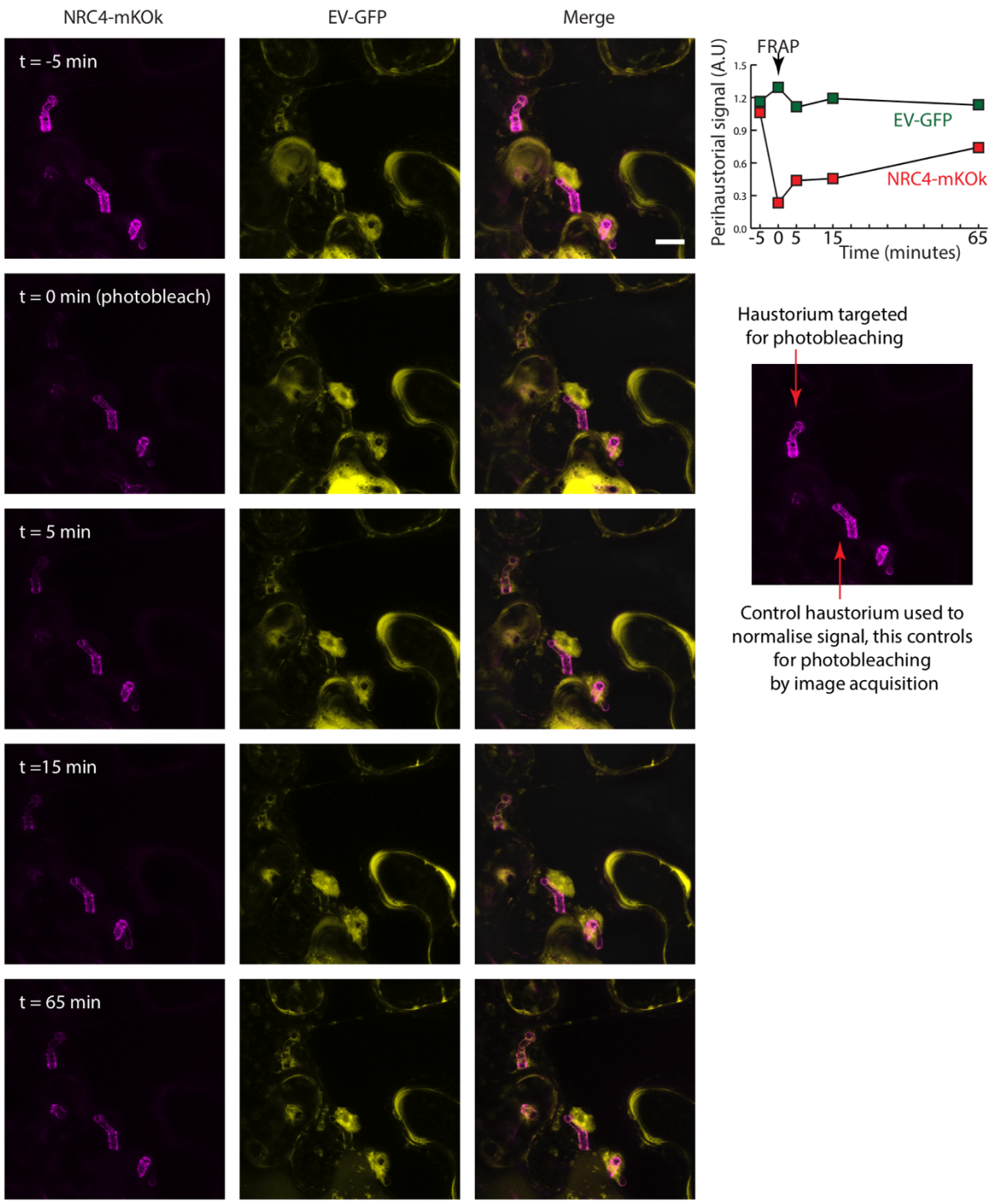


Figure 5.2: NRC4-mKOk fluorescence recovers much slower than cytoplasmic EV-GFP.
Photobleaching of NRC4-mKOk at haustoria and time lapse imaging revealed that NRC4 requires around 19 minutes for half of recovery to take place. An image was first taken 5 minutes before photobleaching (t = -5). At t = 0 strong lasers were focused on the haustorium indicated by the arrow until the haustorium was photobleached. The recovery of NRC4-GFP fluorescence was monitored until recovery plateaued, with perihaustorial signal normalised to a non-photobleached control haustorium in the same cell. EV-GFP was photobleached during this process but its recovery was faster than the image acquisition. Scale bar = 10µm.

5.3.2. Summary of gene silencing screen to determine the cellular components of NRC4 EHM transport

The long time scale for NRC4 EHM fluorescence to recover ($t^{1/2}$=16-19 min; Figure 5.1 and Figure 5.2) implies that a transport machinery is likely involved in this process. Therefore, to elucidate the components involved, Bozkurt et al (unpublished) first employed a co-immunoprecipitation tandem mass-spectrometry (MS) screen to reveal candidate interactors of GFP-NRC4 in non-infected and *P. infestans* infected tissue. The results provided almost 1000 proteins, many of which I immediately removed from consideration as they were also found in the GFP control co-immunoprecipitates. I further narrowed down the list by removing the common proteins found in co-IP assays (Petre et al., 2016). Next, I selected the proteins that appeared or increased in terms of number of peptide hits in the infected tissue and also selected those that had a role in protein transport or associated with protein binding. Additionally, any vesicle transport regulators were selected, whether or not they were found in infected tissue. A table of these proteins of interest is provided below (Table 11).

I aimed to investigate five potential roles of these proteins in NRC4 regulation:

1. Rpi-blb2/NRC4-mediated resistance to *P. infestans*
2. NRC4-mediated HR
3. NRC4 protein levels
4. EHM targeting of NRC4
5. Localisation of fluorescently tagged protein of interest during infection with *P. infestans*

Unfortunately, whilst goal number 4 was highly interesting, it was too risky and labour intensive to immediately investigate as it would require a confocal microscopy screen of infected tissue expressing NRC4-GFP with and without disruption of the gene of interest (GOI). Similarly, for goal number 5, some candidates were selectively cloned, full-length and tagged to fluorescent proteins and their localisation in haustoriated cells gathered. This 'guilt-by-association' method is useful in that proteins involved in NRC4 haustorial transport are likely to be found there. However, in the time-frame of this project it was not feasible to conduct large numbers of confocal microscopy experiments and is risky.

In order to investigate the five goals above, I conducted an RNAi based silencing screen with local hairpin silencing as well as systemic virus induced gene silencing

(VIGS) as outlined (Figure 5.3). The progress so far is summarised in Table 11 and Figure 5.4, however, experimentation is on-going and most results need further verification. Considering the large number of GOIs and the limited time available during this project, I elected to first screen for phenotypes and then validate the efficiency of silencing. In hindsight, this was a quicker but certainly risky strategy as not all silencing constructs can be expected to work efficiently. In order to quickly generate gene silencing constructs for local and systemic silencing, I first generated a golden gate compatible vector for VIGS which I called TRV2gg (Chapter 2, Figure 3). The overhangs of DNA fragments for this vector are compatible with that of the local silencing vector, pRNAiGG, enabling me to clone simultaneously into vectors for systemic and local silencing.

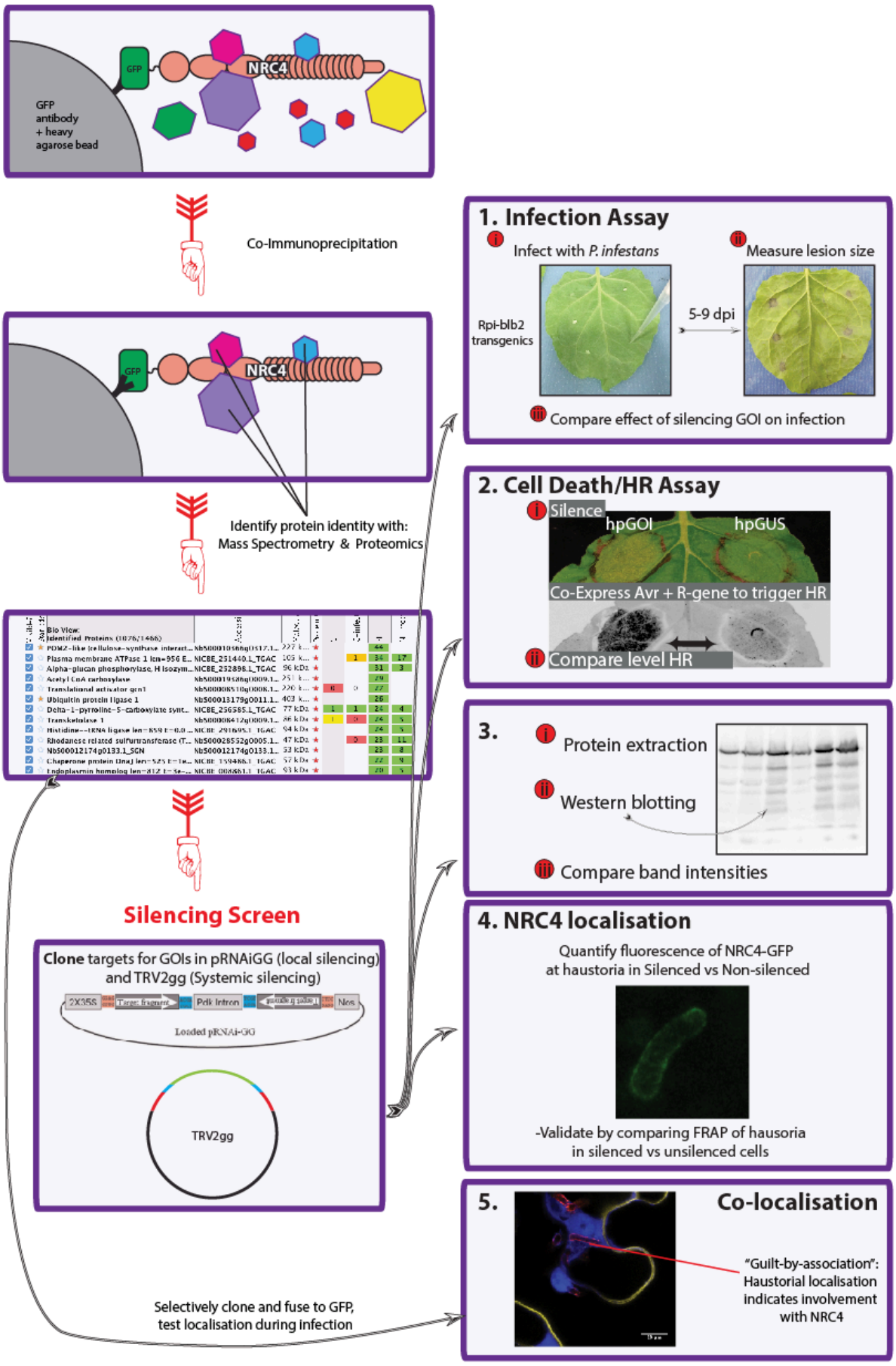

GFP
NRC4
GFP antibody + heavy agarose bead
Co-Immunoprecipitation
Identify protein identity with: Mass Spectrometry & Proteomics
Silencing Screen
Clone targets for GOIs in pRNAiGG (local silencing) and TRV2gg (Systemic silencing)
2X35S
Pdk Intron
Nos
Loaded pRNAi-GG
TRV2gg
Selectively clone and fuse to GFP, test localisation during infection
1. Infection Assay
i Infect with P. infestans
ii Measure lesion size
Rpi-blb2 transgenics
5-9 dpi
iii Compare effect of silencing GOI on infection
2. Cell Death/HR Assay
i Silence
hpGOI
hpGUS
Co-Express Avr + R-gene to trigger HR
ii Compare level HR
3.
i Protein extraction
ii Western blotting
iii Compare band intensities
4. NRC4 localisation
Quantify fluorescence of NRC4-GFP at haustoria in Silenced vs Non-silenced
-Validate by comparing FRAP of hausoria in silenced vs unsilenced cells
5. Co-localisation
"Guilt-by-association": Haustorial localisation indicates involvement with NRC4

Figure 5.3: Reverse genetics screen to identify proteins involved in NRC4-mediated resistance.
GFP-NRC4 was pulled-down with its partner proteins. These were analysed by mass-spectrometry and the identities determined by proteomics. Candidates were narrowed down based on protein function and number of peptide hits. The nucleotide sequence targeted by the gene silencing constructs were 300-600bp in GOIs were selected to be cloned into local silencing and systemic silencing vectors: pRNAiGG and TRV2gg. These silencing constructs were used for three experiments: 1. The effect on Rpi-blb2 resistance due to silencing the GOI was investigated by systemically silencing Rpi-blb2 transgenics and infecting with NL07434 (strain that partially overcomes Rpi-blb2) or 88069 lab strain (avirulent on Rpi-blb2 transgenics). 2. The effect on HR of silencing the GOI was investigated by transiently silencing the GOI vs GUS whilst triggering HR with AVRblb2 and Rpi-blb2. 3. The GOI will be silenced in NRC4-GFP transgenic *N. benthamiana* and the fluorescence at haustoria quantified relative to a non-silenced control. If a GOI is implicated in affecting localisation, this will be validated by comparing the time taken for haustorial signal to FRAP in silenced vs non-silenced cells. 5. GOIs were selected and cloned as fusion proteins and their localisations tested during infection.

Firstly, I tested the effect of systemically silencing a GOI on Rpi-blb2 resistance to the *P. infestans* isolate *NL07434* which is partially virulent on Rpi-blb2 transgenics (Dr Wu, unpublished). This would allow me to assay for quantitative decreases in NRC4-mediated resistance, which is important as partially knocking down one component may not be sufficient to break the complete resistance to *88069* strain. Unfortunately, after several months of trials, this strategy had to be abandoned as *NL07434* infection assays had failed. The spore count of the pathogen was too low, even after revival from liquid nitrogen stocks. Therefore, I decided to conduct the screen with the 88069 isolate. This required making the assumption that NRC4 localisation is required for Rpi-blb2 resistance as I would be unable to determine increases in Rpi-blb2 mediated resistance in silenced plants. In the future the *NL07434* strain should be used to investigate the opposite hypothesis.

Table 11: Summary of Mass Spec candidate interactors investigated for involvement in NRC4-mediated immunity

Construct Name	Full Name	Accession SGN/TGAC	MS Hits uninfected	MS Hits Infected	Additional info	Localisation	VIGS phenotype	Silencing effect on NRC4 HR	Resistance Tested?	Cloning Status
	Predicted Membrane proteins									
GOLD	emp24/gp25L/p24 family/GOLD	NbS00030108g0003.1_SGN	0	2	Golgi & protein trafficking				Yes	VIGS
TM	Small benthi transmembrane protein	NbS00039788g0005.1_SGN		2	mispredicted to be shorter				Yes	hp/VIGS
EF hand	Calcium binding EF hand	NbS00010383g0004.1_SGN		3	transmembrane (x2)				Yes	VIGS
CaCL	Anoctamin Calcium-activated chloride channel	NICBE_366990.1_TGAC		3	transmembrane (x2)				Yes	VIGS
Syt1	Syt1 synaptotagmin	NbS00005170g0006.1_SGN	1	2	Ca2+ dependent lipid binding protein	Haustorial neck				FP
PLAT	PLAT PLAT/LH2 domain	NICBE_226268.1_TGAC		5	membrane lipoxegenase				Yes	VIGS
DUF1295	Protein of unknown function with DUF1295	NbS00008935g0002.1_SGN		2	steroid dehydrogenase-like				Yes	VIGS
DUF2304	ATP-dependent helicase/deoxyribonuclease subunit B (DUF2304)	NICBE_290487.1_TGAC	0	3	Transmembrane, cytoplasmic & non				Yes	VIGS
	Vesicle Transport Regulators									
SNARE	Vesicle fusing ATPase (N-ETHYLMALEIMIDE SENSITIVE FACTOR, NSF)	NbS00011575g0012.1_SGN	2				Dwarf/die	Cytotoxic	n/a	VIGS/hp
Sec3a	Sec3 (Exocyst complex component 1)	NICBE_053349.1_TGAC	5			Pucta at EHM	Dwarf	no change	Yes	FP/VIGS/hp
Sec5	Sec5 (Exocyst complex component 2)	NbS00026473g0006.1_SGN	2					increase	Yes	VIGS/hp
Sec6	Sec6 (Exocyst complex component 3)	NICBE_298622.1_TGAC	6						Yes	VIGS
Sec10	Sec10 (Exocyst complex component 5)	NICBE_108112.1_TGAC	9						Yes	FP/VIGS
Sec15	Sec15 (Exocyst complex component 6)	NICBE_239296.1_TGAC	4						Yes	VIGS
Exo70B1	Exo70B1 (Exocyst complex component 7)	NICBE_366276.1	2			Puncta at EHM			Yes	FP/VIGS/hp
Exo70A1	Exo70A1 (Exocyst complex component 7)	NICBE_208653	1			Puncta at EHM		decrease	Yes	FP/hp/VIGS
Exo84b	Exo84b (Exocyst complex component 8)*	NbS00024919g0014	*not in MS	*not in MS		Haustorial/EHMx	Dwarf/curly leaves		Yes	FP/VIGS/hp
RabD2a	Ras-related protein RABD2a	NICBE_110965.1_TGAC	2	1				decrease	Yes	FP/DN/VIGS/hp
RabE1a	Ras-related protein RABE1a	NICBE_150830.1_TGAC	8	11				increase	Yes	FP/DN/VIGS/hp
	ER Related									
Trap	Translocon-associated protein subunit beta	NICBE_061264.1_TGAC		2	TRAPB				Yes	VIGS
ER3	ER membrane protein complex subunit 3	NICBE_340892.1_TGAC		3	Integral membrane protein DUF106				Yes	VIGS
ER4	ER membrane protein complex subunit 4	NICBE_170029.1_TGAC (+2)		2	DUF1077				Yes	VIGS
	Vacuolar									
VPS16	Vacuolar protein sorting-associated protein 16	NICBE_236764.1_TGAC	9	2	HOPS/CORVET complex		Dwarf/Die		n/a	VIGS
VPS18	Vacuolar protein sorting associated protein 18	NbS00008576g0002.1_SGN	3		HOPS/CORVET complex	EHM/vesicles /cytoplasmic	Dwarf/Die	Increase	n/a	FP/VIGS/hp
VPS41	Vacuolar protein sorting associated protein 41	NbS00045423g0008.1_SGN	5		HOPS complex	EHM/vesicles		Increase		FP/truncates/hp
VSR3	Vacuolar-sorting receptor 3	NICBE_083936.1_TGAC	2	1	Golgi/Prevacuolar				Yes	VIGS/hp
VSR6	Vacuolar-sorting receptor 6	NICBE_031939.1_TGAC (+2)	3		Golgi/Prevacuolar				Yes	VIGS
	Golgi									
COG2	Conserved oligomeric Golgi complex subunit 2	NICBE_396062.1_TGAC	2		Vesicle tethering at Golgi					VIGS
	Misc.									
TPR	Tetratricopeptide repeat (TPR) containing protein	NbS00017326g0002.1_SGN	7		protein binding				Yes	VIGS/hp
	Secreted									
PITP	Putative phosphatidylglycerol/phosphatidylinositol	NICBE_216370.1_TGAC		2	Secreted/sterol transporter				Yes	VIGS
RLP	Secreted LRR (misannotated as receptor serine/threonine protein kinase RLP)	NbS00002113g0001.1_SGN	2	5	secreted				Yes	VIGS/hp
	Enzymes									
Trop	Tropinone reductase	NICBE_060415.1_TGAC		3	NADP to NADH enzyme				Yes	VIGS
Brain	Brain protein 44	NbS00017703g0007.1_SGN		3	mitochondrial pyruvate carrier				Yes	VIGS

5.3.3. VIGS screen of candidate NRC4 interactors reveals secretory components that may positively contribute to Rpi-blb2 mediated resistance

We systemically silenced Rpi-blb2 plants with VIGS and infected leaves with *P. infestans* 88069 isolate. It was not feasible to silence all GOIs in one experiment due to labour and space issues. We therefore silenced groups of four or more GOIs in each experiment. Rpi-blb2 plants are completely resistant and only produce a small necrotic lesion when challenged with droplets containing *P. infestans* spores (Wu et al., 2017). Considering this, we were initially interested in determining whether any pathogen growth would occur in the silenced plants so we did not include a non-silenced control. However, after the first three experiments it became clear that we would require a non-silenced control to compare against if there were small increases in pathogen growth. These are labelled as 'Rpi' (Rpi-blb2 leaves not inoculated with VIGS), or EV (Rpi-blb2 plants with VIGS-EV inoculated). I used a semi-automated colour deconvolution macro for ImageJ produced by FILM at Imperial College (https://www.imperial.ac.uk/medicine/facility-for-imaging-by-light-microscopy/software/fiji/), to measure the necrotic lesion size and found that the most promising constructs were the VIGS-ER4, VIGS-TRAPP, VIGS-ER3, VIGS-Exo70A1, VIGS-Sec15, VIGS-VSR6, VIGS-TPR, VIGS-DUF2304, VIGS-PLAT, VIGS-Sec6 and VIGS-TM (Figure 5.4).

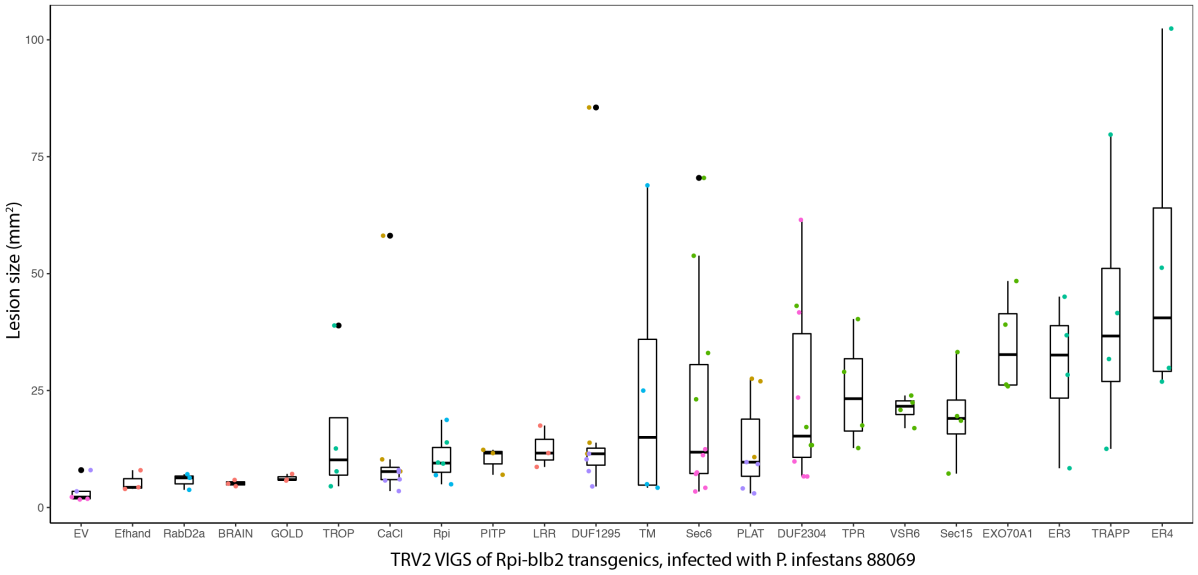


Figure 5.4: VIGS based RNAi screen of candidate NRC4 interactors reveals some possible regulators of Rpi-blb2/NRC4 mediated immunity to *P. infestans.*
Rpi-blb2 seedlings were silenced with VIGS for the gene indicated. At 4-5 weeks these were infected with *P. infestans* 88069 and 7-13 days post infection the lesion size was quantified with the help of a colour deconvolution FIJI macro. Scatter boxplot displays results in order of increasing mean. Colours indicate individual experiments and each dot represents the average lesion size per leaf.

We did not expect to see lesions sizes on GOI-silenced leaves close to that of *NRC4*-silenced leaves as regulation of NRC4 is likely multifaceted, RNAi is inefficient and there could be genetic redundancy. Nevertheless, there were some promising differences worth pursuing in the future. VIGS-Sec15, VIGS-Exo70A1 and VIGS-Sec6 of the Exocyst complex were amongst the most promising as their results correlated with one another. Overall the results in this silencing screen should be considered preliminary as they lack sufficient power for statistical analysis and controls for comparison. It is feasible that the variation in lesion size was partially due to difference in age of leaves chosen for infections. Additionally, using necrotic lesion size as a measure for *P. infestans* growth is useful, but in this situation where *P. infestans* is normally avirulent, could be misleading. These necrotic lesions could be explained by uncontrolled programmed cell death or 'trailing necrosis' due to silencing of a gene required to restrict cell death. For instance, previous studies on autophagy in *Arabidopsis* and *N. benthamiana* which mutated key components of this pathway lead to unrestricted HR (Liu et al., 2005; Patel and Dinesh-Kumar, 2008). An Exo70 paralogue, Exo70D, was recently implicated in a preprint to positively contribute to autophagy (Acheampong et al., 2020). This could therefore explain the results of

silencing exocyst components, for instance. In future, using the red fluorescent strain of *P. infestans,* TD tomato 88069, could discern between run away cell death and actual pathogen growth, as the fluorescent strain would allow me to see the growth of hyphae rather than relying on pathogen induced necrosis as a proxy. The reason I did not do this for the initial screen was due to concerns that the transformed strain is less virulent than the WT.

5.3.4. The exocyst complex is deployed to the EHM but does not seem to regulate NRC4-Rpi-blb2 mediated immunity

Considering the promising results of the VIGS screen on multiple exocyst members, I elected to investigate the involvement of the exocyst complex on NRC4 regulation in further detail. The exocyst complex is an evolutionarily conserved octameric protein complex that directs vesicles to the plasma membrane for exocytosis. The complex consists of Sec3, Sec5, Sec6, Sec8, Sec10, Sec 15, Exo70 and Exo84. In plants the Exo70 component has expanded massively (Du et al., 2018). In our MS data, I found six of the eight exocyst complex components. Additionally, Exo70 was present in two isoforms, Exo70B1 and Exo70A1.

5.3.4.1. RNAi mediated silencing of Exo70A1 did not affect HR triggered by autoactive NRC4

In order to investigate the effect of silencing *Exo70A1* on NRC4 HR we co-expressed autoactive NRC4 ($NRC4^{D478V}$) with hairpin silencing constructs targeting Exo70A1 (hpExo70A1) or GUS control (hpGUS) (Figure 5.5). Visually, it appeared that silencing Exo70A1 reduced the intensity of HR elicited by $NRC4^{D478V}$. We did not observe this with autoactive form of I2, which is believed to be a singleton NLR (Giannakopoulou et al., 2015) that is outside the NRC clade (Wu et al., 2017). However, despite the apparent trend observed on NRC4-triggered HR caused by Exo70A1 knockdown, upon quantification of images taken with blue light (two independent experiments), there was no statistical difference between silencing *Exo70A1* vs GUS. Further replicates of this experiment are warranted to clarify this.

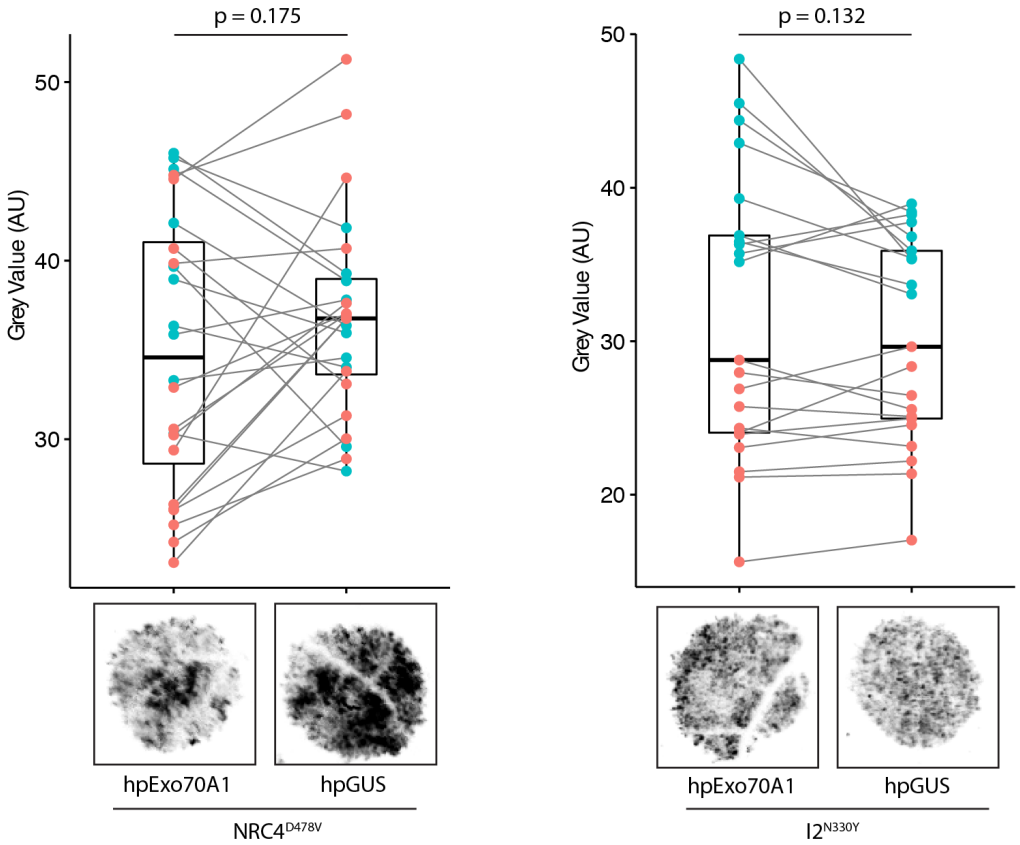


Figure 5.5: hpExo70A1 seems to have no effect on NRC4 or I2 mediated HR. Scatter boxplots representing the intensity of HR imaged with blue light and quantified in terms of mean gray value by FIJI (A) NRC4 autoactive triggered HR is not purturbed by Exo70A1 silencing. $NRC4^{D478V}$ was co-expressed with either hpExo70A1 or hpGUS. (B) I2 autoactive triggered HR is not purturbed by Exo70A1 silencing. $I2^{N330Y}$ was co-expressed with either hpExo70A1 or hpGUS. The resulting HR from the autoactive NLRs was imaged at 3 dpai. Paired t-tests were conducted with p = 0.175 and p = 0.132 respectively. Colours indicate independent replicates and dots represent the signal obtained from a sample of the infiltration patch.

5.3.4.2. NRC4 protein levels are not altered by Exo70A1 silencing

Whilst investigating the visible HR phenotype caused by Exo70A1 silencing, we then investigated whether this is caused by reduced NRC4 protein levels. To do this, we expressed hpExo70A1 side by side with hpGUS silencing control on leaf patches of transgenic NRC4-GFP plants. After three days we harvested leaf disks and detected NRC4-GFP protein levels by western blotting. In immunoblots, there was no clear difference in NRC4-GFP band intensity between *Exo70A1* silenced and GUS control. This experiment was repeated 6 times with similar results each time, with no clear trend between replicates in NRC4 protein levels between silenced and control tissue (Figure 5.6). In the last experiment we included an agro-expressed marker, Luciferase-3xHA to determine whether hpExo70A1 had an effect on *Agrobacterium* transient gene expression. This showed a less intense signal in the hpExo70A1 expressing sample compared with the hpGUS control. Therefore, it is likely the suppression of NRC4-mediated HR observed in some prior experiments was due to decreased *Agrobacterium*-mediated gene expression upon *Exo70A1* silencing. This explanation is not consistent however with no observed difference in I2-mediated HR between *Exo70A1* silenced tissue and control. This immunoblot experiment with *Agrobacterium* expression control should be repeated to see if the results are reproducible, and an HR experiment should be included alongside, to see whether suppression of HR correlates with this result.

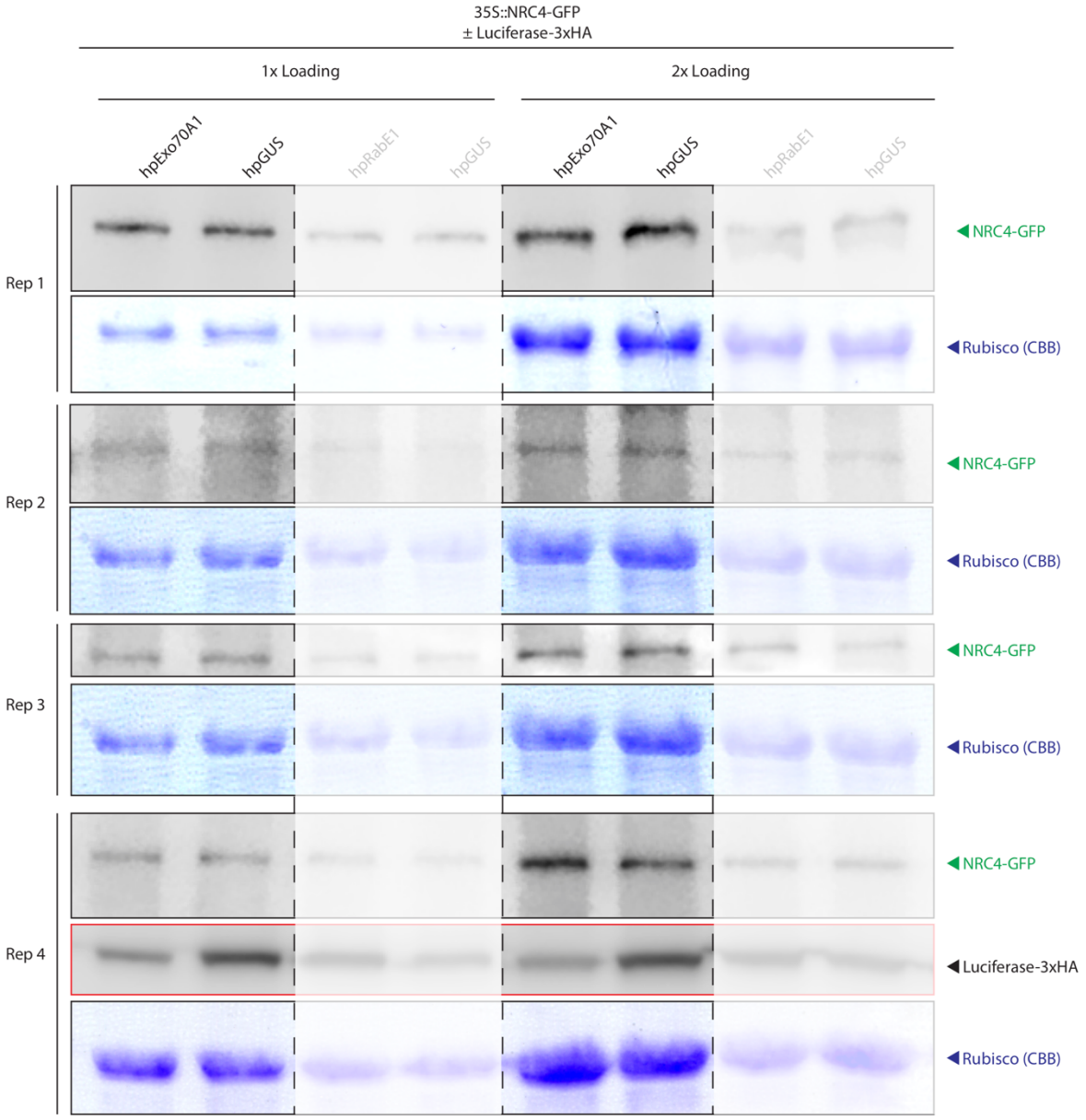


Figure 5.6: Western blotting shows no effect on NRC4 protein levels upon *Exo70A1* silencing.
NRC4 protein levels are not perturbed by Exo70A1 silencing, but *Agrobacterium* mediated gene expression appears to be reduced by Exo70A1 silencing. Transgenic 35S::NRC4-GFP plants were silenced for either Exo70A1 or GUS with hairpin RNAi, and after 3 dpai proteins were crudely extracted, separated by SDS-PAGE (7.5% gel), and immunoblotted for GFP. To assess the relative loading of proteins, the remaining rubisco large subunit after transfer to membrane was detected with Coomassie Brilliant Blue (CBB) staining. Two separate volumes were loaded to reduce the chances of saturation, these were either 10 µl & 20 µl or 5 µl & 10 µl. Four independent experimental replicates were conducted, with the final experiment including co-expression of Luciferase-3xHA as an internal agro-expression control. NOTE: a separate but related experiment involving the silencing of RabE1a was included, but is faded out here as it is discussed in Figure 5.22.

5.3.4.3. The exocyst complex is deployed to the host-pathogen interface

Exo70A1 does not appear to regulate NRC4-mediated HR. Considering this, the preliminary result that VIGS of Exo70A1 may produce susceptibility on Rpi-blb2 plants (Figure 5.4) instead could be due to alteration of NRC4 localisation. To understand whether there is a functional relationship between the exocyst complex and NRC4, I cloned full length constructs of three *N. benthamiana* exocyst subunits and fused them to GFP: Sec3 and Exo70 paralogues Exo70A1 & Exo70B1. I expressed these along with AtExo84b-GFP (provided by Yasin Dagdas at TSL, Norwich) during infection with *P. infestans* and found all show punctate perihaustorial signal (Figure 5.7). Exo70B1 labelled puncta scattered throughout the cell, as well as in a high density at the haustorial interface (Figure 5.7C). This was in contrast to Exo70A1 which was more specific in localising to puncta at the haustorial interface (Figure 5.7D). The finding that the exocyst complex traffics to oomycete haustoria was recently also shown in the *Phytophthora capcisi – Physcomitrella patens* pathosystem (Overdijk et al., 2020), which implies this focal deployment of the plant exocyst complex to oomycete haustoria was an early development in plant evolution.

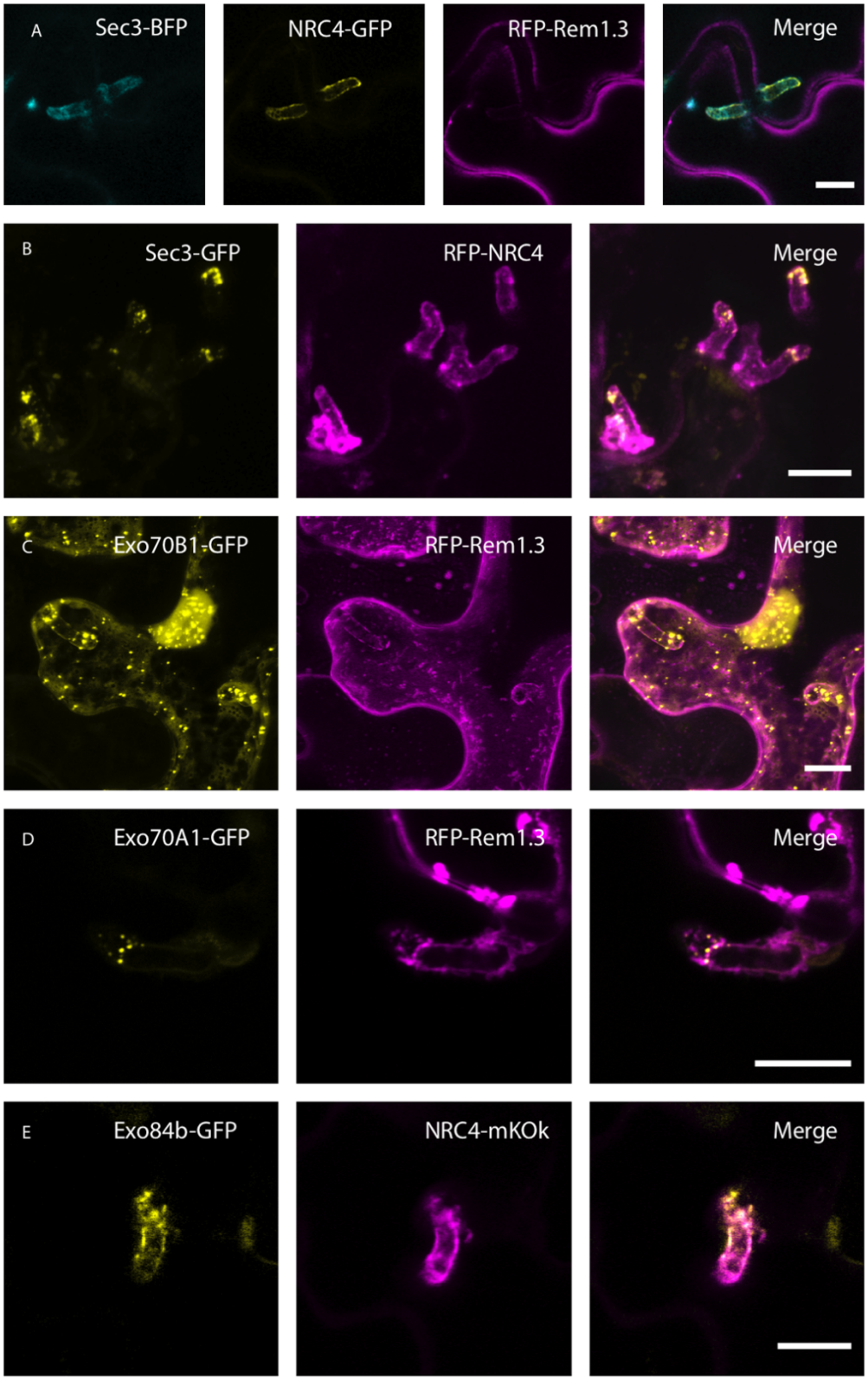


Figure 5.7: Exocyst complex is deployed to the haustorial interface.
NRC4-GFP, NRC4-mKOk, or RFP-Rem1.3 were co-expressed with Sec3-BFP, Sec3-GFP, Exo70B1-GFP, Exo70A1-GFP or Exo84b-GFP in WT *N. benthamiana* leaves. After 3 hours the leaves were infected with *P. infestans.* Images were taken using SP5 confocal microscope (A-C & E) or SP8 confocal microscope (D) after 3 days.

Components of the exocyst complex were tagged with GFP or BFP, N or C terminally and expressed during *P. infestans*. A, E and F are single plane images, whereas B-C are z-projections of z-stacks used to avoid missing haustoria in different z-planes. Scale bars are 10 µm.

The perihaustorial localisation of the components of the exocyst complex presents an intriguing set of hypotheses such as; (i) NRC4 is deployed to the EHM via the exocyst pathway; (ii) Alternatively, NRC4 is directly/indirectly guarding the exocyst pathway by pairing with specific sensor NLRs. Two key experiments should be carried out in the future. Firstly, the association of NRC4 with components of the exocyst complex should be confirmed by immunoprecipitation of exocyst complex and detection of the presence/absence of NRC4 in the co-immunoprecipitates. Secondly, confocal microscopy of exocyst-silenced transgenic NRC4-GFP tissue should be carried out to determine whether NRC4 is depleted from the EHM. This is challenging however, as the plant exocyst complex has diversified, but targeting the components with less diversity such as Sec3 might be a good strategy (Boehm and Field, 2019; Du et al., 2018). Exo70B1 is believed to contribute to autophagy in plants (Kulich et al., 2013; Sabol et al., 2017), however the evidence for this so far is not strong, as this model was built upon a single image of low quality co-localisation microscopy. Nevertheless, the punctate localisation of Exo70B1 during infection with *P. infestans* is reminiscent of our finding that autophagosomes are redirected towards haustoria (Dagdas et al., 2018). Additionally, Exo70B1 was recently reported to deploy FLS2 to the plasma membrane in *Arabidopsis* (Wang et al., 2020). It is possible that Exo70B1 and the rest of the exocyst complex is recycled for endocytosis from the PM and subsequently contributes to autophagic degradation. NRC4 could indeed be guarding this pathway or transported by it. Additionally, Exo70A1 targets exocytosis towards the growing tip of pollen tubes for polar growth (Sekereš et al., 2017). This is an analogous system to haustoria, where the EHM is like an inverted pollen tube.

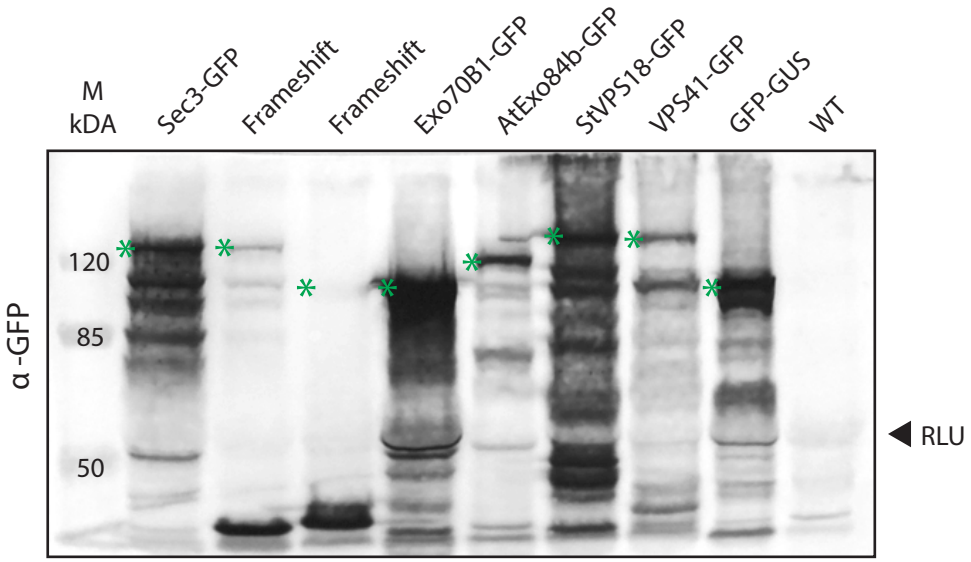


Figure 5.8: Western blotting of GFP fusion proteins confirms stable expression of most constructs.
WT plants were agro-expressed with constructs indicated and after 3 dpai proteins were crudely extracted, separated by SDS-PAGE (7.5% gel), and immunoblotted for GFP. Stars indicate expected band size. RLU indicates Rubisco Large Subunit stained by the colour detection reagent. NOTE: two proteins were incorectly cloned and therefore led to frameshifts. One of these, Exo70A1-GFP was subsequently re-cloned and predicted by sequencing to produce full length protein, however the western blot has not been performed to date. That clone was used for microscopy in Figure 5.7D.

5.3.5. HOPS/CORVET complexes involvement in NRC4-mediated resistance

In eukaryotes there are two hexameric complexes known to mediate endolysosomal tethering, known as CORVET and HOPS (Figure 5.9). These complexes share core components Vacuolar Protein Sorting (VPS) 11, 16, 18 and 33. CORVET has two unique components, VPS3 and VPS8; whereas HOPS contains VPS41 and VPS39 (Takemoto et al., 2018; van der Beek et al., 2019). In our GFP-NRC4 pull-down mass spectrometry data, we identified candidate associations with the core components VPS11/16/18, and HOPS-specific VPS41.

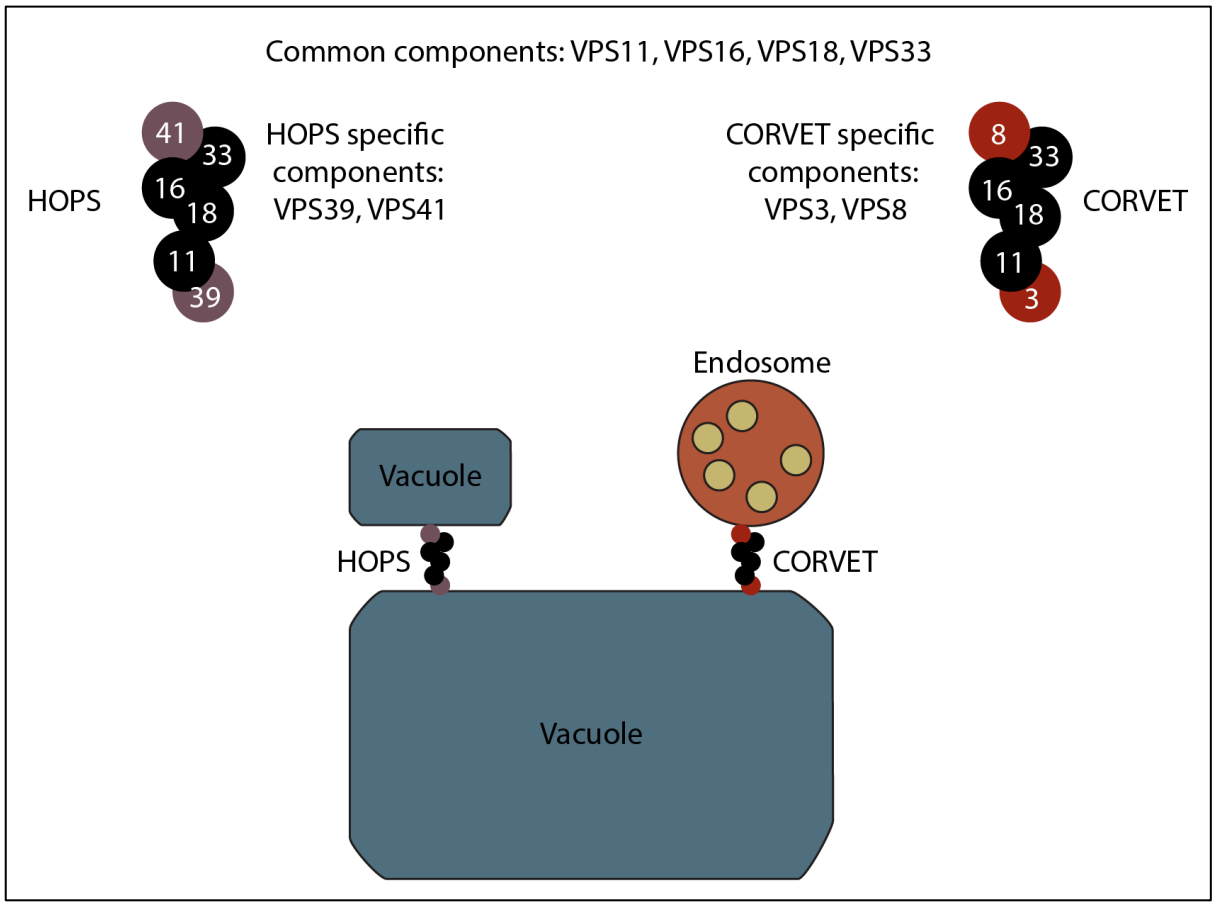


Figure 5.9: Diagram summarising what is known about HOPS and CORVET complexes.
HOPS and CORVET complexes share four components but have two distinct components each, with HOPS mediating Vacuole to Vacuole fusion and CORVET mediating Endosome to Vacuole fusion. VPS = Vacuolar Protein Sorting. Figure adapted from (Takemoto et al., 2018; van der Beek et al., 2019).

5.3.5.1. Systemic silencing of HOPS/CORVET components leads to dwarfing and plant death

To investigate the involvement of these components in NRC4-mediated immunity, we generated VIGS constructs for VPS16 and VPS18. Silencing either led to severe dwarfing of the plants and eventually death, indicating their importance in growth and development. Therefore, we could not complete the VIGS based screen of resistance to *P. infestans.*

5.3.5.2. Hairpin silencing of HOPS/CORVET components amplifies NRC4-mediated HR

To determine whether the HOPS/CORVET complexes were involved in NRC4-triggered HR, I generated hairpin silencing constructs to transiently silence VPS8,

VPS18 or VPS41 during co-expression with the autoactive variant of NRC4 - NRC4^{D478V}. I imaged cell death with a blue light transilluminator and quantified the intensity of HR in terms of the mean grey value per infiltration patch, a system I had previously developed (Dagvadorj et al., 2017). I found a higher intensity of cell death in patches with hpVPS8, hpVPS18 or hpVPS41 (Figure 5.10), indicating silencing of any of these components is sufficient to increase NRC4-mediated cell death. The correlation between hpVPS18 and hpVPS41 phenotypes is not surprising as silencing *VPS18* was successful in disrupting VPS41 association with endosomes in Drosophila, however I did not expect the same phenotype from hpVPS8 as its *overexpression* led to disruption of VPS41 endosomal association through out-competition (Lőrincz et al., 2019).

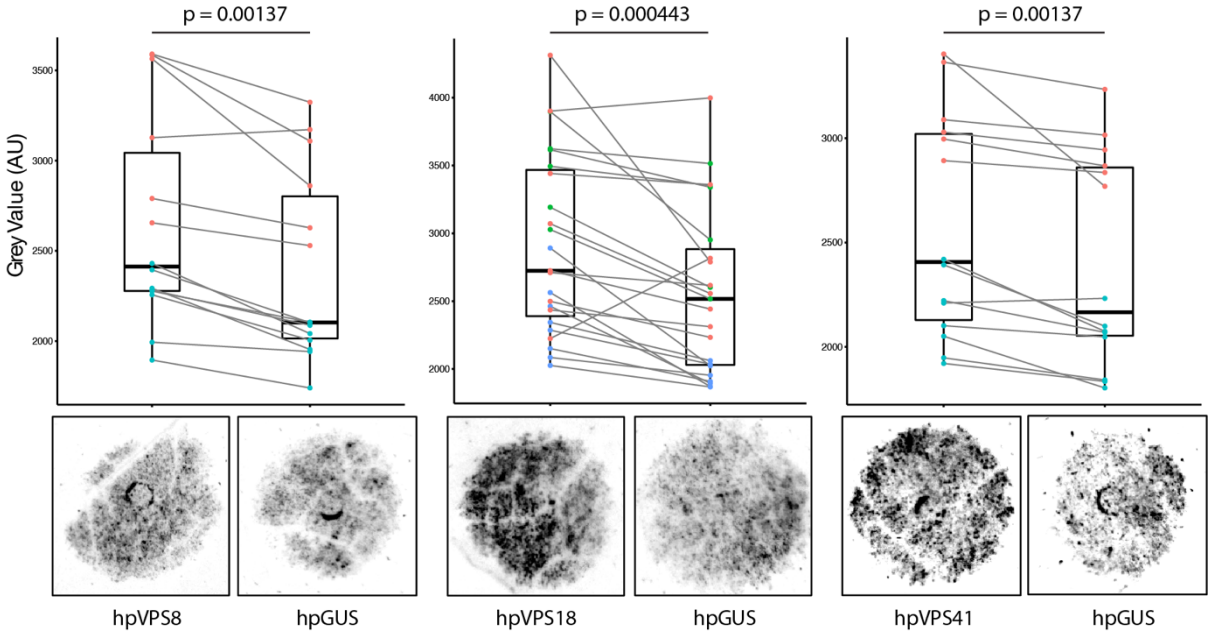


Figure 5.10: Hairpin RNAi of HOPS/CORVET components amplifies NRC4-mediated HR.
Scatter boxplots representing the intensity of HR imaged with blue light and quantified in terms of mean gray value by FIJI. NRC4^{D478V} was co-expressed with either hpVPS8, hpVPS18 or hpVPS41 opposite NRC4^{D478V} with hpGUS. The resulting HR from the autoactive NRC4 was imaged at 3-4 dpai. Paired wilcoxon tests were conducted with p = 0.00137, p = 0.000443 and p = 0.00137 respectively. Colours indicate independent replicates and dots represent the signal obtained from a sample of the infiltration patch.

An increase in cell death could be due to a general effect on programmed cell death, not specific to NRC4. Therefore, we repeated the experiment with a non-NRC dependent 'singleton' CNL, R3a. Expression of hpVPS8, hpVPS18 or hpVPS41 did

not show a visible difference in R3a-triggered HR, but when quantified a mild increase was found with hpVPS41 (Figure 5.11). However, with just one experiment conducted, we did not detect a statistically significant difference. More repeats are required to make it clear whether HOPS/CORVET are acting on non-NRC NLRs. In fact, there was a trend towards increased HR in all patches bar one for VPS8 silencing. If this trend is consistent between replicates, that experiment may reach statistical significance.

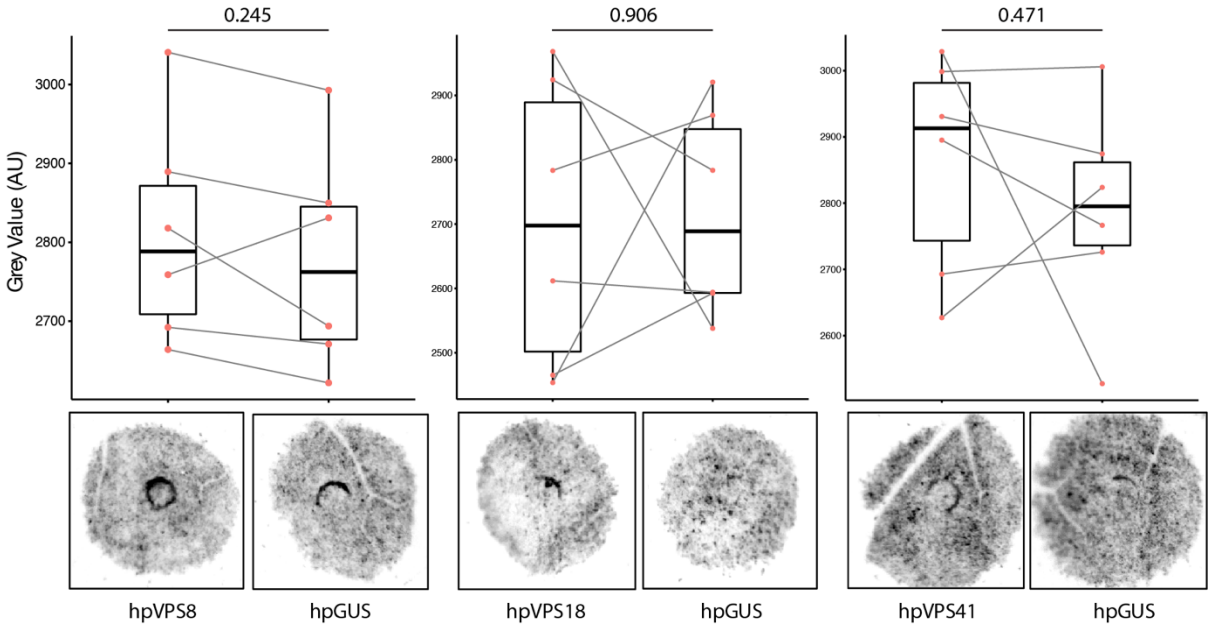


Figure 5.11: Hairpin RNAi of HOPS/CORVET components does not seem to alter R3a-mediated HR.
Scatter boxplots representing the intensity of HR imaged with blue light and quantified in terms of mean gray value by FIJI. R3a & AVR3a were co-expressed with either hpVPS8, hpVPS18 or hpVPS41 opposite R3a & AVR3a with hpGUS. The resulting HR from the R3a was imaged at 3 dpai. Paired t-tests tests were conducted with p = 0.245 , p = 0.906 and p = 0.471 respectively. Only one independent replicate was conducted. Dots represent the signal obtained from a sample of the infiltration patch.

If HOPS/CORVET pathways are regulating HR of NRC4, it is unlikely that this pathway would evolve to control the HR levels of just one NLR. Therefore, we tested whether the paralogue NRC3 was affected by expression of the silencing construct targeting the HOPS/CORVET core component, hpVPS18 (Figure 5.12). There was a large increase in the HR generated by the autoactive mutant NRC3^{D480V}, however there was insufficient data points to conduct a meaningful test. Therefore, as with the previous experiments more repeats are required for sufficient statistical power. The trend indicates that the HOPS/CORVET pathway negatively regulates NRCs.

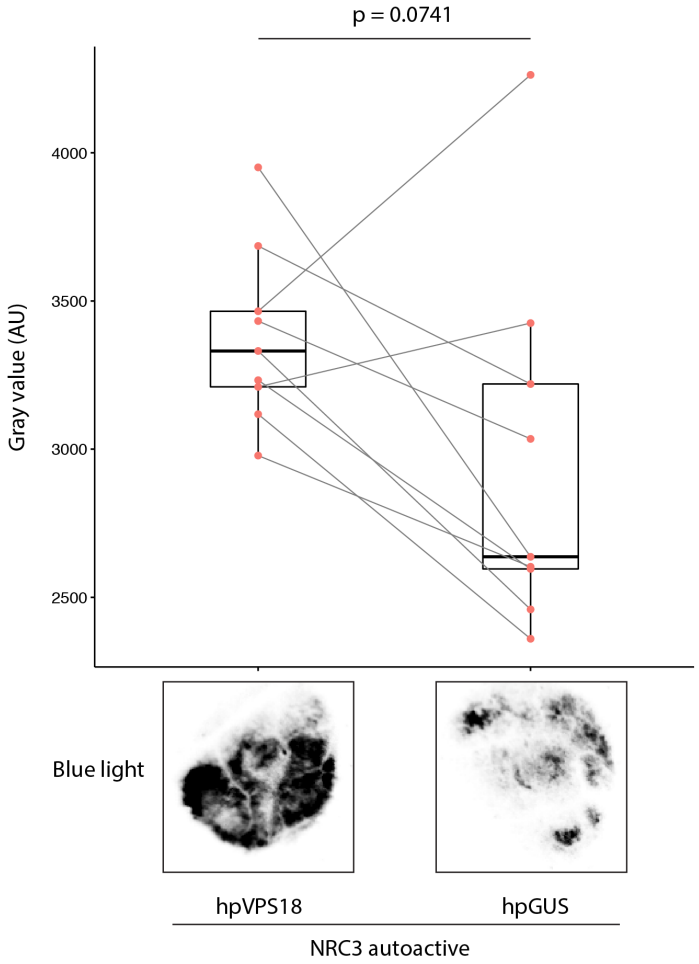


Figure 5.12: Hairpin RNAi of HOPS/CORVET core component VPS18 seems to amplify NRC3-mediated HR, but there is insufficient statistical power present to be conclusive.
Scatter boxplots representing the intensity of HR imaged with blue light and quantified in terms of mean gray value by FIJI. NRC3^{DV} was co-expressed with either hpVPS18 opposite NRC3^{DV} with hpGUS. The resulting HR from the autoactive NRC3 was imaged at 3 dpai. Paired t-test was conducted with p = 0.0741. Only one independent replicate was conducted. Dots represent the signal obtained from a sample of the infiltration patch.

5.3.5.3. *CoIP confirms association of NRC4 with HOPS complex*

To dissect the relationship between NRC4 and the HOPS complex, I set out to validate the associations found in the CoIP/MS screen. I failed to achieve PCR products when amplifying *Nicotiana benthamiana VPS18* from cDNA. Therefore I cloned and expressed StVPS18-GFP and VPS41-GFP and used them for CoIP experiments with NRC4. In both experiments the positive control NRC4-GFP pulled down NRC4-3xHA. VPS18-GFP and VPS41-GFP pulled down NRC4-3xHA (Figure 5.13 and Figure 5.14), but the negative control EV:GFP did not. In the Co-IP experiment with VPS41-GFP, an unusual high molecular weight signal of VPS41-GFP, NRC4-GFP and NRC4-3xHA was seen in the immunoprecipitates (Figure 5.14).

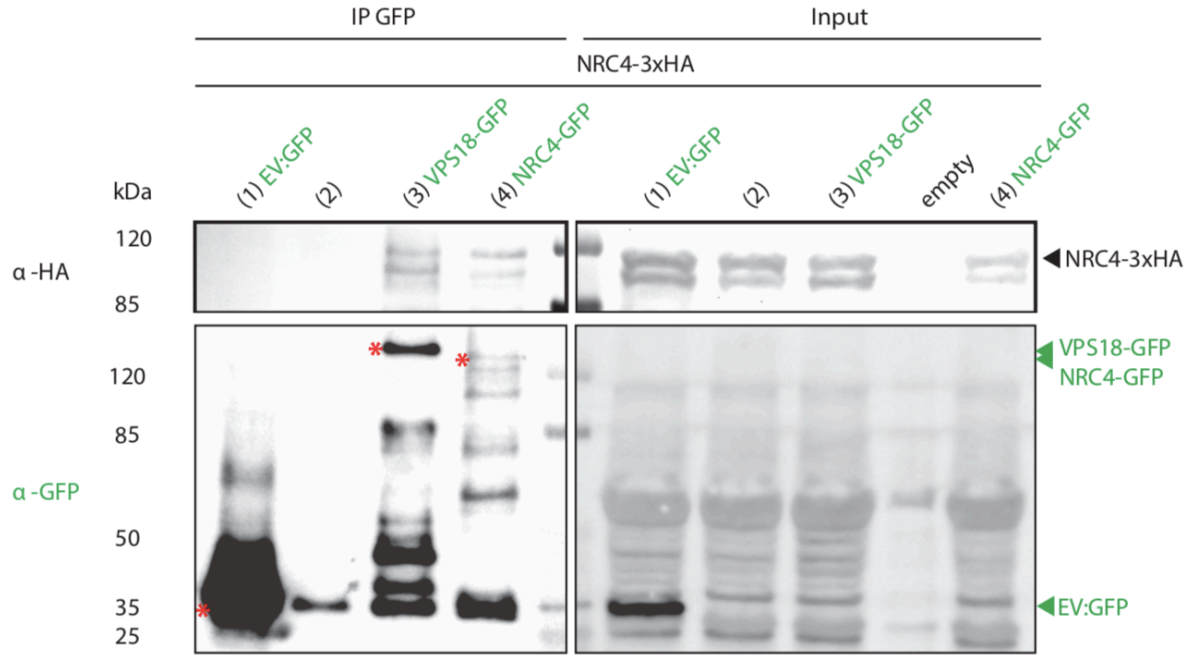


Figure 5.13: NRC4 co-immunoprecipitates with StVPS18-GFP.
NRC4-3xHA co-immunoprecipitated with StVPS18-GFP or NRC4-GFP, but not EV-GFP. *In planta* co-immunoprecipitation or proteins extracted 3 dpai. NRC4-3xHA was transiently co-expressed with either EV-GFP, StVPS18-GFP or NRC4-GFP. IPs were obtained with GFP-trap agarose beads, and GFP and HA was immunoblotted along with total protein extracts (input). Asterisks indicate expected band sizes for proteins in that sample.

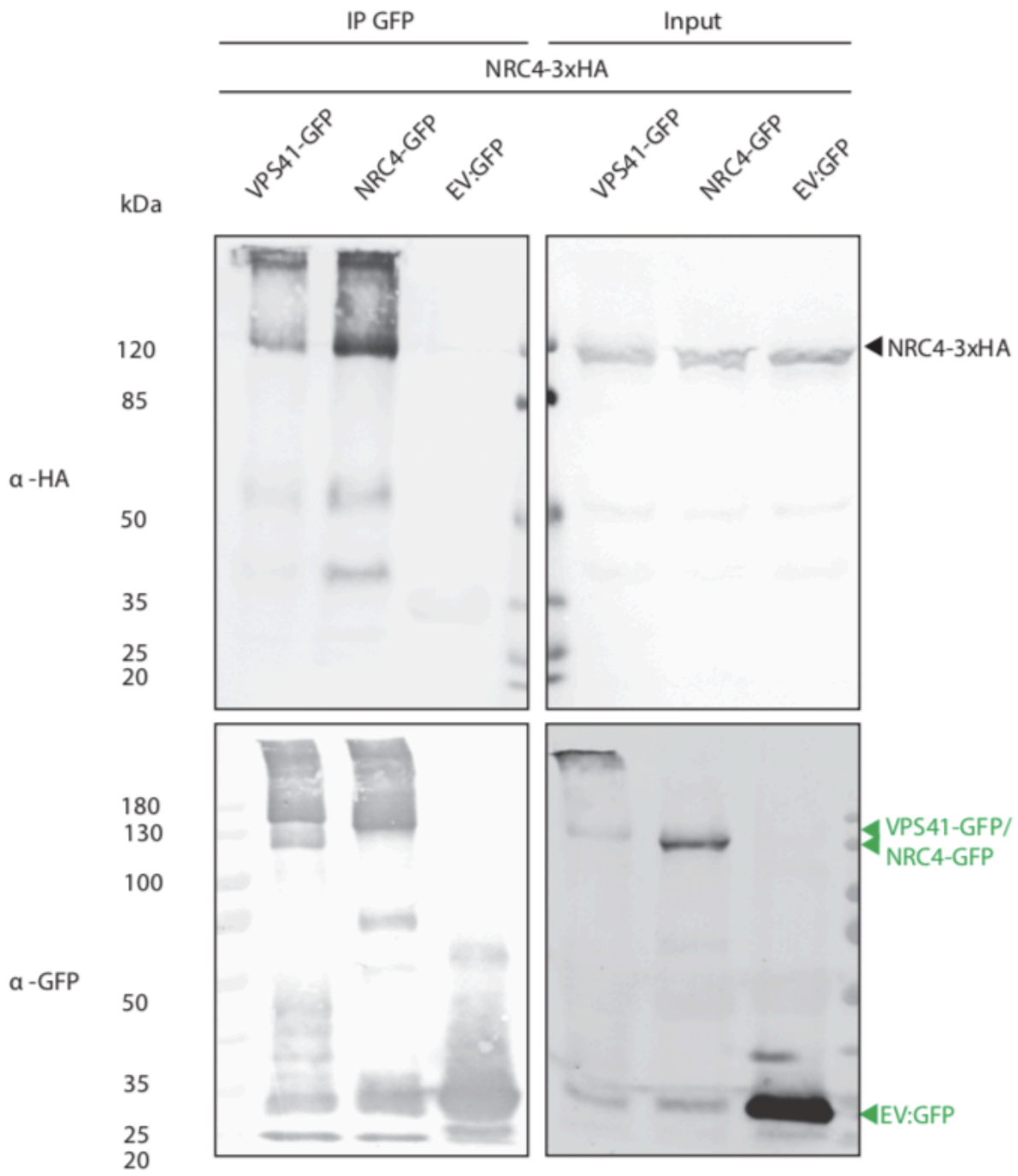


Figure 5.14: NRC4 co-immunoprecipitates with VPS41-GFP.
NRC4-3xHA co-immunoprecipitated with VPS41-GFP or NRC4-GFP, but not EV-GFP. *In planta* co-immunoprecipitation or proteins extracted 3 dpai. NRC4-3xHA was transiently co-expressed with either EV-GFP, VPS41-GFP or NRC4-GFP. IPs were obtained with GFP-trap agarose beads, and GFP and HA was immunoblotted along with total protein extracts (input). Asterisks indicate expected band sizes for proteins in that sample.

5.3.5.4. The HOPS complex is diverted towards haustoria

In order to gain functional insight into association of HOPS with NRC4, I decided to image HOPS components during infection with *P. infestans.* Interestingly, StVPS18-GFP or VPS41-GFP often produced signals focally accumulating around the haustorial interface (Figure 5.15 and Figure 5.16C-D). Some of this fluorescence overlapped with NRC4 across the EHM, however VPS41/18-GFP signals substantially occurred adjacent to the EHM. This may represent vacuole fusion sites with the EHM. HOPS labelling near and at the EHM may be a secretion strategy from the plants, or one hi-jacked by the pathogen. Indeed NRC4 may be guarding this pathway. It could also be a novel mechanism for the endocytosis of pathogen molecules. Interestingly, VPS41-GFP localised to large vesicle like structures that could be small vacuoles (Figure 5.16A-B). This is consistent with its reported role of enabling vacuole to vacuole fusion (Takemoto et al., 2018). Indeed, the signal at these sites was only found where two structures touched and not seen where it bordered the cytoplasm (NRC4-mKOk labelled regions). Some smaller puncta co-localised with NRC4 (Figure 5.16B arrowhead).

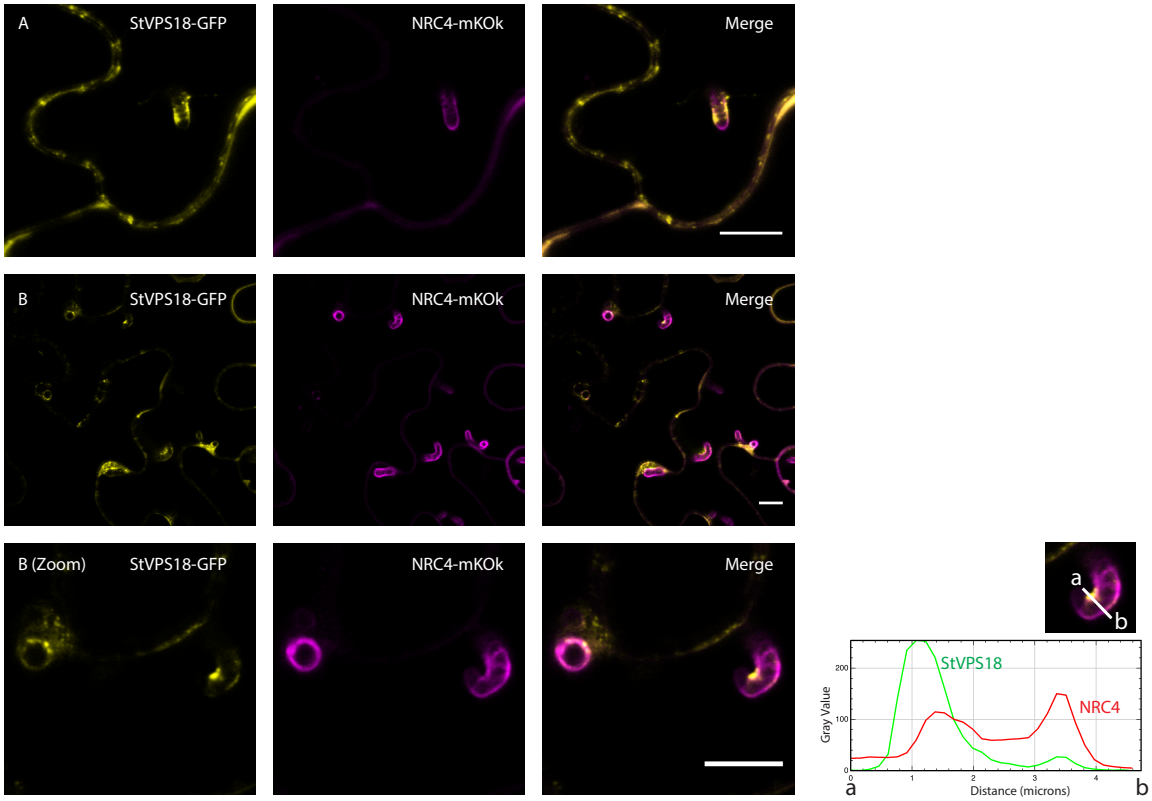


Figure 5.15: HOPS/CORVET core component StVPS18 is deployed to the haustorial interface.
StVPS18-GFP was co-expressed with NRC4-mKOk in WT *N. benthamiana* leaves. After 3 hours the leaves were infected with *P. infestans.* Images were taken using SP5 confocal microscope after 3 days. Single plane images and line profile (right) shows that StVPS18 is focally deployed close to the EHM labelled by NRC4. Scale bars are 10 µm.

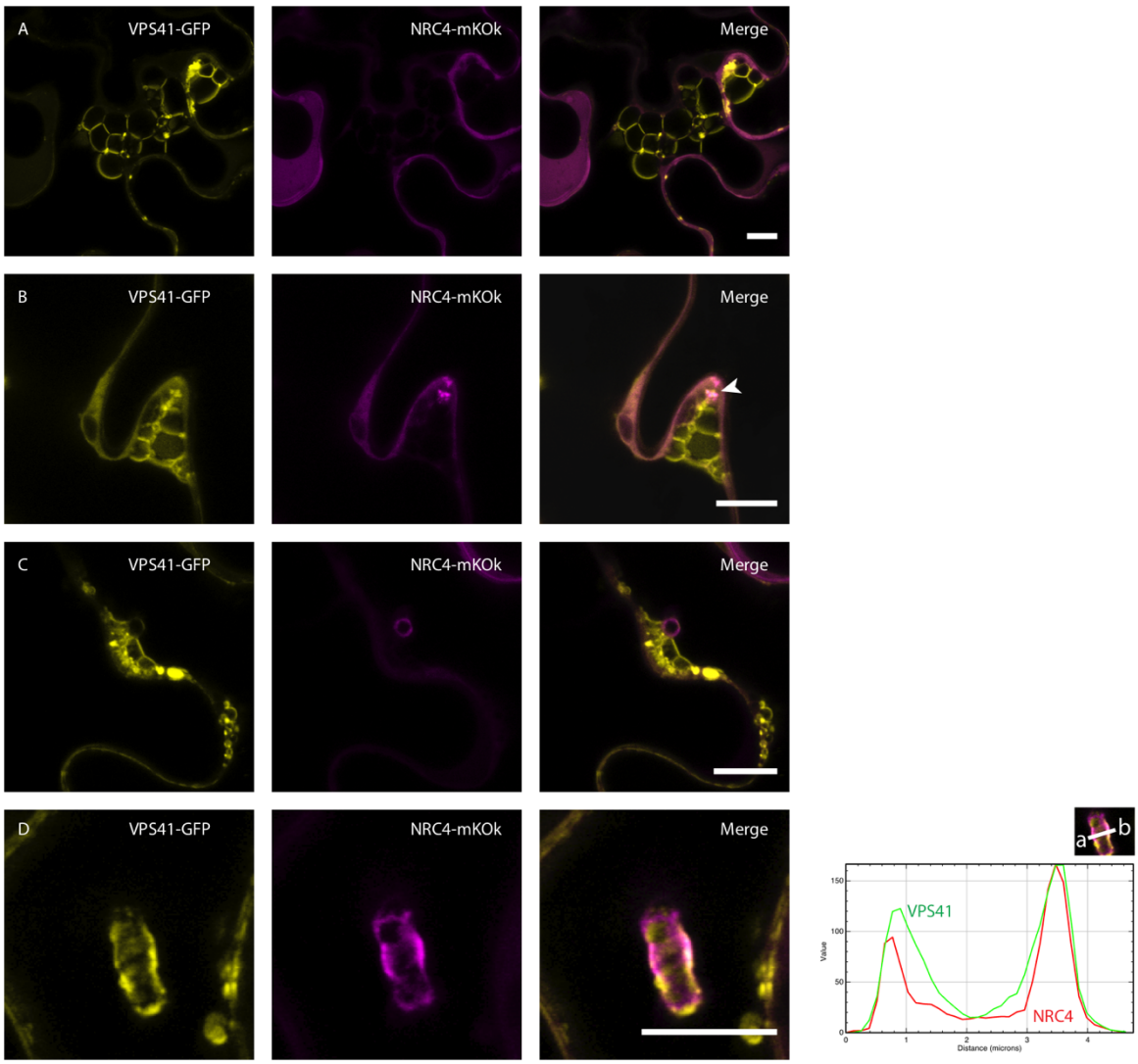


Figure 5.16: HOPS specific component VPS41 is deployed to the haustorial interface.
VPS41-GFP was co-expressed with NRC4-mKOk expressed in WT *N. benthamiana* leaves. After 3 hours the leaves were infected with *P. infestans.* Images were taken using SP5 confocal microscope after 3 days. Single plane images showing VPS41 labels vacuole-like structures and occasionally co-localises with NRC4 (arrowhead). (C-D) Single plane images and line profile (right) shows that VPS41 is focally deployed close to the EHM labelled by NRC4. Scale bars are 10 µm.

5.3.5.5. Hairpin silencing HOPS/CORVET components does not seem to alter NRC4 protein levels

I then set out to determine whether hpVPS18 expression leads to increased NRC4 protein levels which could account for the increased HR. Initially, I transiently co-expressed either NRC4-GFP or EV-GFP with either hpVPS8, hpVPS18, hpVPS41 opposite the hpGUS control (Figure 5.17). This showed no obvious difference between silenced and control samples in NRC4-GFP or EV-GFP expressing tissue. To validate these results, I then used transgenic *35S::NRC4-GFP* lines, and expressed hpVPS18 or hpGUS on either sides of a leaf. I co-expressed Luciferase-3xHA as a marker to determine whether *Agrobacterium* virulence was altered by hpVPS18 expression. It appeared from the first experiment as if NRC4-GFP levels were stabilised in hpVPS18 silencing tissue (Figure 5.18, left). However, the staining of GFP was slightly patchy, raising concerns over the validity of these results. Additionally, there seemed to be more loading in the hpVPS18 sample. We then repeated this experiment (Figure 5.18, right panel), and saw no effect on NRC4-GFP signal or Luciferase-3xHA control. From these experiments, I conclude that there is no effect on NRC4 stability caused by silencing HOPS/CORVET components. However, it would be ideal to conduct western blotting alongside an HR experiment to demonstrate that even when an increase in HR is detected, there is no difference in protein levels.

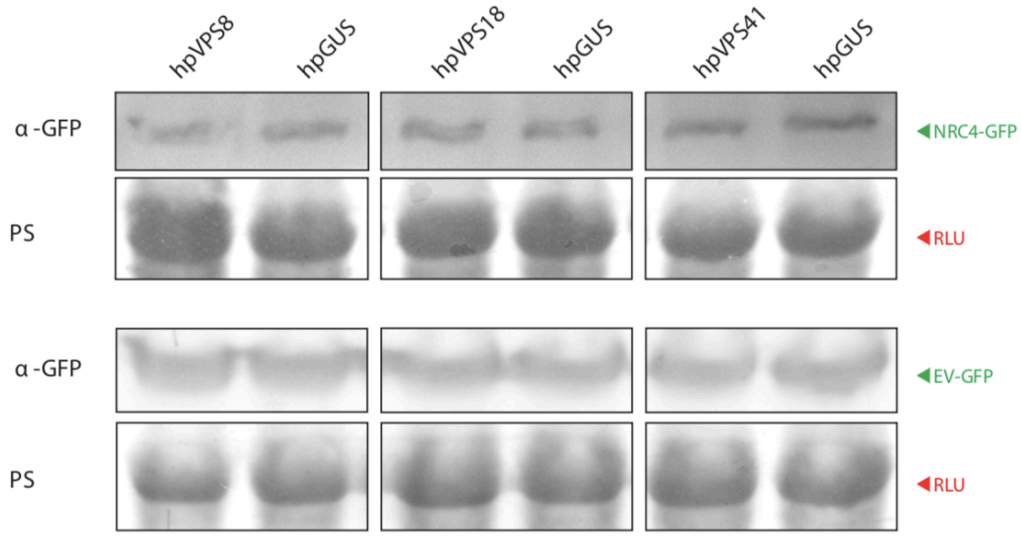


Figure 5.17: Western blotting shows no effect on NRC4 protein levels upon HOPS/CORVET component silencing.
NRC4-GFP or EV-GFP were transiently expressed and co-expressed with either hpVPS8, hpVPS18 or hpVPS41 opposite hpGUS control and after 3 dpai proteins were crudely extracted, separated by SDS-PAGE (7.5% gel for NRC4, 12% gel for EV-GFP), and immunoblotted for GFP. To assess the relative loading of proteins, the rubisco large subunit was stained with Ponceau (PS).

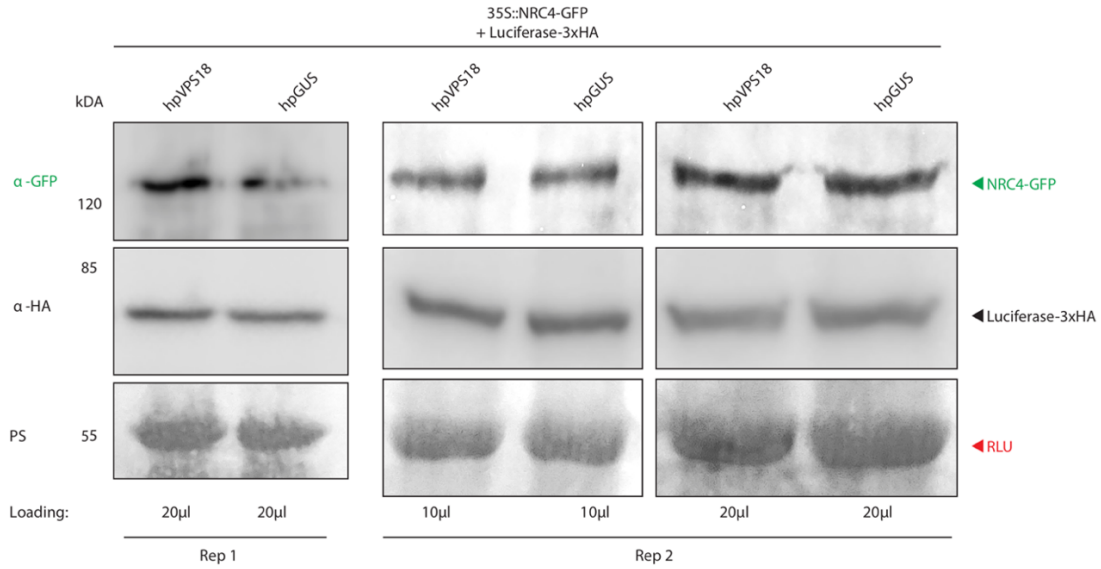


Figure 5.18: Western blotting inconclusive in determining whether hpVPS18 alters NRC4 stability.
NRC4-GFP or Luciferase-3xHA was not affected by VPS18 silencing. Transgenic 35S::NRC4-GFP plants were silenced for either VPS18 or GUS with hairpin RNAi, and after 3 dpai proteins were crudely extracted, separated by SDS-PAGE (7.5% gel), and immunoblotted for GFP. To assess the relative loading of proteins, the rubisco large subunit was stained with Ponceau (PS). Two independent experiments were conducted and in the second experiment two volumes were loaded to reduce the chances of saturation, these were either 10 µl & 20 µl. Luciferase-3xHA was included as an internal agro-expression control.

5.3.6. RabE1 involvement in NRC4-mediated resistance

Rab GTPases are molecular switches that mediate trafficking from donor membranes to recipient membranes via vesicular trafficking (Minamino and Ueda, 2019). The HOPS and CORVET complexes associate with Rab GTPases Rab 7 and Rab5 respectively. We detected Rab5A/RabF2a/Rha1 but did not detect Rab 7 members in the MS analysis. However, lack of detection is not proof of lack of interaction. Rab5A has not been investigated in this project to date. We also detected several others including RabE family members Rab8a/RabE1c, RabE1b and RabE1a; as well as RabD family members Rab1A/RabD2b and Rab1B/RabD2a/Ara-5; Rab2a/RabB1c and Rab11b/RabA1f (Vernoud et al., 2003). RabE1a came with the most peptide hits in uninfected and infected tissue. Therefore I selected it for further study.

5.3.6.1. RabE1 silencing increases HR

To investigate the involvement of RabE1 in NRC4 mediated immunity I generated a hairpin RNAi construct targeting RabE1a's 3'UTR (hpRabE1). Expression of hpRabE1 increased the intensity of the HR generated by AVRblb2/Rpi-blb2 compared with hpGUS expression (Figure 5.19). Conversely *RabE1* silencing didn't result in a measurable effect on HR generated by non-NRC dependent NLR R3a and its cognate effector $AVR3a^{KI}$ (Figure 5.19). However, with p = 0.0583, it is quite possible that this experiment will reach statistical significance when a third or fourth replicate is conducted, as required. Repetition of this experiment with an autoactive mutant of NRC4 ($NRC4^{D478V}$) also resulted in an increase in HR during hpRabE1 expression, however the increase was also seen for an autoactive non-NRC dependent NLR I2 ($I2^{N330Y}$) (Figure 5.20). The HR amplification could be explained by a direct effect on NRC4 or downstream signalling components, as this effect was seen with autoactive NRC4. It's also plausible that RabE1 controls the HR of a number of NLRs, but not all.

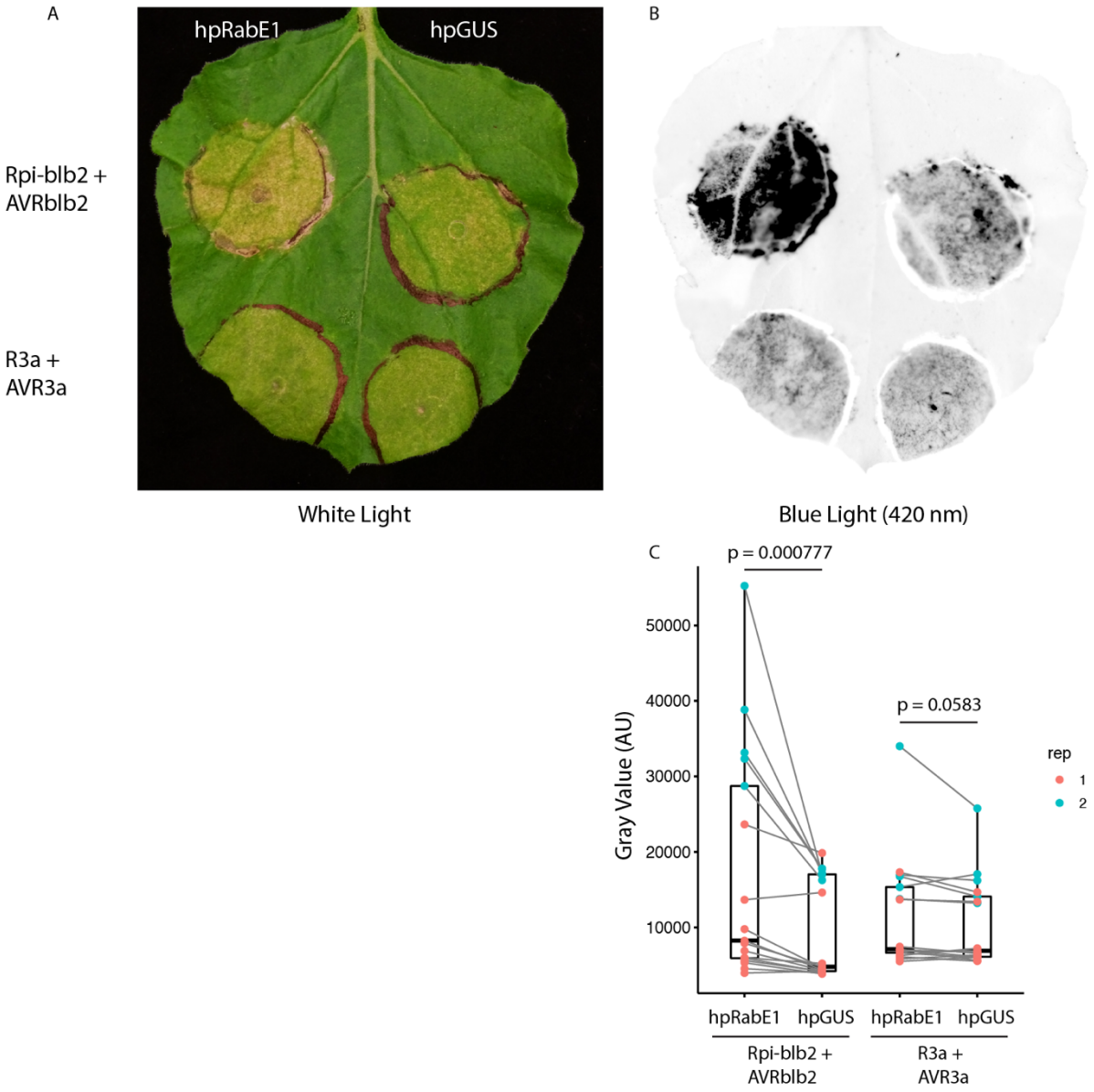


Figure 5.19: Hairpin RNAi of RabE1 amplifes NRC4-mediated HR but not R3a HR. Rpi-blb2 & AVRblb2 were co-expressed with either hpRabE1 or hpGUS and R3a & AVR3a were co-expressed with either hpRabE1 or hpGUS. The resulting HR from the NLRs was imaged at 6 dpai with (A) white light and (B) blue light which was quantified and plotted on a scatterboxplot (C). Paired wilcoxon tests were conducted with p = 0.000777 for Rpi-blb2 HR and p = 0.0583 for R3a HR. Colours indicate independent replicates and dots represent the signal obtained from a sample of the infiltration patch.

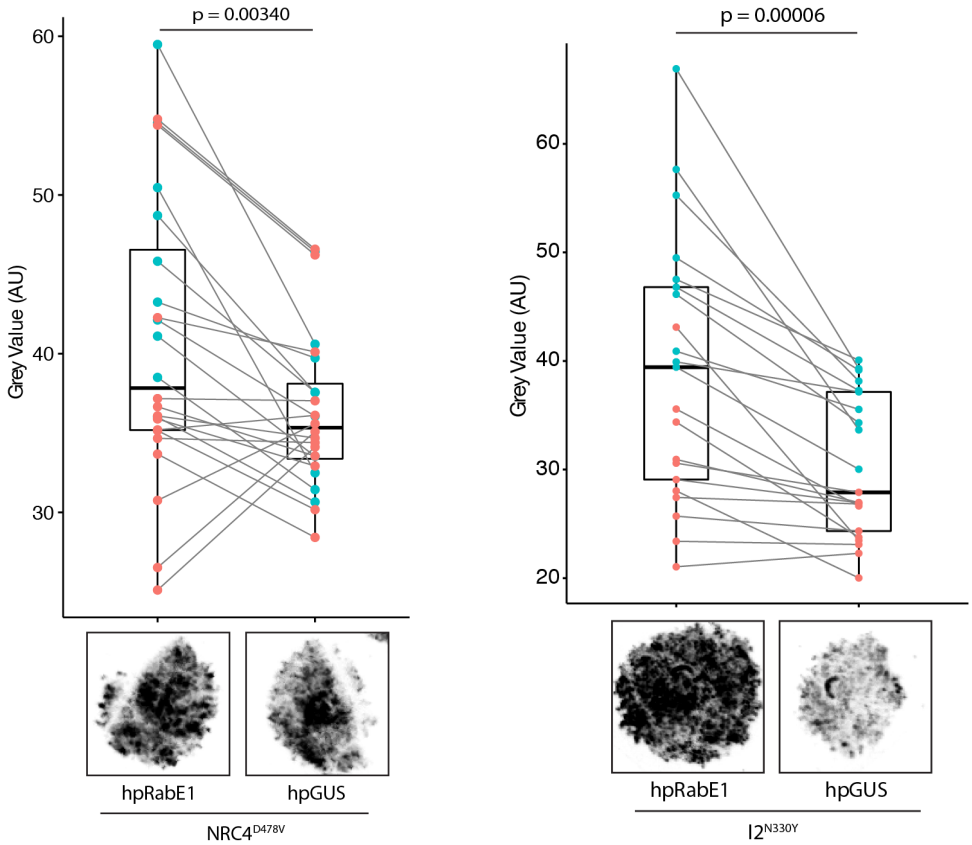


Figure 5.20: hpRabE1 increases the intensity of NRC4 or I2 mediated HRs. Scatter boxplots representing the intensity of HR imaged with blue light and quantified in terms of mean gray value by FIJI (A) NRC4 autoactive triggered HR is not purturbed by RabE1 silencing. $NRC4^{D478V}$ was co-expressed with either hpRabE1 or hpGUS. (B) I2 autoactive triggered HR is not purturbed by RabE1 silencing. $I2^{N330Y}$ was co-expressed with either hpRabE1 or hpGUS. The resulting HR from the autoactive NLRs was imaged at 3 dpai. Paired t-tests were conducted with p = 0.00340 for NRC4 HR and p = 0.0000600 for I2 HR. Colours indicate independent replicates and dots represent the signal obtained from a sample of the infiltration patch.

5.3.6.2. hpRabE1 efficiently silences RabE1, but does not affect NRC4 or Rab8a member mRNA levels

Because of the strong effect on NRC4 HR, I went on to validate the silencing of *RabE1* by RT-PCR. It efficiently silenced *RabE1a*, but did not alter the mRNA levels of NRC4 (Figure 5.21 left). The hairpin construct targets the 3'UTR of RabE1a, but considering there are other Rab8 members with similar sequences, I decided to verify whether the hairpin construct was also silencing Rab8a members, and it was not (Figure 5.21 right & Methods Figure 2.5). Ideally, the gold standard of qRT-PCR would be employed to quantify the degree to which the genes are being silenced.

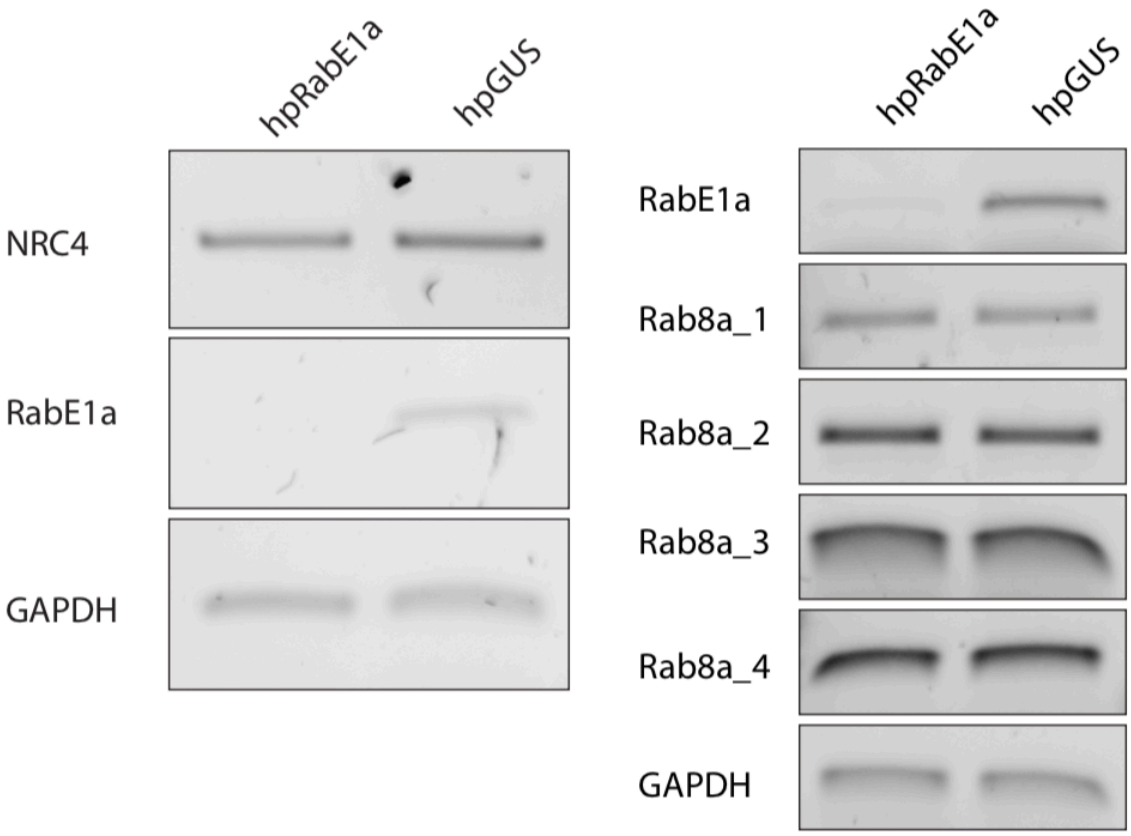


Figure 5.21: Semiquantitative RT-PCR confims silencing by hpRabE1 of RabE1 specifically.
Construct carrying hairpin plasmids (pRNAi-GG) targeting RabE1a or GUS reporter gene were infiltrated to *N. benthamiana* and the expression of targeted genes was assessed by RT-PCR at three days post silencing. RT-PCR verified efficient gene silencing of but did not affect levels of NRC4 (left) or Rab8a members which are closely related. Glyceraldehyde 3-phosphate dehydrogenase (GAPDH) was used as internal control for cDNA loading in the PCR. cDNA was synthesized using total RNA. See methods for further details.

5.3.6.3. RabE1 silencing increases agro-expression

To test whether the increase in HR is caused by enhanced NRC4 protein levels, I compared the protein levels of NRC4 in *35S::NRC4-GFP* transgenics by western blotting in hpRabE1- vs hpGUS-expressing tissue. After six independent experiments I found no clear difference. One experiment contained an agro-expressed marker, Luciferase-3xHA, which showed a strong increase in the hpRabE1 expressing sample compared with the hpGUS control (Figure 5.22). Therefore, it is likely the increase in NRC4-mediated HR is due to increased *Agrobacterium* mediated expression upon RabE1 silencing. This is consistent with our finding that an HR triggered by an independent NLR, $I2^{N330W}$ was also amplified. How this conclusion is compatible with the observation that R3a-HR was unaffected, is unclear, but it's plausible that silencing RabE1 suppressed R3a HR and this effect is negated by the increase in agro-expression of the R3a due to hpRabE1. Additionally, as previously mentioned, when the necessary extra replicates of experiments are conducted, the R3a and I2 data may correlate.

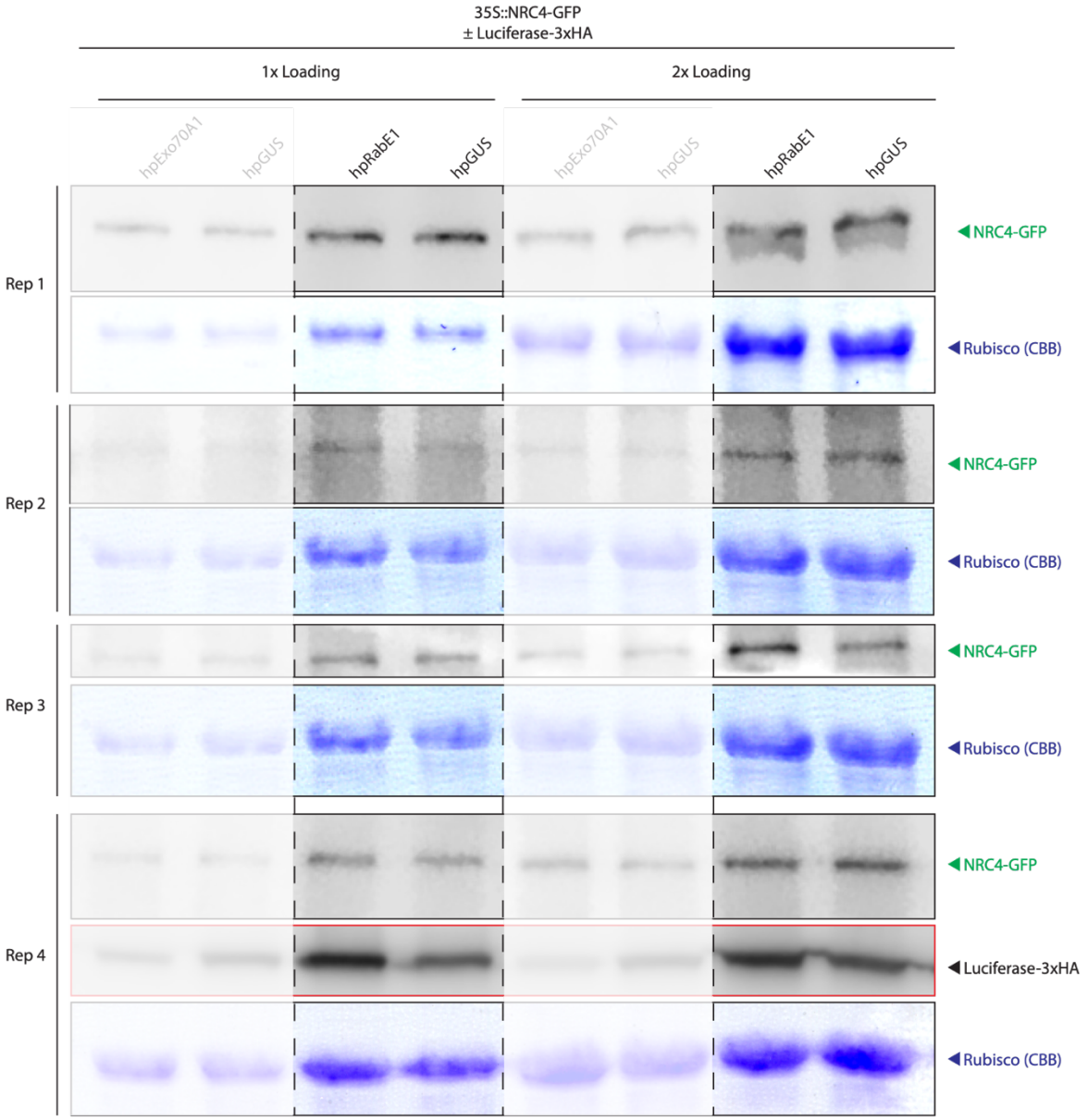


Figure 5.22: Western blotting shows no effect on NRC4 protein levels upon RabE1 silencing, but probable increase in *Agrobacterium* virulence.
NRC4 protein levels are not perturbed by *RabE1* silencing, but *Agrobacterium* mediated gene expression appears to be increased by RabE1 silencing. Transgenic *35S::NRC4-GFP* plants were silenced for either RabE1 or GUS with hairpin RNAi, and after 3 dpai proteins were crudely extracted, separated by SDS-PAGE (7.5% gel), and immunoblotted for GFP. To assess the relative loading of proteins, the remaining rubisco large subunit after transfer to membrane was detected with Coomassie Brilliant Blue (CBB) staining. Two separate volumes were loaded to reduce the chances of saturation, these were either 10 µl & 20 µl or 5 µl & 10 µl. Four independent experimental replicates (different batch of plants, *Agrobacterium,* SDS-PAGE gels etc.) were conducted, with the final experiment including co-expression of Luciferase-3xHA as an internal agro-expression control. NOTE: a separate but related experiment involving the silencing of Exo70A1 was included, but is faded out here as it is discussed in Figure 5.6.

5.3.7. RabD2a involvement in NRC4-mediated resistance

5.3.7.1. Dominant-negative RabD2a suppresses NRC mediated HR

Rab GTPases cycle between GDP-bound typically cytosolic and inactive forms, and GTP-bound typically active forms associated with specific membranes which ensures vesicle targeting specificity. Mutating Asparagine to Isoleucine in the conserved GTP-binding motif GNKxD typically reduces the affinity of RAS or Rab-like GTPases for nucleotide binding, thereby usually rendering them dominant-negative when overexpressed (Zheng et al., 2005). To investigate the involvement of RabD2a in NRC4-mediated immunity, I utilised an existing StRabD2a^{N128I} mutant (DN-RabD2a), presumed to be dominant-negative. Expression of DN-RabD2a suppressed the intensity of the HR generated by autoactive NRC4 compared with EV expression (Figure 5.23). I scored the HR with a HR index due to the risk of the fluorescent tags of the treatment/control being detected by a blue light illuminator. From three independent experiments the difference was clear and statistically highly unlikely to be due to chance. I found a similar trend in HR triggered by the autoactive mutant of the homologue NRC3 (Figure 5.24), indicating the effect was not specific to NRC4.

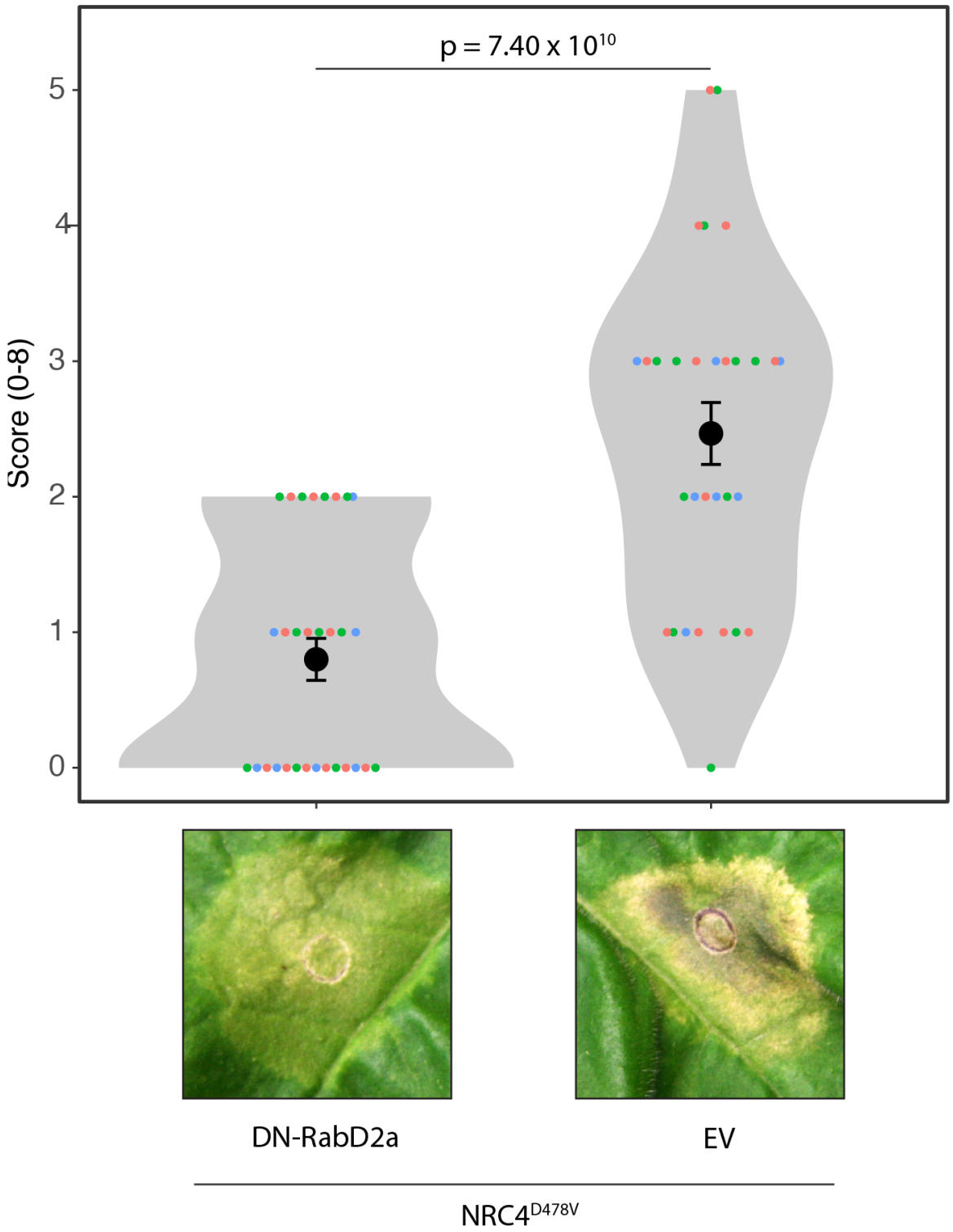


Figure 5.23: Expression of Dominant Negative RabD2a mutant suppresses NRC4-mediated HR.
$NRC4^{D478V}$ was co-expressed with either StRabD2aN128I or EV (GFP or RFP depending on the tag on RabD2a). The resulting HR from the NLRs was imaged at 3-4 dpai with white light quantified by scoring using a HR index, and plotted on a scatter violinplot. Unpaired wilcoxon test was conducted with $p = 7.40 \times 10^{-10}$. Colours indicate each of the three independent replicates and dots represent the score obtained of one infiltration patch.

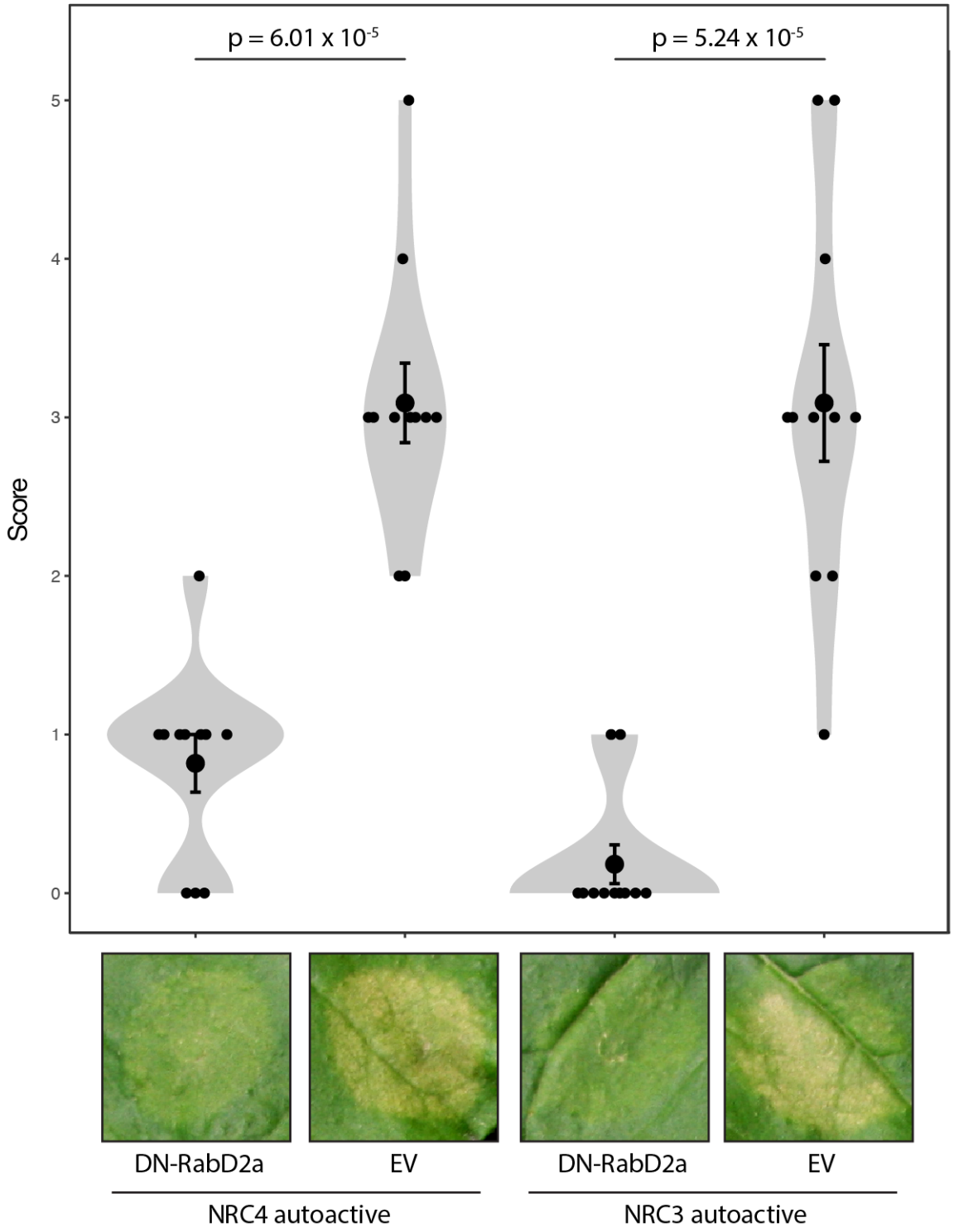


Figure 5.24: Expression of Dominant Negative RabD2a mutant suppresses NRC4 or NRC3 mediated HR.
NRC4 autoactive or NRC3 autoactive were co-expressed with either StRabD2a^{N128I} or EV (GFP or RFP depending on the tag on RabD2a). The resulting HR from the NLRs was imaged at 4 dpai with white light quantified by scoring using a HR index, and plotted on a scatter violinplot. Unpaired wilcoxon tests were conducted with $p = 6.01 \times 10^{-5}$ or $p = 5.24 \times 10^{-5}$ respectively. Only one experiment was conducted. Dots represent the score obtained of one infiltration patch.

5.3.7.2. Western blot analysis shows that DN-RabD2a expression suppresses Agrobacterium-mediated gene expression

To determine whether DN-RabD2a expression resulted in suppression of NRC4 HR due to destabilisation of NRC4, I carried out a western blot on tissue that co-expressed NRC4 with DN-RabD2a or RFP-GUS control. I found a great reduction in NRC4 when co-expressing DN-RabD2a. However, this effect was also seen on EV:GFP internal control which was also *agro*-expressed. Therefore, the effect on HR was probably due to a decrease in *agro*-expression of NRC autoactive constructs and not an effect on the protein stability or cell death itself. The difference was particularly clear as I performed a serial dilution of protein extracts (100%, 75%, 50%, 25%), which aimed to prevent saturation of western blot protein bands.

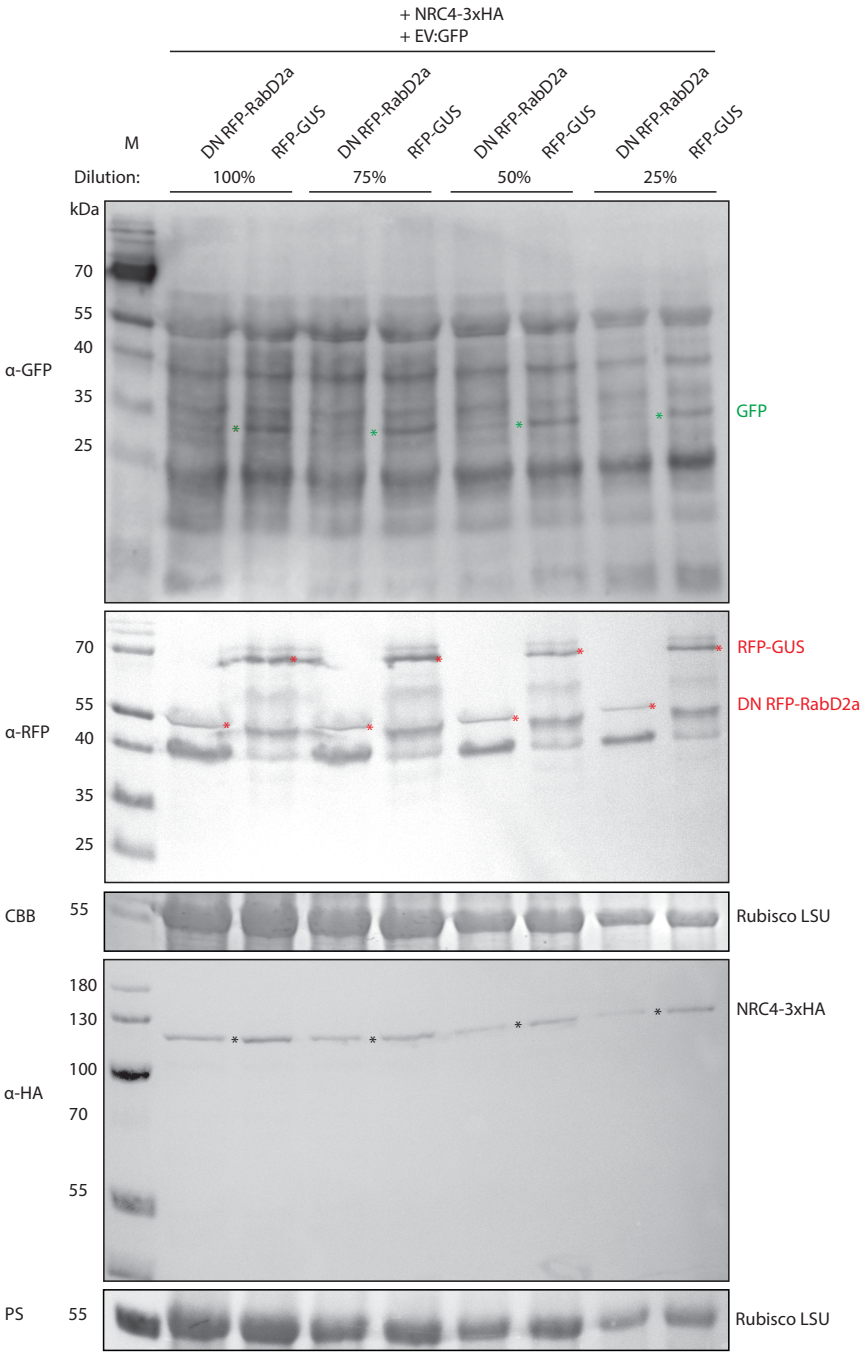


Figure 5.25: Western blotting shows RabD2a suppresses *Agrobacterium* mediated gene expression.
NRC4-3xHA and EV-GFP expression is suppressed by DN-RabD2a expression compared to GUS expression. NRC4-3xHA was co-expressed with EV-GFP and either RFP-StRabD2a^{N128I} (DN RFP-RabD2a) or RFP-GUS, and after 3 dpai proteins were crudely extracted, separated by SDS-PAGE (7.5% gel for HA and 12% for GFP and RFP detections), and immunoblotted for GFP, RFP or HA. To assess the relative loading of proteins, the rubisco large subunit (LSU) was stained with Ponceau (PS) and Coomassie Brilliant Blue (CBB) of leftover proteins after transfer of gel to membrane. Protein extracts were diluted with 1X Laemelli buffer to 75%, 50% and 25% and loaded as with the same volume (20 µl) to reduce chances of saturation. Stars indicate the expected band size.

5.4. Conclusions

The results from FRAP assays indicate NRC4 undergoes a regulated, dynamic process of accumulation at the EHM. This could be mediated by a transport pathway, or could in fact be due to NRC4 diffusion through the cytoplasm and a dynamic process that enables association with the EHM. The innate ability of NLRs to oligomerise suggests a provocative hypothesis that NRC4's accumulation at the EHM is the result of higher order oligomerisation. However, our understanding of NLRs is that they oligomerise upon activation to elicit HR (Cesari, 2017). It is unclear whether NRC4 dimerises or oligomerises before activation. Images in this thesis provide strong evidence that NRC4 tightly associates with the EHM. These observations prompt the question whether NRC4 is embedded in the EHM? This is possible, however NRC4 lacks a predicted transmembrane domain or membrane anchor (Chapter 4, Figure 1). Considering this and the membrane association detected in Chapter 3 (Figure 3), it is likely NRC4 associates with components of the EHM, and this association could be a regulated, dynamic process.

A possible transport pathway will be discussed further in the next chapter. Briefly, the atypical resistance protein RPW8.2 transits to the EHM via a vesicle-mediated secretory pathway (Kim et al., 2014). NRC4 was not detected in RPW8.2-positive vesicles (Figure 3.6). Therefore if NRC4 transits to the EHM via a secretory pathway, it is through a distinct pathway. To identify this putative pathway I included many vesicle transport regulators in our screen in this Chapter, which were detected in the mass spectrometry analysis. The screen was too time-consuming and costly to carry out with confocal microscopy of NRC4 EHM localisation as the readout. Additionally, silencing one component of this pathway may only lead to a small decrease in localisation, if any at all. During the bioinformatic analysis of the targets I chose for the screen, I identified a large amount of potential redundancy in these components. I aimed to silence as many of redundant targets as possible with one construct whilst designing the RNAi tools. However, it is distinctly possible we did not overcome this redundancy. This was one reason why I elected to focus our efforts on phenotypes in the screen and not validate silencing efficiencies for most of the constructs. However, lack of efficient silencing could have led to false-negative results. Therefore the negative results presented here should not be seen as indicating these components

are not involved in NRC4-mediated immunity. These results should be repeated alongside qRT-PCR to demonstrate efficient gene silencing. In the future, the use of chemical treatments to block secretory pathways should be used to determine the involvement in these pathways in NRC4-mediated resistance and EHM targeting. More is discussed in the final chapter.

The HR assays I conducted were a quick and easy way of determining effects on NRC4-mediated immunity. However, I was not very successful in identifying proteins involved in Rpi-blb2/NRC4-mediated immunity to *P. infestans.* I may however, have discovered proteins that impact plant-bacteria interactions. Many of the genes I knocked down led to alterations in efficiency of *Agrobacterium* mediated transient gene expression. These were conducted with the constitutive 35S virus promoter, so it's doubtful the effect is on transcription, however it can't be ruled out with these data. It would be prudent to perform CFU counts of *Pseudomonas syringae* or even *Agrobacterium* itself to determine whether altering the genes of interest indeed has any effect on bacterial titer. We have developed a range of tools to dissect this, including the VIGS constructs and GFP tagged constructs. These could also be used in biopharming practices to increase *Agrobacterium* mediated transient expression of plant made pharmaceuticals. It would be interesting to test in the future whether the components identified here are required for NRC4 dependent sensor NLRs that provide immunity to bacteria such as BS2 which confers resistance to *Xanthomonas campestris* (Wu et al., 2017).

The most successful strategy in determining the potential immune-related roles of candidate NRC4 interactors was live cell imaging for haustorial accumulation. We found that the exocyst and HOPS complexes are diverted to the EHM during infection with *P. infestans.* Given the well-established role of HOPS complex in vacuolar fusion events, these results are consistent with findings that the late endocytic pathway, which is normally targeted to the vacuole, is diverted towards the EHM during *P. infestans* infection (Bozkurt et al., 2015). Whether these complexes are involved in NRC4's localisation at the EHM remains to be determined. Unfortunately, VIGS of HOPS components led to dwarfing or death of the seedlings, so transient silencing or dominant negative mutations will have to be used to dissect this. Silencing the exocyst components doesn't lead to overly severe growth phenotypes, but some of the

components have massively expanded in plants, and whilst our MS analysis didn't reveal all of these, it is possible they are redundant when one component is silenced. It's important to note also, that there is likely more than one pathway diverted to the EHM, and that the correlations I found of NRC4 and HOPS or exocyst complexes, are not proof of causation.

Another quite exciting possible explanation for the EHM association of some candidate NRC4 interactors is that NRC4 does not get transported by them, but guards them together with the NRC4-dependent sensor NLRs. Several pathogen effectors have been found to target exocyst components in the *P. infestans – N. benthamiana* pathosystem. For instance, Sec5 was recently found to be secreted towards haustoria (Wang et al., 2018a), and is known to be targeted by the RXLR effector AVR1 (Du et al., 2015b), which also localises around haustoria (Wang et al., 2018a). Additionally, R1 which detects AVR1, relies on NRC4 for HR and resistance (Wu et al., 2017). Therefore it is possible NRC4 guards this or another pathway directed towards the EHM upon infection. This will be discussed further in the General Discussion and Conclusions Chapter, Chapter 6.

6. General Discussion & Conclusions

The haustorial interface is a critical battleground for fungal and oomycete interactions with plants. Through haustoria, filamentous pathogens deploy a vast array of influential cytoplasmic effectors (Petre and Kamoun, 2014; Wang et al., 2018b, 2017b). Effectors are key in shutting down host immune responses and enabling the pathogen to feed, probably via the haustoria and hyphal structures, although the extent to which both structures feed is unknown and probably varies from pathogen to pathogen (Bozkurt and Kamoun, 2020). Many effectors that are translocated from haustoria localise inside the plant cell but around the haustorial interface (Wang et al., 2018a). These perihaustorial effectors have been implicated in blocking conventional defence-related secretion (Bozkurt et al., 2011), and potentially non-conventional secretory pathways that target the haustoria (Dagdas et al., 2018, 2016).

1. Where does NRC4 localise in the cell?

When considering the mechanisms underlying protein function, understanding localisation in the endogenous circumstance is extremely important. 'Guilt-by-association' in terms of co-localisation within the cell is a good starting point. This is particularly true if a protein has a very specific subcellular localisation. In this thesis I describe the localisation of NRC4 in three states:

1. NRC4 in the absence of infection (inactive)
2. NRC4 in the presence of infection but no sensor NLR (intermediate-inactive)
3. NRC4 in the presence of infection and a compatible sensor NLR (active)

6.1.1. Inactive state – pre-infection

Prior to infection, confocal microscopy data of live cells demonstrated NRC4 is mainly cytoplasmic whereas a subset of the NRC4 pool is membrane associated. Some of my membrane enrichment experiments suggest that NRC4 may be more membrane associated than cytoplasmic (Figure 3.5). However, there are two important considerations: firstly, this is not necessarily the native state of the NLR *in planta*. Protein extraction can alter the state and in particular the enrichment may be biased if precipitation occurs or a portion is lost early in the discarded pellet after the first spin cycle to clear the lysate of debris. These assays need to be repeated with western blotting of the discarded sample to show whether these concerns are unfounded. It would be particularly interesting to repeat the membrane enrichment assay of

transgenic NRC4-GFP in the presence and absence of an *Agrobacterium* challenge, to determine whether *Agrobacterium* presence/recognition is altering the distribution of NRC4. To determine the efficiency of membrane enrichment, it would be important to include a native antibody detection of an intrinsic membrane protein such as ATPase 1, the H^+ ATPase. Also worth considering is that NRC4 may be associating with nano sized vesicles which may not pellet at 21,000 *g*, and may require a two-step sucrose gradient and high centrifugation at 100,000 *g*. However, it has been shown that centrifugation at low speeds can efficiently enrich the heavy domains of membranes (Abas and Luschnig, 2010).

Another unknown aspect of inactive NRC4 is its oligomeric state. This could be ascertained by blue-native PAGE or gel filtration. Considering the dramatic shift from diffuse cytoplasmic signal with the inactive form to intense puncta formation with the autoactive mutant of NRC4 (Chapter 4, Figure 35), I would suggest that NRC4 is probably monomeric or dimeric prior to activation. This is based on the assumption that the puncta are indeed pentameric resistosomes of NRC4 because these puncta can be seen despite the cytoplasmic signal of NRC4.

6.1.2. Inactive state – during infection (intermediate)

Upon infection, NRC4 polarises to the EHM (Chapter 3, Figure 5). This is clear with microscopy, albeit difficult if not impossible to show with biochemistry due to the relatively low abundance of EHM versus plasma membrane and other membranes. Furthermore, the EHM composition is mostly unknown, there are no specific markers for it, and no established protocols to enrich the EHM. NRC4 localises to an EHM microdomain where it may detect AVRblb2 and other perihaustorial effectors via pairing with specific sensor NLRs.

NRC4 is not in the active state when there is no cognate sensor NLR present. So when infection occurs, it does not lead to HR and resistance. It's possible NRC4 is in a primed or intermediate state at the haustorial interface. Targeting of an immune receptor at the pathogen interface suggests that plant has somehow sensed pathogen attempt to form haustoria. But if the plant could sense the haustorium formation, why does the plant not simply trigger HR? When plants conquered land they did so with

the help of symbiotic fungi (Delaux and Schornack, 2021). It could be that the EHM is a hangover from this symbiosis, or indeed extant symbioses. However, it's unclear why the plant would tolerate the existence of the EHM in the leaf. It is possible that EHM-like membranous interfaces emerged during plant development or due to stress conditions during which HR activation may not be suitable for plant fitness. For instance, it is possible NRC4 accumulation is a wounding response and HR would be inappropriate for such abiotic damages. In addition, during invasion attempts by a non-specialized pathogen or unfavourable environmental conditions for the invading pathogen, the plant could prevent penetration via basal immune responses such as papilla formation. It should be more beneficial for plants to detect actual signs of successful pathogen invasion before they commit to HR. In fact, for non-compatible interactions, where the haustorium gets encased, this makes perfect sense. The plant would not benefit from killing a cell unless it detects that the pathogen is trying to manipulate it with effector proteins.

6.1.3. Activated state - pathogen activated vs autoactivated

As well as *P. infestans*, NRC4 is known to provide immunity against viruses, nematodes and bacteria (Wu et al., 2017). We don't know about the localisation of NRC4 during these interactions, but in terms of Rpi-blb2/NRC4 mediated resistance to *P. infestans* we know that NRC4 forms puncta upon activation, and that these sometimes associate with the EHM (Chapter 4, Figure 35). When we pre-activated NRC4 prior to pathogen entry, using an autoactive NRC4 mutant, NRC4^{D478V}, we found it no longer accumulates at the EHM. NRC4 instead forms puncta associated with the PM and EHM linearly. I propose a model in which activated NRC4 assembles into a resistosome-like structure which then associates with the nearest membrane interface. The autoactivated form could therefore be inaccessible to the transport machinery required for haustorial accumulation, and the lack of accumulation at the EHM could explain the loss of resistance.

6.1.3.1. Conservation of ZAR1 resistosome model for NRC4

Considering these observations of activated NRC4 forming resistosome-like puncta associated with the membrane, what other evidence do we have for how well the ZAR1 model of HR elicitation fit NRC4? Our data that α1 (CC domain) is transferrable from

ZAR1 to NRC4 without loss of function suggests functional conservation of this region. Additionally, when we make similar loss of function mutants in this region as were published for ZAR1 (ZAR1$^{F9A/L10A/L14A}$) (Wang et al., 2019a), NRC4 also loses function (NRC4$^{L9A/V10A/L14A}$) (Chapter 4, Figure 34) (Adachi et al., 2019). Inactive ZAR1 was shown to increase its affinity for membranes upon activation. This data is from membrane enrichment assays, but it is important to note that ZAR1 also showed strong affinity for membranes in its inactive state (Wang et al., 2019a). Recently ZAR1 was shown with Blue-Native (BN) PAGE to form oligomers *in planta* of approximately the same size as were observed *in vitro* with the resistosome (Hu et al., 2020). A key goal for us will be to try and replicate this with NRC4, in order to demonstrate that the NRC4 puncta we observe in live cells are indeed resistosomes. It will be interesting to see whether higher order complexes in BN-PAGE are around 900 kDa like ZAR1, or whether NRC4 forms ~500 kDa complexes equal to 5 units of NRC4 and no accessory proteins.

6.2. *How does NRC4 accumulate at the EHM?*

I demonstrated here that NRC4 accumulation at the EHM is a dynamic process which takes more than 30 minutes to occur (Chapter 5, Figure 1-2). There are two models for how NRC4 accumulates at the EHM. Firstly, that NRC4 is carried by some form of transport pathway. Secondly that NRC4 diffuses through the cytoplasm and a regulated process occurs at the EHM-cytoplasm contact points, where NRC4 associates with, or integrates in the EHM.

6.2.1. Transport pathway for NRC4 deployment to the EHM

This is the first instance of a full length NLR which is deployed to the host-pathogen interface, in plant or animal systems. The closest comparison in the literature is the EHM accumulation of the non-NLR CC domain containing R-protein, RPW8.2 and close homologues. RPW8.2 is mostly plasma membrane localised prior to infection with filamentous pathogens, but accumulates at the EHM upon infection (Wang et al., 2009). FRAP data indicates that this process occurs in roughly 5 minutes (Kim et al., 2014; Wang et al., 2009), whereas NRC4 takes more than 30 minutes. RPW8.2 localises to puncta which are labelled with VAMP721 and VAMP722. These mediate membrane fusion and VAMP721 was shown to be required for RPW8.2-mediated

resistance (Kim et al., 2014). NRC4 does not localise to RPW8.2 positive puncta (Chapter 3, Figure 6), and in fact there are no obvious motile puncta of NRC4. These VAMPs are expanded in *N. benthamiana* and so represent a challenging target to study by gene silencing, mutagenesis or knockout. The EHM accumulation of RPW8.2 is insensitive to Brefeldin A (BFA) (Berkey et al., 2016). This experiment could be repeated for NRC4, with RPW8.2 as a negative control, and BFA-sensitive PEN1 as a positive control (Nielsen et al., 2012). We can also investigate whether NRC4 is affected by actin inhibitors, either chemical and/or actin depolymerising factors – both of which inhibit RPW8.2's accumulation at the EHM (Wang et al., 2009). However, it should be noted that these chemical inhibitors target conserved eukaryotic pathways and so will also have an effect on *P. infestans.* Additionally, perturbing key transport pathways and cytoskeleton will lead to cytotoxicity, meaning that imaging this experiment will be technically challenging with the hemibiotrophic lifestyle of potato blight.

6.2.2. Diffusion and EHM association/insertion of NRC4

NRC4 fluorescence recovered from photobleaching much faster than StRemorin1.3 (Chapter 5, Figure 1). Rem1.3 uses a C-terminal positively charged tail to associate with membranes (Perraki et al., 2012). The difference in timing could reflect the small pool of RFP-Rem1.3 in the cytoplasm and/or the long time it takes to laterally diffuse along the membrane to the EHM. NRC4 has a much greater cytoplasmic pool (Chapter 3, Figure 3), and cytoplasmic proteins diffuse quickly, as evidenced by EV:GFP's quick perihaustorial fluorescence recovery (Chapter 5, Figure 2). It is plausible that NRC4 diffuses through the cytoplasm and associates with the EHM, but this association process takes time. However, it is not clear why this process would be time consuming.

6.3. Why does NRC4 accumulate at the EHM?

Since all evidence in this thesis points towards a defence related function of NRC4's EHM accumulation, it is unlikely this localisation is due to pathogen manipulation. This is evident because although NRC4 accumulates at the EHM during *P. infestans* infection of *N. benthamiana*, the resistance mediated by the NRC4 dependent sensor NLRs Rpi-blb2 and R1 are not compromised. Indeed, with the use of nrc4a/b mutant plants and HR suppressed NRC4^{L9E}, I was able to determine that NRC4 accumulates

at the EHM when the disease stopping sensor (Rpi-blb2) is present (Chapter 4, Figure 35). When NRC4 WT is expressed with Rpi-blb2 (Rpi-blb2$^{nrc4a/b}$ plants) it leads to full resistance (Chapter 4, Figure 34). Therefore, it is highly likely that NRC4 accumulation at EHM is primed by immunity, rather than a pathogen strategy to eliminate NRC4 mediated defences. This idea fits with the second of the following three models for why NRC4 accumulates at the EHM. These are discussed in detail below but can be summarised as:

1. Accumulation of NRC4 to increase chances of effector detection
2. Accumulation of NRC4 because it is guarding a secretory pathways that are targeted by the perihaustorial effectors
3. Accumulation of NRC4 in order to disrupt the EHM

It is important to note that these three models are not mutually exclusive. It's distinctly possible that two or more of these models are true. For instance NRC4 accumulation at the EHM may have initially evolved due to plant/pathogen-instigated diversion of an NRC4-guarded secretory pathway, but then the plant equipped sensors to NRC4 that can detect perihaustorial effectors, and activation of NRC4 disrupts the EHM leading to resistance.

6.3.1. NRC4 accumulation at the EHM increase chances of effector detection

Haustoria are the site of conventionally and non-conventionally secreted effectors (Wang et al., 2018b, 2017a). Many of these translocate through the EHM as they have targets on the plant side. The function of NRC4's EHM localisation could be to 'catch' effectors that translocate into the plant cell through the EHM. Therefore my first model to explain why NRC4 accumulates at the EHM is that it aims to increase chances of effector recognition. AVRblb2 concentrates to the EHM to block secretion of C14 proteases (Bozkurt et al., 2011). NRC4 partially co-localises with AVRblb2 at the EHM (Chapter 3, Figure 11). Rpi-blb2 does not accumulate at the EHM with NRC4 (Chapter 3, Figure 12). However, Rpi-blb2 could detect AVRblb2 indirectly and activate NRC4 either through a transient interaction or indirectly. Through a transient interaction, a small amount of Rpi-blb2 in the cytoplasm around the EHM could detect AVRblb2 and activate a large amount of NRC4. This is one possible explanation for why we do not see Rpi-blb2 accumulation at the EHM.

6.3.1.1. Many AVRs are perihaustorial (some of which trigger HR via NRC4)

Several other AVRs have been reported to be perihaustorial. These were summarised in a recent paper and represented in Table 12 below (Wang et al., 2018a). Additionally, we found PexRD54 is a perihaustorial effector (Dagdas et al., 2018).

Table 12: List of perihaustorial effectors (data from (Wang et al., 2018a))

PITG Number	Other name	Localisation without infection
PITG_0821	PexRD21 , CRE1	plasma membrane
PITG_04097	**avrblb2** family, SFI1	nuclear; nucleolar; cytoplasmic background
PITG_04388	PexRD25	nuclear; nucleolar; faintly plasma
PITG_05750	PexRD49 , CRE3	plasma membrane; nuclear/nucleolar
PITG_08943 / 22870	Avr2	plasma membrane
PITG_16427/ 16240/ 16233,	PexRD12 , CRE13	variable, often nucleocytoplasmic but sometimes plasma membrane; occasional faint nucleolar rings
PITG_16663	**AVR1**	nucleocytoplasmic; later peroxisomes
PITG_17316/ 17309	CRE15	plasma membrane; faint nucleolar
PITG_20300	**avrblb2** family, PexRD39 /40	plasma membrane and rarely, faint nucleolar

Of particular interest is the finding that RXLR AVR1 is a perihaustorial effector (Wang et al., 2018a). AVR1 is detected by R1, an NRC4-dependent CNL (Wu et al., 2017). It is plausible that some of NRC4's EHM niche is dedicated to detection of other AVRs. RXLR effector AVR2 partially co-localises with AVRblb2 around haustoria presumably at the EHM (Saunders et al., 2012). However, R2 is not an NRC dependent NLR (Wu et al., 2017). Nevertheless, it shows that the EHM is a hotspot for AVR localisation and adds to the likelihood that NRC4's localisation is at least partially necessitated to enable detection of the effector, via a sensor NLR. In future, investigation of the localisation of NRC4 with other sensors should be conducted. It would important to do so by first disarming the plants with helper NLR knockouts and then complementing with HR-suppressed variants as I have done here, such as NRC4^{L9E}, so that as close to endogenous conditions can be achieved without leading to cell death which prevents microscopy. For some sensor NLRs such as R8, this will require NRC2/NRC3/NRC4 triple knockout plants (Wu et al., 2020).

6.3.2. NRC4 guards a defence-related secretory pathway that targets the haustorial interface

The next model to explain why NRC4 is targeted to the EHM, is that it is guarding a secretory pathway(s) which is diverted to the EHM. There is considerable evidence for this.

6.3.2.1. Does NRC4 guard C14 secretion to the EHM?

The results of this thesis fit remarkably well with previous findings that AVRblb2 blocks defence-related secretion to the EHM (Bozkurt et al., 2011). Dr Bozkurt and colleagues demonstrated that the secretion of the immune protease C14 is blocked by heterologous expression of AVRblb2 in plant cells. They showed that AVRblb2 and C14 are both directed to the EHM. NRC4 could be guarding this defence pathway by recruiting sensors such as Rpi-blb2 to detect perihaustorial effectors like AVRblb2 which perturb cell-intrinsic defence responses. It is important to note that AVRblb2 is a member of expanded effector family in *P. infestans* with multiple copies of *Avrblb2*, and at least four variants of the effector (Oliva et al., 2015). It is yet unknown whether all *Avrblb2* members have the same virulence function.

6.3.2.2. Does NRC4 guard the Exocyst complex?

With our CoIP/MS analysis we found 6 out of 8 components of the Exocyst complex associated with NRC4 in uninfected tissue. Exo70 came in two forms, Exo70A1 and Exo70B1. The reduction in hits associated with NRC4 during infection does not necessarily mean interaction is lost. The total peptide hits associated with NRC4 reduces in the infected sample. More than 5200 unique peptides were found associated with NRC4 in the absence of infection, which weren't associated with the GFP control, whereas in the infected sample this number drops to less than 2200. We found that the exocyst complex is diverted towards haustoria upon infection (Chapter 5, Figure 7). This is in agreement with two other papers (Overdijk et al., 2020; Wang et al., 2018a). It's believed that the exocyst complex is required for the secretion of callose, which is known to be involved in defence against *P. infestans* (Ruano and Scheuring, 2020). It is also plausible that exocyst complex facilitates the secretion of other defence related compounds, to the haustorial penetration. AVR1 targets the exocyst component Sec5 surrounding haustoria (Du et al., 2015b; Wang et al., 2018a). It is unclear how this fits with the finding AVR1 detection by R1 NLR requires nuclear localisation (Du et al., 2015a). This is especially unusual considering R1 requires NRC4 and no other helper, for HR and resistance (Wu et al., 2017). However Du et al., (2015a) did not include any western blotting analysis for R1 variants and the nuclear excluded AVR1 was unstable leading to issues with their conclusions. Considering AVR1 is perihaustorial during infection (Wang et al., 2018a), it is possible AVR1 function and recognition occurs at the EHM.

6.3.2.3. Does NRC4 guard the HOPS/CORVET complex?

The HOPS and CORVET complexes are other interesting candidates supporting the model that NRC4 guard's secretory pathway(s). NRC4 pulled down VPS11, VPS16, VPS18 of the core components and VPS41 of the HOPS-specific components. I found that the StVPS18 and VPS41 were diverted towards the EHM during infection. I need to investigate the localisation of CORVET specific complex VPS8, but currently it seems like HOPS is used for secretion to the pathogen, and/or perhaps to assist with the formation of the EHM. HOPS regulates late endosomal fusion to the vacuole/lysosome or homotypic fusion of vacuoles to vacuoles. In fact, in other systems CORVET and HOPS function sequentially, whereas in plants they are

thought to function on separate pathways. The HOPS process in plants is known to be Rab 7 dependent (Takemoto et al., 2018). Interestingly, a Rab 7 member was shown to be diverted to the EHM during *P. infestans* infection (Bozkurt et al., 2015; Lu et al., 2012), which could represent the same late endosome pathway as we saw with the HOPS complex. Could NRC4 be guarding a late endosome to vacuole pathway that gets diverted to the EHM during infection?

6.3.2.4. Does NRC4 guard other components targeted to the EHM?

There are several other candidate interactors of NRC4 which are vesicle transport regulators reported to accumulate around the haustoria (Bozkurt et al., 2015, 2014; Lu et al., 2012; Pandey et al., 2020). Rab GTPases Rab8a, RabE1d and RabD2a all label perihaustorial vesicles (Lu et al., 2012; Pandey et al., 2020). However, the mass spectroscopy data did not include RabE1d, but the closely related RabE1a and RabE1c. It remains to be validated by CoIP and microscopy whether NRC4 associates with the Rab GTPases on the mass spectrometry list. Synaptotagmin 1 (SYT1) localises to the EHM (Bozkurt et al., 2015, 2014), but mainly at subdomains of EHM that are not labelled by NRC4 fusion proteins (Chapter 3, Figure 6). For this reason, I am doubtful of its involvement in NRC4 trafficking and/or NRC4's role in guarding it. Nevertheless, I was quite successful in identifying new EHM localised or perihaustorial proteins. It remains to be seen if NRC4 has any involvement with these, but regardless they represent interesting candidates for further study on secretion of defence related materials, and for pathogen feeding.

6.3.3. The EHM is required for pathogenesis and targeting NRC4 there allows for efficient destruction of it upon pathogen recognition

Despite their extreme distance phylogenetically (fungi are more closely related to animals than oomycetes) fungi and oomycetes both form haustoria in plant cells and are both surrounded by the EHM (Bozkurt and Kamoun, 2020). The reason for the existence of the EHM is therefore a mystery. Why would a plant tolerate its existence, as surely there are multiple cues that signal its existence? This is a debate among those who work on haustoria forming pathogens, but it is indeed possible that formation of the EHM is primarily a basal plant defence response, in which the

specialized membrane interface mediates focal accumulation of immune components at microbial invasion sites to achieve a stronger antimicrobial effect. Thus, EHM could still serve the plant by reducing pathogen spread, especially when the environmental conditions are not favourable for the pathogen, thereby minimizing the fitness cost imposed by the parasitic infection. When effective, this cell-intrinsic defence response could eliminate many of the pathogenic threats without the cells undergoing HR. It is reasonable that programmed cell death is not the preferred strategy for dealing with these pathogens as it is destructive and irreversible. In line with this view, PTI generally doesn't trigger HR. Indeed NRC4 accumulates at the EHM without triggering an HR unless a sensor for a secreted pathogen effector is present. This was discussed in Section 6.1.2 above. Briefly, the plant may deploy NRC4 to destroy the EHM in the event that pathogen manipulation of the plant is detected. Effectors are deployed to subvert immunity and enable feeding by the pathogen. If the plant detects this, NRC4 could cause rapid destruction of the EHM, if the resistosome model is true and if pore formation leads to membrane lysis. The haustorial interface maybe be an Achilles' heel for *P. infestans* – once the EHM is disrupted plant hydrolytic enzymes (released by vacuole collapse for instance) and ROS from organelles could be directly exposed to haustoria. Oomycete haustoria are vulnerable as they are inside the plant cell wall and, unlike fungi, do not segment haustoria from the rest of the hypha. One could envisage the destruction of the EHM by the plant as a catastrophic event which leads to a chain-reaction like death of the hypha, starting at a single haustorium. This model fits with the fact that haustoria forming pathogens in plants are not known to disrupt the EHM themselves with a pore forming toxin – although, lack of evidence is not proof in itself. Such toxins are a common strategy used by host and pathogens across all kingdoms of life (Peraro and Van Der Goot, 2016). For instance the fungus *Candida albicans* forms hyphal penetrations of human epithelial cells and secretes the pore forming toxin candidalysin to disrupt the membrane of the invasion pocket, promoting further invasion of the tissue (Westman et al., 2019).

6.4. Concluding remarks and future challenges

This work provides evidence that NLRs are dynamic proteins which can change their localisations during infection, rather than being static as previously thought. Here I describe the helper NLR NRC4, which is motile and focally accumulates at an EHM

microdomain surrounding *P. infestans* haustoria. How this system evolved is a mystery and we still lack conclusive evidence for what function NRC4 is providing at the EHM. Considering the spatial separation of *P. infestans* (evolved in Central and South America) and *N. benthamiana* (native to Australia), it's likely NRC4 localises to the EHM formed with other *Phytophthora species.* But what about other oomycetes and fungi? NRC4 is present in potato, tomato, pepper, aubergine and *Nicotiana* (Wu et al., 2017); and so may have evolved in an ancestral solanaceous plant protecting against infections from haustoria forming pathogens. A provocative hypothesis would be that NRC4 localise to different locations for different pathogens, such as viruses, bacteria and nematodes. These could be investigated whilst also determining the localisations of other effectors from these pathogens and sensor NLR which are dependent on NRC4 for HR and resistance. Additionally, what are the localisations of other NLRs during infection with relevant microbes? Particularly interesting would be to determine whether other NRC helpers also accumulate at the EHM, or similar but unrelated helpers such as ADR1 and NRG1? These can probably be dissected with the same strategy as presented here of imaging in the absence of sensor NLRs where possible, or perturbing HR through loss of function N-terminal mutants. NRC4 has an extremely specific localisation in haustoriated cells. We could use this to enrich tissue for EHM in order to analyse the composition of EHM further. This would be a huge feat as it was not possible because we lacked specific EHM markers. One remaining challenge would be to impair NRC4's PM localisation in non-haustoriated cells.

In terms of NRC4 mediated resistance we still do not know what happens when NRC4 becomes activated at the EHM. Does the EHM become destroyed or does the cell die first? Determining this will require a tightly controlled but responsive inducible activation system for NRC4. Dissecting out the transport pathway that deposits NRC4 towards haustoria will require development of an automated process for screening candidates and quantification of small changes in NRC4 EHM accumulation. It would also be useful to find what initial molecular signal targets NRC4 towards haustoria. Finally, it would be key to producing a HR functional variant of NRC4 which does not accumulate at the EHM, in order to decouple the localisation from the resistance phenotype. This however may not be possible as to date all NRC4 variants which lose localisation have also lost cell death capabilities, with the exception of the autoactive mutant. Despite this, the autoactive NRC4 phenotype is difficult to interpret due to

induction of cell death which limits cellular imaging of the infection process. Determining the precise molecular mechanisms behind NRC4-mediated resistance to *P. infestans* could help us engineer more effective and targeted disease resistance controls to haustoria forming pathogens.

7. Bibliography

Abas L, Luschnig C. 2010. Maximum yields of microsomal-type membranes from small amounts of plant material without requiring ultracentrifugation. *Anal Biochem* **401**:217–227. doi:10.1016/j.ab.2010.02.030

Acheampong AK, Shanks C, Chai-Yi C, Schaller GE, Dagdas Y, Kieber JJ. 2020. EXO70D isoforms mediate selective autophagic degradation of Type-A ARR proteins to regulate cytokinin sensitivity. *bioRxiv*. doi:10.1101/2020.02.07.938712

Adachi H, Contreras M, Harant A, Wu C, Derevnina L, Sakai T, Duggan C, Moratto E, Bozkurt TO, Maqbool A, Win J, Kamoun S. 2019. An N-terminal motif in NLR immune receptors is functionally conserved across distantly related plant species. *Elife* **8**:693291. doi:10.7554/eLife.49956

Beck M, Zhou J, Faulkner C, Mac DL, Robatzek S. 2012. Spatio-temporal cellular dynamics of the Arabidopsis flagellin receptor reveal activation status-dependent endosomal sorting. *Plant Cell* **24**:4205–4219. doi:10.1105/tpc.112.100263

Bentham AR, Zdrzałek R, De la Concepcion JC, Banfield MJ. 2018. Uncoiling CNLs: Structure/function approaches to understanding CC domain function in plant NLRs. *Plant Cell Physiol* **59**:2398–2408. doi:10.1093/pcp/pcy185

Berkey R, Zhang Y, Ma X, King H, Zhang Q, Wang W, Xiao S. 2016. Homologues of the RPW8 resistance protein are localized to the extra-haustorial membrane that is likely synthesized de novo. *Plant Physiol* **173**:pp.01539.2016. doi:10.1104/pp.16.01539

Boehm C, Field MC. 2019. Evolution of late steps in exocytosis: Conservation, specialization. *Wellcome Open Res* **4**:1–19. doi:10.12688/wellcomeopenres.15142.1

Boevink PC, Wang S, Pham J, McLellan H, Welsh L, Whisson SC, Birch PRJ. 2019. The oomycete RXLR motif determines non-conventional secretion for effector deliveryIS-MPMI. Glasgow, UK.

Bos JIB, Armstrong MR, Gilroy EM, Boevink PC, Hein I, Taylor RM, Zhendong T, Engelhardt S, Vetukuri RR, Harrower B, Dixelius C, Bryan G, Sadanandom A, Whisson SC, Kamoun S, Birch PRJ. 2010. Phytophthora infestans effector AVR3a is essential for virulence and manipulates plant immunity by stabilizing host E3 ligase CMPG1. *Proc Natl Acad Sci* **107**:9909–9914.

doi:10.1073/pnas.0914408107

Bozkurt TO, Belhaj K, Dagdas YF, Chaparro-Garcia A, Wu C-H, Cano LM, Kamoun S. 2015. Rerouting of plant late endocytic trafficking toward a pathogen interface. *Traffic* **16**:204–26. doi:10.1111/tra.12245

Bozkurt TO, Kamoun S. 2020. The plant-pathogen haustorial interface at a glance. *J Cell Sci* **133**. doi:10.1242/jcs.237958

Bozkurt TO, Richardson A, Dagdas YF, Mongrand S, Kamoun S, Raffaele S. 2014. The plant membrane-associated REMORIN1.3 accumulates in discrete perihaustorial domains and enhances susceptibility to Phytophthora infestans. *Plant Physiol* **165**:1005–1018. doi:10.1104/pp.114.235804

Bozkurt TO, Schornack S, Banfield MJ, Kamoun S. 2012. Oomycetes, effectors, and all that jazz. *Curr Opin Plant Biol* **15**:483–492. doi:10.1016/j.pbi.2012.03.008

Bozkurt TO, Schornack S, Win J, Shindo T, Ilyas M, Oliva R, Cano LM, Jones AME, Huitema E, van der Hoorn R a L, Kamoun S. 2011. Phytophthora infestans effector AVRblb2 prevents secretion of a plant immune protease at the haustorial interface. *Proc Natl Acad Sci U S A* **108**:20832–7. doi:10.1073/pnas.1112708109

Brendolise C, Montefiori M, Dinis R, Peeters N, Storey RD, Rikkerink EH. 2017. A novel hairpin library-based approach to identify NBS–LRR genes required for effector-triggered hypersensitive response in Nicotiana benthamiana. *Plant Methods* **13**:32. doi:10.1186/s13007-017-0181-7

Burdett H, Bentham AR, Williams SJ, Dodds PN, Anderson PA, Banfield MJ, Kobe B. 2019. The plant “resistosome”: structural insights into immune signaling. *Cell Host Microbe* **26**:193–201. doi:10.1016/j.chom.2019.07.020

Casey LW, Lavrencic P, Bentham AR, Cesari S, Ericsson DJ, Croll T, Turk D, Anderson PA, Mark AE, Dodds PN, Mobli M, Kobe B, Williams SJ. 2016. The CC domain structure from the wheat stem rust resistance protein Sr33 challenges paradigms for dimerization in plant NLR proteins. *Proc Natl Acad Sci U S A* **113**:12856–12861. doi:10.1073/pnas.1609922113

Castel B, Ngou PM, Cevik V, Redkar A, Kim DS, Yang Y, Ding P, Jones JDG. 2019a. Diverse NLR immune receptors activate defence via the RPW8-NLR NRG1. *New Phytol*. doi:10.1111/nph.15659

Castel B, Wu Y, Xiao S, Jones JDG. 2019b. An rpw8 quadruple mutant of Arabidopsis Col-0 is partially compromised in bacterial and fungal resistance. *bioRxiv* **4**.

Cesari S. 2017. Multiple strategies for pathogen perception by plant immune

receptors. *New Phytol*. doi:10.1111/nph.14877

Cesari S, Bernoux M, Moncuquet P, Kroj T, Dodds PN. 2014. A novel conserved mechanism for plant NLR protein pairs: the “integrated decoy” hypothesis. *Front Plant Sci* **5**:606. doi:10.3389/fpls.2014.00606

Cesari S, Moore J, Chen C, Webb D, Periyannan S, Mago R, Bernoux M, Lagudah ES, Dodds PN. 2016. Cytosolic activation of cell death and stem rust resistance by cereal MLA-family CC–NLR proteins. *Proc Natl Acad Sci* **113**:10204–10209. doi:10.1073/pnas.1605483113

Chiang Y-H, Coaker G. 2015. Effector triggered immunity: NLR immune perception and downstream defense responses. *Arab B* **13**:e0183. doi:10.1199/tab.0183

Chinchilla D, Zipfel C, Robatzek S, Kemmerling B, Nürnberger T, Jones JDG, Felix G, Boller T. 2007. A flagellin-induced complex of the receptor FLS2 and BAK1 initiates plant defence. *Nature* **448**:497–500. doi:10.1038/nature05999

Dagdas YF, Beihaj K, Maqbool A, Chaparro-Garcia A, Pandey P, Petre B, Tabassum N, Cruz-Mireles N, Hughes RK, Sklenar J, Win J, Menke F, Findlay K, Banfield MJ, Kamoun S, Bozkurt TO. 2016. An effector of the irish potato famine pathogen antagonizes a host autophagy cargo receptor. *Elife* **5**:1–23. doi:10.7554/eLife.10856

Dagdas YF, Pandey P, Tumtas Y, Sanguankiattichai N, Belhaj K, Duggan C, Leary AY, Segretin ME, Contreras MP, Savage Z, Khandare VS, Kamoun S, Bozkurt TO. 2018. Host autophagy machinery is diverted to the pathogen interface to mediate focal defense responses against the Irish potato famine pathogen. *Elife* 1–15. doi:10.7554/eLife.37476

Dagvadorj B, Ozketen AC, Andac A, Duggan C, Osman T, Mahinur SA. 2017. A Puccinia striiformis f . sp . tritici secreted protein activates plant immunity at the cell surface. *Sci Rep* **7**:1–10. doi:10.1038/s41598-017-01100-z

Delaux P-M, Schornack S. 2021. Plant evolution driven by interactions with symbiotic and pathogenic microbes. *Science (80-)* **371**. doi:10.1126/science.aba6605

Derevnina L, Wu C-H, Kamoun S. 2019. Methods and compositions for enhancing the disease resistance of plants. WO2019108619A1.

Du Y, Berg J, Govers F, Bouwmeester K. 2015a. Immune activation mediated by the late blight resistance protein R1 requires nuclear localization of R1 and the effector AVR1. *New Phytol* **207**:735–747. doi:10.1111/nph.13355

Du Y, Mpina MH, Birch PRJ, Bouwmeester K, Govers F. 2015b. Phytophthora

infestans RXLR effector AVR1 interacts with exocyst component Sec5 to manipulate plant immunity. *Plant Physiol* **169**:1975–1990. doi:10.1104/pp.15.01169

Du Y, Overdijk EJRR, Berg JA, Govers F, Bouwmeester K. 2018. Solanaceous exocyst subunits are involved in immunity to diverse plant pathogens. *J Exp Bot* **69**:655–666. doi:10.1093/jxb/erx442

Ellinger D, Voigt CA. 2014. Callose biosynthesis in arabidopsis with a focus on pathogen response: What we have learned within the last decade. *Ann Bot* **114**:1349–1358. doi:10.1093/aob/mcu120

Engelhardt S, Boevink PC, Armstrong MR, Ramos MB, Hein I, Birch PRJ. 2012. Relocalization of late blight resistance protein R3a to endosomal compartments is associated with effector recognition and required for the immune response. *Plant Cell* **24**:5142–5158. doi:10.1105/tpc.112.104992

Fawke S, Doumane M, Schornack S. 2015. Oomycete interactions with plants: infection strategies and resistance principles. *Microbiol Mol Biol Rev* **79**:263–80. doi:10.1128/MMBR.00010-15

Giannakopoulou A, Steele JFC, Segretin ME, Bozkurt TO, Zhou J, Robatzek S, Banfield MJ, Pais M, Kamoun S. 2015. Tomato I2 Immune Receptor Can Be Engineered to Confer Partial Resistance to the Oomycete Phytophthora infestans in Addition to the Fungus Fusarium oxysporum. *Mol Plant Microbe Interact* **28**:1316–29. doi:10.1094/MPMI-07-15-0147-R

Grouffaud S, van West P, Avrova AO, Birch PRJ, Whisson SC. 2008. Plasmodium falciparum and Hyaloperonospora parasitica effector translocation motifs are functional in Phytophthora infestans. *Microbiology* **154**:3743–3751. doi:10.1099/mic.0.2008/021964-0

Grünwald NJ, Flier WG. 2005. The Biology of Phytophthora infestans at Its Center of Origin. *Annu Rev Phytopathol* **43**:171–190. doi:10.1146/annurev.phyto.43.040204.135906

Harant A, Sakai T, Kamoun S, Adachi H. 2020. A vector system for fast-forward in vivo studies of the ZAR1 resistosome in the model plant Nicotiana benthamiana. *bioRxiv* 1–17. doi:https://doi.org/10.1101/2020.05.15.097584

Hiller NL, Bhattacharjee S, van Ooij C, Liolios K, Harrison T, Lopez-Estraño C, Haldar K. 2004. A host-targeting signal in virulence proteins reveals a secretome in malarial infection. *Science (80-)* **306**:1934–7. doi:10.1126/science.1102737

Horsefield S, Burdett H, Zhang X, Manik MK, Shi Y, Chen J, Qi T, Gilley J, Lai J-S, Rank MX, Casey LW, Gu W, Ericsson DJ, Foley G, Hughes RO, Bosanac T, von Itzstein M, Rathjen JP, Nanson JD, Boden M, Dry IB, Williams SJ, Staskawicz BJ, Coleman MP, Ve T, Dodds PN, Kobe B. 2019. NAD+ cleavage activity by animal and plant TIR domains in cell death pathways. *Science (80-)* **365**:793–799. doi:10.1126/science.aax1911

Hu M, Qi J, Bi G, Zhou J-M. 2020. Bacterial effectors induce oligomerization of immune receptor ZAR1 in vivo. *Mol Plant*. doi:10.1016/j.molp.2020.03.004

Jarsch IK, Konrad SSA, Stratil TF, Urbanus SL, Szymanski W, Braun P, Braun KH, Ott T. 2014. Plasma membranes are Subcompartmentalized into a plethora of coexisting and diverse microdomains in Arabidopsis and Nicotiana benthamiana. *Plant Cell* **26**:1698–1711. doi:10.1105/tpc.114.124446

Jones JDG, Dangl JL. 2006. The plant immune system. *Nature* **444**:323–9. doi:10.1038/nature05286

Jones JDG, Vance RE, Dangl JL. 2016. Intracellular innate immune surveillance devices in plants and animals. *Science (80-)* **354**:aaf6395–aaf6395. doi:10.1126/science.aaf6395

Jones P, Binns D, Chang HY, Fraser M, Li W, McAnulla C, McWilliam H, Maslen J, Mitchell A, Nuka G, Pesseat S, Quinn AF, Sangrador-Vegas A, Scheremetjew M, Yong SY, Lopez R, Hunter S. 2014. InterProScan 5: Genome-scale protein function classification. *Bioinformatics* **30**:1236–1240. doi:10.1093/bioinformatics/btu031

Jubic LM, Saile S, Furzer OJ, Kasmi F El, Dangl JL. 2019. Help wanted : helper NLRs and plant immune responses. *Curr Opin Plant Biol* **50**:82–94. doi:10.1016/j.pbi.2019.03.013

Kadota Y, Shirasu K. 2012. The HSP90 complex of plants. *Biochim Biophys Acta - Mol Cell Res* **1823**:689–697. doi:10.1016/j.bbamcr.2011.09.016

Kim H, O'Connell R, Maekawa-Yoshikawa M, Uemura T, Neumann U, Schulze-Lefert P. 2014. The powdery mildew resistance protein RPW8.2 is carried on VAMP721/722 vesicles to the extrahaustorial membrane of haustorial complexes. *Plant J* **79**:835–847. doi:10.1111/tpj.12591

Kim YE, Kim YN, Kim JA, Kim HM, Jung Y. 2015. Green fluorescent protein nanopolygons as monodisperse supramolecular assemblies of functional proteins with defined valency. *Nat Commun* **6**:1–9. doi:10.1038/ncomms8134

Kulich I, Pečenková T, Sekereš J, Smetana O, Fendrych M, Foissner I, Höftberger M, Zárský V. 2013. Arabidopsis exocyst subcomplex containing subunit EXO70B1 is involved in autophagy-related transport to the vacuole. *Traffic* **14**:1155–65. doi:10.1111/tra.12101

Kwon C, Neu C, Pajonk S, Yun HS, Lipka U, Humphry M, Bau S, Straus M, Kwaaitaal M, Rampelt H, El Kasmi F, Jürgens G, Parker J, Panstruga R, Lipka V, Schulze-Lefert P. 2008. Co-option of a default secretory pathway for plant immune responses. *Nature* **451**:835–40. doi:10.1038/nature06545

LAI Y, Eulgem T. 2017. Transcript-level expression control of plant NLR genes. *Mol Plant Pathol* **68**:1–30. doi:10.1111/mpp.12607

Lapin D, Kovacova V, Sun X, Dongus JA, Bhandari D, von Born P, Bautor J, Guarneri N, Rzemieniewski J, Stuttmann J, Beyer A, Parker JE. 2019. A coevolved EDS1-SAG101-NRG1 module mediates cell death signaling by TIR-domain immune receptors. *Plant Cell* **31**:2430–2455. doi:10.1105/tpc.19.00118

Le Roux C, Huet G, Jauneau A, Camborde L, Trémousaygue D, Kraut A, Zhou B, Levaillant M, Adachi H, Yoshioka H, Raffaele S, Berthomé R, Couté Y, Parker JE, Deslandes L. 2015. A receptor pair with an integrated decoy converts pathogen disabling of transcription factors to immunity. *Cell* **161**:1074–1088. doi:10.1016/j.cell.2015.04.025

Lee HA, Kim SY, Oh SK, Yeom SI, Kim SB, Kim MS, Kamoun S, Choi D. 2014. Multiple recognition of RXLR effectors is associated with nonhost resistance of pepper against Phytophthora infestans. *New Phytol* **203**:926–938. doi:10.1111/nph.12861

Lipka V, Dittgen J, Bednarek P, Bhat R, Wiermer M, Stein M, Landtag J, Brandt W, Rosahl S, Scheel D, Llorente F, Molina A, Parker J, Somerville S, Schulze-Lefert P. 2005. Plant science: Pre- and postinvasion defenses both contribute to nonhost resistance in Arabidopsis. *Science (80-)* **310**:1180–1183. doi:10.1126/science.1119409

Liu Y, Schiff M, Czymmek K, Tallóczy Z, Levine B, Dinesh-Kumar SP. 2005. Autophagy regulates programmed cell death during the plant innate immune response. *Cell* **121**:567–577. doi:10.1016/j.cell.2005.03.007

Liu Y, Schiff M, Dinesh-Kumar SP. 2002. Virus-induced gene silencing in tomato. *Plant J* **31**:777–86. doi:10.1046/j.1365-313x.2002.01394.x

Lőrincz P, Kenéz LA, Tóth S, Kiss V, Varga Á, Csizmadia T, Simon-Vecsei Z, Juhász

G. 2019. Vps8 overexpression inhibits HOPS-dependent trafficking routes by outcompeting Vps41/Lt. *Elife* **8**:1–25. doi:10.7554/eLife.45631

Lu R, Malcuit I, Moffett P, Ruiz MT, Peart J, Wu AJ, Rathjen JP, Bendahmane A, Day L, Baulcombe DC. 2003. High throughput virus-induced gene silencing implicates heat shock protein 90 in plant disease resistance. *EMBO J* **22**:5690–5699. doi:10.1093/emboj/cdg546

Lu Y-J, Schornack S, Spallek T, Geldner N, Chory J, Schellmann S, Schumacher K, Kamoun S, Robatzek S. 2012. Patterns of plant subcellular responses to successful oomycete infections reveal differences in host cell reprogramming and endocytic trafficking. *Cell Microbiol* **14**:682–97. doi:10.1111/j.1462-5822.2012.01751.x

Maekawa T, Cheng W, Spiridon LN, Töller A, Lukasik E, Saijo Y, Liu P, Shen QH, Micluta MA, Somssich IE, Takken FLW, Petrescu AJ, Chai J, Schulze-Lefert P. 2011. Coiled-coil domain-dependent homodimerization of intracellular barley immune receptors defines a minimal functional module for triggering cell death. *Cell Host Microbe* **9**:187–199. doi:10.1016/j.chom.2011.02.008

Marti M, Good R, Rug M, Knuepfer E, Cowman A. 2004. Targeting Malaria Virulence and Remodeling Proteins to the Host Erythrocyte. *Science (80-)* **306**:1930–1933. doi:10.1126/science.1102452

Martin R, Qi T, Zhang H, Liu F, King M, Toth C, Nogales E, Staskawicz BJ. 2020. Structure of the activated Roq1 resistosome directly recognizing the pathogen effector XopQ. *bioRxiv*. doi:10.1101/2020.08.13.246413

Martinière A, Lavagi I, Nageswaran G, Rolfe DJ, Maneta-Peyret L, Luu DT, Botchway SW, Webb SED, Mongrand S, Maurel C, Martin-Fernandez ML, Kleine-Vehn J, Friml J, Moreau P, Runions J. 2012. Cell wall constrains lateral diffusion of plant plasma-membrane proteins. *Proc Natl Acad Sci U S A* **109**:12805–12810. doi:10.1073/pnas.1202040109

Minamino N, Ueda T. 2019. RAB GTPases and their effectors in plant endosomal transport. *Curr Opin Plant Biol* **52**:61–68. doi:10.1016/j.pbi.2019.07.007

Nielsen ME, Feechan A, Böhlenius H, Ueda T, Thordal-Christensen H. 2012. Arabidopsis ARF-GTP exchange factor, GNOM, mediates transport required for innate immunity and focal accumulation of syntaxin PEN1. *Proc Natl Acad Sci U S A* **109**:11443–11448. doi:10.1073/pnas.1117596109

Oh S-K, Young C, Lee M, Oliva R, Bozkurt TO, Cano LM, Win J, Bos JIB, Liu H-Y, van

Damme M, Morgan W, Choi D, Van der Vossen EAG, Vleeshouwers VGAA, Kamoun S. 2009. In planta expression screens of Phytophthora infestans RXLR effectors reveal diverse phenotypes, including activation of the Solanum bulbocastanum disease resistance protein Rpi-blb2. *Plant Cell* **21**:2928–47. doi:10.1105/tpc.109.068247

Oh SK, Kwon SY, Choi D. 2014. Rpi-blb2-mediated hypersensitive cell death caused by phytophthora infestans AVRblb2 requires SGT1, but not EDS1, NDR1, salicylic acid-, jasmonic acid-, or ethylene-mediated signaling. *Plant Pathol J* **30**:254–260. doi:10.5423/PPJ.OA.03.2014.0027

Oliva RF, Cano LM, Raffaele S, Win J, Bozkurt TO, Belhaj K, Oh SK, Thines M, Kamoun S. 2015. A recent expansion of the RXLR effector gene Avrblb2 is maintained in global populations of Phytophthora infestans indicating different contributions to virulence. *Mol Plant-Microbe Interact* **28**:901–912. doi:10.1094/MPMI-12-14-0393-R

Overdijk EJR, Tang H, Borst JW, Govers F, Ketelaar T. 2020. Time-gated confocal microscopy reveals accumulation of exocyst subunits at the plant-pathogen interface. *J Exp Bot* **71**:837–849. doi:10.1093/jxb/erz478

Padmanabhan M, Cournoyer P, Dinesh-Kumar SP. 2009. The leucine-rich repeat domain in plant innate immunity: A wealth of possibilities. *Cell Microbiol* **11**:191–198. doi:10.1111/j.1462-5822.2008.01260.x

Pain C, Kriechbaumer V, Kittelmann M, Hawes C, Fricker M. 2019. Quantitative analysis of plant ER architecture and dynamics. *Nat Commun* **10**:1–15. doi:10.1038/s41467-019-08893-9

Pandey P, Leary AY, Tumtas Y, Savage Z, Dagvadorj B, Tan E, Khandare V, Duggan C, Yusunov T, Madalinski M, Mirkin FG, Schornack S, Dagdas Y, Kamoun S, Bozkurt TO, Tümtas Y, Savage Z, Dagvadorj B, Tan E, Khandare V, Duggan C, Yusunov T, Madalinski M, Mirkin FG, Schornack S, Dagdas Y, Kamoun S, Bozkurt TO. 2020. The Irish potato famine pathogen subverts host vesicle trafficking to channel starvation-induced autophagy to the pathogen interface. *bioRxiv*. doi:10.1101/2020.03.20.000117

Patel S, Dinesh-Kumar SP. 2008. Arabidopsis ATG6 is required to limit the pathogen-associated cell death response. *Autophagy* **4**:20–27. doi:10.4161/auto.5056

Peraro MD, Van Der Goot FG. 2016. Pore-forming toxins: Ancient, but never really out of fashion. *Nat Rev Microbiol* **14**:77–92. doi:10.1038/nrmicro.2015.3

Perraki A, Cacas JL, Crowet JM, Lins L, Castroviejo M, German-Retana S, Mongrand S, Raffaele S. 2012. Plasma membrane localization of Solanum tuberosum Remorin from group 1, homolog 3 is mediated by conformational changes in a novel C-terminal anchor and required for the restriction of potato virus X movement. *Plant Physiol* **160**:624–637. doi:10.1104/pp.112.200519

Petre B, Kamoun S. 2014. How do filamentous pathogens deliver effector proteins into plant cells? *PLoS Biol* **12**:e1001801. doi:10.1371/journal.pbio.1001801

Petre B, Saunders DGO, Sklenar J, Lorrain C, Krasileva K V., Win J, Duplessis S, Kamoun S. 2016. Heterologous expression screens in Nicotiana benthamiana identify a candidate effector of the wheat yellow rust pathogen that associates with processing bodies. *PLoS One* **11**. doi:10.1371/journal.pone.0149035

Qi D, Innes RW. 2013. Recent advances in plant NLR structure, function, localization, and signaling. *Front Immunol* **4**:1–10. doi:10.3389/fimmu.2013.00348

Qi T, Seong K, Thomazella DPT, Kim JR, Pham J, Seo E, Cho M-J, Schultink A, Staskawicz BJ. 2018. NRG1 functions downstream of EDS1 to regulate TIR-NLR-mediated plant immunity in *Nicotiana benthamiana*. *Proc Natl Acad Sci* 201814856. doi:10.1073/pnas.1814856115

Rausche J, Stenzel I, Stauder R, Fratini M, Trujillo M, Heilmann I, Rosahl S. 2020. A phosphoinositide 5-phosphatase from Solanum tuberosum is activated by PAMP-treatment and may antagonize phosphatidylinositol 4,5-bisphosphate at Phytophthora infestans infection sites . *New Phytol* 0–2. doi:10.1111/nph.16853

Rocchetti A, Hawes C, Kriechbaumer V. 2014. Fluorescent labelling of the actin cytoskeleton in plants using a cameloid antibody. *Plant Methods* **10**. doi:10.1186/1746-4811-10-12

Roux M, Schwessinger B, Albrecht C, Chinchilla D, Jones A, Holton N, Malinovsky FG, Tör M, de Vries S, Zipfel C. 2011. The arabidopsis leucine-rich repeat receptor-like kinases BAK1/SERK3 and BKK1/SERK4 are required for innate immunity to Hemibiotrophic and Biotrophic pathogens. *Plant Cell* **23**:2440–2455. doi:10.1105/tpc.111.084301

Ruano G, Scheuring D. 2020. Plant cells under attack : Endomembrane dynamics during plant defense. *Plants* 1–15. doi:https://doi.org/10.3390/

Sabol P, Kulich I, Žárský V. 2017. RIN4 recruits the exocyst subunit EXO70B1 to the plasma membrane. *J Exp Bot* 1–13. doi:10.1093/jxb/erx007

Sarris PFF, Duxbury Z, Huh SUU, Ma Y, Segonzac C, Sklenar J, Derbyshire P, Cevik

V, Rallapalli G, Saucet SBB, Wirthmueller L, Menke FLHLH, Sohn KHH, Jones JDGDG. 2015. A plant immune receptor detects pathogen effectors that target WRKY transcription factors. *Cell* **161**:1089–1100. doi:10.1016/j.cell.2015.04.024

Saunders DGO, Breen S, Win J, Schornack S, Hein I, Bozkurt TO, Champouret N, Vleeshouwers VG a a, Birch PRJ, Gilroy EM, Kamoun S. 2012. Host protein BSL1 associates with Phytophthora infestans RXLR effector AVR2 and the Solanum demissum Immune receptor R2 to mediate disease resistance. *Plant Cell* **24**:3420–34. doi:10.1105/tpc.112.099861

Schindelin J, Arganda-Carreras I, Frise E. 2012. Fiji: an open-source platform for biological-image analysis. *Nat Methods* **9**:676–682.

Schmelzer E. 2002. Cell polarization, a crucial process in fungal defence. *Trends Plant Sci* **7**:411–415.

Segretin ME, Pais M, Franceschetti M, Chaparro-Garcia A, Bos JIB, Banfield MJ, Kamoun S. 2014. Single amino acid mutations in the potato immune receptor R3a expand response to Phytophthora effectors. *Mol Plant-Microbe Interact* **27**:624–637. doi:10.1094/MPMI-02-14-0040-R

Sekereš J, Pejchar P, Šantrůček J, Vukašinović N, Žárský V, Potocký M. 2017. Analysis of Exocyst subunit EXO70 family reveals distinct membrane polar domains in tobacco pollen tubes. *Plant Physiol* **173**:1659–1675. doi:10.1104/pp.16.01709

Shen QH, Schulze-Lefert P. 2007. Rumble in the nuclear jungle: Compartmentalization, trafficking, and nuclear action of plant immune receptors. *EMBO J* **26**:4293–4301. doi:10.1038/sj.emboj.7601854

Simon MLA, Platre MP, Assil S, Van Wijk R, Chen WY, Chory J, Dreux M, Munnik T, Jaillais Y. 2014. A multi-colour/multi-affinity marker set to visualize phosphoinositide dynamics in Arabidopsis. *Plant J* **77**:322–337. doi:10.1111/tpj.12358

Song J, Win J, Tian M, Schornack S, Kaschani F, Ilyas M, Hoorn RAL Van Der, Kamoun S. 2009. Apoplastic effectors secreted by two unrelated eukaryotic plant pathogens target the tomato defense protease Rcr3.

Steele JFC, Hughes RK, Banfield MJ. 2019. Structural and biochemical studies of an NB-ARC domain from a plant NLR immune receptor. *PLoS One* **14**:1–20. doi:10.1371/journal.pone.0221226

Takemoto K, Ebine K, Askani JC, Krüger F, Gonzalez ZA, Ito E, Goh T, Schumacher

K, Nakano A, Ueda T. 2018. Distinct sets of tethering complexes, SNARE complexes, and Rab GTPases mediate membrane fusion at the vacuole in Arabidopsis. *Proc Natl Acad Sci* **115**:E2457–E2466. doi:10.1073/pnas.1717839115

Takken FL, Albrecht M, Tameling W IL. 2006. Resistance proteins: molecular switches of plant defence. *Curr Opin Plant Biol* **9**:383–390. doi:10.1016/j.pbi.2006.05.009

Takken FLW, Goverse A. 2012. How to build a pathogen detector: Structural basis of NB-LRR function. *Curr Opin Plant Biol* **15**:375–384. doi:10.1016/j.pbi.2012.05.001

van der Beek J, Jonker C, van der Welle R, Liv N, Klumperman J. 2019. CORVET, CHEVI and HOPS – Multisubunit tethers of the endo-lysosomal system in health and disease. *J Cell Sci* **132**. doi:10.1242/jcs.189134

Van Der Vossen EAG, Gros J, Sikkema A, Muskens M, Wouters D, Wolters P, Pereira A, Allefs S. 2005. The Rpi-blb2 gene from Solanum bulbocastanum is an Mi-1 gene homolog conferring broad-spectrum late blight resistance in potato. *Plant J* **44**:208–222. doi:10.1111/j.1365-313X.2005.02527.x

Van Ooijen G, Mayr G, Kasiem MMA, Albrecht M, Cornelissen BJC, Takken FLW. 2008. Structure-function analysis of the NB-ARC domain of plant disease resistance proteins. *J Exp Bot* **59**:1383–1397. doi:10.1093/jxb/ern045

van Wersch S, Tian L, Hoy R, Li X. 2020. Plant NLRs: the whistleblowers of plant immunity. *Plant Commun* **1**:100016. doi:10.1016/j.xplc.2019.100016

Vernoud V, Horton AC, Yang Z, Nielsen E. 2003. Analysis of the small GTPase gene superfamily of arabidopsis. *Plant Physiol* **131**:1191–1208. doi:10.1104/pp.013052

Wang Jizong, Hu M, Wang Jia, Qi J, Han Z, Wang G, Qi Y, Wang H-W, Zhou J-M, Chai J. 2019a. Reconstitution and structure of a plant NLR resistosome conferring immunity. *Science (80-)* **364**:5870. doi:10.1126/science.aav5870

Wang Jizong, Wang Jia, Hu M, Wu S, Qi J, Wang G, Han Z, Qi Y, Gao N, Wang H-W, Zhou J-M, Chai J. 2019b. Ligand-triggered allosteric ADP release primes a plant NLR complex. *Science (80-)* **364**. doi:10.1126/science.aav5868

Wang S, Boevink PC, Welsh L, Zhang R, Whisson SC, Birch PRJ. 2017a. Delivery of cytoplasmic and apoplastic effectors from *Phytophthora infestans* haustoria by distinct secretion pathways. *New Phytol*. doi:10.1111/nph.14696

Wang S, Boevink PC, Welsh L, Zhang R, Whisson SC, Birch PRJ. 2017b. Delivery of cytoplasmic and apoplastic effectors from Phytophthora infestans haustoria by

distinct secretion pathways. *New Phytol*. doi:10.1111/nph.14696

Wang S, McLellan H, Bukharova T, He Q, Murphy F, Shi J, Sun S, van Weymers P, Ren Y, Thilliez G, Wang H, Chen X, Engelhardt S, Vleeshouwers V, Gilroy EM, Whisson SC, Hein I, Wang X, Tian Z, Birch PRJ, Boevink PC. 2018a. Phytophthora infestans RXLR effectors act in concert at diverse subcellular localisations to enhance host colonisation. *J Exp Bot*. doi:10.1093/jxb/ery360

Wang S, Welsh L, Thorpe P, Whisson SC, Boevink PC, Birch PRJ. 2018b. The Phytophthora infestans haustorium is a site for secretion of diverse classes of infection-associated proteins. *MBio* **9**:1–14. doi:10.1128/mBio.01216-18

Wang W, Liu N, Gao C, Cai H, Romeis T, Tang D. 2020. The Arabidopsis exocyst subunits EXO70B1 and EXO70B2 regulate FLS2 homeostasis at the plasma membrane. *New Phytol* 0–2. doi:10.1111/nph.16515

Wang W, Wen Y, Berkey R, Xiao S. 2009. Specific targeting of the Arabidopsis resistance protein RPW8.2 to the interfacial membrane encasing the fungal Haustorium renders broad-spectrum resistance to powdery mildew. *Plant Cell* **21**:2898–913. doi:10.1105/tpc.109.067587

Wang W, Zhang Y, Wen Y, Berkey R, Ma X, Pan Z, Bendigeri D, King H, Zhang Q, Xiao S. 2013. A comprehensive mutational analysis of the Arabidopsis resistance protein RPW8.2 reveals key amino acids for defense activation and protein targeting. *Plant Cell* **25**:4242–61. doi:10.1105/tpc.113.117226

Westman J, Hube B, Fairn GD. 2019. Integrity under stress: Host membrane remodelling and damage by fungal pathogens. *Cell Microbiol*. doi:10.1111/cmi.13016

Whisson SC, Boevink PC, Moleleki L, Avrova AO, Morales JG, Gilroy EM, Armstrong MR, Grouffaud S, Van West P, Chapman S, Hein I, Toth IK, Pritchard L, Birch PRJ. 2007. A translocation signal for delivery of oomycete effector proteins into host plant cells. *Nature* **450**:115–118. doi:10.1038/nature06203

Whisson SC, Boevink PC, Wang S, Birch PR. 2016. The cell biology of late blight disease. *Curr Opin Microbiol* **34**:127–135. doi:10.1016/j.mib.2016.09.002

Wróblewski T, Spiridon L, Martin EC, Petrescu AJ, Cavanaugh K, Truco MJ, Xu H, Gozdowski D, Pawłowski K, Michelmore RW, Takken FLW. 2018. Genome-wide functional analyses of plant coiled–coil NLR-type pathogen receptors reveal essential roles of their N-terminal domain in oligomerization, networking, and immunity. *PLoS Biol* **16**. doi:10.1371/journal.pbio.2005821

Wu C. 2016. A complex NLR signalling network mediates immunity to diverse plant pathogens. University of East Anglia.

Wu C, Abd-el-haliem A, Bozkurt TO, Belhaj K. 2016. NLR signaling network mediates immunity to diverse plant pathogens. *bioRxiv*. doi:dx.doi.org/10.1101/090449

Wu C, Abd-El-Haliem A, Bozkurt TO, Belhaj K, Terauchi R, Vossen JH, Kamoun S. 2017. NLR network mediates immunity to diverse plant pathogens. *Proc Natl Acad Sci* **114**:8113–8118. doi:10.1073/pnas.1702041114

Wu CH, Adachi H, De La Concepcion JC, Castells-Graells R, Nekrasov V, Kamoun S. 2020. NRC4 gene cluster is not essential for bacterial flagellin-triggered immunity. *Plant Physiol* **182**:455–459. doi:10.1104/pp.19.00859

Xiao S, Ellwood S, Calis O, Patrick E, Li T, Coleman M, Turner JG. 2001. Broad-spectrum mildew resistance in Arabidopsis thaliana mediated by RPW8. *Science (80-)* **291**:118–20. doi:10.1126/science.291.5501.118

Yaeno T, Li H, Chaparro-Garcia A, Schornack S, Koshiba S, Watanabe S, Kigawa T, Kamoun S, Shirasu K. 2011. Phosphatidylinositol monophosphate-binding interface in the oomycete RXLR effector AVR3a is required for its stability in host cells to modulate plant immunity. *Proc Natl Acad Sci U S A* **108**:14682–14687. doi:10.1073/pnas.1106002108

Yoshida K, Schuenemann VJ, Cano LM, Pais M, Mishra B, Sharma R, Lanz C, Martin FN, Kamoun S, Krause J, Thines M, Weigel D, Burbano H a. 2013. The rise and fall of the Phytophthora infestans lineage that triggered the Irish potato famine. *Elife* **2**:e00731. doi:10.7554/eLife.00731

Zhang Q, Berkey R, Pan Z, Wang W, Zhang Y, Ma X, King H, Xiao S. 2015. Dominant negative RPW8.2 fusion proteins reveal the importance of haustorium-oriented protein trafficking for resistance against powdery mildew in Arabidopsis. *Plant Signal Behav* **10**:e989766. doi:10.4161/15592324.2014.989766

Zheng H, Camacho L, Wee E, Batoko H, Legen J, Leaver CJ, Malhó R, Hussey PJ, Moore I. 2005. A Rab-E GTPase mutant acts downstream of the Rab-D subclass in biosynthetic membrane traffic to the plasma membrane in tobacco leaf epidermis. *Plant Cell* **17**:2020–2036. doi:10.1105/tpc.105.031112